CONTRACT REPORT N-69-1

GEOMECHANICAL MODEL STUDY OF THE BEHAVIOR OF UNDERGROUND OPENINGS IN ROCK SUBJECTED TO STATIC LOADS

Report 1

DEVELOPMENT OF MODELING TECHNIQUES

by

R. E. Heuer
A. J. Hendron, Jr.

October 1969

Sponsored by

Defense Atomic Support Agency

Conducted for

U. S. Army Engineer Waterways Experiment Station
CORPS OF ENGINEERS
Vicksburg, Mississippi

under

Contract No. DACA 39-67-C-0009

by

Department of Civil Engineering
University of Illinois
Urbana, Illinois

CONTRACT REPORT N-69-1

GEOMECHANICAL MODEL STUDY OF THE BEHAVIOR OF UNDERGROUND OPENINGS IN ROCK SUBJECTED TO STATIC LOADS

Report 1

DEVELOPMENT OF MODELING TECHNIQUES

by

R. E. Heuer
A. J. Hendron, Jr.

October 1969

Sponsored by

Defense Atomic Support Agency

Conducted for

U. S. Army Engineer Waterways Experiment Station
CORPS OF ENGINEERS
Vicksburg, Mississippi

under

Contract No. DACA 39-67-C-0009

by

Department of Civil Engineering
University of Illinois
Urbana, Illinois

ARMY-MRC VICKSBURG, MISS.

ACKNOWLEDGMENTS

The work described in this report was accomplished in the Department of Civil Engineering at the University of Illinois under Contract No. DACA 39-67-C-0009 for the U. S. Army Engineer Waterways Experiment Station (WES). The work was sponsored by the Defense Atomic Support Agency. Mr. R. E. Heuer, Research Associate in Civil Engineering, was directly responsible for the laboratory work under the direct supervision of Dr. A. J. Hendron, Jr., Associate Professor of Civil Engineering, and the general direction of Dr. D. U. Deere, Professor of Civil Engineering and Geology. The technical assistance of Mr. William Polacek was sincerely appreciated. The cooperation and technical support of Mr. L. F. Ingram, Chief, Physical Sciences Branch; Mr. W. J. Flathau, Chief, Protective Structures Branch; Dr. J. P. Balsara; and Mr. J. L. Drake, Project Monitors, WES, are gratefully acknowledged.

The contract was under the general supervision of Mr. G. L. Arbuthnot, Jr., Chief, Nuclear Weapons Effects Division, WES. Contracting Officer was COL J. R. Oswalt, Jr., succeeded by COL Levi A. Brown, Director, WES.

ABSTRACT

Model laws governing the design of geomechanical model studies of underground openings in rock subjected to static loads are developed using dimensional analysis and the theory of models. The significant variables influencing the prototype which are considered in this study are free-field stresses, intact rock properties, rock mass discontinuity properties, and the opening geometry. Body forces are considered insignificant as a first approximation. The prototype chosen for study is a short section of a long circular tunnel which is underground at a depth of more than 4 tunnel diameters.

The development of a modeling material which successfully models the intact properties of rock is described. It was found that modeling materials described in the literature by previous investigators were not satisfactory because they lacked a sufficiently high angle of internal friction. Satisfactory frictional strength in the materials was achieved by developing mixtures of sand and plaster of Paris with a dense packing of sand grains.

The size of the model tested is 24" x 24" x 8". The design and development of a loading apparatus which allows independent control of the 3 principal stresses on the block is described. Uniformly distributed loads of 96 tons are applied to the 24" x 8" faces of the model. To maintain a plane strain condition in the model, loads of up to 144 tons are applied to the 24" x 24" faces to null strains parallel to the 8" dimension. Friction along the loading faces is controlled with sheets of teflon. Friction losses are reduced to the order of 10% or less of the applied loads.

The development of an instrumentation system for the model is described. Of particular interest is the development of techniques for imbedding electrical resistance strain gages within the model material to measure radial and circumferential strains at points within the model around the tunnel.

Some tentative observations are made concerning the feasibility of utilizing relatively large scale models to study the behavior of underground openings.

CONTENTS

		Page
I.	INTRODUCTION	1
	A. Reasons for Geomechanical Model Studies	1
	B. Scope of Study	6
II.	SIMILITUDE CONSIDERATIONS	7
	A. Fundamental Considerations	7
	B. Selection of Significant Variables	10
	1. Free Field Stresses	10
	2. Intact Rock Properties	15
	3. Discontinuity Properties	17
	4. Opening Geometry	17
	C. Development of Model Laws	18
	D. Model Material Requirements	21
	E. Model Configuration and Boundary Conditions	25
III.	DEVELOPMENT OF GEOMECHANICAL MODELING TECHNIQUES	29
	A. Modeling Materials	29
	1. Introduction and Plaster of Paris Chemistry	29
	2. Plaster of Paris/Kaolinite Curing Characteristics	32
	3. Triaxial Strength Properties of Various Plaster of Paris Mixtures	38
	4. Compaction of Plaster of Paris/Sand Mixtures	43
	5. Triaxial Strength Properties of Compacted Plaster of Paris/Sand Mixtures	45

CONTENTS, Continued

	Page
B. Model Loading Apparatus	50
1. Estimated Model Behavior	50
a. Required Loading Capability	50
b. Blocks Without Tunnels	51
c. Tunnel Behavior	54
2. Lateral Loading Elements	55
a. Loading Methods Considered	55
b. Load Distribution Characteristics of the Triangular Element Lateral Loading System	58
i. Load distribution as measured by the instrumented elements	58
ii. Brittle coating studies	61
3. Longitudinal Restraint and Reaction Frame	66
a. Uniform Restraining Pressure System	67
b. Rigid Heads Tied Across Model	67
c. Controlled Rigid Longitudinal Heads	70
i. Cantilevered lateral reactions	70
ii. Symmetrically supported lateral reactions	71
4. Control of Friction Along Longitudinal Loading Faces	74
C. Instrumentation of the Model	77
1. Applied Stresses and Over-all Block Deformations	77
2. Radial Extensometers	78
3. Internal Electrical Resistance Strain Gages	78
a. General Considerations	78
b. Surface SR4 Gages	82
c. Internal SR4 Gages	89
4. Temperature Compensation and Wiring	90

CONTENTS, Continued

Page

IV. FEASIBILITY OF RELATIVELY LARGE SCALE MODELS - TENTATIVE OBSERVATIONS 94

A. Similitude Considerations 94

B. Modeling Materials 98

C. Model Loading Apparatus 100

D. Instrumentation of the Model 102

REFERENCES 103

FIGURES 107

Geomechanical Model Study of the Behavior of Underground Openings in Rock Subjected to Static Loads

I. INTRODUCTION

A. Reasons for Geomechanical Model Studies

The present needs for the excavation of large underground openings in rock, of unprecedented size and complexity, require a more comprehensive understanding of the influence of the variables which determine the behavior of these openings, if they are to be designed rationally.

Among the variables which play a significant role in the behavior of underground openings are:

1. Free-field stresses;
   - a. Stress magnitude,
   - b. Ratio of minor to major principal stresses, and
   - c. Orientation of the stress field.
2. Intact rock properties;
   - a. Strength parameters such as cohesion, internal friction, and tensile strength, and
   - b. Deformation parameters such as elastic constants, pertinent inelastic deformation parameters, and failure strains.
3. Discontinuities in the rock mass, such as joints, faults, and bedding planes;
   - a. Spacing, location, and orientation,
   - b. Strength parameters, determined by such qualities as shape, roughness, tightness, and filling of the discontinuities, and
   - c. Deformation parameters, which are influenced by qualities such as influence the strength parameters.

4. Geometry of the opening;
    a. Size,
    b. Shape,
    c. Orientation, and
    d. Proximity to adjacent openings.
5. Techniques by which the opening is constructed.

Limited field data concerning the behavior of underground openings are available, but it is not possible to extrapolate these data directly to predict the behavior at other sites where the variables listed above have different values. In order to do this one must have a quantitative basis for determining how changes in the variables will influence the behavior of the opening. To develop such quantitative relationships between the pertinent variables and the behavior of the opening empirically, data must be obtained over a wide range of the variables. The cost and impracticality of obtaining data from many full-scale field construction sites limits the usefulness of this approach. Field data do, however, offer the only ready means of studying the influence of construction techniques.

Analytical methods of predicting the behavior of underground openings in rock are quite limited in applicability. Solutions from the theory of elasticity are directly applicable only to a limited number of rocks which are linearly elastic, and at stress levels below failure. In addition, elastic solutions are tractable for only the most simple opening geometries. Numerical analyses utilizing finite element techniques are much more versatile because they can handle any shape opening in an elastic-plastic material with internal friction governing yield strength (for example, Reyes, 1966) and can account for major discontinuities. These finite element techniques, however, are limited in their ability to accurately account for the actual nonlinear material properties of strength and deformation. All of the analytical methods are also restricted in

their ability to analyze a discontinuous mass such as encountered in practice, where the rock is broken into individual blocks by a number of geologic features. In addition, they are generally not capable of considering simultaneously a number of failure modes.

One of the more widely used experimental techniques for the study of openings is the use of photoelastic models. This technique can be used for openings of any shape, but is restricted to the analysis of the principal stress difference in linearly elastic materials. A superposition of isochromatics determined by photoelastic studies and isopachics determined by a technique such as a conducting paper analog allows a prediction of potential failure zones in a Coulomb-Navier material (Hoek, 1967). Although this method gives much more information than photoelastic techniques alone, it is still restricted to predicting potential failure zones in linearly elastic brittle rocks and does not have general application to more ductile rocks and a prediction of behavior once yielding or fracture has been initiated. It also does not give information about deformations of the opening.

A most promising technique for studying the influence of variables 1 through 4 listed above appears to be the use of geomechanical models. In this technique, a small scale model of the underground opening is constructed in a material which accurately models the properties of the actual rock mass in the field. The model is then loaded in such a manner as to reproduce the stress state which exists in the real prototype underground. If the requirements of similitude are satisfied the behavior of the model then reproduces the behavior of the prototype in all respects: distribution of stresses, distribution of strains and deformations both elastic and inelastic, and failure modes. The main limitation of this technique appears to be the technical problems encountered

in satisfying the requirements of similitude when modeling the details of the geologic environment of the prototype. These problems are not insignificant.

The validity and usefulness of structural models is well established in many phases of engineering research and design. The most notable examples probably are the structural model tests of arch dams at such places as Laboratorio Nacional de Engenharia Civil in Lisbon, Portugal and Istituto Sperimentale Modelli e Strutture in Bergamo, Italy. The next step beyond structural modeling is the use of geomechanical models in which not only the proposed engineering structure (or "anti-structure" in the case of an underground cavity) is modeled, but an attempt is also made to model the details of the geologic environment in which the structure is to exist. For example, the strength and deformability of different rock formations, and the frequency, orientation, and strength and deformation characteristics of discontinuities such as joints, bedding planes, and faults are modeled as accurately as is possible and practical. The engineering structure and surrounding geologic environment are envisioned as a single inter-acting unit in which the behavior of the structure itself cannot be predicted without giving due consideration to the behavior of the surrounding geologic environment.

The use of geomechanical models appears to be the only technique available, analytical or experimental, for determining the behavior of underground openings through all stages of loading and deformation, elastic and inelastic, up to failure.

The theoretical basis of model studies in general (for example, Murphy, 1950; Langhaar, 1951) and of structural and geomechanical models in particular (for example, Preece and Davies, 1964; Rocha, 1958 and 1965;

Fumagalli, 1955, 1959, 1960, and 1964; Mandel, 1964) has been well established. The basis for geomechanical model studies of underground openings in rock (not considering time-dependent behavior) has been discussed and developed to varying degrees by experimentors such as Barron and Larocque (1962), Everling (1964), Hobbs (1966), and Hoek (1965). Some critical aspects of similitude requirements such as boundary loading conditions and model material properties generally have not been adequately satisfied by these investigators and their work is of limited value in a general understanding of the influence of the variables affecting the behavior of underground openings in rock.

B. Scope of Study

This study consists of two phases:

Phase 1. Development of modeling techniques including

a. satisfactory modeling materials,

b. methods of loading the models,

c. instrumentation for quantitatively measuring behavior of the models, and

d. a consideration of the feasibility of testing relatively large scale laboratory models

Phase 2. Tests on a number of small models to study the influence of some of the pertinent variables listed previously.

The techniques developed in this study should be helpful to investigators contemplating geomechanical model studies of proposed engineering structures. The test results on the small models will contribute to the basic understanding of the behavior of underground openings. This information will be particularly invaluable for the design of larger models in which a more detailed study of the behavior can be made. The quantitative results of the study will also be valuable for planning a proper instrumentation program for field measurements because critical areas can be estimated before construction.

This report describes the findings of the first year of work in Phase 1 as outlined above. Studies in Phase 2 will be undertaken in the second year of study.

II. Similitude Considerations

A. Fundamental Considerations

In most physical phenomena considered in civil engineering and geology it is conventionally assumed that a "cause and effect" relationship exists between the various independent and dependent variables which influence and describe a phenomenon. This relationship is assumed to be expressed by some function

$$f(x_1, x_2, x_3, \ldots x_i, \ldots x_n) = 0 \qquad \text{(eq. 1)}$$

where x_i are the pertinent independent and dependent variables. The function $f_{(x_i)}$ can usually be expressed explicitely for only the more simple phenomena. It may be determined from either theoretical considerations or empirical studies. Because the most basic physical laws (such as Newton's Laws) are dimensionally homogeneous, that is their form does not depend upon the units of measurement, it can be hypothesized that the more complex function $f_{(x_i)}$ is also dimensionally homogeneous, even though it is not explicitely known.

The theory of dimensional analysis, founded in the mathematical theories of algebra, is summarized in Buckingham's theorem (Langhaar, 1951, p. 18) which essentially says that from the dimensionally homogeneous function or equation describing the phenomenon, it is possible to develop a relationship in which the variables appear in a set of dimensionless products. (For a more complete discussion see texts such as Murphy, 1950, or Langhaar, 1951). In practice, dimensional analysis allows us to determine these dimensionless products, given the pertinent variables, even though we do not know the form of the function $f_{(x_i)}$ which describes the phenomenon. Thus, from eq. 1, which is the basic function relating the pertinent variables x_i in a description of the phenomenon, we arrive by a dimensional analysis at

$$F(\pi_1, \pi_2, \pi_3 \ldots \pi_i \ldots \pi_m) = 0 \qquad \text{(eq. 2)}$$

as a description of the phenomenon. Each π_i, often called a Buckingham pi term, is a dimensionless product of some number of the original x_i variables. Generally, the number m of independent pi terms is related to the number n of the x_i variables and to the number r of fundamental dimensions (such as mass, length, time, temperature) which are involved in the x_i variables by

$$m = n - r \qquad \text{(eq. 3)}$$

There are several advantages which may be gained from the dimensional analysis. First, the relationship between the x_i variables in the π_i terms often gives valuable insight into the phenomenon being considered. Secondly, the phenomenon is described in terms of a fewer number of variables, only m pi terms instead of the n original variables. This reduction of variables is often important when studying the phenomenon experimentally since it frequently reduces the number of experiments which must be run. A third advantage is that the dimensional analysis provides a theoretical basis for model studies, by which it may be possible to reduce even further the cost involved in studying the phenomenon being considered.

The function given in eq. 2 is dimensionally homogeneous and completely general. If the m pi terms are independent and contain all of the pertinent variables x_i which influence and describe the phenomenon, then the function $F_{(\pi_i)}$ completely describes the phenomenon, regardless of the scale of units with which the quantities x_i are measured, and regardless of the absolute magnitude of the x_i quantities. This means that if we wish to utilize models to study the behavior of a prototype, we can be assured that the behavior of the model duplicates the behavior of the prototype in all respects if each of the pi terms for the model is equal to the equivalent pi term for the prototype, that is, if

$$(\pi_i)_{model} = (\pi_i)_{prototype} \qquad \text{(eq. 4)}$$

If such a condition exists, all requirements of similitude have been satisfied, the model is said to be "completely similar" to the prototype, and the phenomenon in the model is an exact replica of the phenomenon in the prototype.

Several major problems develop in the practical application of dimensional analysis to modeling. One is that it generally is technically impossible to insure that all of the x_i variables which influence the prototype are considered in the dimensional analysis and are accurately reproduced in the model by equating the π_i terms of the model and prototype. For satisfactory modeling it is necessary that the phenomenon be understood well enough to know what variables x_i are most significant and which pi terms π_i must be duplicated most rigorously so that the model gives the most accurate simulation of the prototype which it is both possible and practical to attain.

In this approximation of the prototype by the model a second major problem arises in what are known an "scale effects". For example, as the physical size of the model varies, the relative importance of different forces may vary also. Body forces such as weight due to gravitational attraction vary as the mass of the body, hence as the cube of linear dimensions, while surface forces such as pressures vary as area, hence as the square of linear dimensions. Thus, as the physical size of a model is reduced, the influence of body forces decreases more rapidly than that of surface forces. It is possible that the behavior of the prototype may be strongly influenced by body forces, but when a model is made at a reduced size, its behavior may be strongly influenced by surface forces which are insignificant in the prototype. Careful consideration must be given to the selection of pertinent variables and the possibility of scale effects in developing a model testing program.

B. Selection of Significant Variables

The dimensions of mass M, length L, and time T, are probably the most commonly used dimensions by which physical phenomena are described. An equally valid set of basic dimensions is force F, length L, and time T. For a static system such as is being considered, only force F and length L are involved. This is the set which will be used in the following analysis.

The significant variables associated with the behavior of an underground opening which will be considered are given in Table 1. A number 1 in the dimensions column means that the variable is dimensionless, a pure number.

1. Free Field Stresses

The prototype chosen for study is a segment of a long straight horizontal tunnel buried underground at a depth which is several times greater than the tunnel diameter. The most significant forces influencing the tunnel behavior are assumed to be due to the free field stresses which would exist at the location of the tunnel if it were not present. The two free field stresses considered, σ_v and σ_h, are the vertical and horizontal stresses in a plane perpendicular to the tunnel axis (Fig. 1), and are assumed to be principal stresses (which they would be in an elastic half space with a horizontal surface). The magnitude of the third principal stress, σ_ℓ, the horizontal stress parallel to the tunnel axis, will be considered later.

The vertical free field stress σ_v is assumed to be due to the weight of the overlying material, and at any depth z below the surface, it is given by

$$\sigma_v = \gamma z \qquad \text{(eq. 5)}$$

where γ is the average unit weight of the overburden. Following the arguments of Terzaghi and Richart (1952), the horizontal free field stress σ_h is assumed to be given by

Table 1 Significant Variables

	Variable	Dimensions
1.	1. Free field stresses, assumed to be principal stresses	
	σ_v, the vertical free field stress	FL^{-2}
	σ_h, the horizontal free field stress	FL^{-2}
	2. Intact rock properties	
	c or q_u, cohesion or unconfined compressive strength, use either one	FL^{-2}
	ϕ, angle of internal friction	1
	σ_t, tensile strength	FL^{-2}
	E, modulus of elasticity	FL^{-2}
	ν, Poisson's ratio	1
	3. Properties of joints or other discontinuities in the rock mass	
	s, average spacing of the discontinuities, considering only those parallel or perpendicular to the axis of the opening	L
	α, inclination, with respect to the horizontal, of the discontinuities parallel to the axis of the opening	1
	C_j, cohesion along the discontinuities	FL^{-2}
	ϕ_j, friction angle along the discontinuities . .	1
	4. Geometry of the opening	
	d, diameter	L
	$\ddot{u}$, radial deformations of the opening wall . . .	L
	ε, strain within the rock mass behind the opening .	1

$$\sigma_h = N_{(z)}\ \sigma_v = N_{(z)}\ \gamma\ z \qquad \text{(eq. 6)}$$

The coefficient $N_{(z)}$ relating σ_v and σ_h is intimately related to the present geologic environment and the previous geologic history of the site and may vary over a wide range of values.

One extreme value of $N_{(z)}$ occurs in regions in which high horizontal compressive stresses exist due to tectonic activity in the earth's crust. In such a case σ_h may be significantly greater than σ_v, with $N_{(z)} > 1$. Geological observations and recent rock mechanics investigations offer ample evidence that such stress states have existed in the past and do exist at present in regions of orogenic activity. The probability of a tensile horizontal free field stress in a position such as the crest of an anticline during an orogenic phase is considered to be insigiificant for engineering purposes. It is assumed that jointing and normal faulting would relieve any such stresses which develop. Thus, the other extreme value of $N_{(z)}$ would occur if the rock at the tunnel site had been able to expand laterally due to the Poisson's ratio effect under the gravitational loading of the overlying material. In this case $N_{(z)} = 0$, $\sigma_h = 0$, and a uniaxial gravitational stress field σ_v exists. Generally however, the rock is restrained to some degree by the adjacent portions of the earth's crust, and $N_{(z)} > 0$.

If the portion of the earth's crust under consideration behaved as an ideal elastic half-space loaded by its own weight with no lateral expansion, the horizontal stress at any point would be given by

$$\sigma_h = \left(\frac{\nu}{1-\nu}\right)\ \sigma_v = \left(\frac{\nu}{1-\nu}\right)\ \gamma\ z \qquad \text{(eq. 7)}$$

where ν is the Poisson's ratio of the material. In the absence of tectonic stresses, such a stress state might be considered typical for a sedimentary rock mass deposited in horizontal beds with no lateral expansion of underlying beds during the deposition of overlying sediments. However, there are a number of reasons why such an assumption may be seriously in error. The erosion of

stream valleys through the sedimentary sequence may relieve horizontal stresses near the valley walls, but lead to a stress concentration near the valley floor, analogous to the stress rarefactions and concentrations around a notch in a tension member. The erosion and removal of a significant depth of overlying material over a wide area will lead to a reduction of the vertical stress σ_v proportional to the depth removed. But the horizontal stress σ_h is not reduced proportionally because of the inelastic nature of the rock. This leaves a residual "locked-in" component of the horizontal stress so that the resultant horizontal stress σ_h is not related to the existing depth of overburden as predicted by eq. 7, but is larger. This phenomenon has been verified experimentally for sands and clays by Hendron (1963) and Brooker (1964), respectively. The same effect can be produced by the melting of great thicknesses of ice such as existed in areas of continental glaciation during the Pleistocene.

The only conclusion which can be drawn concerning the function $N_{(z)}$, then, is that it is very intimately related to unknown details of the geologic environment and history of the site and can not be predicted with any accuracy. It will be assumed for this study that $N_{(z)}$ is a constant for the tunnel site and is not a function of depth z, hence it will be symbolized by N rather than $N_{(z)}$. The concept and symbol of K_o, the coefficient of earth pressure at rest, as presented by Terzaghi (1943), is not used here because it is understood to mean a condition of gravity loading with no lateral deformation in the earth's mantle or crust. This would not include, then, the possibility of horizontal deformation and very high horizontal stresses due to tectonic forces, a condition which must be considered in rock masses. Instead of arbitrarily choosing a numerical value of N for the model testing program, so that only two of the variables, σ_v or σ_h, is independent, both σ_v and σ_h will be considered as independent variables.

Mindlin (1939) has developed rigorous solutions for stress distributions around a circular tunnel in an elastic half space under gravity loading

with N values of 0, $\nu/1-\nu$, and 1. His results (see Panek, 1951; or Caudle and Clark, 1955, for more detail) show that if the tunnel is at a depth of 3 tunnel diameters or more, the stress distribution around the tunnel can be approximated very closely by the distribution of stresses about a circular hole in a biaxially loaded elastic flat plate, as determined by the Kirsch equations (see for example Timoshenko and Goodier, 1951; or Obert and Duval, 1967). In both cases the zone in which stresses are significantly influenced by the tunnel has a width of about 4 times the diameter of the tunnel.

These observations allow a considerable simplification in modeling the stress field about the tunnel. The observation that the zone of influence of the tunnel is about 4 tunnel diameters wide means that the stress distribution on a square whose sides are 4 tunnel diameters long, concentric with the tunnel, is very closely approximated by that illustrated in Fig. 1, where σ_v and σ_h are the free field stresses at the location of the tunnel axis, and $\Delta\sigma_v$ and $\Delta\sigma_h$ are the changes in the free field stresses between the top and the bottom of the zone due to the weight of the material within it. This is the free field stress distribution due to gravity loading of the elastic half space.

The observation that Mindlin's (1939) solutions for tunnels buried at more than 3 tunnel diameters are closely approximated by Kirsch's solution means that the stress distribution of Fig. 1 can be approximated by that of Fig. 2 with negligible error. This means that for the elastic case the stress distribution around a tunnel underground at a depth of more than 3 tunnel diameters is more strongly influenced by the average free field stresses at the tunnel location than by the gravity forces on the material within the zone influenced by the tunnel. When modeling the static behavior of a tunnel in this situation only the average free field stresses as illustrated by Fig. 2 need

be modeled and the body forces can be neglected. On the basis of the preceding arguments the body forces and associated variables such as the density of the material are not considered in the list of significant variables for the present study.

2. Intact Rock Properties

A discussion of the failure mechanism of rock materials is beyond the scope of this project. The reader is referred to papers such as Bieniawski (1967) as an example of recent work in this area. Regardless of the actual failure mechanism in rock materials, it is generally observed that some form of Mohr envelope can be fitted to observed experimental data and used to predict rock strength. In order to simplify the dimensional analysis and subsequent discussions, it will be assumed that the general curvilinear Mohr envelope can be approximated by a straight line in the compression pressure range of interest, so that the general Mohr failure criteria

$$\tau = F_{(\sigma)} \qquad \text{(eq. 8)}$$

can be replaced by the more specialized Coulomb-Navier failure criteria

$$\tau = c + \sigma \tan \phi \qquad \text{(eq. 9)}$$

(For a more detailed discussion of failure criteria, see Nadai, 1950; Seely and Smith, 1952; Jaeger, 1962; Obert and Duval, 1967).

The two independent Coulomb-Navier strength parameters are the cohesion c and the angle of internal friction ϕ. An alternate and equally valid pair are the unconfined compressive strength q_u, and the angle of internal friction ϕ. Either c or q_u, in conjunction with ϕ, are necessary and sufficient to define the failure state and describe the failure envelope. In addition, the tensile strength σ_t must be defined, since eq. 9 is not valid in the tensile strength range. The complete failure envelope, then, is as shown in Fig. 3. A rigorous

consideration of the actual curvilinear Mohr envelope does not change the basic conclusions of the dimensional analysis.

The elastic constants, the modulus of elasticity E and Poisson's ratio ν, relate stress and strain assuming the intact rock exhibits a quasi-elastic behavior at low and intermediate stress levels. In general this quasi-elastic range is followed by a range in which inelastic strains occur, and then by some form of failure such as fracture or plastic deformation (Fig. 4). No variables are included to describe the inelastic and plastic regions for two reasons: 1) the wide range of behavior exhibited by different rocks, and 2) the scarcity of real numerical description and data for this portion of the stress-strain curve. It is recognized that the other types of behavior exist. For example, a concave upward stress-strain curve is commonly observed at low stress levels for very porous rocks, for highly weathered rocks, and for thinly bedded or foliated rocks compressed perpendicular to the bedding or foliation. The initial quasi-elastic behavior is probably more common, however, and is much more simple to consider and model.

Time-dependent behavior such as creep or viscous deformation is not considered. These properties of real rock are so poorly known and understood that any attempt to consider them in modeling the behavior of underground openings must be considered a very questionable practice for the "present state of the art." The one exception to this statement would be in the case of underground openings in the evaporites: rock salt, potash, and possibly gypsum and anhydrite. For these rocks viscous behavior is so pronounced that it must be considered. Indeed, because it is so pronounced it can be and has been studied enough so that intelligent attempts to model the viscous behavior of such rocks can be made.

3. Discontinuity Properties

The influence of discontinuities such as joints, faults, and bedding planes upon the mechanical behavior of a rock mass is well recognized by competent workers in the field of rock mechanics and their inclusion in the list of significant variables influencing the behavior of underground openings needs no justification here.

The geometry of the discontinuities is defined by their average spacing s and their orientation α. The possibility of discontinuities intersecting the tunnel axis at an acute angle will not be considered in this initial modeling program. The significance of these variables is widely recognized and their selection needs no defense. An attempt to consider the details of the discontinuity surface, such as surface roughness, is beyond the scope of the initial model testing program. Moreover, the influence of these details is inherent in the shear strength parameters of the joints. Hence these details are considered indirectly.

Theoretical considerations and model studies (Patton, 1966) and tests on actual rock surfaces (Patton, 1966; Corps of Engineers, 1964, 1965; Lane and Heck, 1964; and Jaegar, 1959) indicate that the shear strength of rock mass discontinuities may be represented by a Mohr Failure Envelope which may be approximated by segments of 1 or 2 straight lines, and that both a cohesion intercept c_j and a friction angle ϕ_j are needed to define the segments (Fig. 5; see Patton, 1966, for a more complete discussion). Hence the variables c_j and ϕ_j are included in the dimensional analysis.

4. Opening Geometry

The variables selected to describe the geometry and behavior of the opening are well understood and their selection needs no explanation.

C. Development of Model Laws

The behavior of the prototype tunnel is assumed to be determined and described with sufficient accuracy by the variables given in Table 1. These variables are the x_i terms of Eq. 1, which then becomes

$$f\ (\sigma_v, \sigma_h,\ c \text{ or } q_u,\ \phi,\ \sigma_t,\ E,\ \nu,\ s,\ \alpha,\ c_j,\ \phi_j,\ d,\ u,\ \varepsilon) = 0 \quad \text{(eq. 10)}$$

The next step in the determination of the similitude requirements governing a model study of this phenomenon is to perform a dimensional analysis, that is, to determine a set of pi terms as in Eq. 2. By inspection of Table 1 and Eq. 3 it is seen that there are $m = n - r = 14 - 2 = 12$ dimensionless pi terms which describe the phenomenon. Rigorous methods are available for determining a complete set of independent pi terms (see for example, Langhaar, 1951; or Murphy, 1950). However, a complete set for the variables in Table 1 can be determined by inspection, and are given in Table 2.

Table 2
Dimensionless Pi Terms

defining loading:	$\frac{\sigma_h}{\sigma_v}$, $\frac{\sigma_v}{q_u}$
defining intact rock:	$\frac{\sigma_t}{q_u}$, ϕ, $\frac{E}{q_u}$,, ν
defining discontinuities:	$\frac{s}{d}$, α, $\frac{c_j}{c}$, ϕ_j
defining geometry and deformations:	$\frac{u}{d}$, ε

Equation 2 then becomes

$$F\ (\frac{\sigma_h}{\sigma_v}, \frac{\sigma_v}{q_u}, \frac{\sigma_t}{q_u}, \phi, \frac{E}{q_u}, \nu, \frac{s}{d}, \alpha, \frac{c_j}{c}, \phi_j, \frac{u}{d}, \varepsilon) = 0 \qquad \text{(Eq. 11)}$$

This is the dimensionless functional relationship describing the phenomenon. If the model study is to accurately reproduce the prototype field behavior, it is necessary that the pi terms as given in Table 2 and Eq. 11 be identical for the model and the prototype, as indicated by Eq. 4. That is, for example:

$$\left(\frac{\sigma_h}{\sigma_v}\right)_{\text{model}} = \left(\frac{\sigma_h}{\sigma_v}\right)_{\text{prototype}}$$

$$(\phi)_{\text{model}} = (\phi)_{\text{prototype}} \qquad \text{(Eq. 12)}$$

and so on for the rest of the pi terms.

If the symbol K_{x_i} is used to represent the ratio between the value of one of the x_i terms in the model and in the prototype, for example:

$$K_{\sigma_v} = \frac{(\sigma_v)_{\text{model}}}{(\sigma_v)_{\text{prototype}}} \quad \text{or} \quad K_d = \frac{(d)\ \text{model}}{(d)\ \text{prototype}} \qquad \text{(Eq. 13)}$$

then the requirements of similitude as given in Eqs. 4 and 12 dictate certain relationships which must exist between the K_{x_i} terms. The K_{x_i} ratios are called the scale factors, and the relationships between them are called the model laws. The model laws for this phenomenon, as derived from the pi terms of Table 2 by simple algebraic manipulation, are given in Table 3.

Table 3
Model Laws

linear dimensions L:	$K_L = K_d = K_u = K_s$
stresses σ:	$K_\sigma = K_{\sigma_v} = K_{\sigma_h} = K_{q_u} = K_{\sigma_t} = K_E = K_{c_j}$
strains ε:	$K_\varepsilon = K_\nu = 1$
angles ϕ:	$K_\phi = K_{\phi_j} = K_\alpha = 1$

The model laws of Table 3 show that all of the x_i quantities having the dimensions of length L scale in the same ratio K_L between the model and the prototype, all x_i quantities having the dimensions of stress F/L^2 scale in the same ratio K_σ, and all dimensionless quantities such as strains and angles have the same magnitude in the model as in the prototype. Furthermore, the model laws show that the scale factors for lengths and stresses, K_L and K_σ, are independent and may be chosen arbitrarily.

If the model laws of Table 3 are satisfied, the requirements of Eq. 4 are satisfied, the model is "similar" to the prototype, and it behaves exactly as the prototype. By measuring the x_i quantities in the model, the x_i quantities of the prototype can be predicted through the scale factors. The accuracy with which the predicted prototype behavior matches the actual prototype behavior depends upon two factors:

1. The accuracy of the assumption that the x_i quantities of Table 1 are the quantities which determine and describe the phenomenon, and
2. The accuracy with which the model laws are satisfied.

D. Model Material Requirements

Some very stringent requirements on the behavior of the model material are implicit in the modeling ratios given above. The model laws $K_{\sigma_t} = K_{q_u} = K_{\sigma_v} = K_{\sigma_h}$ and $K_\phi = 1$ require that on any dimensionless plot of strengths, the data for both the model and prototype materials must collapse onto a single line. For example, if Fig. 6 were the Mohr envelopes for the prototype and model materials, then on a dimensionless plot of τ/q_u vs σ/q_u such as Fig. 7, the envelopes for the two materials must coincide. On any other dimensionless strength plot, such as $(\sigma_1 - \sigma_3)/q_u$ vs σ_3/q_u, the strength envelopes for the two materials must also coincide.

A similar relationship exists for the deformation characteristics of the model and prototype materials. The modeling ratios $K_E = K_{q_u}$, $K_\varepsilon = 1$, $K_\nu = 1$, and the strength requirements given above require that the materials have the same Poisson's ratio and that on all dimensionless plots of strains or deformations vs stress the curves for the two materials must coincide. For example, if Fig. 8 were the stress-strain curves for the model and prototype materials at comparable confining pressures, i.e., at a value of σ_3/q_u which is the same for both materials, then on a dimensionless plot of $(\sigma_1-\sigma_3)/q_u$ vs ε, the curves for both materials must coincide as in Fig. 9. This means, for example, that in triaxial compression tests at comparable confining pressures, the materials must fail at the same strains. Hence, on a dimensionless plot of $\varepsilon_{failure}$ vs σ_3/q_u, the data for the two materials must collapse onto a single line.

In practice these requirements are almost impossible to satisfy. In a model study of a linearly elastic phenomenon, the strength modeling laws do not exist, and the deformation modeling laws are not so critical since the stress-deformation relationships are linear. For example, $K_\varepsilon = 2$ may be

allowed without seriously affecting the accuracy of the model. For a model study in which inelastic deformations and failure conditions are important, however, the model laws must be satisfied as nearly as possible. Patterns of stress and strain distribution in the prototype may change markedly as non-linear, inelastic deformations occur and as failure conditions are approached or reached. If the model laws are not satisfied and the model materials do not fulfill the requirements outlined above, the patterns of stress and strain distribution in the model may differ considerably from those of the prototype.

In modeling studies the most common solutions of this dilemna are either 1) to conduct tests in only the quasi-elastic, working-stress range, where the model material requirements are not so critical; or 2) to build the model from essentially the same material as the prototype, as is done in microconcrete model studies of reinforced concrete structures. These approaches are not feasible in geomechanical model studies of underground openings, however.

In the first case, underground structures are highly indeterminant so that local failures can develop without leading to complete failure of the structure. In fact, the economics of underground construction often demand that such local failures be tolerated. Hence, a study of the low stress, quasi-elastic behavior is not sufficient.

The second approach is not feasible for two reasons. First, the discontinuities in the actual rock mass exist on a physical scale such that it is impossible to obtain samples of the rock mass small enough so that accurate model studies can be performed. Secondly, the strength of the rock materials is generally so great that the size of models constructed of the prototype material which can economically be loaded to failure in the laboratory are too small to be of interest. Hence it is necessary to use artificial, low strength materials for the construction of geomechanical models.

Data for intact rock (for example, Deere and Miller, 1966; Deere and Hendron, 1965; Handin and Hager, 1957; Handin, et al, 1963; Corps of Engineers, 1964, 1965, and 1966; and Robertson, 1955) indicate that on the average, the properties of intact rock are such that the tensile strength is about 5% to 10% of the unconfined compressive strength and the modulus of elasticity is about 250 to 500 times the unconfined compressive strength (E being the tangent modulus at 50% of q_u), while the angle of internal friction commonly varies between 25° and 60°, and ν is between 0.1 and 0.3. That is, for actual rock:

$$5\% < \frac{\sigma_t}{q_u} < 10\%; \quad 250 < \frac{E}{q_u} < 500; \quad 25° < \phi < 60°; \quad 0.1 < \nu < 0.3$$

The material chosen for the construction of the model must also have properties within these ranges if similitude is to be achieved.

Test data indicate that rock specimens typically fail in unconfined compression at axial strains of 0.2 to 1.0 percent. In triaxial compression at confining pressures equal to their unconfined compression strength, rock specimens reach a peak stress difference $(\sigma_1 - \sigma_3)$ at axial strains which may range widely, from around 1% for dense igneous rocks up to 10% to 20% or more for ductile shales or evaporites. Rocks commonly exhibit dilation during shear, possible exceptions being very porous sedimentary or volcanic rocks whose porous structure collapses during shear, or some evaporites which may fail by intercrystalline gliding with no volume change. A general modeling material should exhibit dilation during shear to satisfy similitude.

Typical stress-strain curves for a wide range of rock types are given in the references listed above. The modeling material chosen should possess stress-strain curves which are of the same shape as those of a typical rock, as in Fig. 4.

Experimental studies of the frictional properties of natural joints in rock (Deere and Hendron, 1964; Lane and Heck, 1964; Corps of Engineers, 1964, 1965; Jaeger, 1959) suggest that the angle of friction along a rock joint may range from about 25° to 40°, i.e., $25° < \phi_j < 40°$. The model material should have a similar value of ϕ_j.

If a modeling material is being chosen to model the general behavior of rock, it should have properties falling within the ranges given above. Preferably it would have intermediate properties and would not be at the extreme of any of the ranges listed. More difficulty would be experienced if a modeling material were being selected to model the behavior of a particular rock type, or more specifically, rock from a given formation at a given locality.

E. Model Configuration and Boundary Conditions

For the initial testing program a model configuration should be chosen such that it is easy to construct, load, and monitor, and so that it may be compared with theoretical predictions of behavior as a test of the accuracy of the modeling techniques. A circular, cylindrical opening modeling a long tunnel satisfies these requirements best. It could readily be cored out of a block of model material, it would be most easily monitored by various types of instrumentation, and its mathematical simplicity and symmetry have made it most conducive to theoretical consideration so that a number of relationships are available for predicting its behavior.

An inspection of the scale factors and modeling laws presented previously shows that the length scale factor K_L may be chosen arbitrarily. The only modeling requirements on linear dimensions are that joint spacing be modeled in the same ratio as the tunnel diameter, and that the deformation of the tunnel will have this same scale factor. For ease of instrumentation of the model it is desirable that the model be as large as possible, but for economy in the construction of loading apparatus, it is necessary to keep the model as small as possible.

The tunnel opening should be about 4 to 6 inches in diameter for ease of installation of various instrumentation for monitoring the behavior of the tunnel and the mass in which it is contained. The block containing the tunnel should be a rectangular shape for ease of application of a polyaxial stress state. It should be at least 4 to 6 tunnel diameters in width so that a relatively uniform "free field stress state" can be achieved in the area in which the tunnel is to be placed, away from the loading heads. The length of the tunnel should be at least twice the tunnel diameter in order to minimize

"edge effects" on instrumentation placed at the center of the model around the tunnel. It is believed that a 4" diameter tunnel in a model block 24" x 24" x 8" would satisfactorily meet the requirements (Fig. 10).

As a matter of convenience, and since body forces are being neglected the model would be tested on its side, that is, with the 24" x 24" faces horizontal. This would greatly simplify the design of the loading apparatus. However, this testing position might disturb the tunnel behavior once failure has been initiated. In the prototype, gravity body forces acting on the rock around the tunnel will often cause rock to fall from the crown after failure has been initiated by the free field stress concentrations around the tunnel. This behavior would not be duplicated when the model is tested lying on its side. Observation of the model behavior will be a means of evaluating the significance of this discrepancy.

As discussed previously, the lateral loading boundary condition would be uniform lateral pressures on the sides of the model, that is, a uniform distribution of the σ_v and σ_h pressures (Fig. 2). This would simulate a uniform distribution of the vertical and horizontal free field stresses some distance from the tunnel.

If the model is to represent a segment of a long tunnel, the boundary condition in the longitudinal direction, parallel to the tunnel axis, would be that of plane strain, with no deformation in the σ_ℓ direction (Fig. 10). In order to duplicate this plane strain condition in the laboratory it would be necessary to place some sort of restraint against the 24" x 24" faces of the model, such as:

1. Uniform pressures against the two faces, controlled during the test to null any longitudinal expansion which tends to develop as the lateral loads are applied, or

2. Rigid heads against the two faces, tied together across the model to prevent longitudinal expansion, or
3. A combination of the first two concepts, consisting of rigid heads placed against the faces of the model, with a controlled load applied to the two heads to null any longitudinal expansion which tends to develop as the lateral loads are applied.

The only reasonable alternate laboratory loading condition would be a biaxial plane stress loading.

In the elastic case, for a given set of free field stresses σ_h and σ_v, the lateral stress distribution around the tunnel is independent of the longitudinal stress σ_ℓ. That is, stresses in the plane perpendicular to the tunnel axis are the same for both the plane strain and the plane stress conditions.

When the elastic range is exceeded and failure is initiated, both stresses and strains in the lateral directions would be influenced by the longitudinal stress. Failure, whether in the form of a shear fracture or plastic deformation, would in general be accompanied by dilation of the mass. If the plane strain condition is maintained, this volume increase must be expressed by inward movements of the tunnel walls and an increase of compressive stresses around the zones of dilating material. But if a plane stress condition exists, the volume increase may be relieved by expansion in the longitudinal direction, resulting in a significantly different distribution of stresses and strains.

Also, if a plane stress condition exists, with $\sigma_\ell = 0$ and both σ_h and σ_v being compression, then it would be expected that a shear fracture might develop in a plane which is perpendicular to the plane containing σ_ℓ and the highest compressive stress, either σ_v or σ_h, independent of the existence of

of the tunnel. This type of failure was observed by Muller and Pacher (1965) on similarly shaped blocks which were loaded in a plane stress condition.

Hence, it is imperative that a restraint be placed in the longitudinal direction and that a condition of plane strain be maintained or approximated in the model in some manner such as the three listed above.

In summary, the boundary conditions for the model are that it be loaded under plane strain conditions, with no longitudinal deformation and with a uniform distribution of applied lateral pressures.

III. Development of Geomechanical Modeling Techniques

Because one of the major objectives of this study is to develop basic techniques of geomechanical modeling which may be of use to future investigators, the failures as well as the successes of the study will be presented in some detail. An attempt will be made to present the reasoning which led to the development of the different techniques and to present alternate solutions to the different problems which were considered but rejected for one reason or another.

A. Modeling Materials

1. Introduction and Plaster of Paris Chemistry

A literature study has indicated that the materials which have been used most widely and with the most success for modeling rock have been a mortar or matrix material such as Portland cement or plaster of Paris with or without an aggregate or filler such as a diatomaceous earth, sand, kaolinite, pumice, or a number of heavy minerals such as galena and barite. The most commonly used material has probably been a mixture of water, plaster of Paris, and diatomaceous earth. This material is quite easily mixed, molded, cured, and cut or shaped when dry. Data from the literature (Barron and Larocque, 1962; Raphael, 1960; Rocha and Serafim, 1955) show that the unconfined compressive strength and modulus of elasticity of this material can be varied over a wide range by varying the water/plaster ratio of the mix. Diatomaceous earth is added as an inert filler to the mixtures of high water/plaster ratio to reduce bleeding problems and segregation of the water and plaster during mixing and molding. These materials model the behavior of rock quite well in uniaxial compression with the exceptions of having a somewhat high E/q_u ratio of 500 to 800, and high tensile strengths of 15% to 30% of the

unconfined compression strength. No data were found in the literature on the behavior of these materials in triaxial compression. Some data was available on the behavior in direct shear of plaster-kaolinite and plaster-sand mixtures (Patton, 1966). The direct shear properties of these two materials were almost identical, but the plaster-kaolinite material had better unconfined compression and tensile strength properties than both the plaster-sand mixtures and plaster-diatomaceous earth mixtures. Hence, material studies were begun with plaster-kaolinite mixtures.

The plaster used was U.S. Gypsum Red Top No. 1 white molding plaster, which the manufacturer describes as being 97% to 98% calcium sulfate hemihydrate, $CaSo_4 \cdot 1/2\ H_2O$, commonly known as plaster of Paris. This material is manufactured by calcinating gypsum (calcium sulfate dihydrate) according to the equation:

$$CaSo_4 \cdot 2H_2O \xrightarrow[\Delta]{} CaSo_4 \cdot 1/2\ H_2O + 3/2\ H_2O \qquad \text{(Eq. 14)}$$

$$\text{Gypsum + heat} \rightarrow \text{Plaster of Paris + Water}$$

When the plaster is mixed with water the reaction is reversed and the hemihydrate dissolves and recrystallizes as the dihydrate, forming an inter-knitted network of monoclinic gypsum crystals which give the mass its strength (see Raphael, 1960; Eckel, 1922; Ladoo and Myers, 1951; and White, 1926, for more detail).

Very little water is needed to convert the hemihydrate to the dihydrate, the weight of water required being only 18.6% of the weight of the plaster. A greater amount of water is needed, even for a pure water-plaster mixture, to produce a mix that is fluid enough to be poured. This excess, free water serves as a medium in which the hemihydrate solution and dihydrate crystallization occurs, and may easily be lost by evaporation in air at

standard room atmospheric conditions. The loss may be speeded by oven drying if desired. The hemihydrate, plaster of Paris, is produced from gypsum commercially by heating the gypsum to temperatures in the range of 300° F. It is frequently stated in texts that the dehydration occurs at temperatures above about 212° F, the boiling point of water. It was found that water content determinations as usually performed on soils, heating samples of 20 to 40 grams at about 225° F for 24 hours, completely converted the dihydrate back to the hemihydrate. This is the procedure which was adopted for water content determinations for this study. Hence, the reported water contents are based upon the combined oven dry weights of the hemihydrate and the inert filler, kaolinite in this initial case, and the water considered includes both the chemically unbound free water in the pores of the model material and the chemically bound water of hydration which combines with the hemihydrate to form the dihydrate.

The setting and hardening of plaster of Paris is a very rapid reaction. A water/plaster/kaolinite mixture of 2/1/2 becomes solid enough within 11 or 12 minutes to support the Gillmore needle used to define the initial set of concrete mortar. This rapid reaction rate does not allow enough time for large volumes or a number of cylinders to be mixed and cast before the mixture sets. Various chemicals can be added to slow down the process of hemihydrate solution and dihydrate crystallization. Anhydrous dibasic sodium phosphate, Na_2HPO_4, was used as a retarder. Figure 11 shows the effect of adding small amounts of this retarder as a powder to the dry mixture of plaster and kaolinite before they were added to water. It was decided to use 0.5% of this retarder giving a setting time of about 60 minutes, which was adequate for mixing and casting large batches.

2. Plaster of Paris/Kaolinite Curing Characteristics

A modeling material with a low unconfined strength is necessary for economy of design of the model testing and loading apparatus. A water/plaster ratio of 2/1 was chosen to give this low strength. Data in the literature indicated that an unconfined strength of 200 psi to 500 psi could be expected from this water/plaster ratio. The kaolinite used was Kaolin NF, 400 clay, code 5643, obtained from the Mallinckrodt Chemical Works, St. Louis, Mo. Initial tests indicated that a water/plaster/kaolinite mixture of 2/1/2 gave a quite workable mix which was easily mixed and poured, although it exhibited considerable shrinkage during drying. A number of cylinders were tested in unconfined compression after being subjected to several different curing procedures in an attempt to study the different variables of significance in curing the material.

A parameter which proved useful in this study was called the weight ratio, WR, which is defined as $WR = \frac{1 + w}{1 + w_i}$, where w_i is the initial water content at the time of mixing, and w is the water content at any particular time. The weight ratio WR at any time is also equal to the weight of the material at the given time divided by the initial wet weight immediately after casting. For the mix used, considering the water content of the air dried plaster and kaolinite, the initial water content w_i was 70.0%, hence, the relationship between WR and w is $WR = 0.589\ (1 + w)$. It was found that almost all the free water was removed from the material at an air dry equilibrium water content w of about 8 1/2 %, which corresponds to a weight ratio WR of about 63.9%. If a specimen is at a water content or weight ratio above these values it contains excess free water in the pores of the material, but if it is below these values, part of the water adsorbed by the kaolin has been removed and/or part of the

dihydrate, gypsum, has been dehydrated to the hemihydrate, plaster of Paris.

Figure 12 shows drying curves for cylinders cured in air in the ambient atmosphere of the laboratory. The rate at which the cylinders dried was controlled by varying their exposure. One group of cylinders were extruded from their molds at 2 days after casting and dried to an equilibrium water content by about 14 days after casting. A second group which was left in the mold until 8 1/2 days before being extruded reached equilibrium at about 20 days. A third group was left in open-end molds until dry, and reached equilibrium in about 32 days. All groups reached essentially the same equilibrium water content of 8 1/2% to 9%, corresponding to a weight ratio of about 64%.

Drying curves for cylinders in ovens at different temperatures are shown in Figure 13. Specimens dried at 225° F dropped within 1 1/2 days to a weight ratio of 59%, then lost no more water, indicating a loss of all free water and removal of enough water of hydration to convert the dihydrate to hemihydrate, i.e., they dropped to 0 water content. Specimens dried at 115° F dropped within 2 days to a weight ratio of 64 1/2%, then lost no more, indicating evaporation of all the free water but no loss of water of hydration. Specimens dried at 145° F and 170° F lost water rapidly for 1 to 2 days, then continued to lose water at slower rates, the specimens at lower temperatures losing water less rapidly. The rapid initial loss represents removal of the free, chemically unbound water, while the subsequent slower loss represents removal of the chemically bound water of hydration, slowly transforming the dihydrate into the hemihydrate. It will be noted that this loss occurs at temperatures well below that often given in texts as the temperatures at which the dihydrate is converted

into the hemihydrate and that, as would be expected, the rate of this loss increases with the temperature.

The drying behavior of larger blocks is shown in Figure 14. As would be expected, the behavior of these larger blocks is the same as that of the smaller cylinders except a longer time is required to dry the larger volumes. A block 8" x 24" x 24" such as suggested for the model could not be expected to air dry more rapidly than the 5" long cylinders in molds with both ends open. Thus, a drying time of 1 1/2 to 2 months might be expected for the model blocks if they are air dried. All of the free water is removed from the oven dried block after 5 or 6 days in the oven, after which dehydration of the gypsum proceeds slowly. This suggests that the free water in an 8" x 24" x 24" block for the model could be removed in a maximum of 8 to 10 days after casting the blocks. The problem of possible water content variations across the larger blocks was investigated by coring the blocks a number of times during drying and determining water contents of the cored samples. The water content profiles of the 7" x 10" by 11" block while oven drying is shown in Figure 15. It is seen that water contents are remarkably uniform across the block, particularly when all the free water is removed after 5 or 6 days in the oven, at water contents of 8% or 9%.

Data shown in Figure 16 for oven dried cylinders indicates that they absorb very little water from the atmosphere after being removed from the oven. Specimens dried to a water content of 0% increase in weight by a maximum of 1% to 1 1/2%, indicating only partial rehydration of the dissociated dihydrate, while specimens oven dried to a water content of 8% to 9% (the air dry equilibrium water content, no free water) showed no change when taken from the oven.

In summary, it was found that the most stable condition for the water/plaster/kaolinite mixture of 2/1/2 is at a water content of around 8% to 9%, at which nearly all of the free water has been removed from the material. This condition may be achieved either by air drying or by oven drying at temperatures of 115° F or lower. Oven drying at higher temperatures result in some dissociation of the dihydrate unless the specimen is weighed frequently and removed from the oven when the weight ratio reaches 64%. At higher water contents or weight ratios the material loses water to the atmosphere readily and its properties change considerably within a few days time. Specimens of the plaster-kaolinite mixture can be extruded from their molds within 2 days after casting and oven dried within an additional 3 to 10 days, depending upon the size of the specimen.

A study was also made of the cylinders cured by the different methods to observe the influence of both curing time and water content upon the strength and stress-strain characteristics of the plaster-kaolinite mixture. The specimens were cast in 2 1/4" diameter by 6" long plastic cylinders which had one end plugged by a rubber stopper. After extrusion and drying the cylinders were cut to lengths of about 4" before testing. The curing time and weight ratios at which air dried cylinders were tested in unconfined compression are shown in Figure 12. The drying curves for different methods of oven drying specimens are shown in Figure 16. The variation of unconfined compression strength with curing time is shown in Figure 17. It can be seen that there is essentially no direct correlation and that at any particular time, specimens can exhibit a wide range of strengths depending upon their water content. Dashed lines in the figure roughly represent the variation of strength with time if water content is held constant. These suggest a small increase of strength with time in the range of 8 to 24 days.

Figure 18 shows a well defined relationship between the unconfined compressive strength and water content, independent of curing time. From these two figures (17 and 18) it can be seen that the critical factor influencing the strength of the plaster-kaolinite mixture is the water content of the sample, and that the behavior is nearly independent of the time required to reach that water content, over a range of curing times from 8 to 24 days. The influence of the water content may be due to 2 factors: 1) a mechanical effect in which the free pore water may develop significant positive pore pressures during shear, or 2) a chemical effect in which the excessive amount of free water may soften the inter-knitted network of gypsum crystals which gives the material its cohesive strength.

The only apparent major influence of curing time for air dried specimens seems to be either at short times and high water contents, or at longer curing times over 30 days. Specimens B-1b and B-1f which were tested 7 days after molding at water contents around 30% had strengths significantly lower than the general trend. Specimens A-4a and A4c which were tested at air dry equilibrium water contents at 42 days were significantly stronger than the general trend. It is hypothesized that these variations may represent changes in the inter-knitted network of gypsum crystals which develops as the dihydrate crystalizes from solution. At short times and high water contents the network may not have had a chance to develop fully, while a very strong network may have developed in the specimens which were allowed to dry very slowly. (White, 1926, discusses some observations of changes in gypsum crystal structure for different drying times.)

It is seen in Figure 18 that if cylinders are dried so far that dissociation of the dihydrate begins, the strength falls off rapidly. This is assumed to reflect the destruction of the gypsum crystal network.

Figure 19 shows the relationship between failure strain and water content. The minimum failure strain of around 0.5% is reached when all of the free water is removed, corresponding to the development of the maximum strength.

Typical unconfined compression stress-strain curves for typical specimens at various water contents are shown in Figure 20. It is seen that lowering the water content increases the specimen's initial tangent modulus of elasticity and causes a more brittle behavior. Specimens air dried or oven dried to remove all free water are the most satisfactory for modeling rock. They possess a relatively low compressive strength of 500 to 600 psi, fail at strains of about 0.5% to 0.6%, are linearly elastic up to about 50% of their ultimate strength after which they exhibit some non-linear deformation, and have a modulus/strength ratio of 250 to 350.

The variations in the behavior of the water/plaster/kaolinite mixture of 2/1/2 in unconfined compression with changing water content and curing procedure agrees well with the behavior of plaster-sand mixtures as determined by Hobbs (1966) and of plaster-diatomaceous earth mixtures as determined by Raphael (1960). It appears then, that these variations are due entirely to the plaster-gypsum matrix material and are not significantly influenced by the type of inert filler material being used. Hence, in all subsequent work with plaster of Paris mixtures, the material has been oven dried at 110° F until all the free water is removed. This is done to develop the most satisfactory material behavior and also because if not fully dry, the physical properties will change considerably over a few days time due to water evaporation.

3. Triaxial Strength Properties of Various Plaster Mixtures

Both triaxial and unconfined compression test specimens were cast extra long and cut to length on a 8" diameter rock saw running at 20,000 rpm. The test specimens were approximately 2" in diameter and 4" long.

Unconfined compression tests were run in a small hydraulic loading frame in which axial load is measured by an electrical load cell. Axial deformation was determined by three mechanical dial gages 120° apart measuring the relative movement between the loading platens.

Tensile strengths were determined by Reichmuth point load tension tests.

Triaxial tests were run with conventional equipment. Test specimens were encased in membranes cut from a bicycle inner tube, and confining pressures were applied by hydraulic oil. Axial loads were applied and registered by a 60,000 lb Reihle test machine. Axial strain of the cylinders was determined by a 0.0001" mechanical dial gage measuring the relative movement between the triaxial cell base and the axial loading piston.

The Reichmuth point load tension tests on the plaster-kaolinite material showed the tensile strength to be about 11% of the unconfined compression strength. A complete Mohr envelope determined by triaxial compression and point load tensile tests is shown in Figure 21. The plaster-kaolinite mixture has a quite low angle of internal friction, which is about 17° at normal stresses of 300 psi and around 5° at normal stresses of 900 psi. The material behaves very ductilely in triaxial compression, going to strains of 1%, 3%, and 10% at confining pressures of 125, 250, and 500 psi. It is seen, then, that the water/plaster/kaolinite mixture of 2/1/2 is quite satisfactory for modeling rock in uniaxial stress states, but has an angle of internal friction

lower than is acceptable for modeling rock behavior under triaxial stress conditions.

Since diatomaceous earth-plaster of Paris mixtures are used so extensively in modeling work, a mixture of these materials was tried. The diatomaceous earth used was Hyflo Supercell, processed by Johns Manville Co. A water/plaster/diatomaceous earth mixture of 2/1/0.7 proved satisfactory in unconfined compression, but was very unsatisfactory in triaxial compression, showing a decrease in strength at confining pressures greater than about 1/2 its unconfined strength due to a collapse of the structure of the material under the influence of the confining pressure alone (Fig. 22). This behavior is attributed to the very porous, low density structure of the material (unit weight = 44 pcf), which resulted from the low bulk density of the diatomaceous earth.

Various sand mixtures were tried next. A mixture of water/plaster/kaolinite/sand of 2/1.6/1/7 exhibited an acceptable behavior in unconfined compression but showed essentially a $\phi=0$ condition in triaxial compression (Fig. 23). The Mohr-Coulomb envelope of the previously studied water/plaster/kaolinite mixture of 2/1/2 also appeared to be approaching a horizontal asymptote. This suggests a maximum shear stress, $\phi=0$, failure criteria for the gypsum matrix and/or kaolinite.

Recent studies (Polacek, 1967) on a pure plaster of Paris material substantiate the hypothesis of a $\phi=0$ behavior in the gypsum matrix. Cylinders of a water/plaster mixture of 1.2/1.0 were tested in unconfined and triaxial compression. The material exhibited significant bleeding and shrinkage during casting and curing, and had a density of 62 pcf. Water content determinations on this material indicated an average value of 18.8% for 5 cylinders, in good

agreement with the value of 18.6% predicted from the chemical equation (Eq. 15) for the plaster → gypsum reaction. The Mohr-Coulomb envelope for these cylinders is shown in Fig. 24. The ϕ=0 behavior is presumably due to intra-crystalline gliding in the gypsum, which is not surprising considering the behavior of other evaporite rocks such as rock salt and potash.

Further testing was confined to plaster/sand mixtures. Using the fine Wabash sand, Fig. 25, a water/plaster/sand mixture of 1.85/1/8.15 exhibited an unconfined strength of 400 psi and an angle of internal friction of approximaterly 22° at confining pressures up to 500 psi, but troubles were encountered in the crushing of cylinders under the confining pressures of 1000 psi alone, without any increased axial load, similar to the behavior of the plaster-diatomaceous earth mixture. Accompanying this crushing was a densification of the material, hence, a significantly higher strength was developed at σ_3 = 1000 psi and the Mohr envelope for this material turned upward (Fig. 26).

Increasing the unconfined compression strength to about 1000 psi by decreasing the water/plaster ratio to 1.0, and adding as much sand as possible while maintaining fluidity gave water/plaster/sand mixtures of 1/1/3.7. This material could take confining pressures of 1000 psi but exhibited nearly a ϕ=0 behavior, presumably due to plastic flow in the gypsum matrix. A sample taken from the triaxial cell after about 5% strain at a constant axial load showed no visible signs of failure, except for axial shortening and diametrical extension, and had a strength of about 220 psi when subsequently tested unconfined.

It was decided that water/plaster/sand mixtures fluid enough to be poured into molds will not give satisfactory modeling materials. After such materials are cured and dried, the removal of mix water in excess of that required for chemical reaction with the plaster results in a very porous

structure. Porosities calculated for the various mixes tested range from 30% to 35%. This porous structure, at unconfined compression strengths of 400 psi, is not capable of supporting a hydrostatic loading of 1000 psi. This behavior is inacceptable since model loadings to 1000 psi would crush the whole model. However, if the material is strengthened by increasing the plaster content, so that a hydrostatic loading of 1000 psi can be supported, the internal friction drops, presumably due to plastic deformation in the gypsum matrix. Even at low stress levels the crushable materials with the higher sand contents do not exhibit a sufficiently high angle of internal friction for modeling rock, the highest achieved being 22° before crushing. The sand grains in these materials have been at void ratios of 0.76 to 0.88 (calculated including the volume of the gypsum matrix as part of the volume of voids), which is a "relative density" of around zero for the sand. Thus the low friction angles are not surprising.

The results of these studies suggest that previous investigators (excluding from consideration the various model studies of creep behavior) using geomechanical models to study the behavior of underground openings have failed to adequately satisfy one of the most critical requirements of similitude. One of the most distinguishing characteristics of most geologic materials is their frictional strength. A failure to model this characteristic would make the results of any geomechanical model subject to serious question. The modeling laws derived from dimensional analysis, as discussed previously, require that the angle of internal friction of the modeling material be the same as that of the prototype material, i.e., in the range of 25° to 60°. Yet almost without exception previous investigators have failed to report the triaxial compressive strength properties of their modeling materials. Moreover, the data reported herein on materials quite similar to those used by most of the previous

investigators has shown these materials to be very unsatisfactory for modeling rock behavior in triaxial stress states such as exist around underground openings. The only experimental studies which have come to the attention of the authors in which the internal friction properties of model materials have been considered is the work of ISMES in Bergamo, Italy on geomechanical model using pumice stone mortars (Fumagalli, 1959, 1960, and 1964). In general, their materials appear to have rather low angles of internal friction ranging from 20° to 25°.

Hence, significantly more study was required to develop acceptable modeling materials. Studies by Horn and Deere (1962) indicate that the friction angle between dry polished mineral surfaces is rather low, ranging from 14° to 20° for layer-lattice minerals such as muscovite and biotite and 6° to 9° for space lattice minerals such as quartz, calcite, and microcline. Studies by Patton (1966) indicate that the friction angle along dry polished rock surfaces is also low, ranging mostly from 10° to 20° for carbonate rocks up to 22° to 24° for sandstone. These values from Patton (1966) are the initial friction angles which developed before the surfaces were gouged and roughened during shear. It is hypothesized, therefore, that any portion of the angle of internal friction of rock materials in excess of these values reported for polished mineral and rock surfaces must come from dilation of the rock material during shear. This dilation during shearing deformation is pictured as being a "moving apart" or loosening of the very dense packing of the mineral grains of which the rock is composed.

It was hypothesized that the duplication of high angles of internal friction in a model material would similarly require the manufacture of a material with a very dense packing of mineral grains, such as sand grains. The material would require a weak cementing matrix to give a low cohesion and a low

unconfined compression strength. It was decided to use plaster of Paris as the matrix material because of its rapid curing properties, which were well known.

4. Compaction of Plaster of Paris/Sand Mixtures

Using the fine Wabash sand, a number of different techniques for producing dense sand/plaster mixtures were tried, including:

1) dry plaster/sand mixtures vibrated into molds, then saturated,
2) moist water/plaster/sand mixtures placed by
   a) vibration under static load - applying an axial load to the material with a hand press while vibrating the mold with a concrete vibrator,
   b) static compaction - placing the material in the molds in 1" thick lifts, each lift being subjected to a static load of 500 psi,
   c) impact compaction - compacting in thin layers with a dropping weight.

The highest densities were achieved by the impact compaction. Samples were compacted in 2" diameter x 4" long molds with a Vicksburg tamper, a 4 lb. weight dropping 12 inches.

Dry mixtures of plaster of Paris and fine Wabash sand at a ratio of 1/8 were compacted first. As seen in Fig. 27, the maximum density was achieved by compacting in 1/2" layers at 25 blows per layer. Compaction in layers of less than 1/2" thickness was considered to be impractical. The average density of the material in the mold was increased by compacting an extra thickness of material in an extension above the top of the mold, then trimming off the upper

material (Fig. 28). The compaction procedure adopted for the 2" x 4" molds was to compact in 1/2" layers at 25 blows per layer with the Vicksburg tamper, and to compact an extra inch of material in an extension of the mold, then trim off the excess length. This procedure gives a compaction energy of 64 ft lbs/in^3.

Tests were run to determine the optimum water content for compaction of the plaster/sand mixtures. The moisture-density curves for the plaster of Paris/fine Wabash sand mixture of 1/8 are shown in Fig. 29. It is seen that for the compaction procedures and equipment used, the highest density of the cured material is achieved when a water/plaster/sand mixture of 0.9/1.0/8.0 is used. In order to retard the set of the plaster, an amount of $Na_2 HPO_4$ equal to 1% of the weight of plaster was used, giving a total mix of water/plaster of Paris/fine Wabash sand/Na_2HPO_4 in the proportions 0.9/1.0/8.0/0.01. This percentage of Na_2HPO_4 retarder was added to all subsequent compacted plaster/sand mixtures.

Similar tests were run with the fine Sangamon sand (Fig. 25) at a plaster/sand ratio of 1/9. The results are shown in Fig. 30. It is seen that within the range of mix water contents considered, the density of the cured plaster/sand material increases continuously and does not reach a peak value at some intermediate mix water ratio. Above a mix water content of about 13% water flows from the material during the hammer impact. Because this results in sample inhomogeneity, a mix water content of 12% was chosen as optimum, giving a water/plaster of Paris/fine Sangamon sand/Na_2HPO_4 mix in the proportions of 1.2/1.0/9.0/0.01. This mixture and the one selected for the fine Wabash sand, above, is essentially a damp, bulking sand and has no fluidity.

Unconfined and triaxial compression test specimens of the plaster of Paris and fine Wabash and fine Sangamon mixtures were compacted by the procedures and in the proportions described above. Larger volume specimens of the fine

Sangamon sand mixture were compacted to see if the same densities and material behavior could be produced as in the small cylinders. The 1.2/1.0/9.0/0.01 mixture was compacted into a 3" x 4" x 8" mold with a 4" square foot on the Marshall hammer (a 10 lb. weight dropping 18") at 3 different compaction energies. The results, Fig. 31, show that for the same compaction energy, the same density can be achieved in the larger mold as in the small cylinders. Specimens of NX diameter cored from these blocks showed essentially the same strength and deformation properties as specimens of comparable density compacted in the 2" diameter cylinders.

It was estimated that a minimum of 10 to 12 hours would be required to compact a 24" x 24" x 8" model block by hand with the Marshall hammer, hence, a more rapid compaction method was needed. A pneumatic chipping hammer equipped with a 4" square tamping foot produced the same densities in the 3" x 4" x 8" mold as were achieved by hand compaction with the Marshall hammer. It is not easy to vary at will the density of blocks compacted in this manner, however, because of the difficulty of controlling the compaction energy.

With an 8" square foot on the pneumatic hammer, operating at an air pressure of 100 psi, an average density of 1.82 gm/cc has been achieved in a block 24" x 24" x 3". The density of seventeen cylinders of NX diameter and 4" length cored from the block had a coefficient of variation of 1.2%, indicating that this procedure can yield a block of a relatively uniform density. It is planned that this method will be used to prepare the models blocks 24" x 24" x 8".

5. Triaxial Strength Properties of Compacted Plaster/Sand Mixture

A summary of strengths exhibited by compacted plaster/fine Wabash sand mixtures of 1/8 is shown in Figs. 32 through 37. It is seen in Fig. 32 that the angle of internal friction is linearly related to the void ratio of

the sand (computed considering the gypsum matrix as a part of the void volume). The sand used is essentially a fine grained fraction of the Wabash Sand used by Hendron (1963). The points in Fig. 33 show that the relationship between ϕ and e_s determined for the fine Wabash sand in sand/plaster mixtures is a direct extrapolation of the relationship determined by Hendron for the coarser, more well-graded sand which he used. The data seem to substantiate the hypothesis that the internal friction of such materials is entirely determined by the sand grain structure, and that the gypsum plaster matrix exhibits plastic yield at low shear stress levels and does not contribute significantly to the internal friction of the material. The Mohr envelopes determined for these plaster of Paris/fine Wabash sand materials up to confining pressures of 1000 psi actually generally exhibit a slight curvature, but for simplicity the inclination of the average straight line has been given here as the angle of internal friction of the material.

It was found that as the compacted density of the 1/8 mixture of plaster/sand increased, the unconfined compression strength increased markedly (Fig. 34). The unconfined compression strength, q_u, of a material whose strength is determined by the Coulomb-Navier failure criterion is a function of both the angle of internal friction ϕ, and the cohesion intercept c, of the Mohr diagram. The previous discussion of internal friction showed that part of the increase of q_u is due to the increase of ϕ with density (lower e_s). It was also found that the cohesion intercept of the material increased as the density increased, as shown in Fig. 35. It is hypothesized that the cohesion intercept is determined by the gypsum matrix, and that an increase in the matrix density produces a higher cohesion. This relationship is shown in Fig. 36. The one deviation from these generalizations concerning q_u and c is batch S18 which was vibrated into

the mold dry, then saturated. The deviation may be related to the poor control of the material resulting from this method of preparation.

Previous investigators using gypsum plaster for modeling materials have generally stated or suggested that the unconfined compression strength of the plaster materials could be controlled at will by varying the water/plaster ratio of the mix. It is generally stated that increasing the water/plaster ratio decreases the strength. The data in Fig. 37 shows that this is not a complete valid generalization. In fact, although batch S22 had a slightly higher mix water content than batches S19 to S21, its unconfined strength was higher rather than lower. Batch S4 had twice as much mix water as S19, but nearly the same unconfined strength. A similar relationship exists for the cohesion intercept of the material. In keeping with the previous discussion, it is hypothesized that the significant variable influencing the cohesion is the density of the gypsum matrix, and that it is independent of the mix water used. The mix water in excess of the amount required for chemical combination with the plaster simply occupies volume during the initial setting and hardening, serving as a medium for the plaster solution and gypsum crystallization, then evaporates when the specimen is dried. This produces a porous structure and a low bulk matrix density, resulting in a low cohesion. Batch S4 is an example of such a situation. The same strength and the same bulk matrix density were produced in batch S19 at a lower mix water content because the mix of S19 was a bulking material cast with a significant volume of minute air voids. On the other hand, batch S22, with a slightly higher mix water content than S19, was compacted to a greater density with less air voids. This gave a greater bulk matrix density and a higher strength, in spite of the higher mix water content.

Additional testing was conducted on a somewhat more angular sand, the subangular fine Sangamon sand whose gradation is essentially identical to that of the fine Wabash sand. A summary of strength data obtained to date for the two different sands is shown in Figs. 38 and 39. Fig. 38 suggests that the internal friction is primarily determined by the relative density of the sand grains and is not increased by the slightly increased angularity of the fine Sangamon sand. Fig. 39 indicates the cohesion intercept is determined by the matrix density alone, and, over the range of variables studied, is independent of internal friction, mix water content, and the angularity of the sand. All data obtained so far with these material has indicated that the two strength parameters, cohesion and internal friction, can be controlled independently by independently varying the gypsum matrix density and the density of the sand grain structure. This control would be restricted by the practical problems associated with compacting and molding different mixtures of water, plaster, and sand. For example, it might be possible to hold ϕ constant by producing a material with a given sand void ratio, and vary c by varying the sand/plaster ratio, hence the gypsum matrix density. The range of c which might be achieved would be restricted, however, by the relative volumes of the two mix components, the compaction characteristics of the different mixtures, and the resulting capability of compacting the sand to the same void ratio for the different mixtures.

The material which has been tentatively selected for construction of the models is a water/plaster/sand mixture of 1.2/1/9, using the fine Sangamon sand. Fig. 40 shows the Mohr envelope and Fig. 41 shows the stress-strain curves for cylinders of this mix tested at 6 different confining pressures. The cylinders tested were from two separate batches of 5 cylinders each, molded several days apart and cured independently. The average densities for the

two batches were 1.875 gm/cc and 1.870 gm/cc. The average of the 10 cylinders was 1.873 gm/cc, the range was 1.860 to 1.888, and the coefficient of variation was 0.4%. Thus, the material is reproducible. The Mohr envelope and the stress-strain curves also indicate a reproducible material with the exception of an apparently stronger cylinder tested at σ_3 = 500 psi. This cylinder was the densest, at 1.888 gm/cc, of those tested.

The suitability of this material for modeling rock in triaxial stress states is shown by Figs. 42 and 43. Fig. 42 is a dimensionless plot comparing the triaxial compression strength of the selected model material and a number of different rocks. Fig. 43 is a similar dimensionless plot comparing failure strains for the different materials. The data for the different rocks were obtained from the published reports indicated. The data from Handin and Hager (1947) were selected as illustrating typical average behavior for the 23 sedimentary rocks which they studied. The data shown include sandstones, shales, limestone, dolomite, and anhydrite. Other data in Figs. 42 and 43 are for a granite, a quartz monzonite, and a schistose gneiss in the igneous and metamorphic rocks. The shape of the stress-strain curves in Fig. 41 is quite similar to many rocks, as substantiated in the references cited.

In summary, it is seen that modeling materials with strength and deformation characteristics satisfactory for modeling the behavior of rock materials can be produced from compacted moist mixtures of plaster of Paris and sand. More detailed stress-strain data as measured by electrical resistance gages will be given in the section on instrumentation.

B. Model Loading Apparatus

1. Estimated Model Behavior

a. Required Loading Capability. In order to design a loading apparatus and later the instrumentation system, it is necessary to have some estimate of the model behavior. First consider a model of a tunnel in an intact rock mass. Failure may be expected to be initiated when the tangential stress at the edge of the opening equals q_u, the unconfined compression strength of the rock. The extreme values of stress concentration factors about an opening, for the elastic solution of a plane strain or plane stress condition about a circular opening, occur at the crown and invert and at the spring line of the opening, assuming that σ_v and σ_h are the major and minor principal stresses. The magnitude of the stress concentration factor, SCF = σ_θ/σ_v, where σ_θ is the tangential stress at the edge of the opening, at both the spring line and the crown and invert is given in Fig. 44 for an elastic material for different values of σ_h/σ_v. Consideration of this figure indicates that a minimum stress concentration factor of 2.0 in compression is available for initiating failure around the opening. This means that for all possible loadings a minimum "free field stress" of 300 psi would be required to initiate compression failure in the model material with $q_u \simeq 600$ psi.

Since the initiation of compression failure at the wall of the opening will not necessarily mean failure of the whole mass, but merely a yielding of the material adjacent to the wall and a redistribution of load back away from the opening, the loading apparatus should probably have a loading capacity of perhaps three times the magnitude required to initiate failure. As an estimate, then, the loading required might be a 1000 psi capability for σ_h and σ_v. Since this acts over a 24" x 8" face, a total reaction capability of about 192,000 lbs is desirable for the lateral reactions.

For a plane strain condition, the maximum capability for the longitudinal stress σ_ℓ in the elastic case is the requirement that $\sigma_\ell = \nu(\sigma_v + \sigma_h)$. A value of $\sigma_\ell = 0.25\ (1000 + 1000) = 500$ psi is the maximum that should be required, assuming that ν of the model material would not exceed 0.25. This requires a reaction capability of 288,000 lbs on the longitudinal 24" x 24" faces.

b. Blocks Without Tunnels. Consider a solid, elastic block loaded polyaxially in plane strain with the 3 principle stresses σ_v, $\sigma_h = N\sigma_v$, and $\sigma_\ell = \nu\ (\sigma_v + \sigma_h) = \nu\sigma_v\ (1 + N)$ on the faces. Assuming $0 < N < 1$, the major principal stress, σ_1, will be σ_v, but the minor principal stress σ_3 may be either σ_h or σ_ℓ depending upon the magnitudes of N and ν. The longitudinal stress σ_ℓ will be the minor principal stress, $\sigma_\ell < \sigma_h$, i.e. $\nu\sigma_v\ (1 + N) < N\sigma_v$, when $\nu < N/(1 + N)$. The range of values of N and ν for which $\sigma_h = \sigma_3$ and for which $\sigma_\ell = \sigma_3$ are shown in Fig. 45.

If a solid model block is loaded at N values of 1/3, 2/3, and 1; if the relationship shown in Fig. 45 is valid; if the strength of the model material can be approximated by the relationship in Fig. 40; and if the material has a Poisson's ratio of 0.25; then the relationship of the stress paths during loading to the failure envelope is as shown in Fig. 46. It is seen that for plane strain loading there is no chance for a failure of the solid block.

If the model block is jointed, there is a possibility for a failure of the whole mass. Fig. 47 shows this, assuming a friction angle as low as 20° along the joint planes. If a joint were critically oriented with respect to the applied stresses, failure could occur for loadings of N = 1/3 or 2/3, but not for N = 1 unless a tunnel were present to initiate failure. The critical orientation of the joints which are the potential failure surfaces is at an angle of $(45° + \phi_j/2)$ to the tunnel axis. As discussed previously, only joints

either parallel or perpendicular to the tunnel axis will be considered for the initial model tests, hence, this failure mode is of no practical significance.

Another failure mode which should be considered is movement along joints parallel to the tunnel axis, at an angle of $45° + \phi_j/2$ to the direction of σ_h. In this case, the significant stresses are those in a plane perpendicular to the tunnel axis, σ_v and σ_h, which are the major and intermediate principal stresses, σ_1 and σ_2. The relationship between the failure envelopes and the loading curves for these stresses is shown in Fig. 48. It is seen that failure can occur for critically oriented joints at a lateral stress ratio of N = 1/3, but not for N > 1/2 regardless of the joint orientation.

A consideration of Figs. 46, 47 and 48 shows that the initiation of failure would coincide with the first application of load since the stress loading paths are always above the failure envelopes for the critically oriented surfaces. The assumption of a Poisson's ratio of 0.25 has been made for these calculations. As can be seen in Fig. 45, lower values of Poisson's ratio simply mean that σ_3 will be σ_ℓ for all loadings (except for very small N); and because ν is smaller, $\sigma_3 = \sigma_\ell$ will be smaller. The conclusions drawn from Fig. 48 would not be influenced because σ_h and σ_v are not influenced by ν. The possibility of failure along joint surfaces inclined at an acute angle to the tunnel axis (Fig. 47) would be increased, but this is of no significance because these joints are not being modeled. The loading curves of Fig. 46 would be steeper if $\nu < 0.25$, hence failure of an intact model could occur if it is loaded to very high stress levels where the steep loading curves might intersect the flatter failure envelope of the intact material. This would not occur for the planned stress levels (up to σ_v = 1000 psi), though, except for extreme values of N and ν.

In summary, it is seen that for the material properties and loadings being considered, a general failure of the model block could occur only if a joint set parallel to the tunnel axis were inclined at angles of $45° + \phi_j/2$ or more to the direction of σ_h. Hence, the loading apparatus will not have to be designed to accommodate large, irregular deformations which might be associated with a general failure of the model block, but rather, only movements of the same order of magnitude as the elastic deformations which can be expected.

A study of Fig. 41 shows that the elastic modulus of the model material can range between 100,000 and 200,000 psi. Using a value of 200,000 psi and an assumed Poisson's ratio of 0.25, the elastic deformation of a 24" x 24" x 8" block predicted by elastic equations of the form

$$\varepsilon_v = \frac{\sigma_v}{E} - \frac{\nu}{E}(\sigma_H + \sigma_\ell)$$

$$\varepsilon_H = \frac{\sigma_H}{E} - \frac{\nu}{E}(\sigma_v + \sigma_\ell) \qquad \text{(Eq. 15)}$$

$$\varepsilon_\ell = \frac{\sigma_\ell}{E} - \frac{\nu}{E}(\sigma_v + \sigma_H)$$

are as given in Table 4 for both plane strain and plane stress conditions at the maximum anticipated loading. These values show that a maximum movement of the lateral faces of 0.05" for a modulus of 200,000 psi and an upper limit of 0.1" for a lower modulus can be expected in plane strain conditions. The loading apparatus, then, should be designed to accommodate perhaps 0.5" of movement of each lateral face. The figures for plane stress deformations indicate a maximum longitudinal movement of each 24" x 24" face up to 0.01" could be expected, for a total thickness increase of 0.02" for the model block. If a plane strain condition is to be approximated in the model the total longitudinal expansion of the model must be restricted to the order of 0.0001" to 0.0005".

Table 4. Estimated elastic deformations of each face of model block, assuming E = 200,000 psi, $\nu = 0.25$, σ_v = 1000 psi (-) indicate extension

Plane Strain

	Δ_v	Δ_h	Δ_ℓ
N = 1	0.0375"	0.0375	0
N = 1/4	0.0516"	-0.0047"	0

Plane Stress

	Δ_v	Δ_h	Δ_ℓ
N = 1	0.0450"	0.0450"	-0.0100"
N = 1/4	0.0570"	0	-0.0062"

c. Tunnel Behavior. Calculations have been made for elastic deformations and for both elastic and plastic stress distributions using material properties of E = 100,000 psi, $\nu = 0.25$, $\phi = 35°$, and q_u = 400 psi; at applied free-field stresses of up to 1000 psi under N = 1, plane strain conditions; for a 4" diameter tunnel. Elastic deformations were calculated from Lame's thick walled cylinder equations (Seely and Smith, 1952; Obert and Duval, 1967). The deformations which would result are shown in Figures 49 and 50. Stress-distributions around the tunnel for both the elastic case and for an elastic-perfectly plastic Coulomb-Navier material have been calculated following assumptions such as given by Jeager (1962, pp. 186-192). The results are shown in Figs. 51 through 54. Fig. 51 shows the development of the plastic zone at the applied free field stress of 1000 psi, and how it differs from the elastic stress distribution. Fig. 52 shows how the plastic zone develops for increasing values

of applied free field stress. Figs. 53 and 54 show how the depth of the plastic zone varies with the strength of the material. The significance of these figures will be discussed later.

2. Lateral Loading Elements

The requirements of the lateral loading apparatus, as developed previously, are that it be able to apply a uniform pressure up to 1000 psi on the 24" x 8" faces of the model for a total reaction of 192,000 lbs, and that it be able to deform up to 0.5" as the model is loaded. Although large, irregular deformations of the faces are not anticipated, a nonuniform deformation must be expected for two reasons: (1) the presence of the tunnel and (2) restraining friction along the loading faces. Hence, the lateral loads must be applied by a flexible loading system which can adjust to the irregular model deformations, rather than by a rigid loading head.

For the methods considered for applying the lateral loads it was decided that the load should be actively applied to all four lateral sides, rather than actively loading the model on 2 adjacent sides and pushing it against a passive reaction on the opposing sides. Although this increased the complexity of the loading system, it was done to maintain loading symmetry in the model for two basic reasons: (1) so that the tunnel axis would remain stationary with respect to the loading frame, which could serve as a reference frame for measuring movement of the tunnel walls, and (2) so friction between the model and the longitudinal and lateral loading heads would be symmetrical about the tunnel.

a. Loading Methods Considered. Several methods for applying the lateral pressures were considered. The first was some sort of hydraulic "flat jack," such as those used in in-situ stress measurements in tunnel walls or similar to the Fressinet jacks used in plate jacking tests of rock

deformability. This system was rejected in anticipation of the problems associated with constructing such a jack which is rectangular in shape, operates to 1000 psi internal pressure, and will expand up to 0.5".

The second system considered is sketched in Fig. 55. It consists of an oil filled hydraulic cushion against the model, backed by channel iron stiffeners, and pushed against the model by hydraulic jacks. The hydraulic cushion would consist of a channel iron with a thin metal membrane between the flanges, the ends covered with steel plates, and filled with oil. An alternative to the thin membrane would be an oil filled rubber bag placed inside the open-faced rectangular box formed by the channel iron and its end plates. The hydraulic cushion serves only as a means of applying a uniform pressure to the model. The required 0.5" of movement would be supplied by hydraulic jacks pushing the loading head forward. As the hydraulic cushion is forced against the model the flexible metal membrane or rubber bag would transmit to the model the uniform pressure which exists in the oil within the cushion. By monitoring this pressure the load on the model would be known. A problem which is anticipated with a system of this sort would be the tendency for the membrane to develop a concave surface as the oil is compressed. This would cause the flanges of the channel iron to pick up load and produce a concentration of stress at the edges of the specimen. To offset this effect it would be necessary to pump oil into the cushion during the model loading.

Calculations of the stresses in the membrane indicate that a steel membrane capable of supporting the internal pressure of 1000 psi would have to be 1/8" thick or more for the system shown in Fig. 55, i.e. it would not have the required flexibility. The same problem would probably be encountered in the manufacture of a rubber bag for the hydraulic cushion. This requirement that the membrane or rubber bag be capable of supporting an internal pressure

of 1000 psi by itself is unrealistically severe, however, since the membrane or bag would be completely contained and supported by the model and the channel iron of the hydraulic cushion. Because of the problems anticipated in the development of a dependable, rectangular shaped hydraulic cushion which is sufficiently flexible and capable of going to pressures of 1000 psi, this system was rejected. It is believed however, that a loading system of this nature is promising, particularly at lower pressure levels, and would merit consideration in future studies.

The system which was finally chosen is a completely mechanical one whose basic operation is quite similar to a system used by Hoek (1965) on small models 6" x 6" x 1". It consists of a pyramid of increasingly larger triangular elements produced by welding angle irons and flat plates together, as shown in Fig. 56. Two such sets of elements are used to apply the load to each lateral face of the model, as shown in Fig. 57. The load is applied by a hydraulic jack against the transition head element and distributed down through the pyramid to the model, which is in contact with the smallest triangular elements, Element No. 3. At the contact between the elements, grooves 1/16" deep with a 1" radius are cut into the plates and the angle corners are rounded on a 1/2" radius. The purpose of the grooves and rounded corners is threefold: (1) to allow the elements to rotate with respect to each other and to adjust to any irregular deformations of the model while carrying equal loads, (2) to aid in aligning the elements, and (3) to provide a large enough bearing area at the contacts to prevent local yielding of the steel and flattening of the contacts. Even so, high contact stresses exist and a high yield steel (T-1 steel) was used for the transition heads and the angles of Element No. 1. This system of applying the lateral loads was chosen for two reasons: (1) the successful operation of the

similar loading system used by Hoek (1965), and (2) the simple, completely mechanical nature of the system, which suggests that it would be very dependable and rugged.

b. Load Distribution Characteristics of the Triangular Element Lateral Loading System. The load distribution characteristics of the triangular loading element assembly were studied in some detail to determine how well they satisfy the lateral boundary condition; that of a uniform lateral stress distribution some distance from the tunnel. It is recognized that the stress distribution on the face of the model will be quite irregular due to the finite width and the finite stiffness of the loading elements. The philosophy guiding the design of the elements was that they should be relatively narrow, stiff, and closely spaced, and that each should apply the same total force to the model even if it deforms unevenly. Then, within a short depth into the model, approximately equal to the width of the elements, the actual stress distribution would deviate only slightly from the average stress applied to the boundary. To check the behavior of the loading apparatus, two things were done. First, one set of loading elements was instrumented to determine the loads being carried by the smallest triangles, under uneven deformations of the assembly. Secondly, concrete blocks the size of the actual model blocks, 24" x 24" x 8", both with and without tunnels, were tested on biaxial compression. These were sprayed with a brittle lacquer coating on an unloaded 24" x 24" face to study the strain distribution in the block. These studies, discussed in some detail below, led to the conclusion that the lateral loading system was performing satisfactorily and fulfilling the design requirements and boundary condition.

i. Load distribution as measured by the instrumented elements. One set of triangular elements as shown in Fig. 56 was used for this study. An electrical resistance strain gage (SR4 gage, type A-7) was placed on the center

of each leg of each of the 4 small triangular elements (Elements No. 3) as shown in Fig. 58. The two gages from each element were wired into opposite arms of a 4-arm Wheatstone bridge and monitored by a strain indicator. Each of the small triangular elements was then loaded invididually with the transition head to obtain a calibration curve showing SR4 gage reading vs. total load carried by the individual element. The entire pyramid of triangular loading elements and transition head was then loaded and at successive stages of loading the strain indicated by the SR4 gages on each of the small elements (No. 3) was recorded and compared with the calibration curves to determine how much of the total applied load was being carried by each individual element.

This method of monitoring the loads carried by individual elements is not satisfactory for general usage, although it was sufficient for the purpose of the immediate investigation. The problem with this method is that it is very sensitive to bending moments in the triangle legs, which are in turn caused by bending of the bottom flat plate of the element at the contact with the model. This system of instrumentation is thus quite sensitive to pressure distribution on the base of the elements. Ideally, the instrumentation would be sensitive only to the average compression strain in the legs of the angles. This might be achieved, for example, by placing another A-7 gage on the inside of each angle leg, opposite each existing gage and either wiring it in series with the opposing existing gage, or into an adjacent arm of the Wheatstone bridge. The inside of the angle legs is inaccessible, however, so this could not be done.

The result of this sensitivity to pressure distribution is that the calibration curves are quite sensitive to the nature of the surface against which the element is placed. This is illustrated by calibration curves for element No. 3-1, shown in Fig. 60. Curve A of Fig. 60 shows the calibration for element

No. 3-1 placed against the surface of a concrete block used in the brittle coating studies. The negative reading at low loads means the SR4 gages are in tension, although an over-all compressive strain must exist in the legs of the triangle. This would mean high bending moments in the legs, which might be caused by a high spot on the concrete block under the center of the element's flat base plate. If a 1/8" thick rubber pad is placed between the element and the concrete, the calibration of curve B (Fig. 60) is obtained. If the element is loaded in a Reihle test machine with two rubber pads 1/8" thick between the base of the element and the loading machine head, curve C (Fig. 60) is obtained. This sensitivity to base conditions means that each element must be calibrated in exactly the position in which it is to be used, and recalibrated every time it is moved to a new position or whenever the character of the base changes. For the immediate investigation, this difficulty was solved in the manner shown in Fig. 59. A steel bar 1/2" wide x 1/8" thick was placed under each edge of each element and these in turn were placed upon a 1/8" thick strip of rubber. Rubber strips of different stiffness were used to induce differential movement of the elements during loading. The use of narrow strips under the edges of the elements elminiated the problem of pressure distribution across the base. In addition the elements were placed upon a 12" x 8" x 1 1/2" steel plate which could be moved freely so that the individual elements could be centered in the test machine for calibration, and then the whole assembly could be centered for loading. In this way the whole loading assembly could be tested with the small elements in exactly the same position and with exactly the same base conditions with which they were calibrated. Using this technique, the calibration of each element became fairly constant, as shown by curve D in Fig. 60.

The results of the tests on the whole assembly are shown in Fig. 61. The maximum variation between elements is approximately ± 2.3% of the total assembly load and was generally around ± 1%. The variation between the load carried by each element is almost equal to the variation in the calibration of the individual elements (as shown in Fig. 60, curve D, for example), so that within the accuracy of this method of measurement, the elements are carrying equal loads. This was measured during tests in which the movement of the whole assembly and the relative movements of individual elements was of the same order of magnitude as is expected in the models, as shown in Fig. 61.

The assembly was subjected to a more rigorous test by loading it with wide strips of 3/8" soft pine under each element. The results are shown in Figs. 62 and 63. The differences between individual element loads shown in Fig. 63 is within the uncertainty of the calibration of each element due to the pressure distribution across the base of the elements. Element No. 3-2 indicated no increased load after about 1/5 of the total load was applied because the wood strip under its base was relatively narrow, concentrating load near the center of the base and producing high bending stresses in the legs.

In summary, this study shows that this lateral loading assembly can accommodate substantial differential movements of its base while distributing the total load equally across the base.

ii. Brittle coating studies. While the tests outlined above show that the pyramid of triangular loading elements is capable of rotating and distributing the load uniformly to the elements in contact with the model, they do not indicate how well the entire lateral loading apparatus is able to fulfill its design function, that of producing a uniform free field stress distribution in the model. To study this, concrete blocks the size of the model were loaded

under plane stress conditions in biaxial compression by the lateral loading assembly at stresses of σ_v = 1000 psi and N values of 1/3 and 1. Brittle coatings on an unloaded 24" x 24" longitudinal face were used to study the strain distribution in the block. The brittle coating is a specially prepared lacquer which cracks at a low tensile strain (on the order of 800 micro inches per inch for the test conditions), the cracks being perpendicular to the direction of maximum tensile strain. When an object coated with the lacquer is strained enough to develop cracks in the lacquer coating it is possible to determine the orientation of the strain field by studying the crack pattern in the lacquer. Under carefully controlled conditions it is also possible to determine the magnitude of the maximum tensile strain if one knows the strain at which the lacquer cracks. For the present study, however, only a knowledge of the strain direction was desired.

Two concrete blocks 24" x 24" x 8" were cast from a cement:sand:gravel mixture of 1:2:3 to which enough water was added to give a 3" to 4" slump. One of the blocks was cast with a 4 1/4" diameter "model tunnel" in the center of the 24" x 24" sides. One 24" x 24" face of each block was prepared for the brittle lacquer by rubbing it smooth with emery cloth wrapped around a hand-held wooden block and then spray painting it with a white flat base enamel. The brittle coating used was Stresscoat lacquer, manufactured by Magnaflux Corporation. The lacquer was sprayed on the prepared surface to obtain a thin, even coating and then allowed to dry for 24 hours. Because the lacquer cracks in tension and the concrete model is loaded in compression, the crack pattern is developed when the model expands upon release of the load. The concrete model was loaded slowly in small increments over a period of about 30 minutes, then the load was held constant for about 5 hours. This was done to

allow creep to relax the compressive stresses in the lacquer. The load on the model was then dropped to zero in a few seconds and as the model expanded, tensile strains were developed in the brittle lacquer coating. Because the stress level to which the model was loaded is low compared to the strength and modulus of concrete, the strains developed (on the order of 300 micro inches per inch) were not enough to crack the lacquer and it was necessary to chill the lacquer with a short blast from a CO_2 fire extinguisher. This commonly used technique, known as sensitizing, superimposes a uniform, temperature-induced strain upon the existing load-induced strain field and results in strains large enough to crack the lacquer, with the cracks developing perpendicular to the direction of the maximum tensile strain of the load-induced strain field. Because the cracks are very small and closely spaced, a black wax pencil was used to outline the crack pattern for photographic purposes. It was not possible to show all the cracks in this manner, but only to sketch the general pattern of cracking.

A total of 4 tests were run, using 2 values of N for each of the 2 concrete blocks. The first test was conducted on the solid block at N = 1. Lacquers of three different sensitivities, Stresscoat 60, Stresscoat 90, and a mixture of the two, were used in different quadrants of the block, and the coatings were sprayed to different thicknesses. The resulting crack pattern is shown in Fig. 64. It was found that the crack development was essentially independent of the lacquer sensitivity, but was quite strongly influenced by the thickness of the coating. The crack pattern developed very poorly in quadrant 1, on the upper left, where the coating was the thinnest, and was much clearer and more intense in the other quadrants, where the lacquer was thicker. Chips of the coating from the quadrants where the cracks were well developed were about 0.01"

thick as measured by a micrometer, and were of a deep lemon color. Based upon the results of this test, it was decided that Stresscoat 60 would be used and an attempt would be made to obtain a coating thickness of 0.01" by spraying the lacquer until the coating was a deep lemon color.

Several significant features can be observed in the crack pattern shown in Fig. 64. The most prominent feature of the pattern is the strong lineation of cracks on the right and left edges, parallel to the edges, with less development along the top edge and almost none along the bottom. A pattern of randomly oriented cracks was present over the rest of the block (with the exception of quadrant 1). On the right and left edges the strong lineation extends for about 5" into the model. Because the block was loaded at N = 1, the strains ideally would be equal in all directions and the random crack pattern which developed in the center should have been present over the whole face. The strong lineation around the edges is attributed to the influence of friction along the loading faces, which disrupted the ideal stress and strain distribution. The more pronounced pattern on the right and left sides is attributed to the fact that during each increment in load, the increase was first applied to the right and left sides, and then to the top and bottom. It is assumed that the increase in friction along the right and left sides due to the increased normal force prevented the subsequently increased normal force on the top and bottom from producing an equal strain in that direction. Hence, throughout the loading the strain at the edges was unequal in the two directions.

It is seen, then, that the "edge effects" extend for about 5" into the model from each side, leaving a central area about 14" square in which a uniform strain field exists. This is considered to be too small. In an attempt to increase the size of the uniform strain area in subsequent tests,

a 1/8" thick rubber pad was placed between the loading elements and the model block. It was believed that the shearing deformations in the rubber pad would allow the model to move relative to the loading elements unhindered by friction along the faces.

Another significant feature seen in Fig. 64 is the arcuate pattern immediately adjacent to the edges, showing the influence of the individual loading elements. It can be seen that this influence extends to a maximum depth of 1 1/2 to 2 inches.

The next test was run on the solid block at N = 1/3. The resultant crack pattern is shown in Fig. 65. Some difficulty was experienced with the spray nozzle when applying the lacquer, resulting in a less uniform coating on the right half of the block, as evidenced by the less uniform intensity on that half. The dominant cracks developed perpendicular to the 1000 psi stress direction, as would be expected. A very uniform crack orientation parallel to the right and left sides exists over the whole block except in the upper right hand quadrant, where the cracks on the right half of the quadrant seem to trend into the upper corner, indicating a distortion of the strain field. It is not known whether this resulted because of an improper alignment of the loading elements or a low force in the hydraulic jack in that corner. In any case it is rather localized and not considered serious. The en-echelon pattern observed in a number of places is attributed to the influence of aggregate particles in the concrete. The conclusion drawn from this test is that with the 1/8" thick rubber pad between the concrete and the loading elements, a sufficiently uniform strain field is produced in the model.

The crack pattern from the next test, on the block containing the tunnel at N = 1, is shown in Fig. 66. As would be expected, a random crack

pattern is developed everywhere except immediately adjacent to the tunnel. Because of the circumferential compressive stress concentration around the tunnel during loading, a circumferential tensile strain developed in the lacquer during unloading, giving the radial crack pattern. The pattern appears to be symmetrical, indicating a uniform stress field around the tunnel. The only apparent significant deviation from a uniform strain field in the block is immediately adjacent to the edges where there seems to be a preferential development of cracks perpendicular to the edges. This phenomena extends to a depth of perhaps 1 1/2" and is attributed to the influence of the loading elements and the rubber pad.

The fourth test, with N = 1/3 on the block containing the tunnel, was not entirely satisfactory and is not shown. A good crack pattern did not develop because the lacquer coating was made too thin due to a shortage of lacquer. This test did not show anything different from the first 3 tests.

In summary, it is seen that with a friction reducing pad between the model and the loading elements, the edge effects extend only 1 1/2" into the model, giving a uniform strain distribution over a central area 21" square. This extends to a depth of 4 tunnel radii behind the tunnel wall and is considered to be quite satisfactory. The results of these brittle coating tests and the previously described tests with the instrumented loading elements indicate that the system chosen for applying the lateral loads will satisfactorily satisfy the lateral boundary conditions of the model.

3. Longitudinal Restraint and Reaction Frame

The method of applying the longitudinal restraint and the method of supplying the lateral jacking reactions are intimately related and must be considered together. As discussed previously, a condition of plane strain should

be approximated in the model. Three methods of achieving this result were listed previously:

1) a uniform pressure against the longitudinal faces, controlled to null any longitudinal expansion which tends to develop,
2) rigid heads against the longitudinal faces, tied rigidly together across the model, and
3) rigid heads against the longitudinal faces, with a controlled load applied to them to null any longitudinal expansion which tends to develop.

a. Uniform Restraining Pressure System. It is believed that the uniform pressure method would not satisfy the boundary condition satisfactorily. Dilation of the material is expected in failure zones which develop around the tunnel, with some expansion occurring in the longitudinal direction. More pressure would be required to null longitudinal strains in these regions than in regions away from the tunnel which are still behaving elastically. A uniform nulling pressure would then be too low to prevent expansion in the plastic zones and/or too high to exactly null strains in the elastic zones. Hence, the longitudinal faces would not remain plane during the loading, but would warp. Thus, the system is unsatisfactory.

b. Rigid Heads Tied Across Model. The second method suggested has the obvious advantage of greatly simplifying the test procedure. Once the model is in testing position, the longitudinal heads are brought into contact with it and tied together across the model, probably at the corners of the model, Then, during the lateral loading the model is restrained from longitudinal expansion by the rigid heads and ties. This would eliminate the need for monitoring and regulating the longitudinal deformations and loads. A serious problem which must be given careful consideration with an apparatus of this sort is the

difficulty of seating the restraining heads against the model. Because of the very small (0.02") longitudinal expansion which would occur even in the plane stress condition, the restraining heads must be seated very carefully and tightly. Otherwise, the expansion of the model which would occur before intimate contact with the restraining loads was developed would be of the same order of magnitude as the total expansion during the test. In such a case the actual test condition would approximate plane stress more closely than plane strain. In spite of this problem, the anticipated simplicity of the testing procedure with an apparatus of this sort was very attractive and the design of such a system was carefully considered.

Consideration was first given to a restraint consisting of heads about 24" square tied together at the corners, such as sketched in Fig. 67. If the deformation of the restraining heads is estimated by analysing the heads as plates simply supported at 4 corners and subjected to a uniformly distributed load of 500 psi, it is found that to prevent 90% of the plane stress longitudinal expansion at the center, a steel plate 12" thick would be required. This is considering only bending deformations in the "plate" and does not include shearing deformations and extension of the ties between the heads, which are probably of the same order of magnitude as the bending deformations. Clearly, this sort of restraint is not satisfactory.

Deformations would be significantly reduced if the edges of the heads could be kept from rotating. A design such as shown in Figs. 68 to 75 was considered for achieving this result. The top and the bottom heads are x-shaped members, each arm of which is about 24" wide and 82" long and is made of 8" channel irons, as shown in Figs. 68 and 69. The central 48" of each arm is covered top and bottom by a 1/2" cover plate. At each corner of the model

the top and bottom heads would be tied together by a connection such as shown in Figs. 70 and 71. The reactions for the lateral loading jacks and the end ties between the top and bottom heads are combined as shown in Figs. 72 to 75.

After the model is placed in position on the bottom head, it would be covered by the top head and the two heads would be fastened tightly together by the bolts in the corner connections (Fig. 70 and 71) in order to seat the heads tightly against the model. Next, the connections between the heads at the ends of the arms would be made. Because a tight bearing is necessary between the heads and at the jacking reactions, and because different model blocks can be expected to vary slightly in thickness, the wedge blocks a and b (Figs. 74 and 75) are necessary. They will allow solid bearing between the bottom head and the top head but will still allow the position of the top head to vary.

Calculations were made to determine the deformations of the centers of the top and bottom heads under a uniformly distributed load of 500 psi over the location of the model. Both bending in the heads and extension of the corner ties was considered. Two different analyses were considered: 1) analyzing the central 24" x 24" section of the head as a square plate simply supported at the corners and with some degree of fixity at the edges, and 2) considering each cross arm of the head to be a continuous beam from one end to the other, each subjected to 1/2 of the 500 psi uniform load from the model. It was found that the center deformation would be between 0.0030" and 0.0050", i.e., when subjected to the stress needed to maintain a plane strain condition, the center of the heads would move outward between 30% and 50% of the amount that the block would expand longitudinally under plane stress conditions. Roughly 1/2 of this movement would occur because of strain in the ties between the heads

at the corners of the model. This calculated deformation is an overestimate because it assumes the full 500 psi acts as the head deforms while in reality, the pressure would decrease as the head deforms and the model is allowed to expand. Shearing deformations are not considered, however, and would probably be of the same order of magnitude. The conclusion reached is that this design would not be rigid enough.

To be acceptable, the calculated deformation should not exceed about 10% of the plane stress expansion, i.e., it should be 1/3 to 1/5 of that allowed by this design, requiring perhaps 3 to 5 times as much steel as the design shown in Figs. 68 to 75. Such an apparatus is considered too massive to be practical. The problem of adequately seating a model in an apparatus of this design remains an unsettled question. Furthermore, such an apparatus, representing a sizable investment, would not have the adaptability and general capabilities of the design finally chosen. For these reasons, it was decided that rigid heads tied together across the model were not a satisfactory design.

c. Controlled Rigid Longitudinal Heads.

i. Cantilevered lateral reactions. The next system which was considered is shown schematically in Fig. 76. The bottom frame and lateral reactions would be combined into a single unit very similar to that of the previous rigid design. Details of the ends are shown in Figs. 77, 78, and 79. The top head would consist of a grill work as shown in Fig. 80 with a 1" bottom cover plate in contact with the model and a 1/2" top cover plate. The 1/4" rod threaded into the bottom plate is part of the longitudinal deformation monitoring system which will be discussed in more detail later. Hydraulic jacks would force the head against the model to null longitudinal expansion of the model.

Calculation of the deformation of this "rigid" head, assuming a 500 psi uniformly distributed load from the model and point loads from the jacks indicate the surface in contact with the model would deform on the order of ± 0.0002" from a plane, considering both shearing and bending deformations. This is considered satisfactory and is actually an over-estimate since the jack reactions would be spread over the area of the jack bases and would not be point loads. The reaction for these longitudinal jacks would be provided by a grillwork such as shown in Fig. 81, tied to the bottom frame by angle irons at the corners of the model.

The difficulty with a design such as this is that the support for the lateral jacks is not symmetrical, but is cantilevered off the bottom frame. This produces bending stresses in the bottom frame and results in a convex upward curvature under the base of the model, which is intolerably large. A number of schemes were considered for reducing this curvature but calculations for all schemes showed that the maximum deformation of the center would be up to 20% of the plane stress deformation, unless steel sections much larger than shown are used. The conclusion reached is that an eccentric support of the lateral reactions is unsatisfactory.

ii. Symmetrically supported lateral reactions. Utilizing experience gained from previous designs, a final design was arrived at in which the reactions are symmetrically supported and deformations of the reaction frame are not a major problem. This design is shown in Figs. 82 to 97. Overall views of the apparatus are shown in Figs. 82 to 84. The lateral loads are applied by the pyramids of triangular elements discussed previously, which are arranged as shown in Figs. 85 and 86. The reactions for the lateral jacks are supplied as shown in Figs. 82 to 85, with details of the end reactions given in

Figs. 87 to 90. The horizontal 1 3/4" rods are removed while positioning the model in the loading frame and setting up the test. These rods have the same cross sectional area as the horizontal 3" x 3" x 7/16" angle iron ties, and the axis of the lateral jacks is spaced vertically midway between the centroid of the rods and the centroid of the angles, in both the σ_v and σ_h directions. Hence, bending moments in the lateral reaction frame are kept to a minimum. Moreover, the lateral reaction system is independent of the longitudinal system, and deformations and moments in the lateral system have no effect upon the longitudinal deformations.

The longitudinal restraint is supplied by the apparatus shown in Figs. 91 to 96. The top longitudinal head is the same as shown in Fig. 80. The bottom restraint is a passive element, the 2' x 2' x 2' concrete cube shown in Figs. 91 and 93. The reactions are supplied by the top and bottom longitudinal reaction heads shown in Figs. 92 to 96, which are tied together by the 4 vertical 1 3/4" diameter rods. While considerable deformation of these top and bottom reaction heads will occur, it is of no significance because the model does not rest directly against them. The model is shielded from irregular deformation of the bottom frame by the 2' concrete cube, while being loaded from the top by the hydraulic jacks acting against the top head shown in Fig. 80.

The system for monitoring the longitudinal deformations is shown in Figs. 93 and 97. The horizontal 1 1/4" x 1 1/4" x 1/8" angle iron above the top loading head is coupled to the 3/8" plates under the model by the short 1/2" diameter rods and the horizontal 1" x 1" x 1/4" angle irons which are in "tunnels" in the concrete cube, and it moves with the bottom of the model block. The 1/4" rods through the top loading head are screwed into the 1" plate in contact with the top of the model, and move with the top of the model.

Mechanical dial gages measure the movement between the 1 1/4" angle iron and the 1/4" diameter rods, i.e. they measure the relative movement between the top and bottom of the model. The load applied by the longitudinal jacks will be controlled to null any longitudinal expansion of the model which tends to develop during the application of the lateral loads, as measured by this null strain monitoring system.

For those members in which deformations was not a controlling factor, the reaction frame has been designed for an extreme fiber stress of 20,000 psi in both tension and compression in the rolled steel sections, which are of A36 steel. The horizontal and vertical tie rods are subjected to higher stresses in the threaded sections, and are of higher yield steel.

To ensure adequate seating of the loading heads (and longitudinal deformation measuring points) against the model, the following procedure is suggested: The top 3/8" plate beneath the model is the bottom of the mold in which the model is compacted, hence it should be well seated against the model. The bottom 3/8 plate was cast against the concrete cube and will not move. As the model is put in testing position a thin film of hydrocal, or a similar material, will be placed between the 3/8 plates to ensure complete contact between them. The top loading head will be placed on the model immediately after it is compacted and before it hardens so that the model surface conforms to the bottom of the 1" plate of the loading head. When testing is ready to begin, a longitudinal seating load of perhaps 50 to 100 psi will be applied before the lateral loads are applied.

The hydraulic jacks used are 12 Simplex RC-6010 double-acting 60 ton hydraulic rams. They are actuated by the pressure console shown in Figs. 82, 83 and 98. The console is driven by air pressure and features two

independent hydraulic systems each capable of producing pressures of 10,000 psi from an air pressure of 100 psi. The four jacks applying the σ_v loads to the model are driven by one of the consoles' hydraulic systems, while the four applying the σ_h loads are driven by the other system. A hydraulic pressure of 7000 psi is required to develop the average stress of 1000 psi against the model. The longitudinal jacks are driven by a hand pump.

The lateral loading assembly has been thoroughly tested in conjunction with the brittle coating studies described previously, and has been found to operate very satisfactorily. At the time of this writing, the longitudinal restraint system has been assembled, but not tested. It is anticipated that minor modifications of the apparatus will have to be made as the model testing program develops.

4. Control of Friction Along Longitudinal Loading Faces

A very critical problem is that of friction between the model and the large area of the longitudinal loading surfaces. Hobbs (1966) in similar experiments experienced losses of 35% to 68% of the applied lateral loads into friction along the longitudinal faces. Friction losses of this magnitude are intolerably large.

The first method considered for reducing the friction between the model and the loading heads utilized a set of thin, square steel plates spread over the longitudinal faces of the model (as shown in Fig. 99), between the model and the loading heads. The plates would be placed directly against the model surface and would move with it. They would be separated from the steel head by some sort of friction reducing system and would move relative to the head. It was believed that friction between the two steel surfaces could be controlled better than friction between the model material and steel.

A system of ball bearings between the plates and loading heads would probably give the lowest friction, but was rejected because of the anticipated cost and complexity. A film of dry lubricant of some sort (Fig. 100) was considered to be more practical and easy to use. Discussions with members of the mechanical engineering staff at the University of Illinois suggested that the small square steel plates would be unnecessary and the model could be placed directly against the lubricant and the loading heads.

A simple double direct shear device was constructed for investigating the friction between the model material and steel (Fig. 101). Tests indicated a coefficient of friction of 0.35 between the 1/1/9 mixture of water/plaster/fine Sangamon sand and steel (friction angle = 19°). A number of combinations of aluminum foil, wax paper, vaseline, light oil, molybdenum disulfide powder (Molykote) and teflon were tried in an attempt to reduce this friction. Representative test results are shown in Fig. 102. The combination of a thin coating of vaseline covered by a layer of wax paper against the surface of the model material proved to be most effective in "smoothing out" the surface of the model and minimizing the roughness produced by individual sand grains on the surface. Aluminum foil proved to be less satisfactory than wax paper because it was easily punctured and torn by individual sand grains. The dry Molykote powder was more effective as a lubricant than vaseline, light oil, or a mixture of molykote and light oil because the latter were extruded from the sliding surfaces under the normal loads, whereas the powder was not. Hence attention was concentrated on dry lubricants. The lowest coefficient of friction which has been achieved is 0.05 ($\phi = 3°$), using two sheets of 0.005" thick teflon placed between two sheets of wax paper. The most common readily available dry lubricants and representative ranges of coefficients of friction found in the

literature are: graphite, 0.10-0.19; molybdenum disulfide, 0.05-0.15; teflon, 0.03-0.04. The presently achieved values are within these ranges. A further reduction of friction with these lubricants would probably require flatter, smoother surfaces, which may be difficult to achieve with the model material. Sheets of 0.005" thick teflon 24" wide have been obtained. This material seems to be quite tough, and no difficulties due to tearing of the teflon sheets is expected.

Calculations have been made to determine the loss of applied lateral load due to friction between the model and top and bottom loading faces, based upon the assumptions of plane strain, a 100 psi top head seating load, and a Poisson's ratio of 0.25 for the model material. The results are shown in Fig. 103 for different values of N and friction properties. It is seen that over the range of N values considered, for a coefficient of friction of 0.05, between 85% and 95% of the applied lateral loads are felt by the model tunnel, except for the loads in the σ_h direction at N = 1/4. For $N = \frac{\nu + \nu^2}{1 - \nu^2}$, there is no strain in the direction of the minimum applied lateral loads, while for lower values of N, the block tends to expand in this direction, even though in compression. For $\nu = 0.25$, this occurs for $N < 1/3$, hence at $N = 1/4$, the friction on the heads opposing the outward movement of the model increases the loads in the σ_h direction, as shown. The 100 psi seating load and Poisson's ratio of 0.25 are probably overconservative estimates, so that actually an even higher percentage of the applied load will reach the tunnel.

C. Instrumentation of the Model

A great deal of qualitative information could be obtained from the model tests simply by measuring the applied loads and by observing the failure modes and noting how they are influenced by changes in the variables being studied. However, a much greater understanding of tunnel behavior would result if quantitative measurements could be made through an appropriate instrumentation system.

1. Applied Stresses and Over-all Block Deformations

The applied loads could best be measured by simply monitoring the pressure supplied to the hydraulic jacks. While this is not entirely satisfactory because it is a rather remote measurement, it seems to be the most practical for the present testing program. Experience with the instrumented set of loading elements, presented earlier, indicates that strain gage instrumentation is not a satisfactory method of monitoring the individual loading elements. Some sort of hydraulic cushion or flat-jack system against the model would probably be required for a direct measurement of the applied stresses. It is expected that this would be rather expensive to develop. Furthermore, the studies of the load distribution properties of the lateral loading assembly, presented earlier, have shown that the assumption of uniform free field stresses equal to the total applied load divided by the total area is a reasonable one.

The over-all lateral deformations of the model block could be measured with mechanical dials attached to the loading frame and should present no particular problems. The mechanical dials can be placed against the model at the center of each lateral side, between the two pyramids of triangular loading elements. The longitudinal deformations would be monitored as discussed previously.

2. Radial Extensometers

Measurements of the radial movements of the tunnel wall would be quite valuable. Because the first models tested will not contain tunnels, a method for monitoring these deformations has not been studied in great detail yet. It is planned that these deformations be monitored by radial extensometers utilizing LVDT's, potentiometers, or some similar linear displacement transducer as sensing elements. These extensometers might be mounted in a manner such as shown in Fig. 104, measuring to the tunnel wall and to a depth of 1 tunnel radius behind the wall, as shown in Fig. 105. The bore holes for the extensometers could be drilled with a dental drill. The extensometers would be mounted in the 0°, 90°, and 225° directions, as shown in Fig. 105, to measure deformations in the directions of the free field principle stresses and at 45° to them. This 45° direction was chosen because the work in Reyes (1966) predicts the growth of plastic zones away from the tunnel in the 45° directions for loadings of $N \neq 1$. A maximum of about 6 such extensometers could be used because of space limitations. The estimated elastic deformations as shown in Figs. 49 and 50 indicate that the sensing elements of the extensometers should have an accuracy of 0.001 inch and an operating range of at least 0.100 inch.

3. Internal Electrical Resistance Strain Gages

a. General Considerations. It would be desirable to have more quantitative measurements of the model behavior than can be obtained from the 6 radial extensometers. To obtain additional data it would be necessary to imbed some sort of instrumentation gages within the model, behind the tunnel walls. Before these gages can be selected, it is necessary to have some idea of the

model behavior. As previously presented (Sect. II. B. 1. c.), one estimate of stress distribution around the tunnel is shown in Figs. 50 to 53. If a plastic zone such as represented actually develops, then in order to place instrumentation in it, it is desirable to have as wide a plastic zone as possible, hence as weak a material as possible. Yet to properly model the strength and deformation characteristics of rock, higher strengths are developed in the model materials. A reasonable compromise appears to be a 4" diameter tunnel in a material with a ϕ of around 35° and a q_u of 500 psi to 600 psi. This would give a plastic zone about 1" thick.

An instrumentation layout such as shown in Fig. 106 seems desirable. This system would allow the behavior to be monitored at depths of 1/4, 1/2, 1, 2, and 3 tunnel radii behind the tunnel wall in the 0°, 90°, and 225° directions. The suggested gage locations are staggered on opposite sides of the tunnel for two reasons: 1) to increase the number of gages which can be placed along a diameter while allowing sufficient spacing of reasonably large gages, and 2) to give some indication of the symmetry of the model behavior. The data from 5 gages on one diameter will be plotted on a graph as if they were all on one side of the tunnel. If the two data points from one side line up reasonably well with the three data points from the other side to define some sort of curve, it will be assumed that the model behavior is symmetrical about the tunnel. If not, it may reflect on assymmetrical behavior and some changes in the instrumentation may be required. As discussed previously, the work of Reyes (1966) indicates the development of the plastic zone along 45° lines for $\sigma_v \neq \sigma_h$, hence, the need for instrumentation along 45° radii. If failure occurs by formation of extension fractures parallel to the tunnel wall or by the tunnel walls raveling and falling in as the failure zone grows, instead of by

the full development of a plastic zone such as shown in the graphs, the instrumentation shown in Figs. 105 and 106 should still allow a reasonably complete monitoring of the model behavior.

A satisfactory method of imbedding gages within the model block poses some problems. Some requirements of the internal gages are:

1) They must not significantly disturb the model behavior,

2) They must be capable of being placed within a block of sand/plaster material which will probably be molded by impact compaction,

3) They must have a remote readout linearly proportional to strain in the model (it is assumed that such a strain gage will be much easier to construct than a device whose output is linearly proportional to the stresses in the model),

4) They must measure strains in a material whose deformation modulus will vary from a maximum of about 200,000 psi in the elastic regions at high confining pressures to a minimum of 0 in the plastic zones; hence it will be impossible to match the modulus of the gage with the modulus of the material.

5) They should operate over a strain range approaching 4% (40,000μ in/in).

6) They should measure strains in the midplane of the model in 2 or 3 directions at the gage point.

7) The gage length must be small, particularly near the tunnel, because the strain gradients may be large,

8) The gage length must be significantly larger than the size of individual sand grains so that the strain readings are meaningful,

9) The gages must not be adversely influenced by perpendicular pressures of up to 500 psi which may be required to maintain plane strain in the model.

It seems that sensing elements consisting of SR4 foil rosette gages of about 1/4" gage length such as the BLH FAR-50-12(45)S6 gage will most nearly satisfy the requirements listed above. The best method of encapsulating these elements

within the model is not certain. A literature survey has not disclosed any completely satisfactory methods which have been used by other investigators. A study by Loh (1954) indicates that the most desirable configuration for an internal strain gage is a long dimension parallel to the direction in which strain is being measured, and short perpendicular dimensions. This configuration would result in the smallest error in gage reading due to a mismatch of gage and model moduli. A foil SR4 gage in a thin wafer would best satisfy this requirement. Personal communication with Mr. Leo Ingram of U.S. Army Waterways Experiment Station indicates that they have satisfactorily imbedded SR4 gages in cement grouts by sandwiching the gages between 2 pieces of 0.005" copper shim stock, then casting this into a 2" x 1" diameter cylinder which is mounted in the grout mass. Loh (1954) discusses somewhat similar techniques. Barron and Larocque (1962) and Barron (1962) report partial success in installing similar gage "sandwiches" in slits cut into cured plaster-diatomaceous earth materials. To date, no other record has been found of satisfactory placement of SR4 gages in materials such as are being used. Some literature is available on the casting of SR4 gages in epoxy bars and cylinders, (Baker and Dove, 1962 and 1963; Brazier and Dove, 1961; Dove, Brazier, and Baker, 1962) but the techniques do not seem to be applicable to the problem at hand.

Present study suggests that the most practical method of imbedding internal gages would be to first cast the model in two 4" thick slabs. To insure complete contact between the two halves, the bottom half may be compacted in the bottom of an 8" deep mold, then a layer of metal foil placed at the mid-plane of the model and covered by compacting the top half in place. After

drilling the tunnel, the two halves would be separated and the foil removed, then the SR4 foil gages would be glued to the top surface of the bottom 4" slab. The top slab would then be placed in position over this. For satisfactory performance of the model it should not be necessary to glue the top and bottom halves together since theoretically no shear or tensile stresses will be transmitted across the midplane because of the symmetry of the model and because considerable normal stress will be applied to this plane to maintain plane strain in the model.

It would be necessary to test cylinders with gages mounted internally in a similar manner so that readings of the internal gages may be compared with readings of surface mounted SR4 and dial gages, to test the accuracy of the internal gages.

b. Surface SR4 Gages. The first study, then, was directed toward mounting SR4 gages on the surface of cylinders of the model material. As an estimate of the accuracy of the surface SR4 gages, the stress-strain curve determined by them was compared with that determined by a dial gage measuring the deformation between the loading heads. It was assumed that the SR4 gages would be working properly if the central linear portion of the dial gage stress-strain curves was parallel to the central linear portion of the curve determined by the SR4 gages.

To date, a satisfactory comparison between the two has not been observed. The SR4 gages have always registered considerably less strain than the dial gage. Typical curves from an unconfined specimen are shown in Fig. 107. In this figure, the dial gage curve has been shifted to the left so the central linear portion extends through the origin, in a crude attempt to correct for seating errors at low stress levels.

A number of different gage mounting techniques were tried in an attempt to increase the "strain pick-up" of the SR4 gages, including:

1. Mounting the SR4 gages (BLH type A-1) on the specimen with Duco cement and various epoxies such as Budd GA2, a BLH two-component epoxy, and Armstrong A35.
2. Coating the specimen at the gage location with a sub-base of Duco cement diluted with acetone, then mounting the gages on the sub-base with the epoxies listed above and with Eastman 910 adhesive.
3. Coating the specimen at the gage locations with a very thin layer of plaster of Paris, then mounting the gage with Armstrong A35 on the smooth plaster surface.

Only the use of undiluted Duco cement and the thin plaster layer developed visibly unsatisfactory bonds. The undiluted Duco cement was too viscous to penetrate into the material and peeled off readily carrying the first layer of sand grains. The gages on the plaster layer registered almost no strain, and the plaster layer spalled off as the cylinder approached failure. A visual inspection of all other methods suggested the bonds were quite satisfactory, penetrating sufficiently deep into the material to bond well, but not so deeply as to form a rigid button which spalls prematurely.

Of the various gluing techniques tried, the most strain has been registered by gages bonded with Eastman 910 adhesive on the dilute Duco sub-base, presumably because a thinner bond is obtained, which transmits strains to the gages more efficiently. The dilute Duco sub-base consists of a mixture of Duco cement and acetone (1:1 by weight) which is dried at 110°F for 24 hours. This sub-base serves to seal the pores of the material and prevent excessive

penetration of the very fluid Eastman 910 adhesive. Budd GA-1A1 accelerator has proven most satisfactory for use with the Eastman 910 on this sub-base. A-1 gages mounted in the above manner on the surface of cylinders tested in unconfined compression have registered about 1/4 the strain indicated by the mechanical dials measuring between the loading heads, in the central linear part of the stress-strain curves.

The reason for this descrepancy between the SR4 gages and the mechanical dial gages was not immediately apparent. One possible explanation was associated with the weak, friable nature of the material. Dove (1955) has shown that the stiffening influence of two paper-backed Al gages and the associated nitrocellulose cement on materials of modulus around 100,000 to 200,000 psi is almost negligible, being only 3% to 6% for a tensile specimen 3/8" thick by 1" wide. It was thought that it might be possible that this stiffening affect is magnified on friable materials such as are being tested, however, because it may be easier to develop a non-uniform strain distribution across this very heterogeneous gypsum matrix-sand grain structure. It was hypothesized that a sharp strain gradient might develop in the cylinder immediately behind the SR4 gage and the portion of the cylinder which is impregnated with glue, with the central portion of the cylinder experiencing more strain than the SR4 gage. If such a phenomenon actually exists, it might be expected that the gage would spall off as failure of the cylinder is approached. However, this has not been observed. If this strain gradient does tend to develop, it would be expected that it would be reduced by application of normal stresses to the surface of the cylinder through confining pressure in triaxial tests. A cylinder tested at a confining pressure of 500 psi showed a much better correlation between the surface A-1 gages and the external dial gage (Fig. 108), lending support to this hypothesis.

If this hypothesis is the major reason for the poor correlation between the SR4 and dial gages, it would be expected that the best correlation would be obtained on triaxial compression specimens with SR4 gages imbedded internally, along the axis of the specimen, since such a gage would have the maximum surface area of bond between the gage and the specimen. However, the stress-strain curves from internal gages, which will be presented later, matched closely those from the surface gages, so that doubling the bonding area had little effect on the strain pick-up. This discounts the explanation of the hypothesized strain gradient causing the discrepancy between the SR4 gages and the dial gages.

Another explanation might be associated with seating of the loading heads. The model material is quite friable because of the weak bonding between sand grains. Hence it is impossible to get a very smooth surface on the cut ends of the test cylinders. The ends of the test cylinders are relatively flat, parallel, and perpendicular to the cylinder axis, but are smooth only to within approximately $\pm$ the sand grain diameter. As load is applied the protruding sand grains take up load and are pushed down into cylinder giving a very pronounced concave upward curvature on the stress-strain curve determined by the dial gage measuring between loading heads. It has been assumed that this effect does not extend beyond stress levels of approximately 1/3 to 1/4 the maximum strength, where the stress-strain curve becomes linear. If, however, the effect is present to some extent at higher stress levels, the dial gage would yield stress-strain curves which are flatter than the actual material behavior and are not valid for a comparison with the SR4 gages. In essence, this is hypothesizing the existence of a strain gradient along the axis of the cylinder, with a higher strain at the ends due to a progressive failure mechanism.

Several things were tried to test this hypothesis. For one thing, the ends of cylinders were capped with Hydrocal to give a smooth, hard surface in an attempt to reduce this progressive failure. A comparison of the stress-strain curves for the dials between platens in Fig. 107 for a cylinder without end capping, and that for a cylinder with end capping in Fig. 109 shows a considerable difference. Although a concave upward curvature exists to about the same stress level for both cylinders, much less strain occurred both for the initial curvature and for the total stress to failure in the cylinder with the end capping. This supports the hypothesized progressive failure phenomenon and seating problem at the ends of the specimen.

As a further test of this hypothesis, a mechanical extensometer was mounted on the cylinder to measure deformations along the central 2 1/8" of the cylinder. The extensometer consists of 2 brass rings of about 3" internal diameter mounted concentric with the cylinder about 2 1/8" apart. Each ring is supported by 3 screws 120° apart which are brought into contact with the surface of the cylinder. Three 0.0001 dial gages mounted on the rings 120° apart measure the relative movement of the two rings and allow the axial strain in center of the cylinder to be determined. Because the model material is so weak and friable the weight of the extensometer rings and dial gages can not be supported adequately by screws seated directly in the cylinder surface. To overcome this problem, a small patch of the dilute Duco cement is placed on the cylinder at the location of the screw contacts and the screws are seated in the Duco patch. The results of an unconfined compression test with such a set-up are shown in Fig. 109. It is seen that the surface mounted A-1 gages register very nearly the same strain as the extensometer does, in fact, they register slightly more. This indicates that the SR4 gages are properly bonded

and are actually registering the strain which the cylinder is experiencing through its central portion. Again, this is a confirmation of the existence of a strain gradient down the axis of the cylinder, with higher strains occurring at the ends.

In an attempt to document the existence of this hypothesized strain gradient, several cylinders were tested with a series of SR4 gages glued in a line parallel to the axis of the cylinder. Two cylinders were tested with 2 lines of A-7 gages (1/4" gage length) and 2 A-1 gages (13/16" gage length) arranged as shown in Fig. 110. A third cylinder was tested with gages arranged as shown in Fig. 112. The resulting stress-strain curves for 2 of the cylinders are shown in Figs. 110 and 112, and the measured strain gradients are shown in Figs. 111 and 113.

It is seen that the strain as measured by the SR4 gages is definitely not uniform along the axis of the specimen. The two cylinders show the highest strain at the bottom and the least at the top. It should be noted that the strain measured by the A-1 gages in the middle is roughly the average of the strain measured by the A-7 gages. In general, the strain variation along the axis as measured by the SR4 gages is not enough to account for the variation between the middle A-1 gage and the external dial gage. Only the stress-strain curve for the A-7 gage at the bottom of cylinder B4-3 (Figs. 110 and 111) roughly parallels the stress-strain curve determined by the mechanical dial measuring between the loading heads.

An interesting feature which can be observed in both Figs. 110 and 112 is that just before the cylinder fails, the stress-strain curve for the bottom A-7 gage, which is recording the most strain, exhibits a reversal of curvature, i.e. it becomes concave to the upper left. This indicates a relaxation of

stresses at the gage location caused by the development of a fracture in the high strain regions under the gage, preceding the complete failure of the cylinder.

The data from these tests are inconclusive. They indicate the existence of a considerable variation in strain along the axis, but only in the case of cylinder B4-3 was the strain measured by the end SR4 gages large enough to account for the difference between the middle A-1 gages and the dials between the loading heads. This suggests that the highest strains occur quite near the end of the specimen. The fact that the highest strains were measured at the bottom of the cylinders suggests that the physical arrangement of the testing apparatus may be of some importance. The bottom loading head was rigidly attached to the loading machine whereas the top loading head continued a spherical seat. It is conceivable that the rigid bottom head may produce an uneven stress distribution at the bottom, intensifying the unequal strain distribution in the cylinder.

The important conclusions which can be reached from the study of surface SR4 gages on the cylinders are:

1. Electrical resistance strain gages can be satisfactorily mounted on surface of cylinders of the model material with Eastman 910 adhesive over a sub-base of dilute Duco cement (Duco cement: acetone in a mixture of 1:1 by weight).
2. The SR4 gages mounted along the center of test cylinders in the manner described above give a reasonable indication of the strain which actually occurs at the gage locations. This strain is significantly less than the average strain of the specimen measured by relative movement of the loading platens because of

a strain gradient along the axis of the specimens, with the greatest strains occurring at the ends.

c. Internal SR4 Gages. Several cylinders of the model material have been tested with foil SR4 gages placed on an axial plane inside the cylinder. The internal surface has been prepared in two ways. One is by simply sawing the cylinder along an axial plane and splitting it in half. The other method used is that suggested for the model, which is to compact a block with a metal foil separation along a mid plane, then to separate the two halves and remove the foil after the block has cured. The test cylinders were cored from the block with their axis in this plane of separation.

Two different types of gages, one and two element foil rosettes, were used for different cylinders. The gage is glued to the axial plane on one half of the cylinder in the same manner as surface gages, with Eastman 910 adhesive on a dilute Duco sub-base. The lead wires are then soldered to the gage and brought out of the cylinder in small grooves cut into the exposed axial plane. A slight hollow is then formed in the axial plane on the other half of the cylinder directly opposite the gage location, to prevent sand grains from being in direct contact with the foil. This hollow is then filled with Duco cement, the gage on the first half is coated with Duco cement, and the two halves are clamped together. After the Duco cement has dried, surrounding the gage and glueing the two halves together, the cylinder is ready for testing.

The results of tests on three cylinders are shown in Figs. 114, 115, and 116. The data in Figs. 114 and 115 give a comparison between the readings of the internal foil gages and surface of A-1 gages. It is seen that the two agree favorably, indicating that the internal gages are functioning properly. A careful study of Figs. 114 to 116 shows that the SR4 gages show better agreement with the external dials in triaxial compression than in unconfined

compression, but at best they only register about 50% of the strain indicated by the dial gages, even when the curves are shifted to correct for the initial seating error.

The data of Figs. 115 and 116 indicate reasonable values of Poisson's ratio and dilation of the material at failure. The volume change characteristics of these cylinders are quite similar to those observed in real rocks (See for example, Corps of Engineers, 1964 and 1965). This is a further indication of the suitability of this material for modeling rock.

The conclusion which has been reached in these instrumentation studies is that foil rosette SR4 gages mounted in the manner described operate satisfactorily in triaxial tests at confining pressures at least as high as 500 psi and should prove satisfactory for monitoring the model behavior.

4. Temperature Compensation and Wiring

Raphael (1960) describes the use of SR4 gages on a plaster-diatomaceous earth model of a dam in which temperature compensation of active gages was a problem. He found that the use of a single compensating gage with a number of active gages caused intolerably large temperature induced false strain readings because of heating of the compensating gage. This problem is not so severe when working with metals since the heat evolved by the gages is rapidly dissipated because of the metal's high thermal conductivity. But the plaster-diatomaceous earth material has a much lower thermal conductivity and does not dissipate the heat rapidly enough. Raphael (1960) found it necessary to reduce the bridge voltage to 2 1/2 volts and to switch compensating gages as well as active gages, using 24 compensating gages with 215 active gages. The time lapse between successive uses of any one compensating gage was then sufficiently long to allow dissipation of the heat evolved by the gage during the time it was part of the bridge circuit.

In anticipation of similar problems, several tests were performed using one element of Budd C6-141-R2TC foil rosette gages imbedded within test cylinders of the model material in the manner described previously, and wire SR4 gages mounted on a steel plate. For switching, 10 position silver contact switches were used. Strains were read with a BLH Model 120 Indicator powered by 110 volt 60 cycle alternating current and supplying a bridge voltage of 2.7 volts. The first test consisted of switching two of the wire gages on the steel plate into adjacent arms of the bridge and observing the bridge balance for periods of up to 30 minutes. It was found that no drift occurred, indicating that the strain indicator was stable. Next, two of the foil gages inside the model material cylinders were subjected to the same test. Again no drift was observed, indicating that temperature effects on gages mounted on the model material can be compensated for adequately. Next one of the foil elements in the model material cylinders was switched into the bridge as a compensating gage and a wire gage on the steel plate was switched in as an active gage. The bridge was balanced and observed for a period of time. It was found that over a period of 40 minutes the bridge drifted a total of 10 μ in/in out of balance. It was assumed that the heat was able to dissipate from the wire gage on the steel plate as rapidly as it was produced by the gage. The observed drift, then, indicates that the thermal conductivity of the model material was sufficiently low to allow the temperature to build up around the foil gage, and a temperature induced strain was read. The rather low magnitude of this strain may be due to two reasons: 1) the thermal conductivity of the model material may be nearly high enough to dissipate the heat (the low thermal conductivity of the plaster-diatomaceous earth materials used by Raphael (1960) may be due to the large percentage of air voids in such low density materials), and 2) the thermal coefficient of expansion

of the model material may be sufficiently close to that of steel so that the temperature compensation of the gage is almost exact (both quartz and plaster have thermal expansion coefficients close to that of steel). Although this temperature induced false strain is so small as to be almost negligible, it is felt that it should be eliminated if possible.

Switching tests indicated that the combined error in switching and reading the strain indicator is approximately $\pm$ 2 μ in/in, and that a total of about 20 seconds is required for one man to switch to a gage, balance and read the indicator, and record the reading. A test was next run using a wire gage on steel as the compensating gage, and switching between another wire gage on steel and one of the internally imbedded foil gages for the active gage. The foil gage was switched into the circuit for a reading for 20 seconds every 3 minutes. The rest of the time the wire gage on steel was left in the circuit. This was done for a period of one-half hour. The strain indicated by the foil gage remained the same within $\pm$ 2 μ in/in, the accuracy with which the readings can be made. This indicated that the time lapse between successive readings of the foil gage was enough to allow complete dissipation of the heat evolved while the gage was in the circuit, so that no temperature induced false strains were produced. Duplication of this timing in the model would require 9 compensating gages which would be switched each time an active gage is read. Each compensating gage would then be used for 20 seconds out of every 3 minutes.

The switching system shown in Figure 117 is planned for the model. It is designed for manual switching, reading, and recording using a single strain indicator and a bank of 10 position silver contact switches. For the sake of symmetry it is planned that 10 compensating gages be used. It is estimated that about 20 minutes would be required to read the gages on the model.

A wiring system such as shown in Figure 118 is suggested for the model. The leads for the SR4 gages would be brought out the sides of the model rather than through the tunnel in an attempt to minimize disturbance of the tunnel.

IV. FEASIBILITY OF RELATIVELY LARGE SCALE MODELS - TENTATIVE OBSERVATIONS

Because the presently proposed testing programs on small scale models has not yet been conducted, it is too early to present many definite suggestions. Some tentative observations can be made, however.

A. Similitude Considerations

Body forces are a major consideration which have been ignored in the present study. As discussed previously (II.B.1. and II.E) this can be done as a "first approximation" in a study of the behavior of underground openings. In a more refined study, however, the influence of body forces such as gravity should be considered. If they are to be considered, the body forces must be modeled in the same scale as the surface forces (such as the free field stresses which are considered in this study). That is

$$K_{(\text{body forces})} = K_{(\text{surface forces})} \qquad \text{Eq. 16}$$

This is the same as $$K_{(mg)} = K_{(\sigma A)} \qquad \text{Eq. 17}$$

which is $$K_{(\rho L^3 g)} = K_{(\sigma L^2)} \qquad \text{Eq. 18}$$

or $$K_\rho K_L^3 K_g = K_\sigma K_L^2 \qquad \text{Eq. 19}$$

which simplifies to $$K_\rho K_L K_g = K_\sigma \qquad \text{Eq. 20}$$

That is, the product of the density, length, and gravitational acceleration scale factors must be equal to the stress scale factor. (See Langhaar, 1951, for an explanation of this method of developing model laws.)

The modeling law expressed by Eq. 20 places rather severe limitations on model studies, and a number of techniques have been developed by

previous investigators in an attempt to satisfy this requirement. The problem is particularly difficult in studies such as the present one in which both elastic and inelastic deformations and "failure" are significant and must be considered. In such cases it is very difficult to find or develop a low strength material for accurately modeling the behavior of the prototype material. Hence it is quite common to use the same material in the model as exists in the prototype. In such a case corresponding stresses in the model and in the prototype are identical, i.e. $K_\sigma = 1$. Hence, in modeling, the requirement of Eq. 20 becomes

$$K_\rho \, K_L \, K_g = 1 \qquad \text{Eq. 21}$$

The length scale factor K_L is dictated by the size of the prototype and the size of the available laboratory testing facilities. Since K_L is generally less than unity ($K_L < 1$) it is necessary that the product of the density and the gravitational accelerator scale factors be greater than unity ($K_\rho \, K_g > 1$). The material density can be varied by a factor of perhaps 2 or 3 by incorporating heavy minerals such as barite or galena into the model material. The gravitational acceleration of course can not be controlled. A technique frequently used is to place the model in a centrifuge and simulate the prototype gravitational field by centrifugal force in the model. The centrifugal force can be controlled at will and the requirements of Eqs. 21 and 21 can be satisfied.

Many of these problems can be eliminated by using a model material such as developed in the present study, and by reducing the stress scale factor. For example, consider the compacted plaster/sand material which was developed, with an unconfined strength $q_u = 550$ psi and a unit weight $\rho g = 1.875$ gm/cc = 117 pcf. Assume the prototype rock is a granite with a density of 160 pcf

and an unconfined strength of 25,000 psi. The scale factor for the product $K_\rho K_g$ would be 117/160 = 0.73, and the stress scale factor would be 550/25,000 = 0.022. Equation 20 then becomes

$$K_L = 0.03 \qquad \text{Eq. 22}$$

The 4" tunnel presently being considered would then model a 10' diameter tunnel through the granite, while a 33' diameter prototype would require a 12" diameter model.

In other words, gravitational body forces can be accurately modeled with the present material without resorting to a heavy mineral aggregate or centrifuge loading. The gravitational body forces in the present modeling program are being disregarded as a "first approximation" solely for the sake of simplicity in the design of the loading apparatus and the testing procedures. It is strongly recommended that for future testing programs serious consideration should be given to modeling the gravitational body forces.

In a similar manner, with these low strength materials it may be possible to model the dynamic loading of underground openings. In such a case the significant body forces are the inertial forces due to the dynamic loading, rather than the gravitational forces. Instead of Eq. 20, the modeling requirement becomes

$$K_\rho K_L K_a = K_\sigma \qquad \text{Eq. 23}$$

where a is the particle acceleration in the rock mass. Since acceleration has the dimensions LT^{-2}, we have the model law

$$K_a = \frac{K_L}{K_t^2} \qquad \text{Eq. 24}$$

where K_t is the scale factor between analogous times in the model and in the prototype. When Eq. 24 is substituted into Eq. 23 we obtain

$$\frac{K_\rho K_L^2}{K_t^2} = K_\sigma \qquad \text{Eq. 25}$$

as the model law defining the relationship between the 4 basic scale factors defining the model. Because the ability to vary K_ρ and K_t is severaly restricted by technical difficulties and limitations, it is apparent that in general a reduced strength material is needed in a reduced scale model of dynamic phenomena.

B. Modeling Materials

The study of modeling materials described previously has led to the conclusion that mixes sufficiently fluid to be poured into a mold will not have properties satisfactory for modeling the mechanical behavior of rock unless a high percentage of the mix water will combine chemically to form the matrix of the cured material, and unless the matrix material has a sufficiently high angle of internal friction. The authors know of no such materials.

It was concluded and observed that satisfactory mechanical properties can be obtained by producing a structure of mineral grains which is sufficiently dense to give the desired angle of internal friction, and by including the amount of matrix material required to give the desired unconfined compression strength and cohesion. The plaster of Paris and sand material developed is considered satisfactory for modeling the behavior of rocks in general. Additional study is needed to determine how the material properties can be varied by varying the matrix material (different plasters and cements could be studied), the aggregate material (grain size distribution and angularity of sands, and the possible addition of some clay could be studied), the mix proportions, and the molding techniques. Additional study is also necessary to determine the variation of material properties with time and moisture content after the initial curing is completed.

Impact compaction to produce the required material density was chosen as being most practical for the present study. For larger models this may prove difficult and inefficient. Large scale models of a jointed rock mass could be fabricated from individual bricks the size of the joint blocks. These could be mass produced in individual molds, and compacted possibly by vibration or by static compaction in a hydraulic press. Fumagalli (1967) mentions the

use of a hydraulic press in this manner, and Rosenblad (1967) has used a vibratory table for such a purpose. It should be noted, however, that the data available to the authors indicate that these investigators have not achieved as satisfactory behavior in their materials as has been observed in the materials described herein. Similar techniques were tried in the present investigation, but with the equipment available the impact compaction produced the highest densities.

One thing worthy of note concerning modeling of a jointed rock mass is that Fumagalli (1967) describes various materials with which joint surfaces can be coated in order to vary at will the friction along the joints, thus simulating varying degrees of smoothness, decomposition, and filling along the joints. Personal communication with Dr. Fumagalli indicated, however, that these results were for low normal stress levels, well below 100 psi.

The material presently being used has an unconfined compression strength of about 550 psi. Complete data are not available, but it is believed that the unconfined strength can be varied from a low of approximately 250 psi to as high as a few thousand psi while maintaining the same angle of internal friction by varying the percentage of plaster of Paris in the mix. The value of 250 psi probably represents as low a value as is practical because of the difficulties involved in handling such a low strength material.

C. Model Loading Apparatus

Four major problems were encountered in the design of a loading apparatus to satisfy the design requirements:

1) the magnitude of the loads applied, resulting from the size of the loaded area,
2) the necessity of applying a uniformly distributed lateral pressure, even if uneven deformations develop,
3) the very small allowable deformation in the longitudinal direction (ideally none),
4) the development of large frictional forces over the loading faces.

Some of these problems can be expected to be magnified in larger models, while others will not. If the teflon sheets prove adequate in reducing friction during the actual model tests, the same method of friction reduction could probably be used on larger models with very little alteration of techniques. On larger models, the absolute magnitude of allowable longitudinal deformations would not be so small, but relative to the total magnitude of the forces and the size of the apparatus the problems in keeping deformations within tolerable limits will be just as difficult.

The magnitude of the reactions needed will increase as the square of the linear dimension, hence they can grow quite large on large models. Two basic concepts observed in the design of the present reaction frame should have application to a model loading frame of any size if it is a self-contained system:

1) reactions should be symmetrically supported with loads being carried as much as possible in direct tension or compression, rather than by moments in beams, and

2) the reactions in each direction should be supported independent of those in the other directions.

Following these concepts should reduce the amount of material required for the reaction frame and keep deformations to a minimum.

It is felt that the application of uniformly distributed lateral loads of the magnitude considered may best be accomplished by a mechanical system. Such a system has the advantages of being reliable (no worry about weaks or punctured membranes), adaptable to different tests and configurations, and able to give the required deformations. A lateral loading system of hydraulic flat jacks at first appears attractive, but to the author's knowledge, rectangular metal flat jacks with the required pressure and deformation capabilities are not standard items. Some sort of rubber bag may be capable of giving the desired results and is worthy of consideration in future work.

In the design of future model loading devices, consideration should be given to the possibility of orienting the model with the tunnel axis horizontal so that body forces may be simulated in the model. In such an apparatus it would be desirable to apply a load distribution approximating that shown in Fig. 1.

It is anticipated that it will be possible to make more definite recommendations concerning the model loading apparatus at the conclusion of the model testing program.

D. Instrumentation of the Model

Data available to date from cylinders tested triaxially with the internal SR4 gages suggests they will work quite satisfactorily. The technique for installing these gages is adapted to the requirement that the model must be made of compacted material, hence the gage must be placed after curing rather than having the material poured around the gage. This method of installing the internal gages is quite simple and should be easily adapted to instrumentation of larger models fabricated from individual joint blocks.

In jointed rock masses it would be expected that stresses might vary erratically from joint block to joint block, hence the radial extensometers may prove more valuable in measuring the behavior of a tunnel in a jointed mass. In the small models, the size of the radial extensometers will seriously restrict their use, but in larger models this should be much less of a problem, and the behavior of the tunnel could be monitored by miniature multiple position borehole extensometers. Herein lies a major advantage of larger models.

REFERENCES

Baker, W. E., and Dove, R. C., (1962), "Measurement of Internal Strains in a Bar Subjected to Longitudinal Impact," Proc. S.E.S.A., v. 19, pt. 2, pp. 307-311.

_____, (1963), "Construction and Evaluation of a Three-Dimensional Strain Rosette," Proc. S.E.S.A., v. 20, pt. 2, pp. 201-206.

Barron, K., (1962), "Some Aspects of Instrumentation for the Structural Model," Wabana Model Study, Rept. No. 7, Internal Rept. FMP 62/22-MIN, Fuels and Min. Prac. Div., Mines Br., Can. Dept. Mines and Tech. Surv.

Barron, K., and Larocque, G., (1962), "Development of a Model for a Mine Structure," Proc. Rock Mech. Symp., McGill Univ., Montreal, Sept. 7-8, 1962, pp. 145-190.

Bieniawski, Z. T., (1967), "Mechanism of Brittle Fracture of Rock," Int. Journ. Rock Mech. and Mining Sciences, Oct. 1967, pp. 395-430.

Brazier, R. I., and Dove, R. C., (1961), "Use of Electrical-Resistance Strain Elements in Three Dimensional Stress Analysis," Proc. S.E.S.A., v. 18, pt. 1, pp. 186-191.

Brooker, E. W., (1964), The Influence of Stress History on Certain Properties of Remolded Cohesive Soils, Ph.D. thesis, University of Illinois, 216 pp.

Caudle, R. D., and Clark, G. B., (1955), Stresses Around Mine Openings in Some Simple Geologic Structures, Univ. of Illinois, Eng. Exp. Sta., Bull. No. 430, Urbana, Illinois, 42 pp.

Corps of Engineers, MRD Lab, (1964), Tests for Strength Characteristics of Rock, Pile Driver Project, MRD Lab No. 64/90, Sept. 1964, Corps of Eng., U.S. Army, Mo. Riv. Div. Lab, Omaha, Neb.

_____, (1965), Tests for Strength Characteristics of a Schistose Gneiss, MRD Lab No. 64/126, May 1965, Corps of Eng., U.S. Army, Mo. Riv. Div. Lab., Omaha, Neb.

_____, (1966), Strength Parameters of Selected Intermediate Quality Rocks, MRD Lab No. 64/493, July 1966, Corps of Eng., U.S. Army, Mo. Riv. Div. Lab, Omaha, Neb.

Deere, D. U., and Hendron, A. J., (1965), Lecture notes from graduate courses in rock mechanics, Univ. of Ill.

Deere, D. U., and Miller, R. P., (1966), Engineering Classification and Index Properties for Intact Rock, Tech. Rept. No. AFWL-TR-65-116, Air Force Weap. Lab, Kirtland AFB, New Mexico, Dec., 1966.

Dove, R. C., (1955), "Strain Measurement Errors in Materials of Low Modulus," Proc. A.S.C.E., v. 81, Sep. 691, 10 pp.

Dove, R. C., Brazier, R. I., and Baker, W. E., (1962), "Selection of Gages for Strain Measurement at Interior Points," Proc. S.E.S.A., v. 19, pt. 1, pp. 189-190.

Eckel, E. C., (1922), Cements, Limes and Plasters, 2nd Ed., John Wiley and Sons, N. Y., 655 pp.

Everling, G., (1964), "Model Tests Concerning the Interaction of Ground and Roof Support in Gate-Roads," Int. Journ. Rock Mech. and Min. Sci., v. 1, n. 3, pp. 319-326.

Fumagalli, E., (1955), "Communication Sur Les Materiaux Pour Modeles Statiques De Barrages En Beton," 5th Int. Cong. on Large Dams, Paris, v. IV, c. 26, 1955, pp. 1039-1074.

_____, (1959), "Materiaux Pour Modeles Reduit et Installations de Charge," Madrid Symp. on Models of Structures, June 1959, in RILEM Bull. n. 8, Sept. 1960, pp. 27-40.

_____, (1960), "The Use of Models in Reinforced Concrete Structures," Mag. of Conc. Res., v. 12, n. 35, July 1960, pp. 63-72.

_____, (1964), "Modeles Geomecaniques des Reservoirs Artificiels: Materiaux, Technique D'essais, Exampler de Reproduction Sur Modeles," ISMES Pub. No. 26, Bergamo, Italy, Oct. 1964.

_____, (1967), Paper presented to short course in Rock Mech., Univ. of Swansea; April 1967, Proc. to be published.

Handin, J., and Hager, R. V., Jr., (1957), "Experimental Deformation of Sedimentary Rocks Under Confining Pressures: Tests at Room Temperature on Dry Samples," Bull. A.A.P.G., Vol. 41, No. 1, pp. 1-50, January 1957.

Handin, J., Hager, R. V., Jr., Friedman, M., and Feather, J. N., (1963), "Experimental Deformation of Sedimentary Rocks Under Confining Pressure: Pore Pressure Results," Bull. A.A.P.G., Vol. 47, No. 5, pp. 717-755, May 1963.

Hendron, A. J., Jr., (1963), The Behavior of Sand in One-Dimensional Compression, Tech. Doc. Rept. RTD-TDR-63-3089, Air Force Weapons Lab, Kirtland AFB, N. M., 285 pp.

Hobbs, D. W., (1966), "Scale Model Studies of Strata Movement Around Mine Roadways, Apparatus, Technique, and some Preliminary Results," Int. Journ. of Rock Mech. and Min. Sci., v. 3, n. 2, pp. 101-128, May, 1966.

Hoek, E., (1965), Rock Fracture Under Static Stress Conditions,"Nat. Mech. Eng. Res. Inst., Council for Sci. and Ind. Res., CSIR Rept. MEG 383, Pretoria, South Africa, Oct. 1965, 228 pp.

_____, (1967), "A Photoelastic Technique for the Determination of Potential Fracture Zones," Failure and Breakage of Rock, 8th Symposium on Rock Mech., pp. 94-112, Soc. of Mining Eng. of A.I.M.E.

Horn, H. M., and Deere, D. U., (1962), "Frictional Characteristics of Minerals: Geotechnique, V. XII, pp. 319-335.

Jeager, J. C., (1959), "The Frictional Properties of Joints in Rock," Geofisica Pura e Applicata, Milano, v. 43, p. 148.

_____, (1962), Elasticity, Fracture, and Flow, Methuen and Co. Ltd, London, 2nd Ed., 212 pp.

Ladoo and Myers, (1951), Non-Metallic Minerals, 2nd Ed., McGraw-Hill, 605 pp.

Lane, K. S., and W. J. Heck, (1964), "Triaxial Testing for Strength of Rock Joints," Sixth Symp. on Rock Mech., Univ. of Missouri, pp. 98-108.

Langhaar, H. L., (1951), Dimensional Analysis and Theory of Models, John Wiley and Sons, Inc., New York, 166 pp.

Loh, Y. C., (1954), "Internal Stress Gages for Cementitious Materials," Proc. S.E.S.A., v. 11, pt. 2, pp. 13-28.

Mandel, J., (1964), "Tests on Reduced Scale Models in Soil and Rock Mechanics, A Study of the Conditions of Similitude," Int. Journ. Rock Mech. and Min. Sci., v. 1, n. 1, pp. 31-42.

Mindlin, R. D., (1939), "Stress Distribution Around a Tunnel," Proc. A.S.C.E., pp. 619-642, April 1939 (Also in Trans. A.S.C.E., v. 105, pp. 1117-1140, 1940).

Muller, L., and Pacher, F., (1965), "Modellversuche zur Klarung der Bruchgefahr geklufteter Medien," Safety in Rock Engineering, 15th Symp. of Aust. Reg. Group of Int. Soc. for Rock Mech., in Felsmechanik and Ingenieurgelogie, Supp. II, 1965, pp. 7-24.

Murphy, G., (1950), Similitude in Engineering, Ronald Press, N. Y., 302 pp.

Nadai, A., (1950), Theory of Flow and Fracture of Solids, 2 vol., McGraw-Hill.

Obert, L., and Duvall, W. I., (1967), Rock Mechanics and the Design of Structures in Rock, John Wiley and Sons, New York, 650 pp.

Panek, L. A., (1951), Stresses About Mine Openings in a Homogeneous Rock Body, New York, 50 pp.

Patton, F. D., (1966), Multiple Modes of Shear Failure in Rock and Related Materials, Ph.D. Thesis, Univ. of Illinois.

Polacek, W., (1967), private communication concerning undergraduate research at the Univ. of Illinois, sponsored by NSF, under general guidance of the authors.

Preece, B. W., and Davies, J. W., (1964), Models for Structural Concrete, C. R. Books Ltd., London, 1964, 252 pp.

Raphael, J. M., (1960), Structural Model Investigations for Oroville Dam, Series 100, Issue 6, Inst. of Engr. Res., Univ. of Calif., Berkeley, Feb. 1960, 164 pp.

Reyes, S. F., (1966), Elastic-Plastic Analysis of Underground Openings by the Finite Element Method, Ph.D. Thesis, Univ. of Illinois.

Robertson, E. C., (1955), "Experimental Study of the Strength of Rocks," Bull. G.S.A., Vol. 66, pp. 1275-1314, October 1955.

Rocha, M., (1958), "Model Tests in Portugal," Civ. Engr. and Pub. Work Rev., v. 53, n. 619, Jan. 1958, pp. 49-53, and n. 620, Feb. 1958, pp. 179-182.

_____, (1965), "Structural Model Techniques - Some Recent Developments," Chapr. 16, pp. 385-424 in Stress Analysis by Zienkiewicz and Hollister, (1965), John Wiley and Sons, Ltd.

Rocha, M., and Serafim, J. L., (1955), "Analysis of Concrete Dams by Model Tests," 5th Int. Cong. on Large Dams, v. 4, comm. 36, pp. 1307-1344.

Rosenblad, J. L., (1967), Personal communication concerning research being conducted at U.S. Army Corps of Engr., Mo. Riv. Div. Lab, Omaha, Neb.

Seely, F. B., and Smith, J. O., Jr., (1952), Advanced Mechanics of Materials, John Wiley and Sons, New York, 680 pp.

Terzaghi, K., (1943), Theoretical Soil Mechanics, John Wiley and Sons, New York, 510 pp.

Terzaghi, K., and Richart, F. E., Jr., (1952), "Stresses in Rock About Cavities," Geotechnique, v. 3, pp. 57-90.

Timoshenko, S., and Goodier, J. N., (1951), Theory of Elasticity, McGraw-Hill Book Co., New York.

White, A. H., (1926), "Volume Changes in Gypsum Structures Due to Atmospheric Humidity," Eng. Res. Bull. No. 2, Univ. of Michigan, Dept. of Eng. Res.

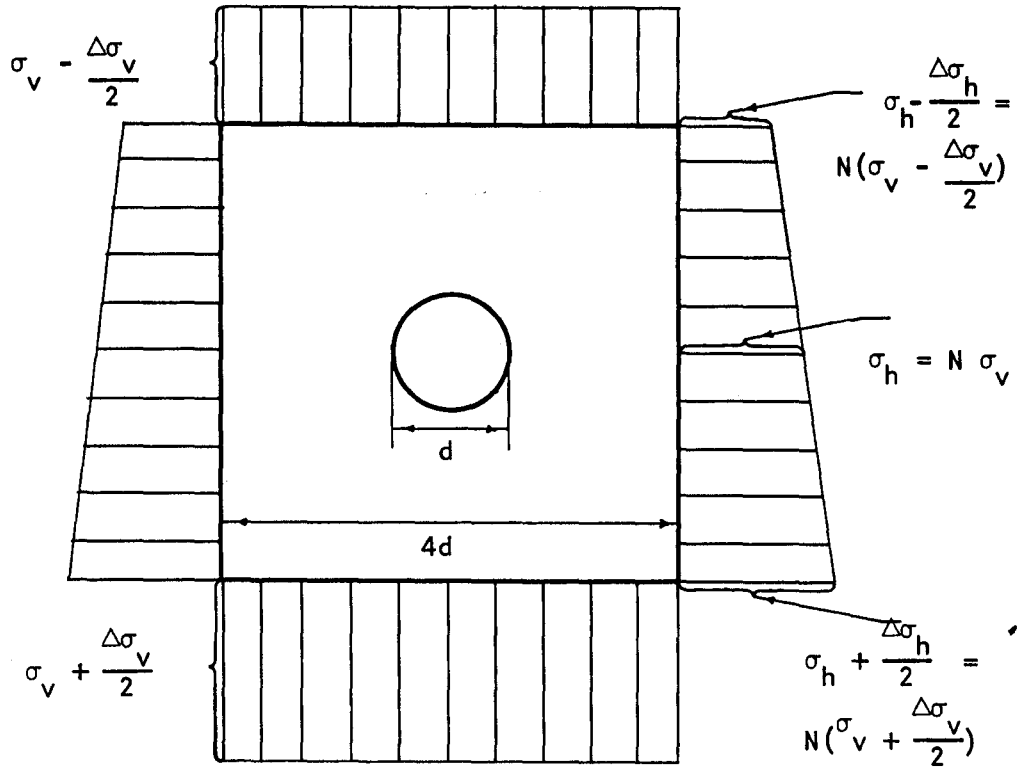

Figure 1 Stress Distribution Some Distance From Tunnel

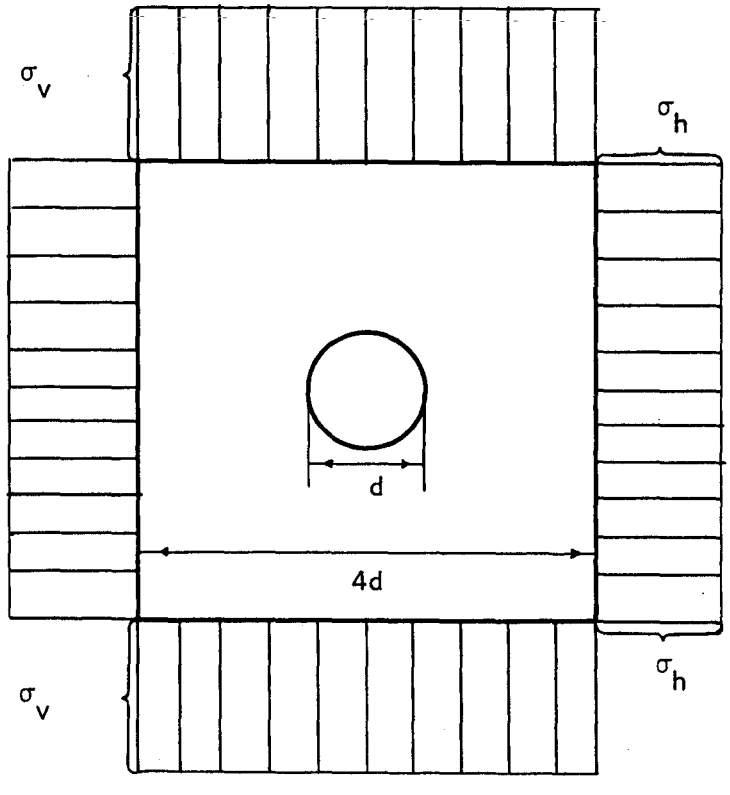

Figure 2 Approximate Stress Distribution Some Distance From Tunnel

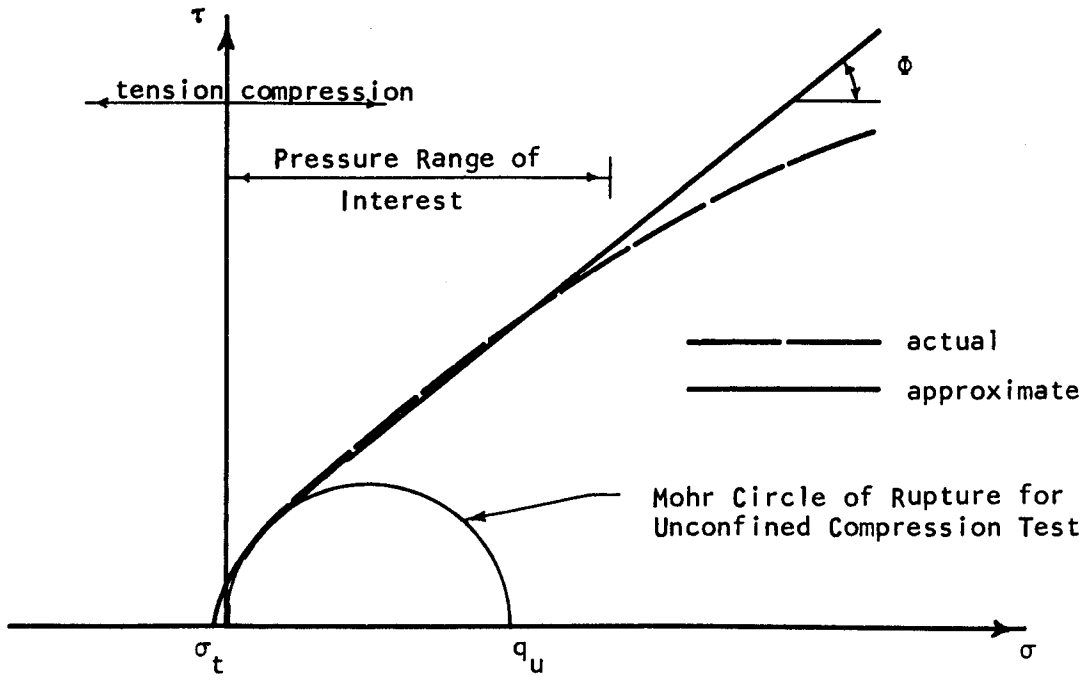

Figure 3 Failure Envelope Considered Typical For Rock

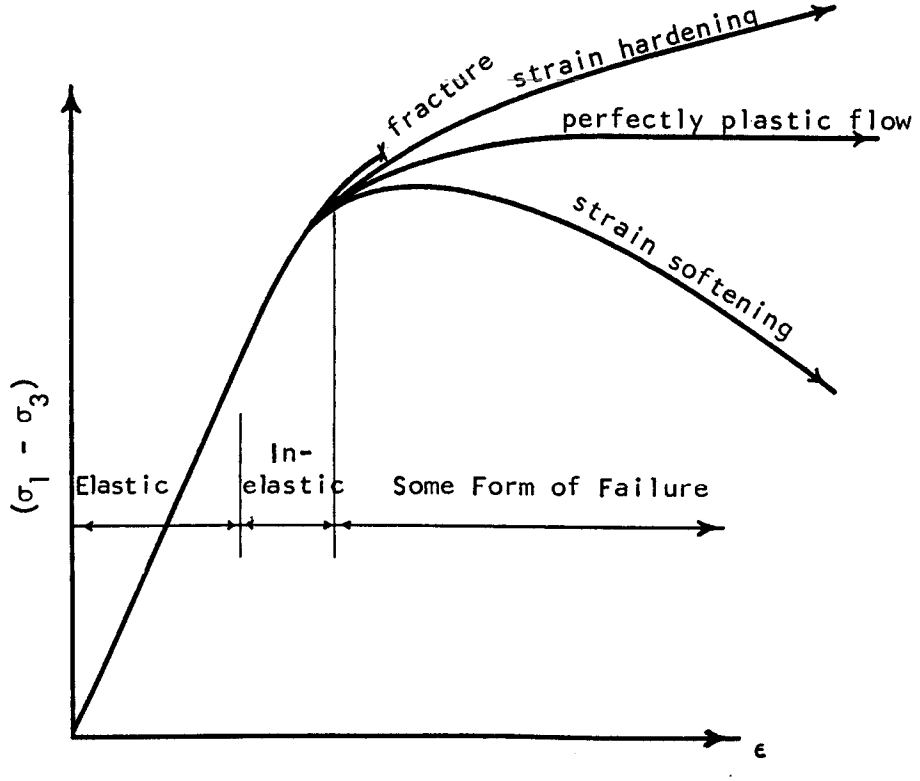

Figure 4 Stress-Strain Curve Considered Typical for Rock

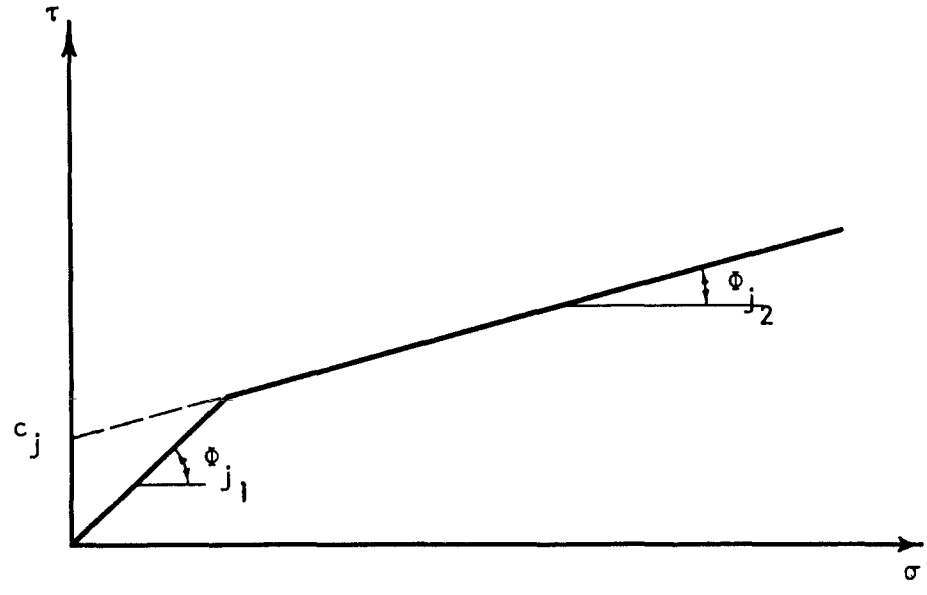

Figure 5 Typical Failure Envelope Along Rock Mass Discontinuities

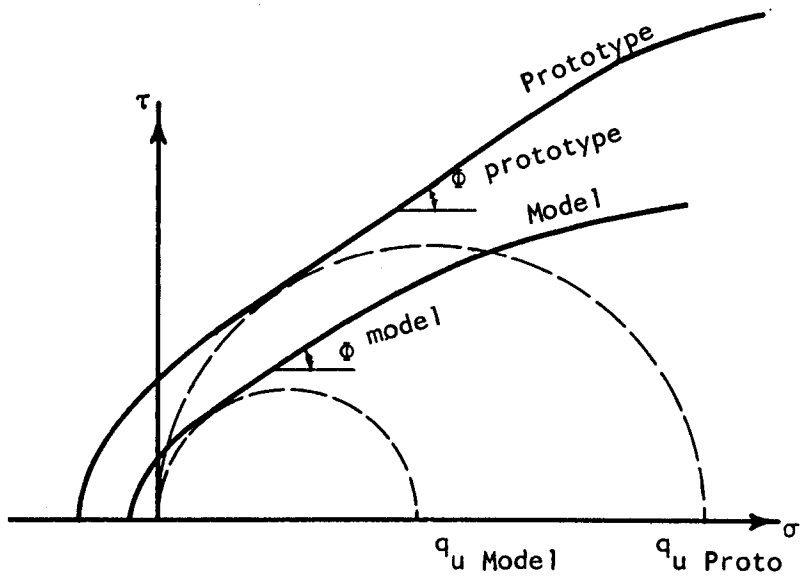

Figure 6 Prototype and Model Mohr Envelopes

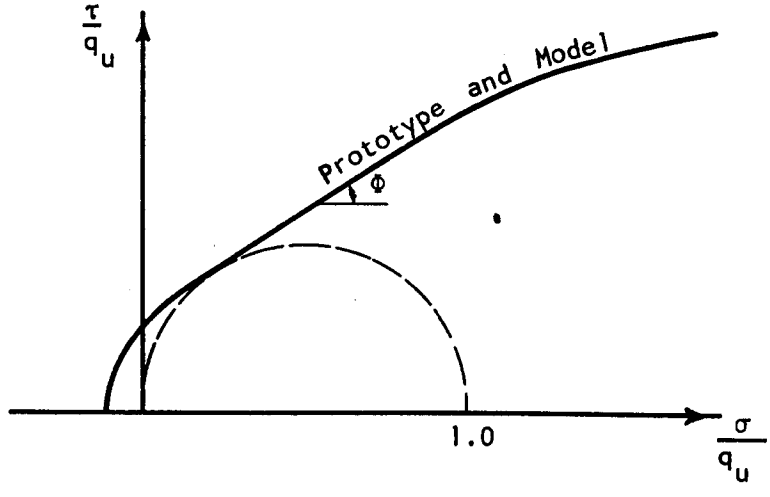

Figure 7 Dimensionless Prototype and Model Mohr Envelopes

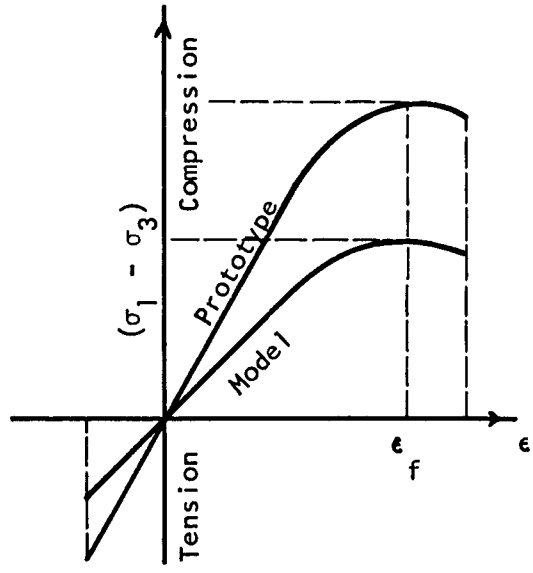

Figure 8 Prototype and Model Stress-Strain Curves

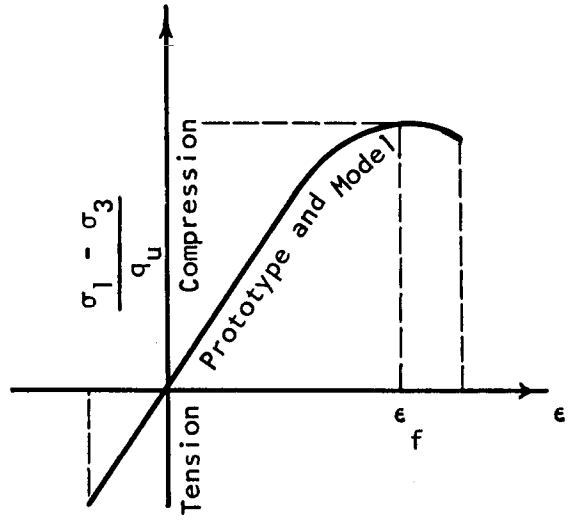

Figure 9 Dimensionless Prototype and Model Stress-Strain Curve

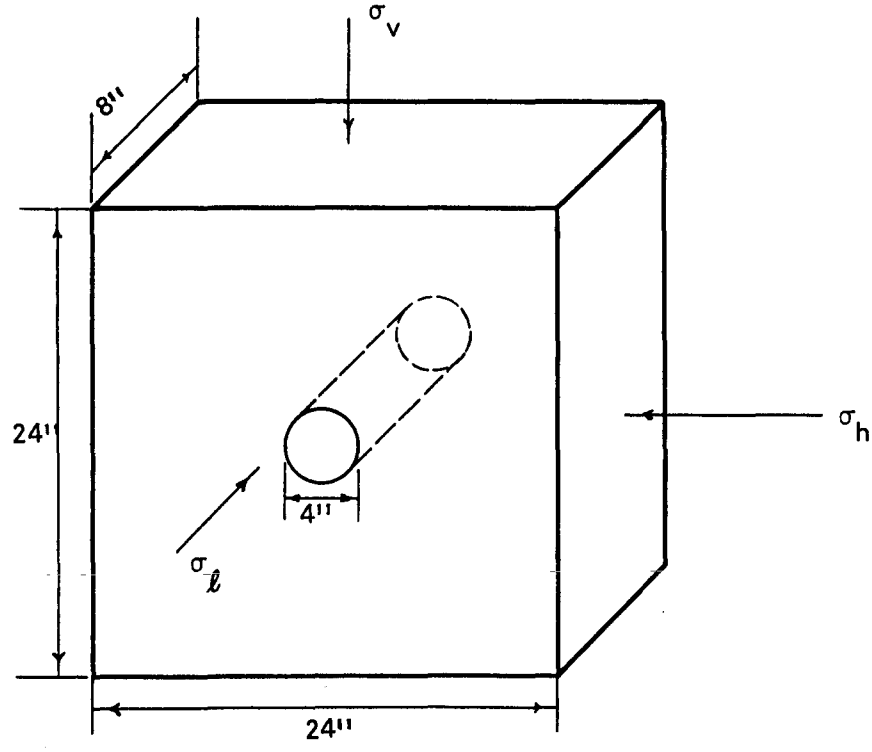

Figure 10 Proposed Model Block

Figure 11 Retarding Effect of $Na_2 HPO_4$ on Water/Plaster/ Kaolinite Mixtures of 2/1/2

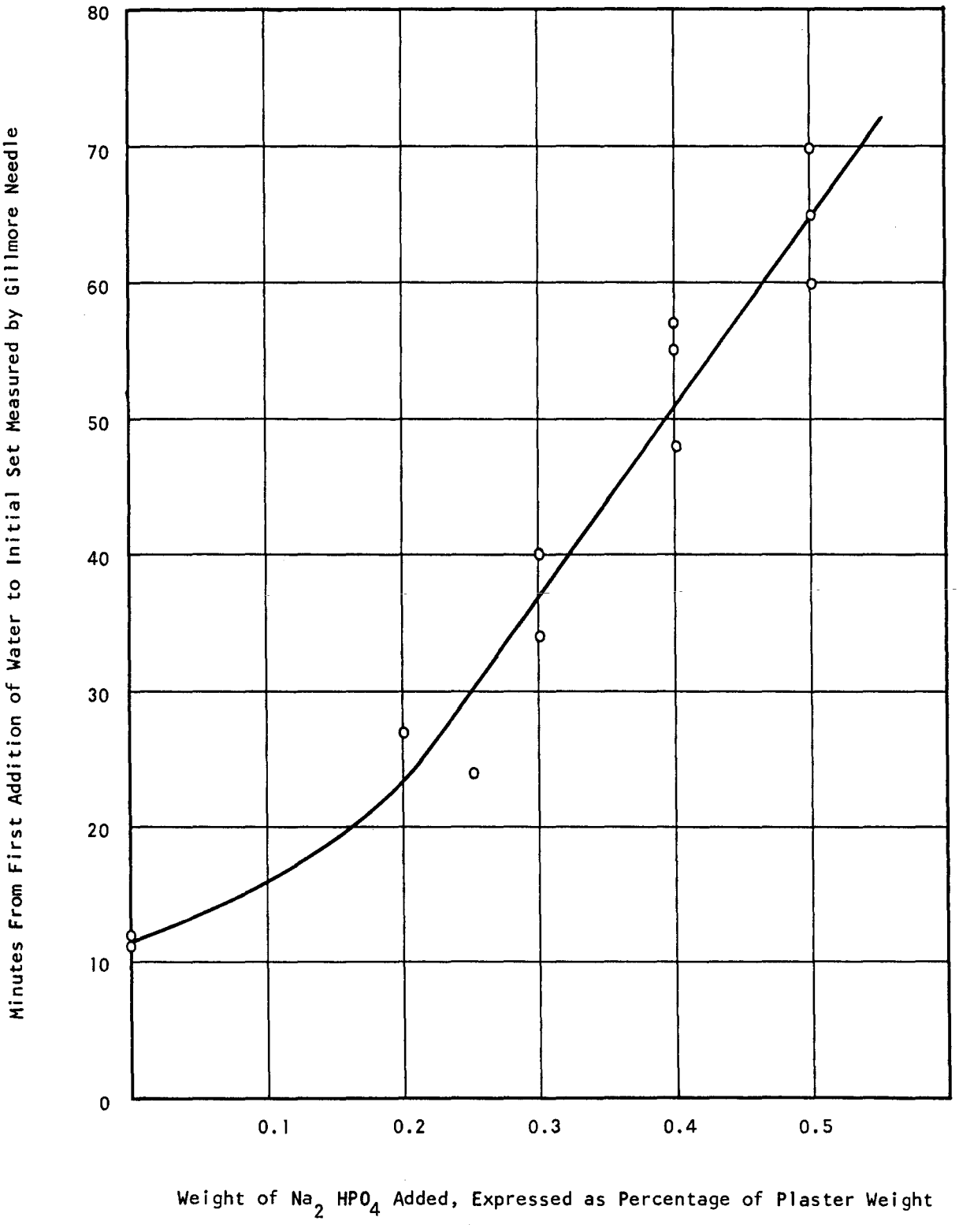

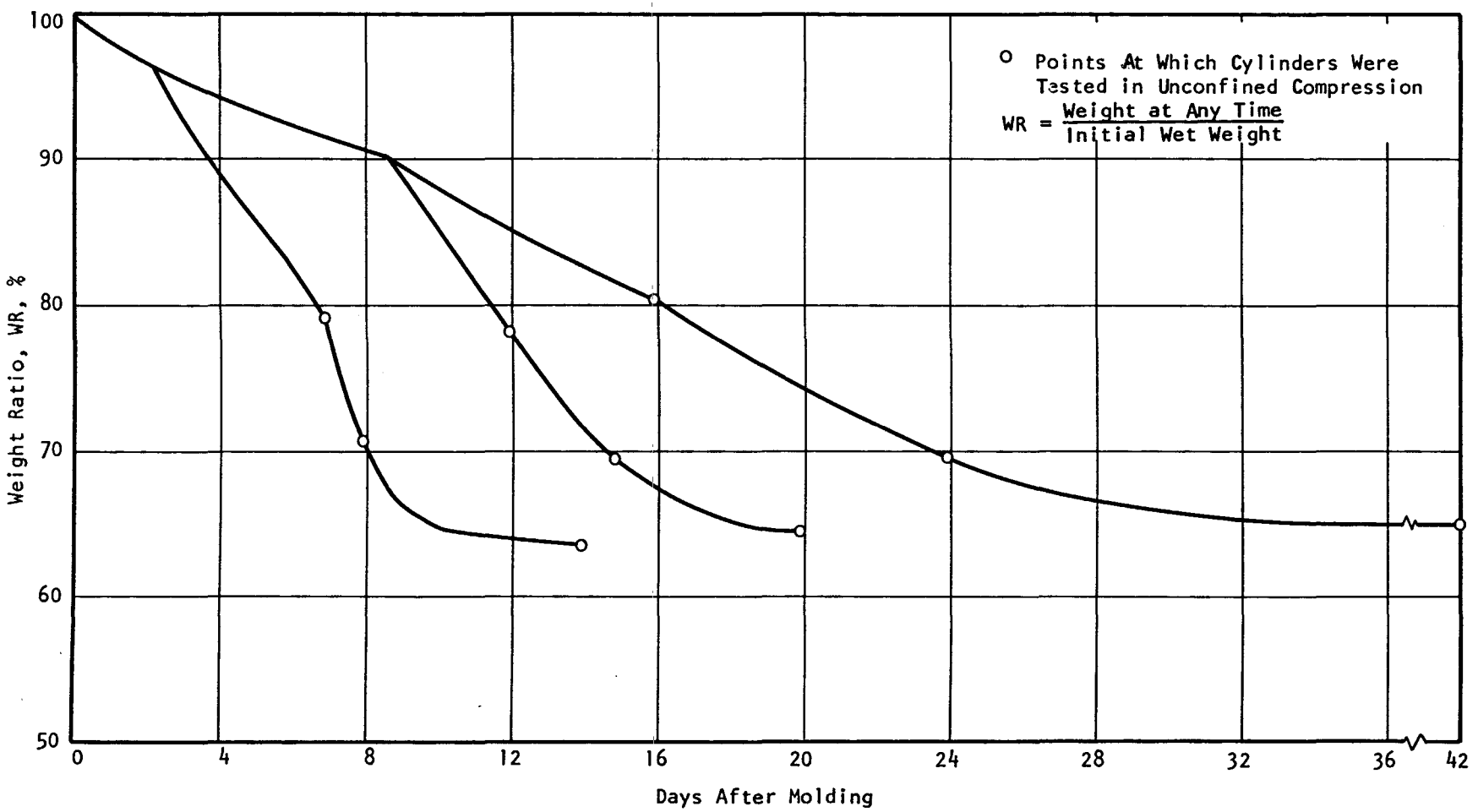

Figure 12

Cylinder Drying Curves in Air

Figure 13 Effect of Different Oven Temperatures Upon Drying Curves of Cylinders

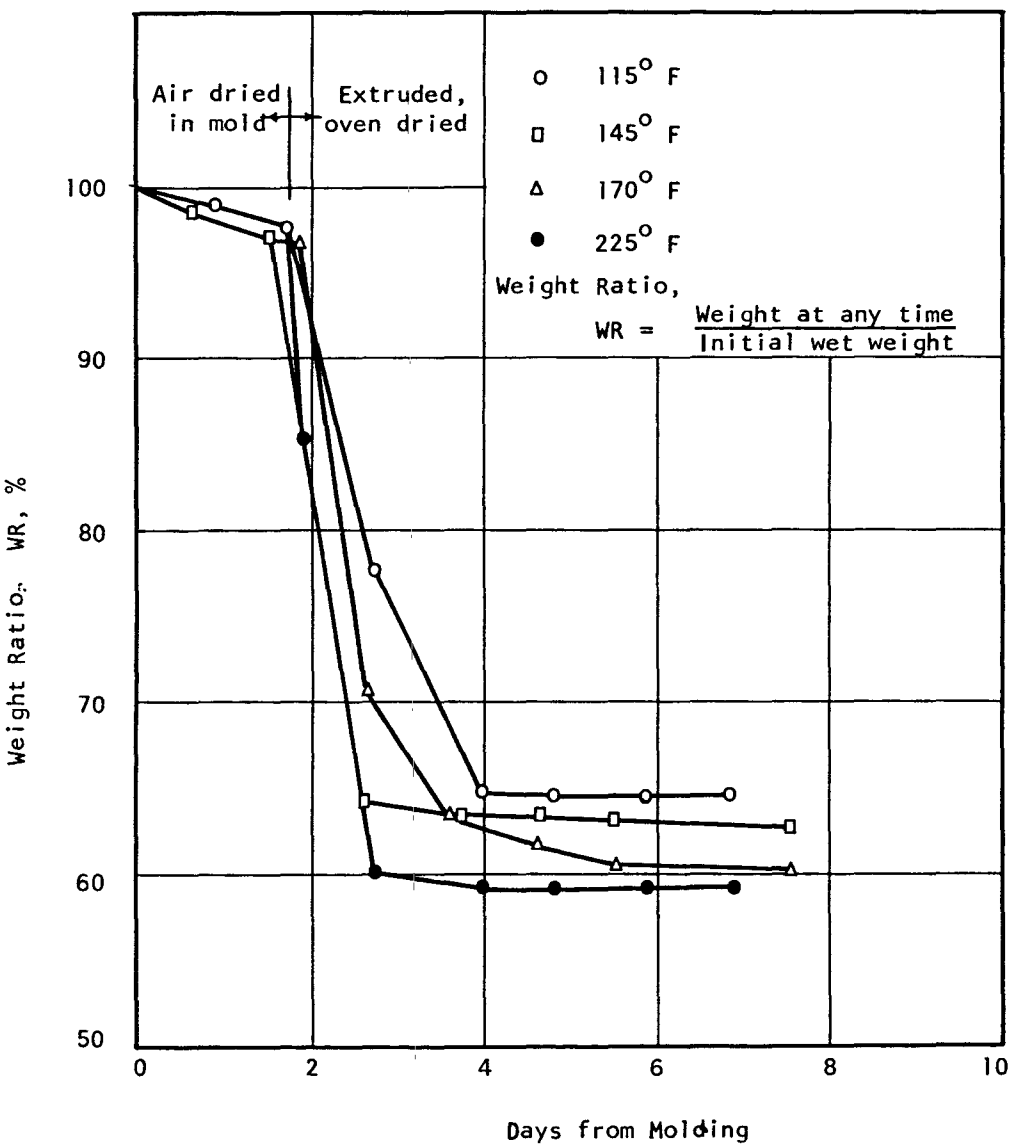

Figure 14 Drying Curves of "Large" Volumes Weight Ratio, WR, = $\frac{\text{weight at any time}}{\text{initial wet weight}}$

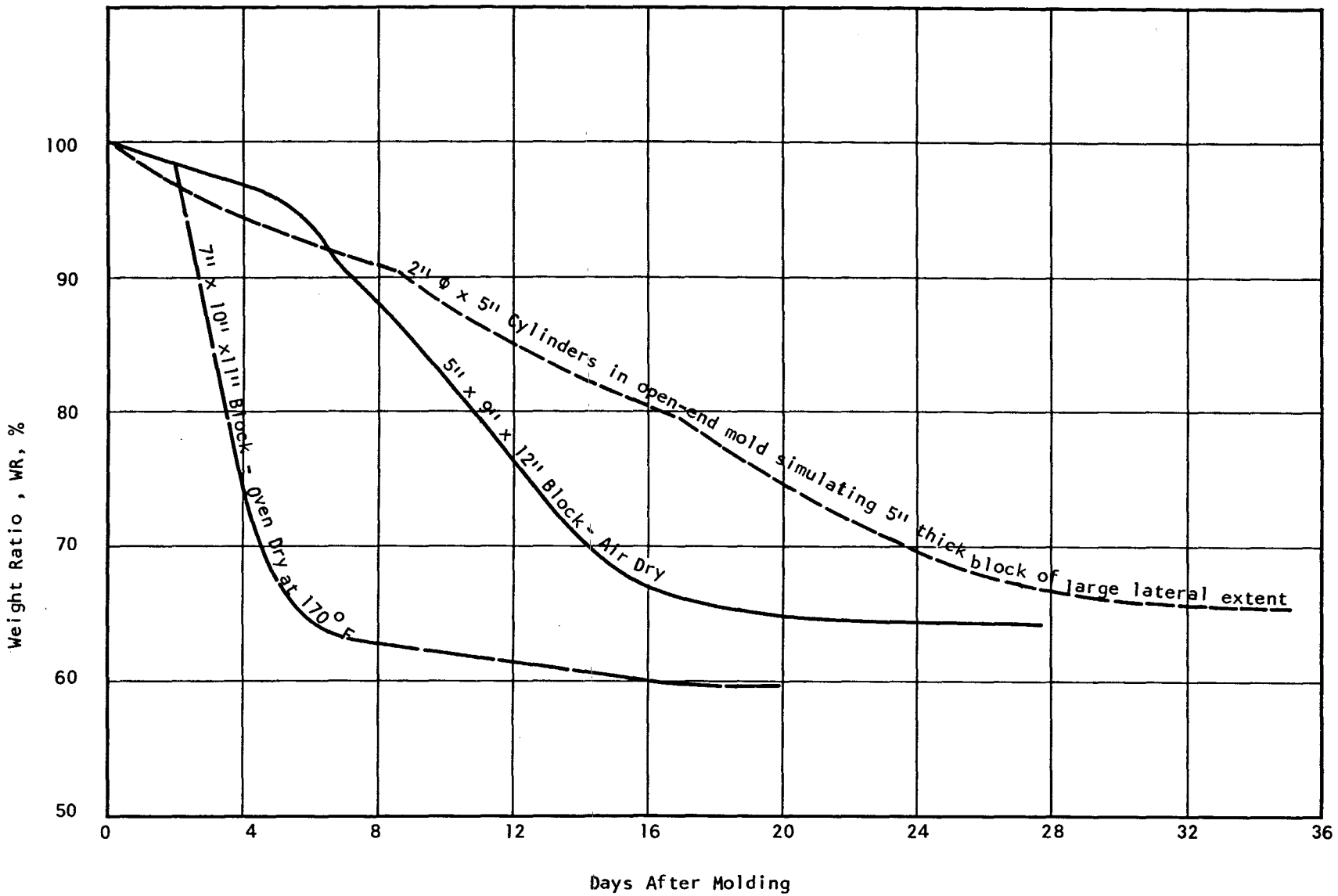

Figure 15 Water Content Profiles During Drying in Oven 7" x 10" x 11" Block at 170° F

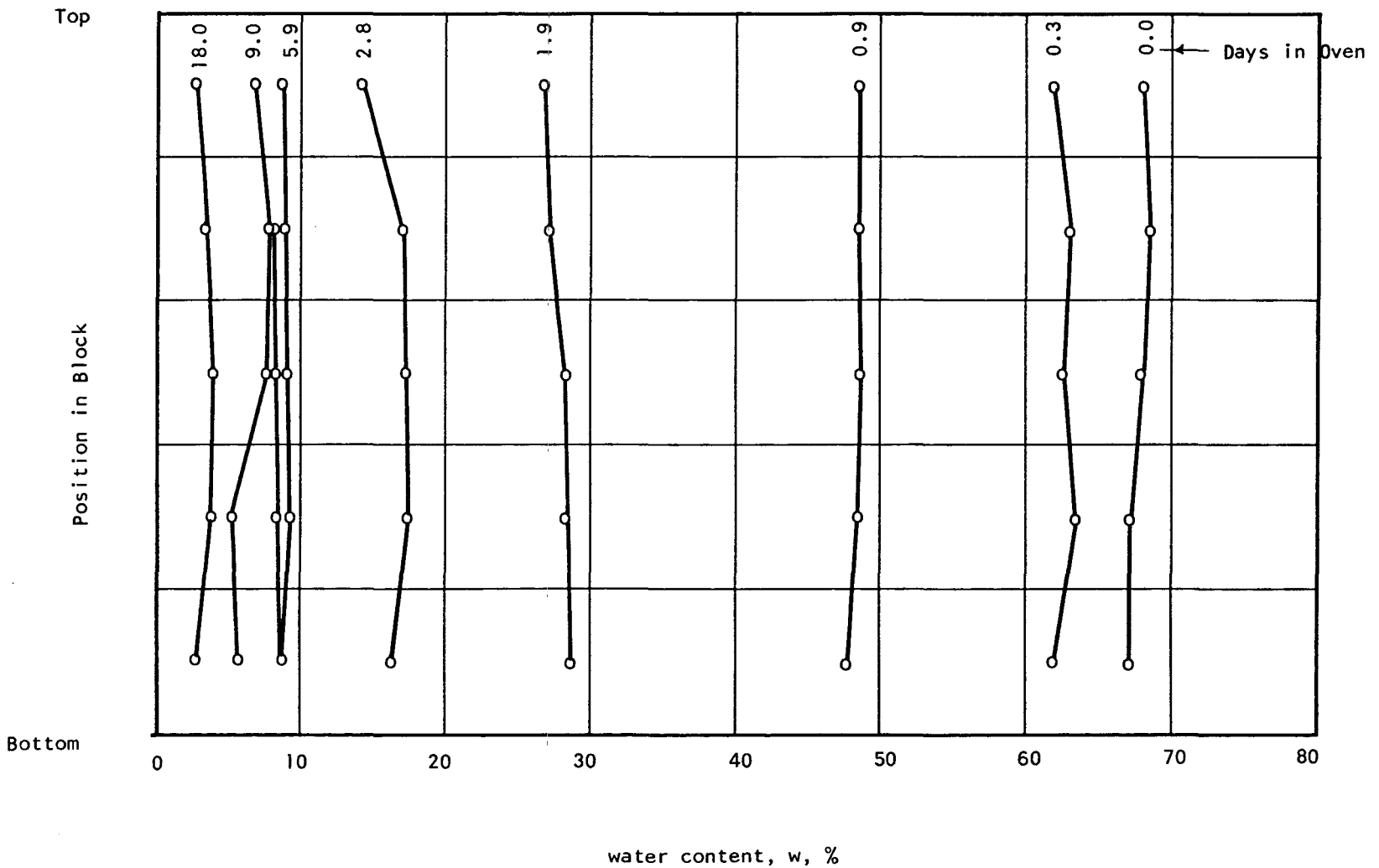

Figure 16 Cylinder Drying Curves

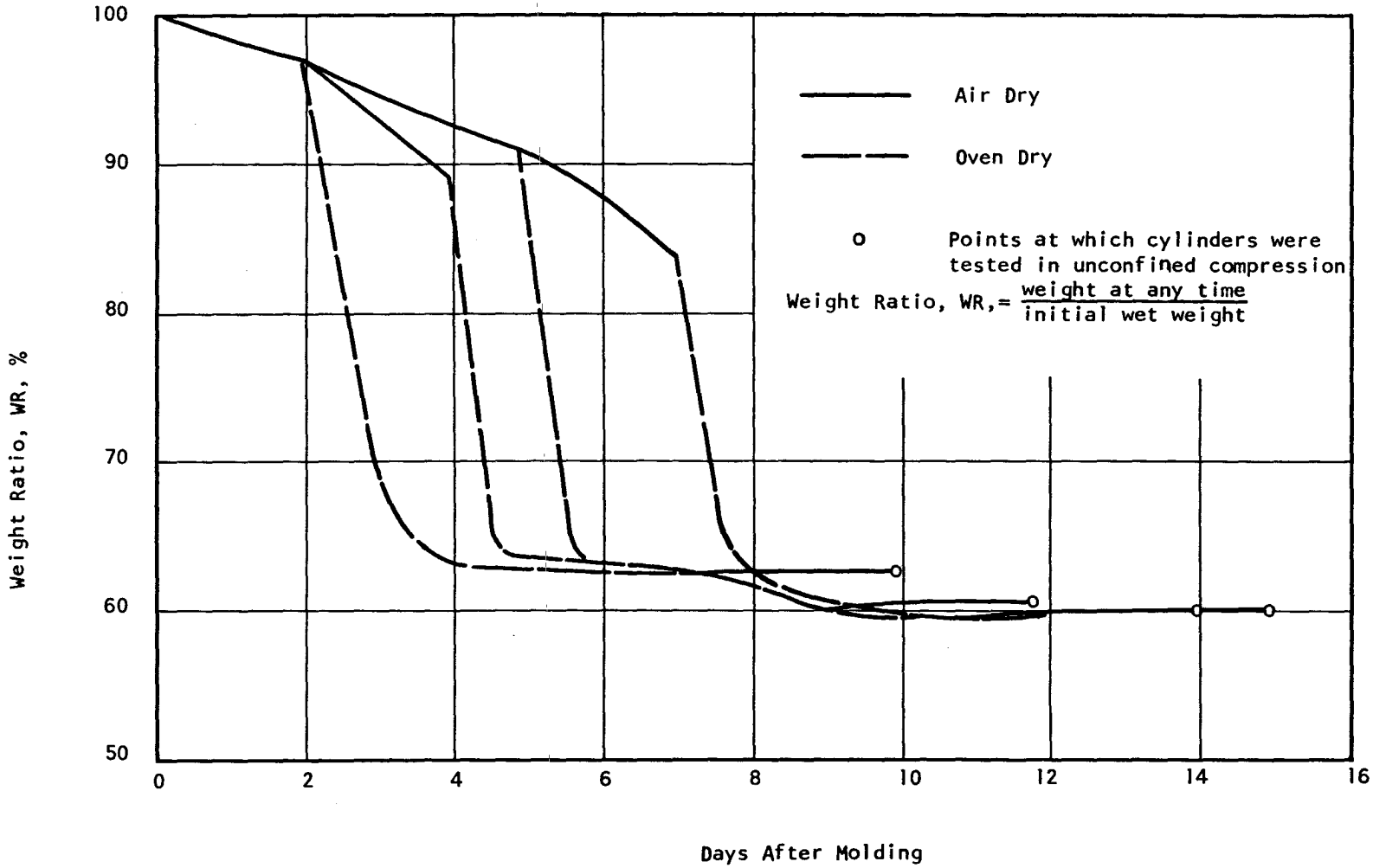

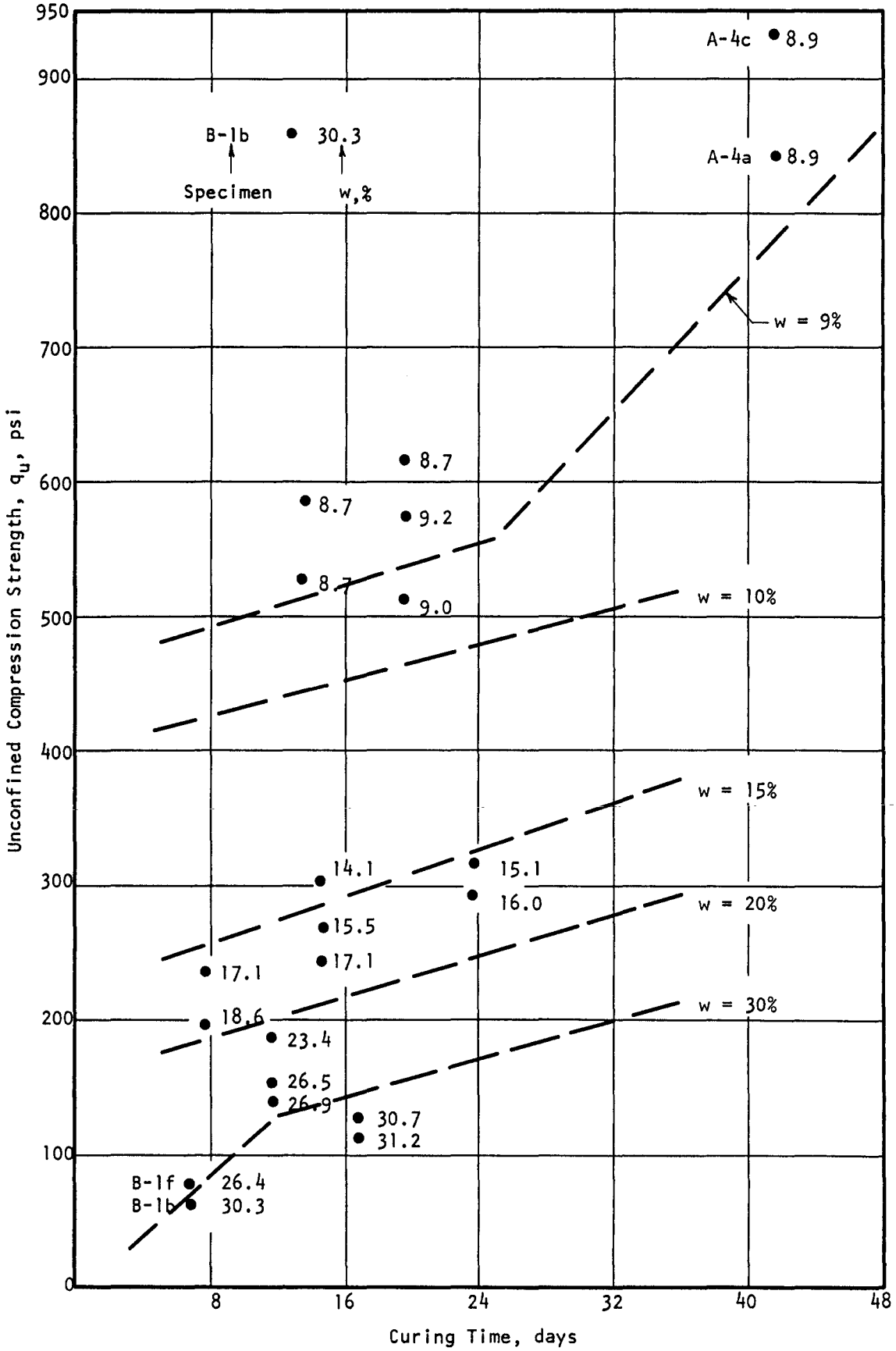

Figure 17

Unconfined Compression Strength vs Curing Time, Air Dried Cylinders

Figure 18 Unconfined Compression Strength vs. Water Content

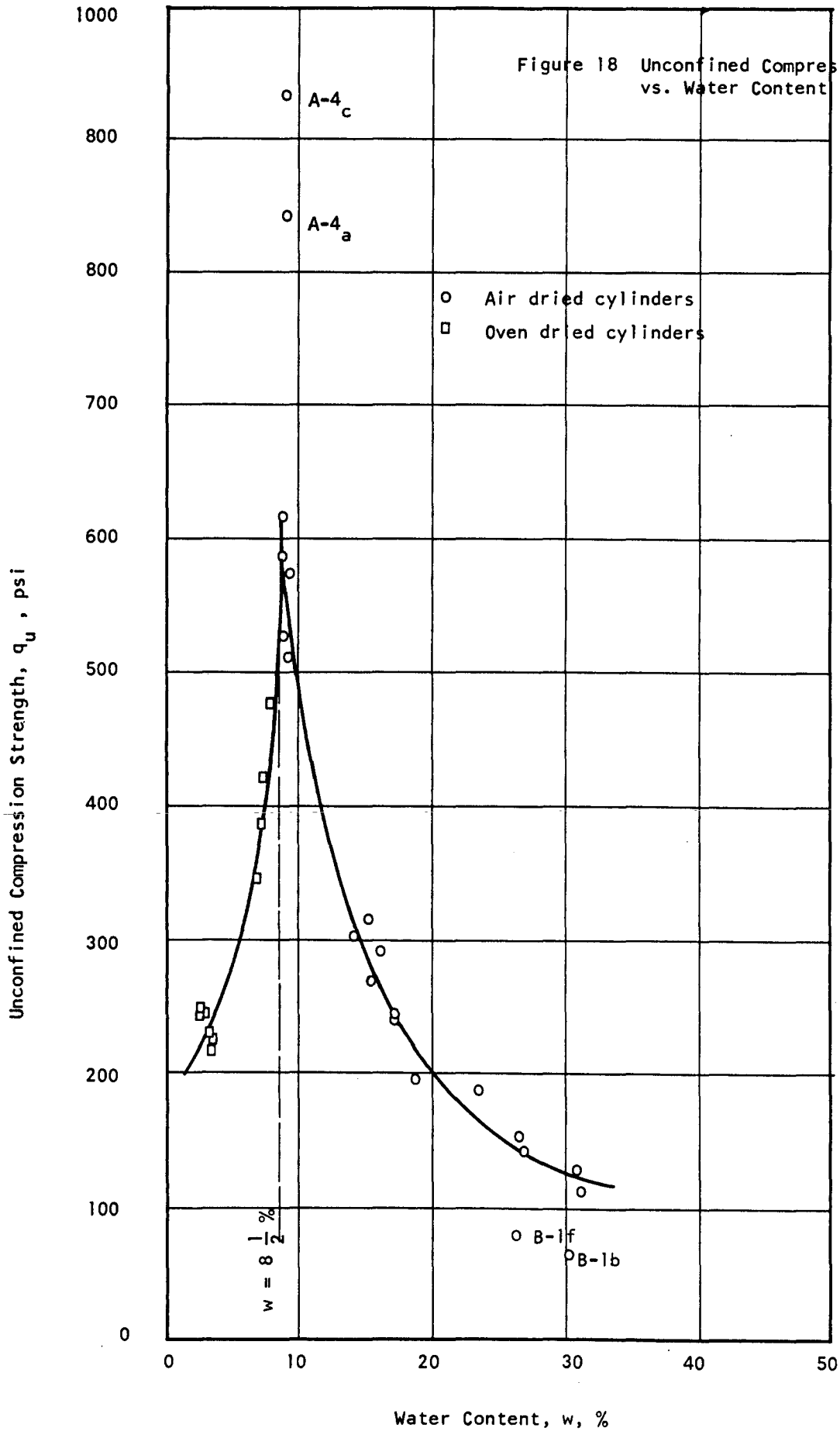

Figure 19 Failure Strain vs Water Content
Unconfined Compression

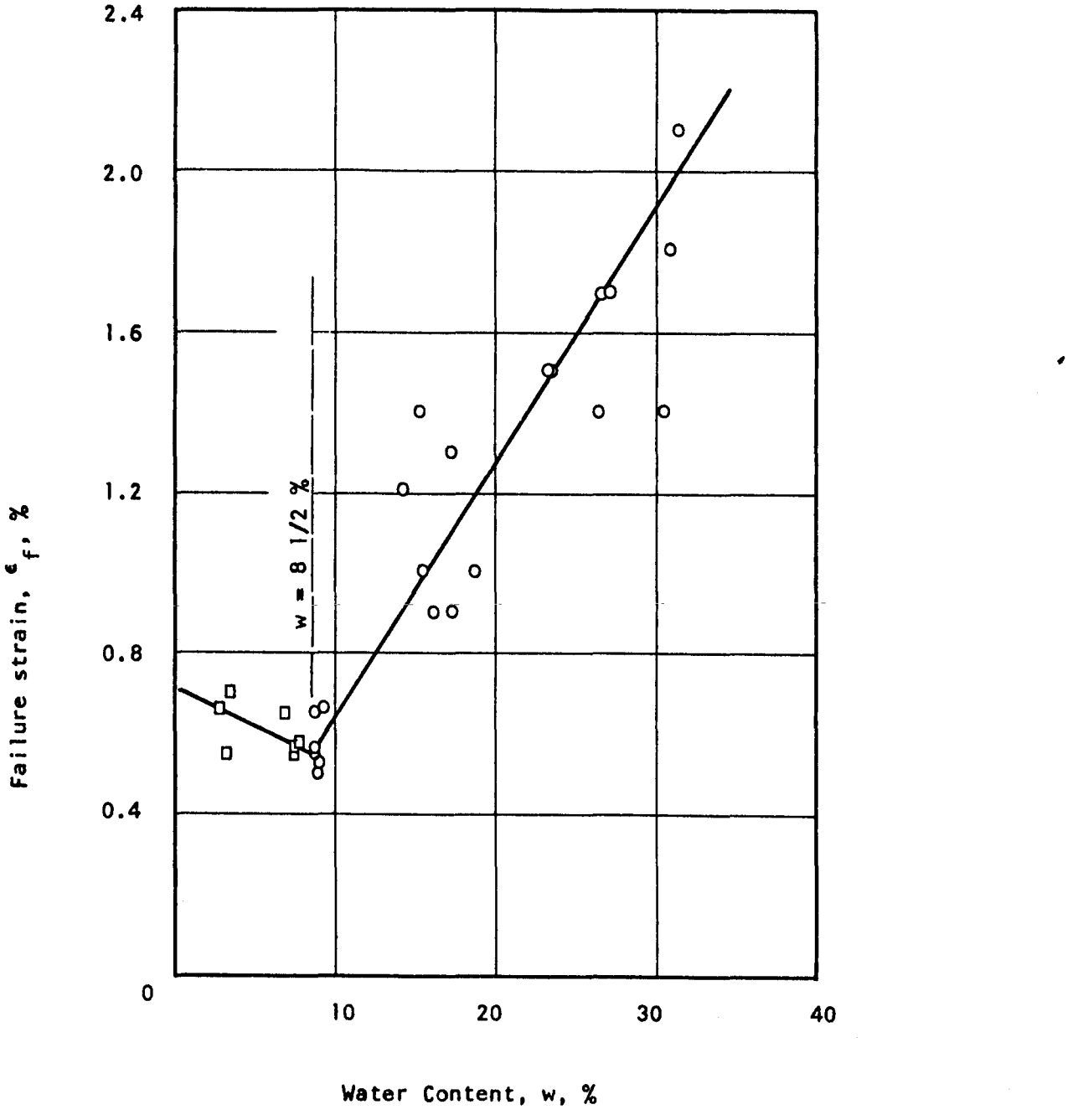

Figure 20 Typical Stress-Strain Curves Unconfined Compression

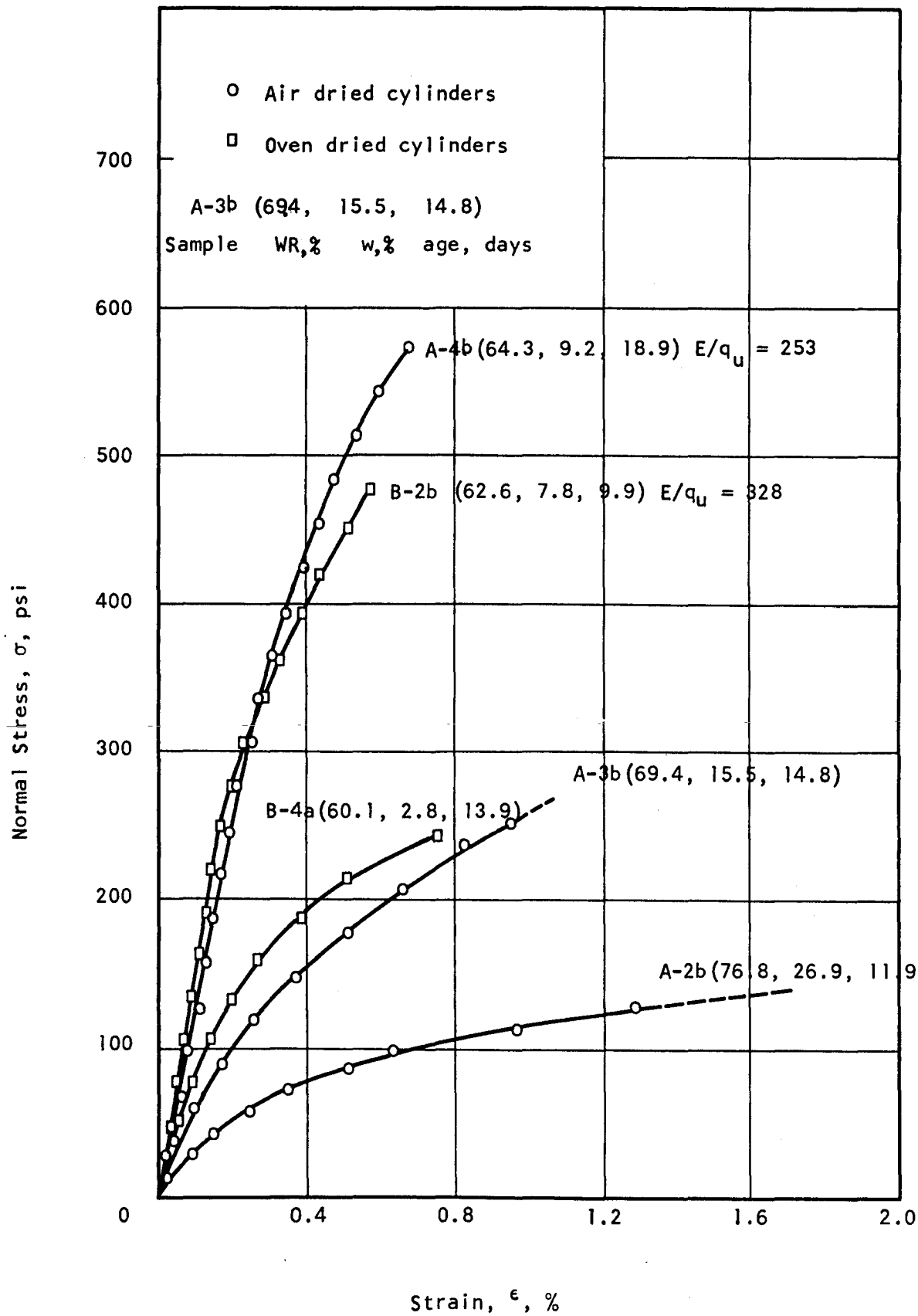

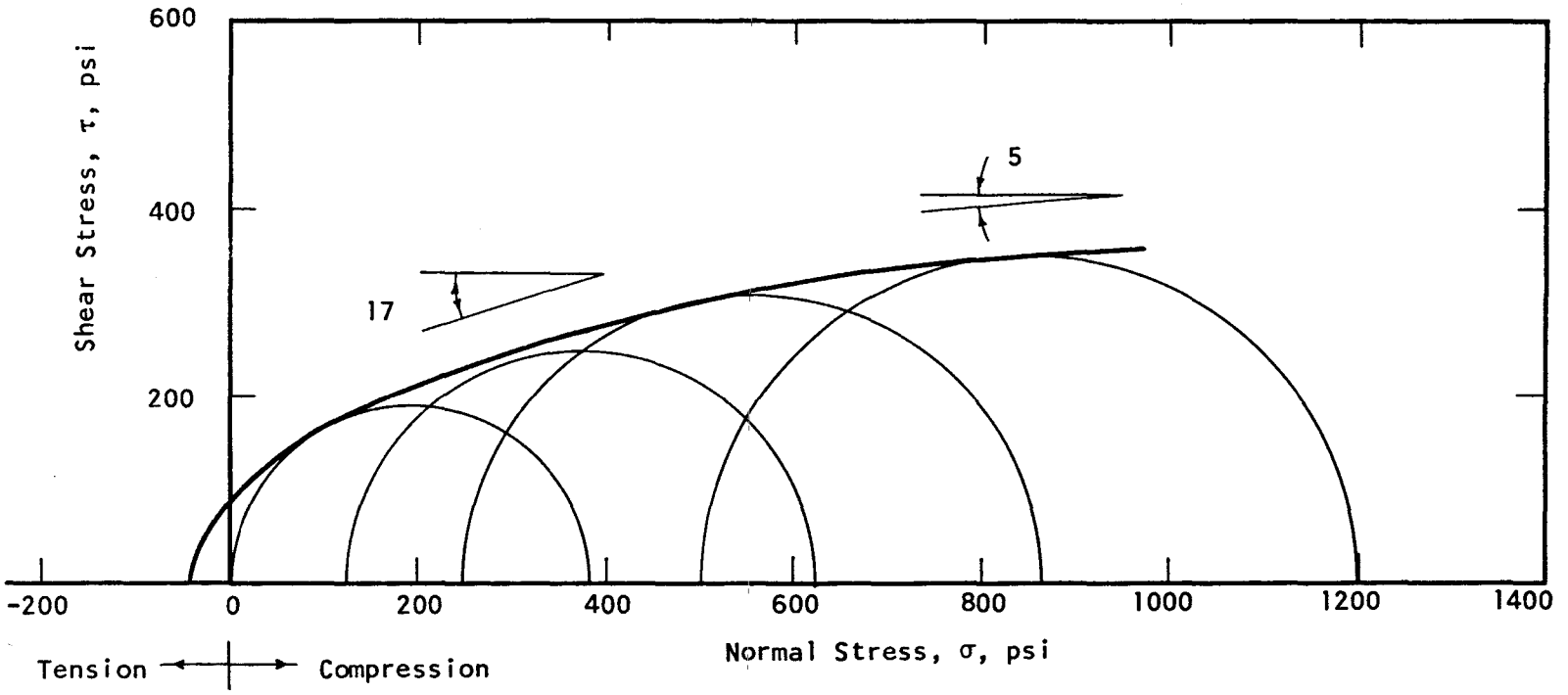

Figured 21 Mohr Envelope - Triaxial Compression
Water/Plaster/Kaolinite/Na_2HPo_4 Mixture
of 2/1/2/.005

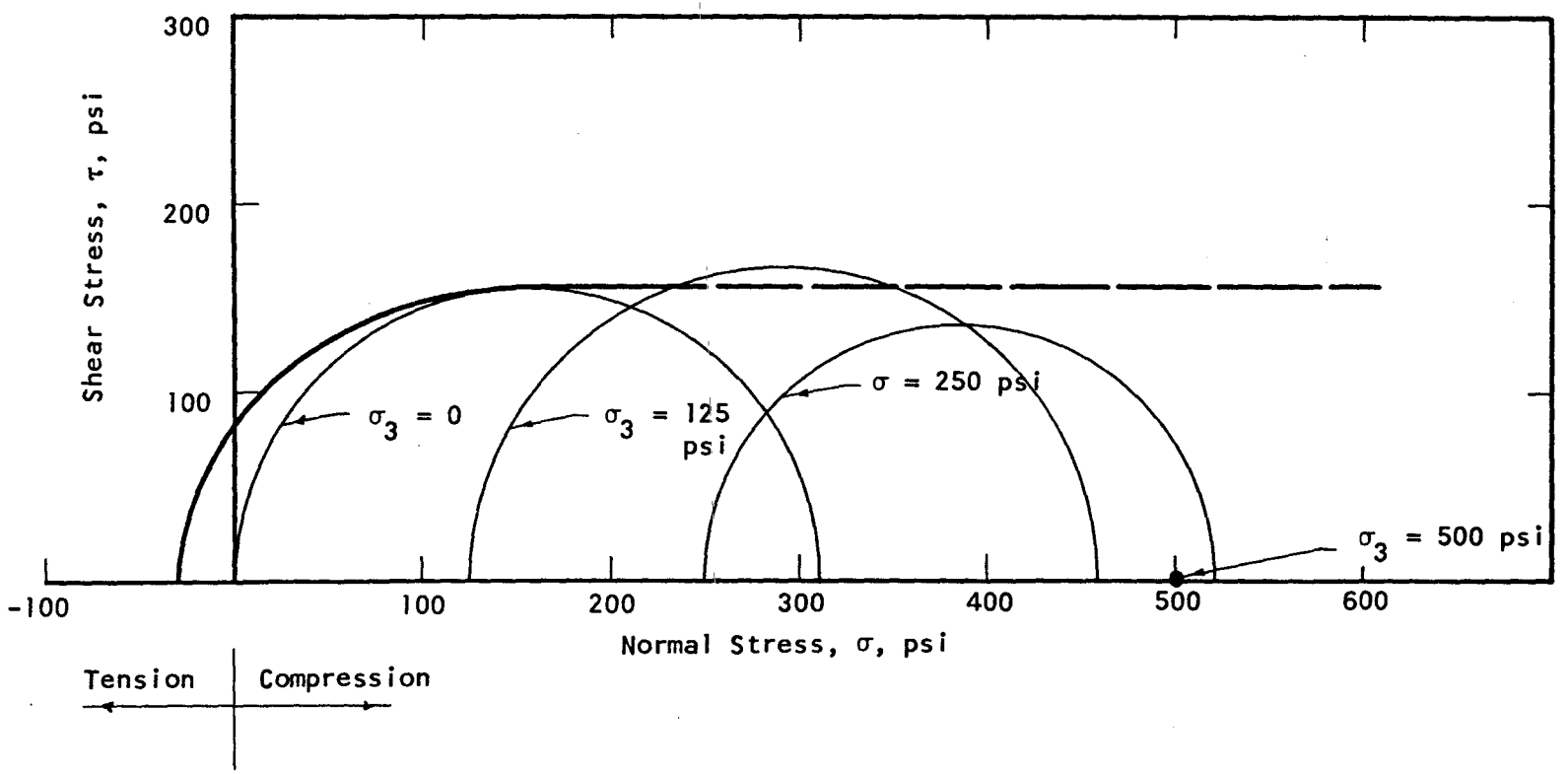

Figure 22 Mohr Envelope - Triaxial Compression Water/Plaster/Diatomite Mixture of 2/1/0.7

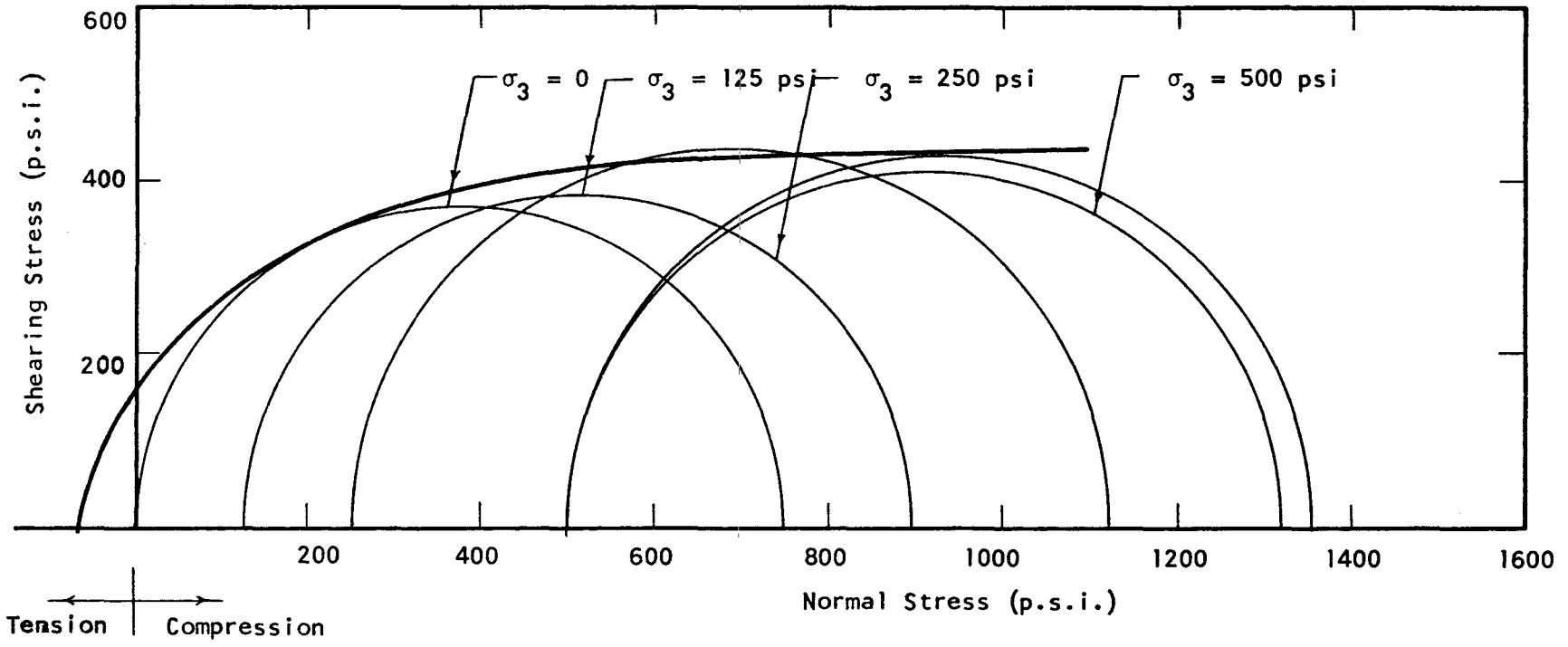

Figure 23 Mohr Envelope - Triaxial Compression
Water/Plaster/Kaolinite/Sand Mixture
of 2/1.6/1/7

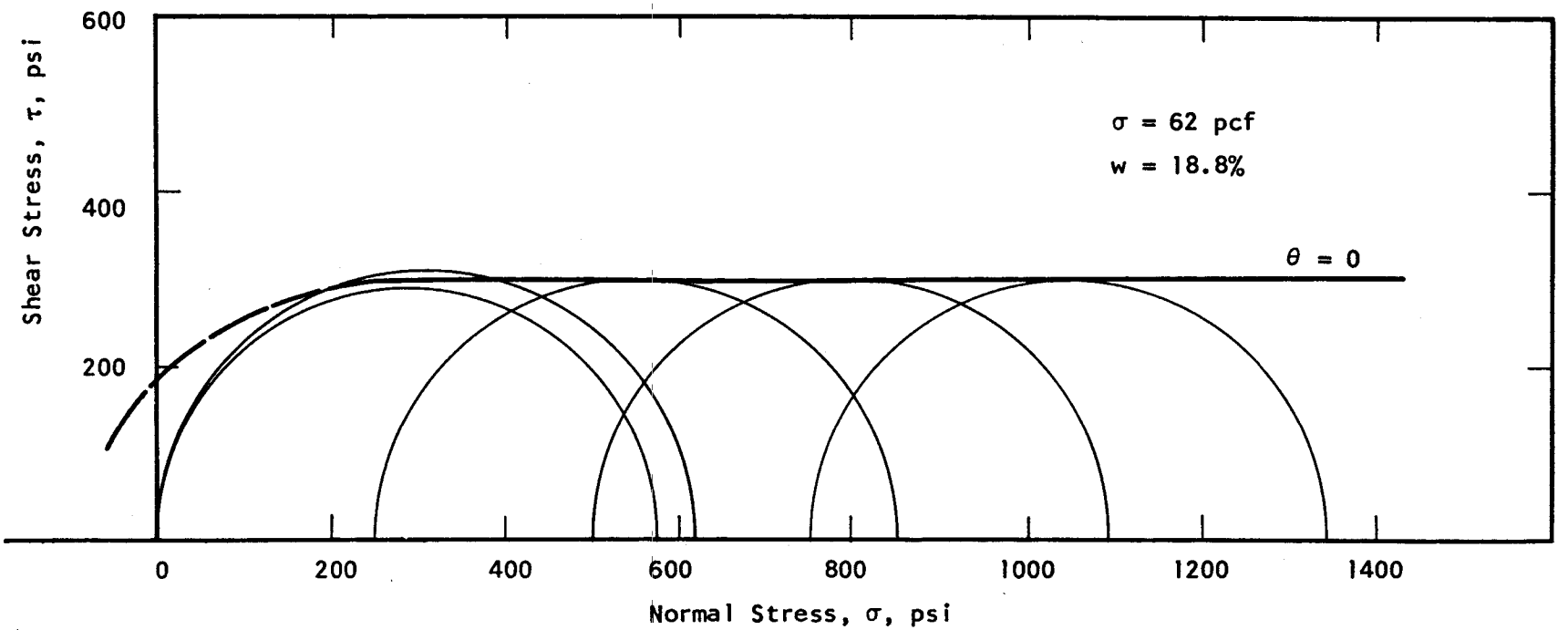

Figure 24 Mohr Envelope - Triaxial Compression
Water/Plaster Mixture of 1.2/1.0

Figure 25 Grain Size Distribution of Different Sands Tested

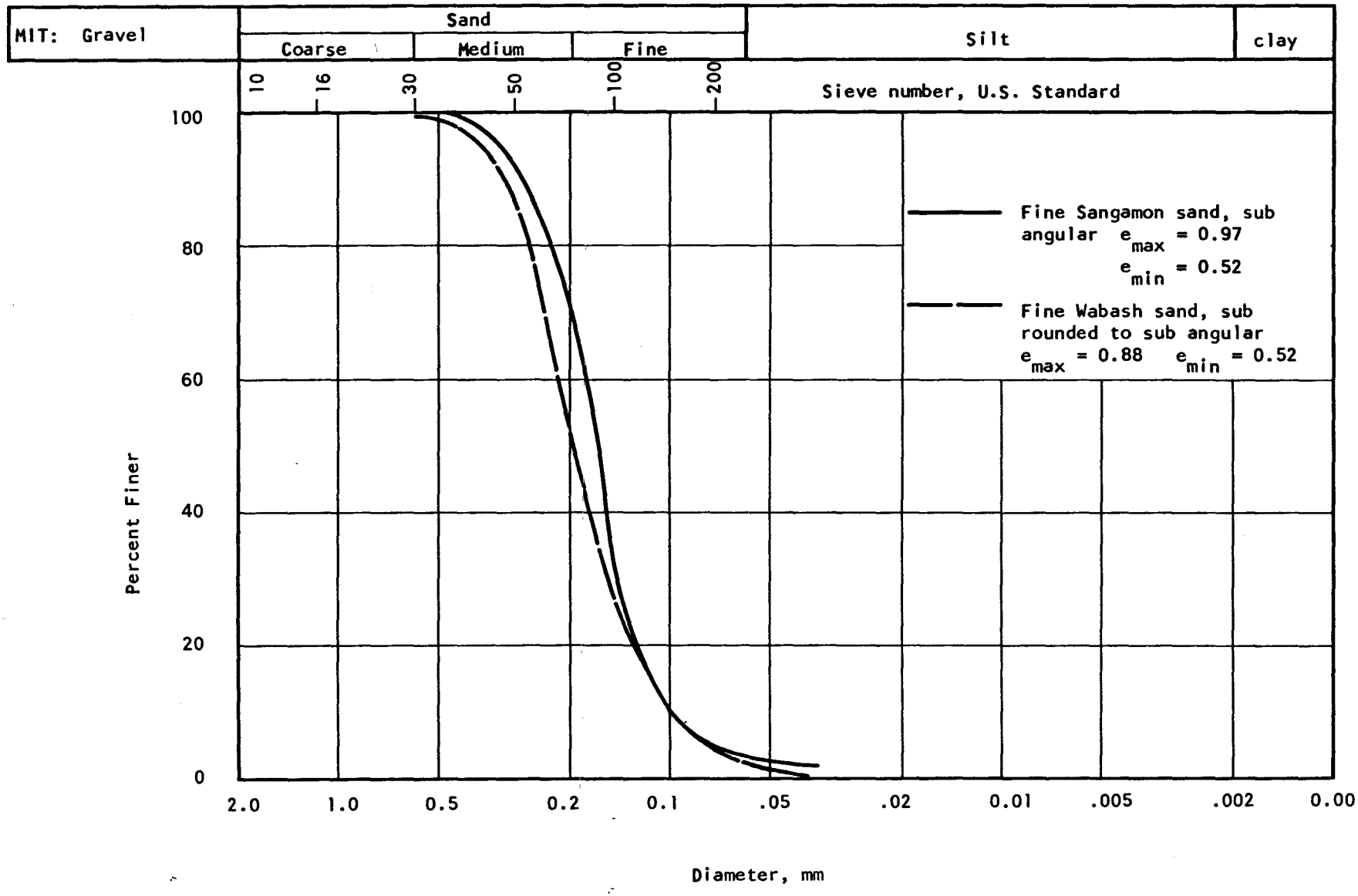

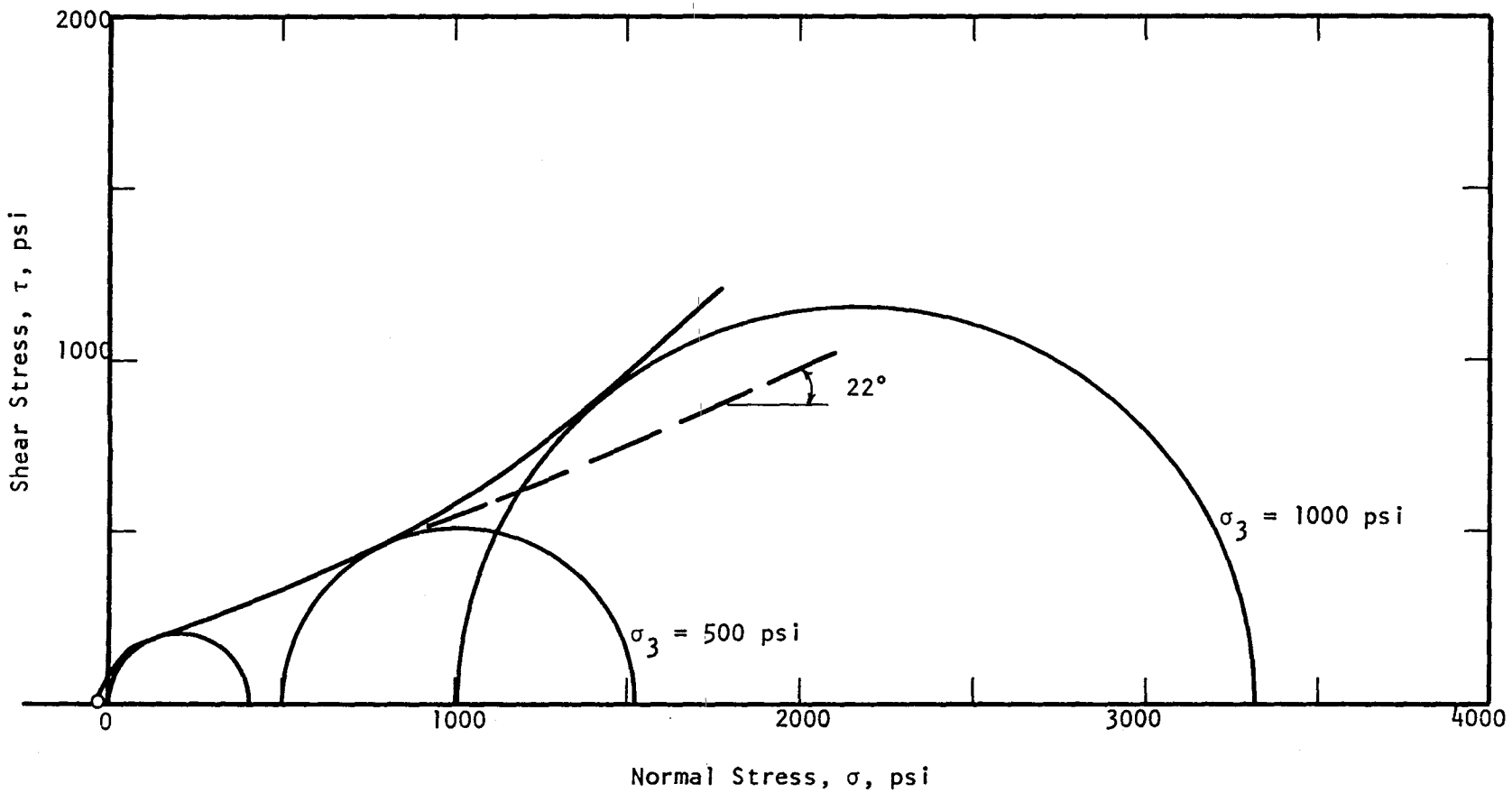

Figure 26

Mohr Envelope - Triaxial Compression
Water/Plaster/Sand Mixture of 1.8/1/8.1

Figure 27 Compaction of Dry Plaster of Paris and Fine Wabash Sand, Mixed at 1/8, in 2" Diam. x 4" Long Molds with Vicksburg Tamper, No Extension on Mold

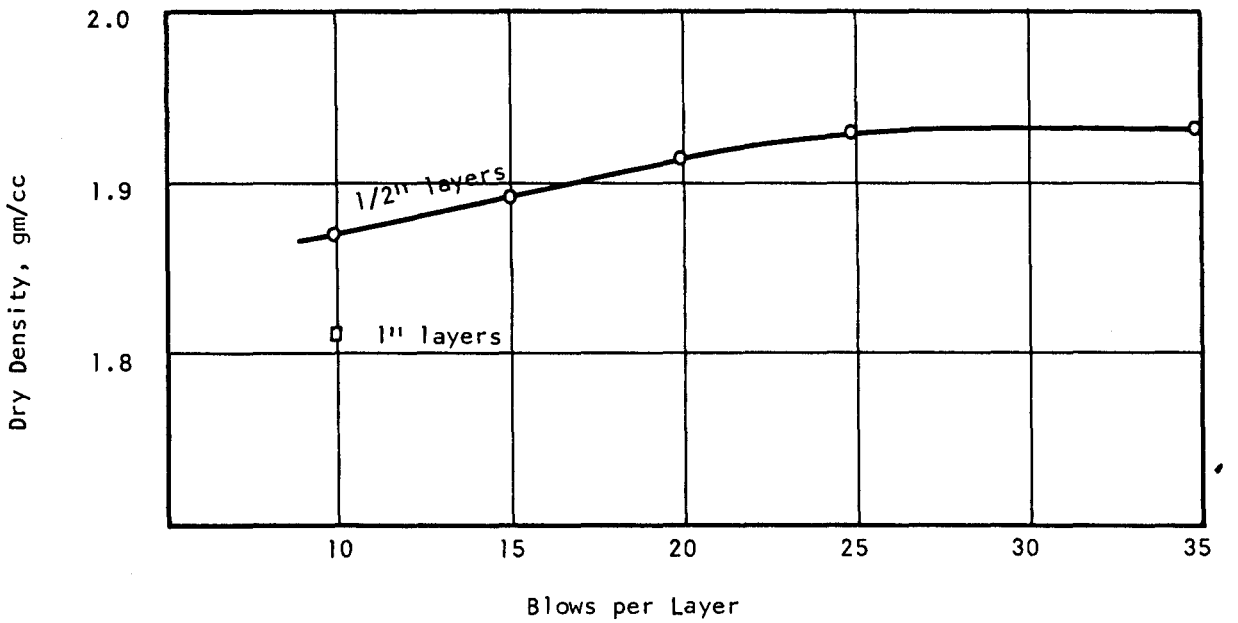

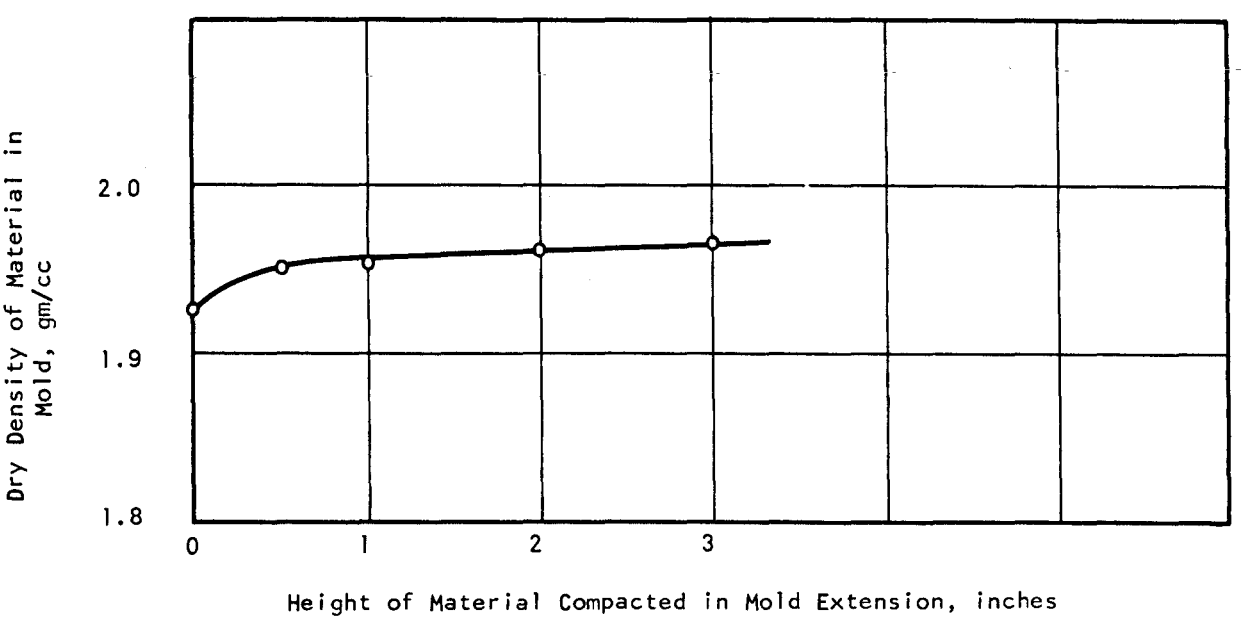

Figure 28 Compaction of Dry Plaster of Paris and Fine Wabash Sand, Mixed at 1/8, in 1/2" Layers, 25 Blows per Layer With Vicksburg Tamper - Using Mold Extension

Figure 29 Moisture-Density Curve For a Plaster of Paris/Fine Wabash Sand Mix Ratio of 1/8 Compacted in 2" Diam x 4" Long Cylinders with Vicksburg Tamper, 1/2" Layers, 25 Blows/Layer

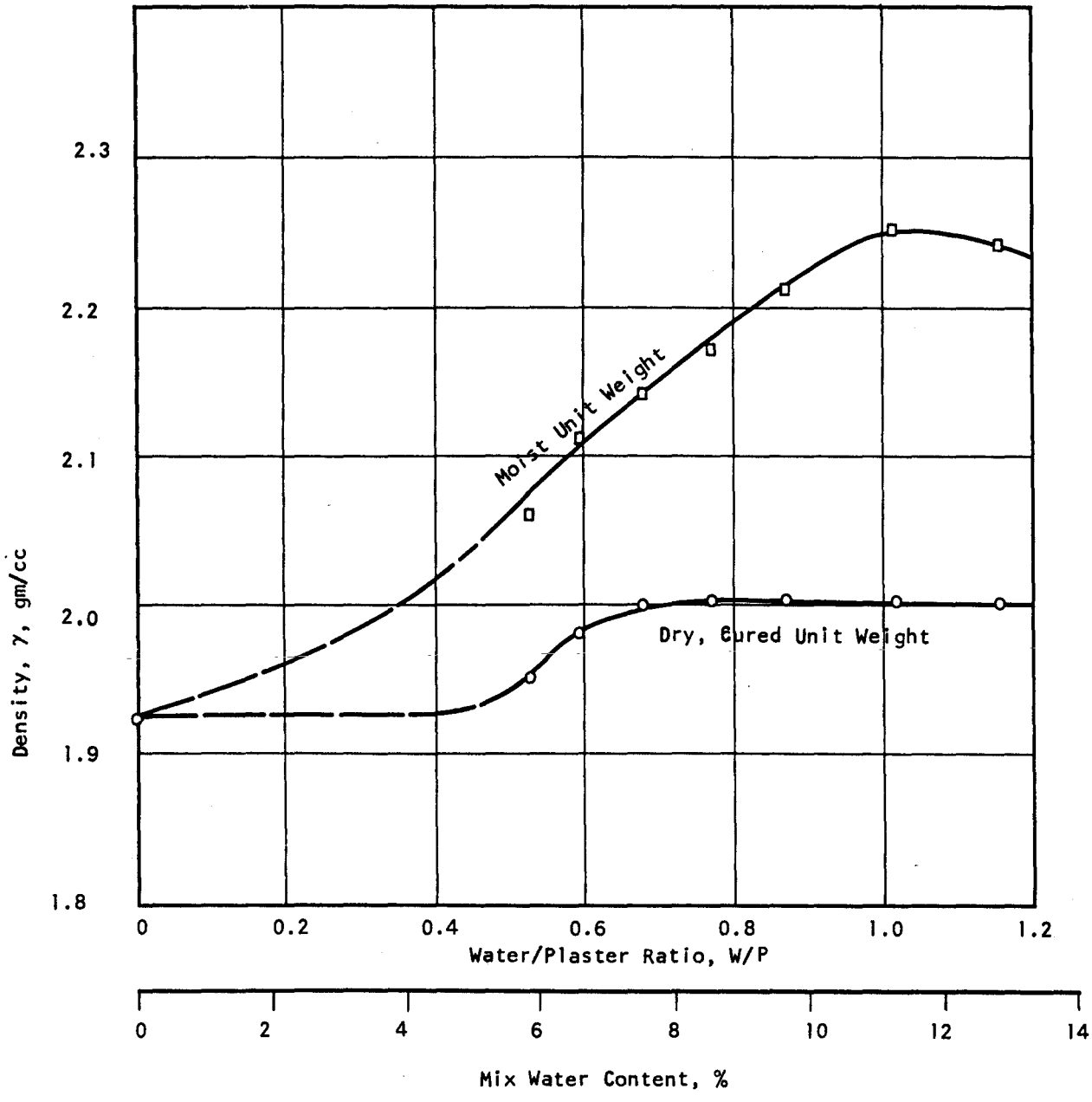

Figure 30 Moisture-Density Curve For a Plaster of Paris/Fine Sangamon Sand Mix Ratio of 1/9 Compacted in 2" Diameter x 4" Long Cylinders with Vicksburg Tamper, 1/2" Lifts, 25 Blows/Lift
○ , □ Two Different Series of Tests

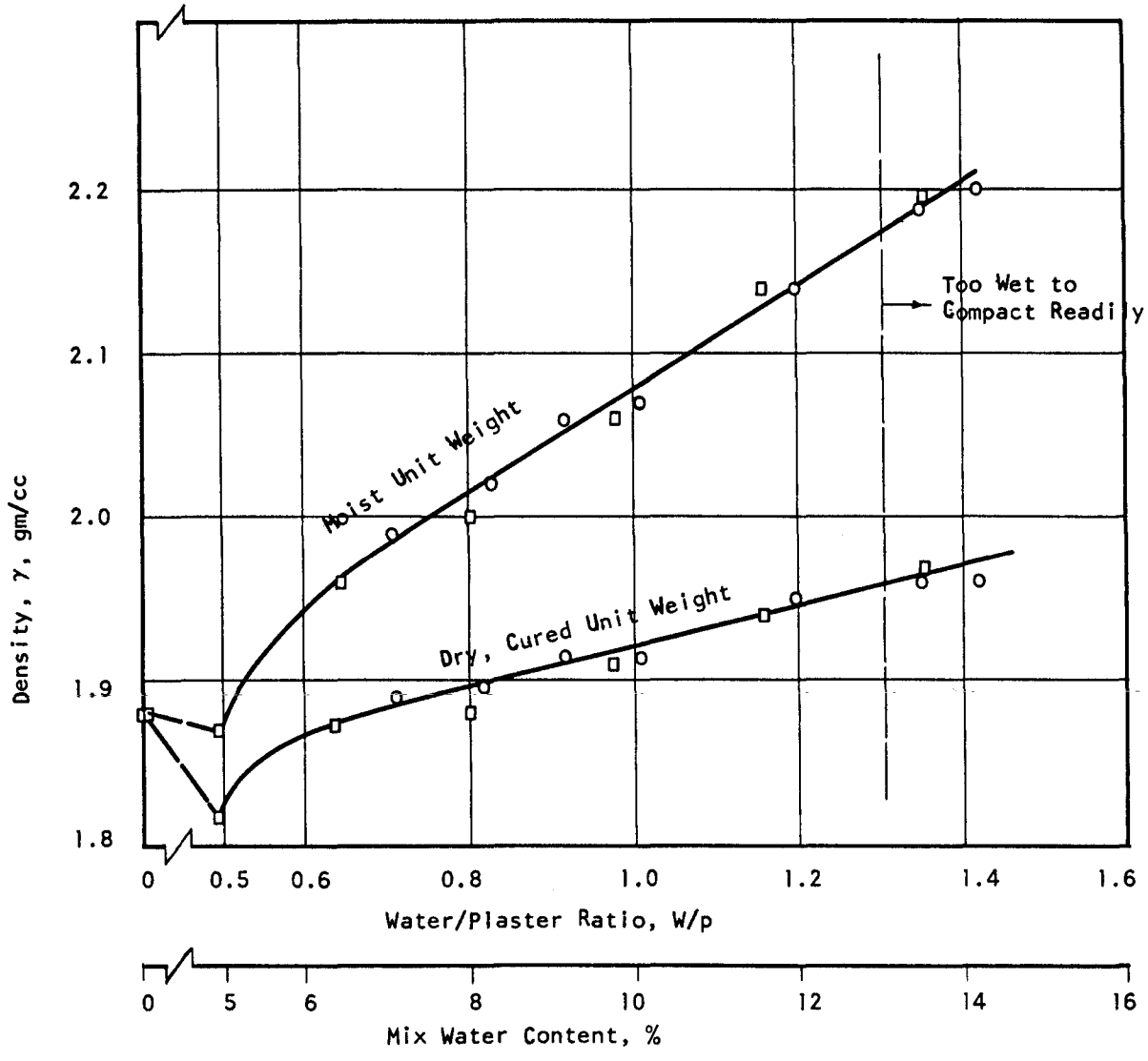

Figure 31 Variation of Density With Compaction Energy Water/Plaster/Fine Sangamon Sand Mixture of 1.2/1.0/9.0. Compacted in 3" x 4" x 8" mold with Marshall hammer (10 lb hammer, 18" drop)

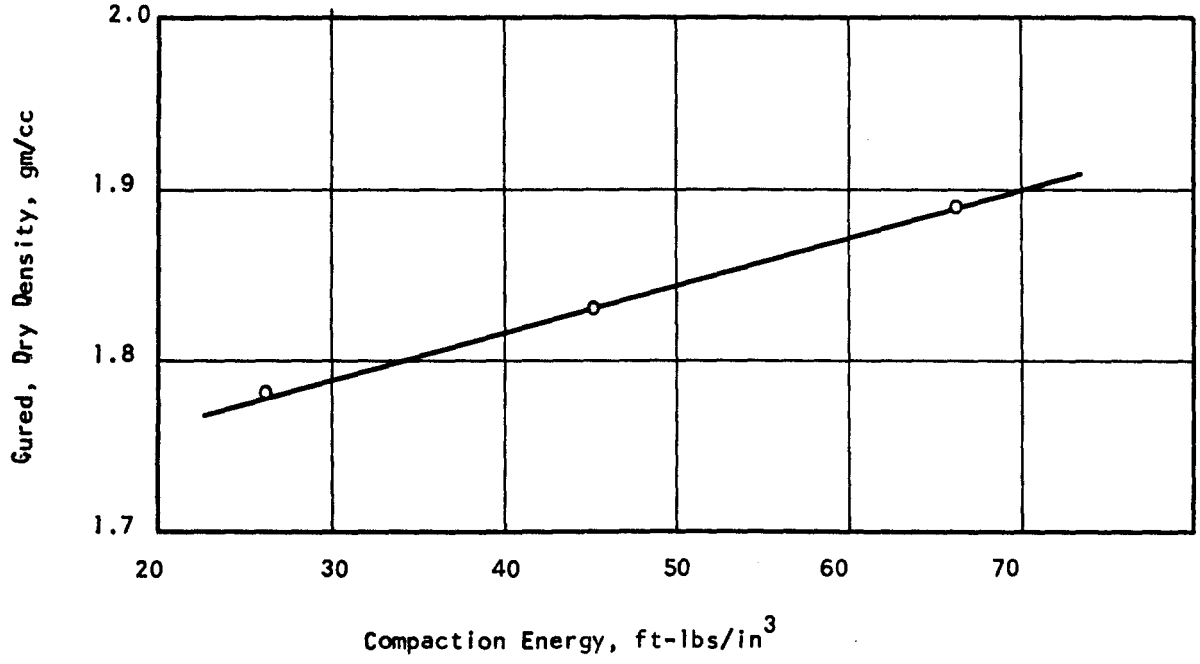

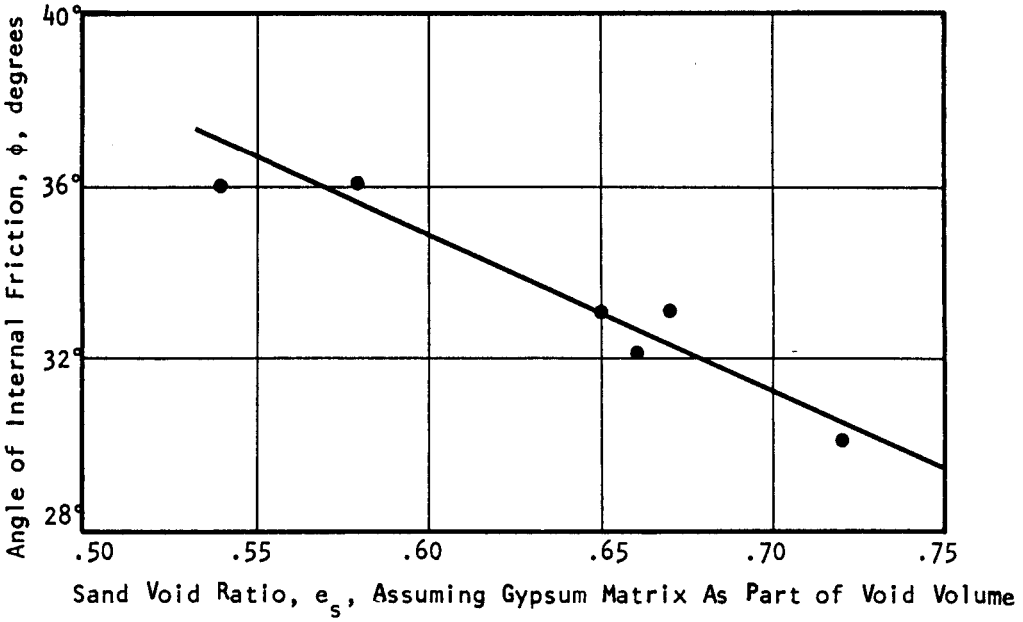

Figure 32

Variation of Angle of Internal Friction with Sand Void Ratio,
Plaster/Fine Wabash Sand Mixtures of 1/8

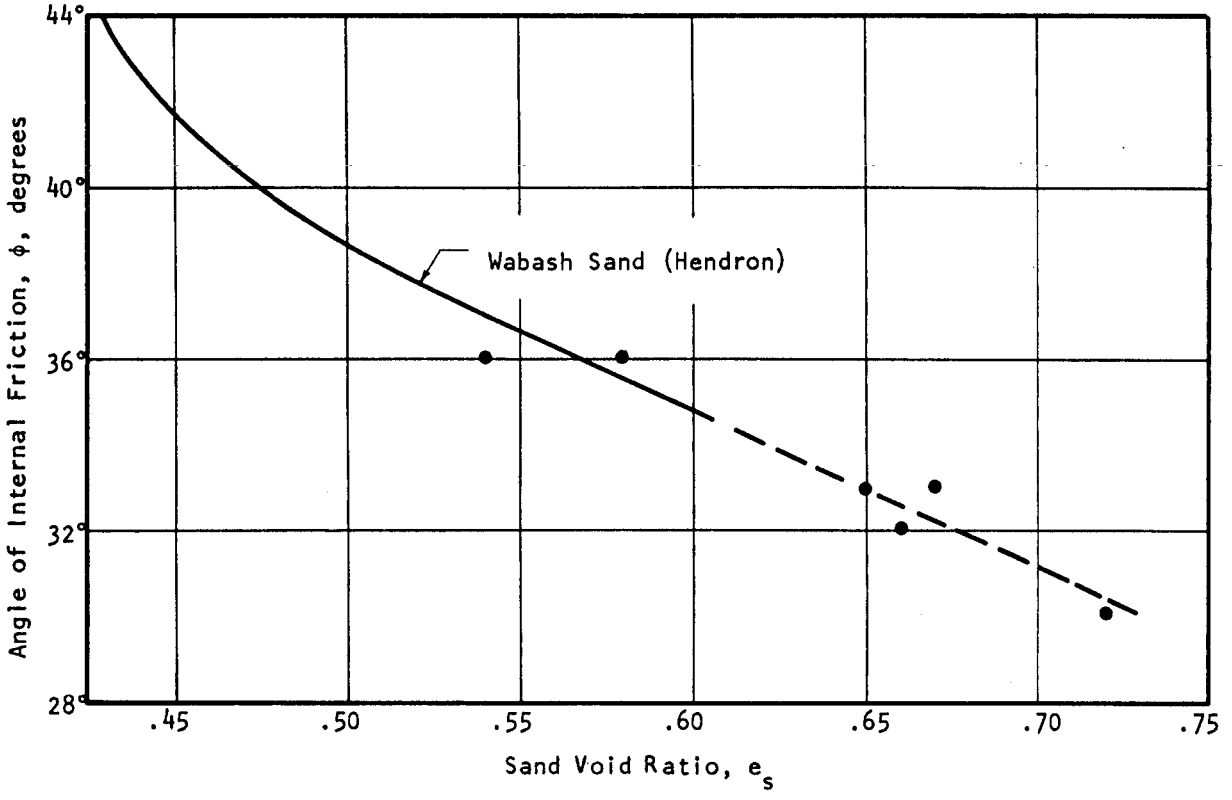

Figure 33

Comparison Between Angle of Internal Friction of Wabash Sand (Hendron, 1963)
and Plaster of Paris/Fine Wabash Sand Mixtures of 1/8

Figure 34 Variation of Unconfined Compression Strength With Compacted Density of Plaster of Paris/ Fine Wabash Sand Mixtures of 1/8

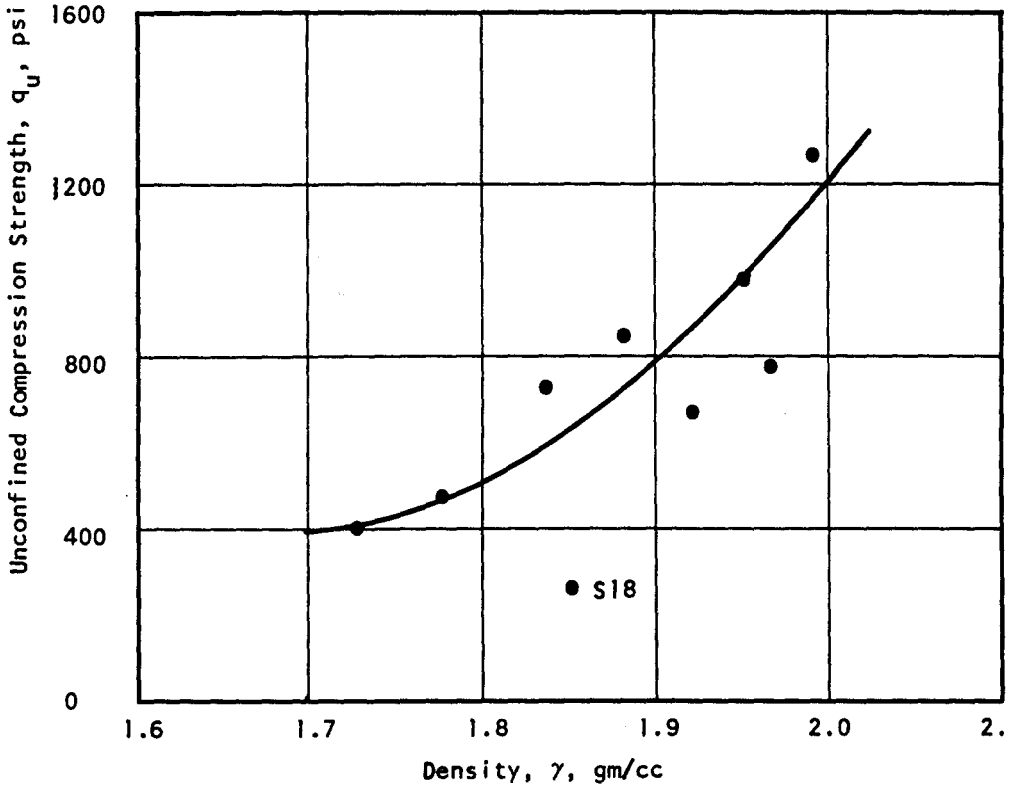

Figure 35 Variation of Cohesion Intercept of Mohr Diagram with Compacted Density of Plaster of Paris/Fine Wabash Sand Mixtures of 1/8

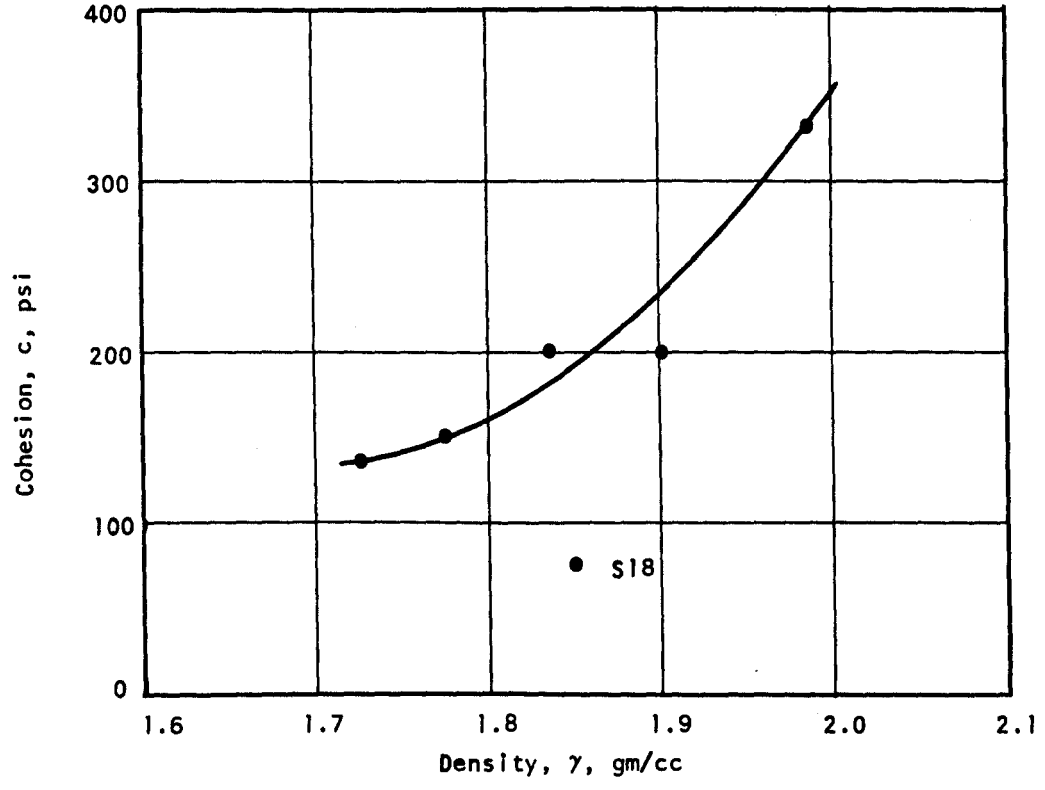

Figure 36 Variation of Cohesion Intercept of Mohr Diagram with Bulk Gypsum Matrix Density in Compacted Mixtures of Plaster of Paris/Fine Wabash Sand of 1/8

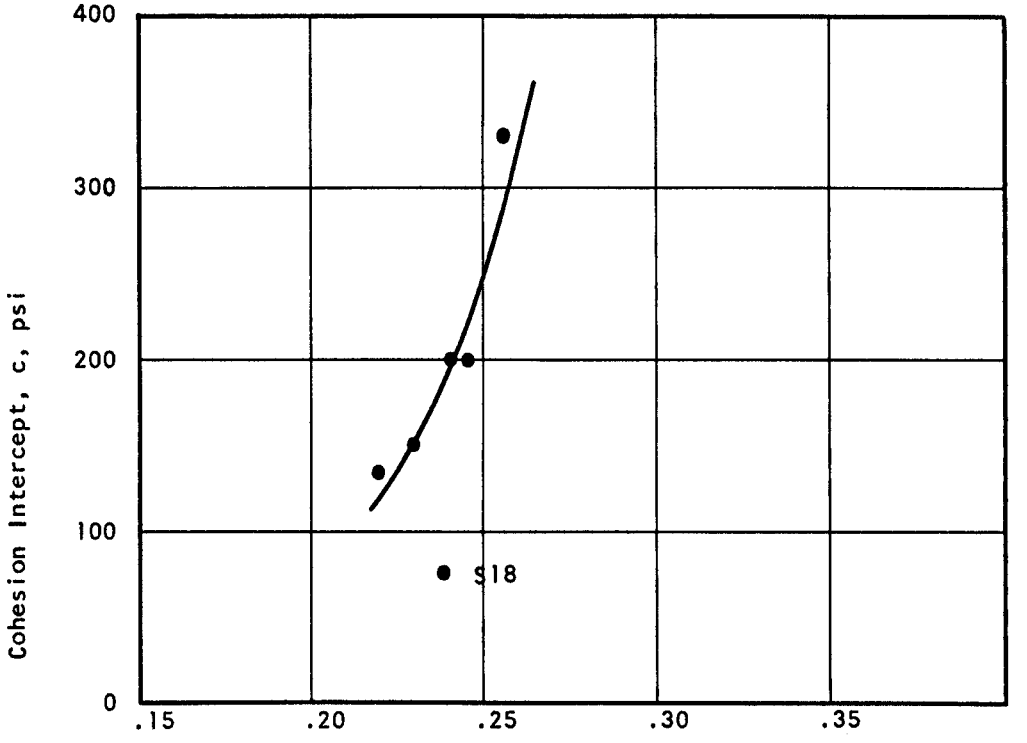

Fig. 37 Variation of Unconfined Compression Strength with Water/Plaster Ratio in Compacted Plaster of Paris/Fine Wabash Sand Mixtures of 1/8

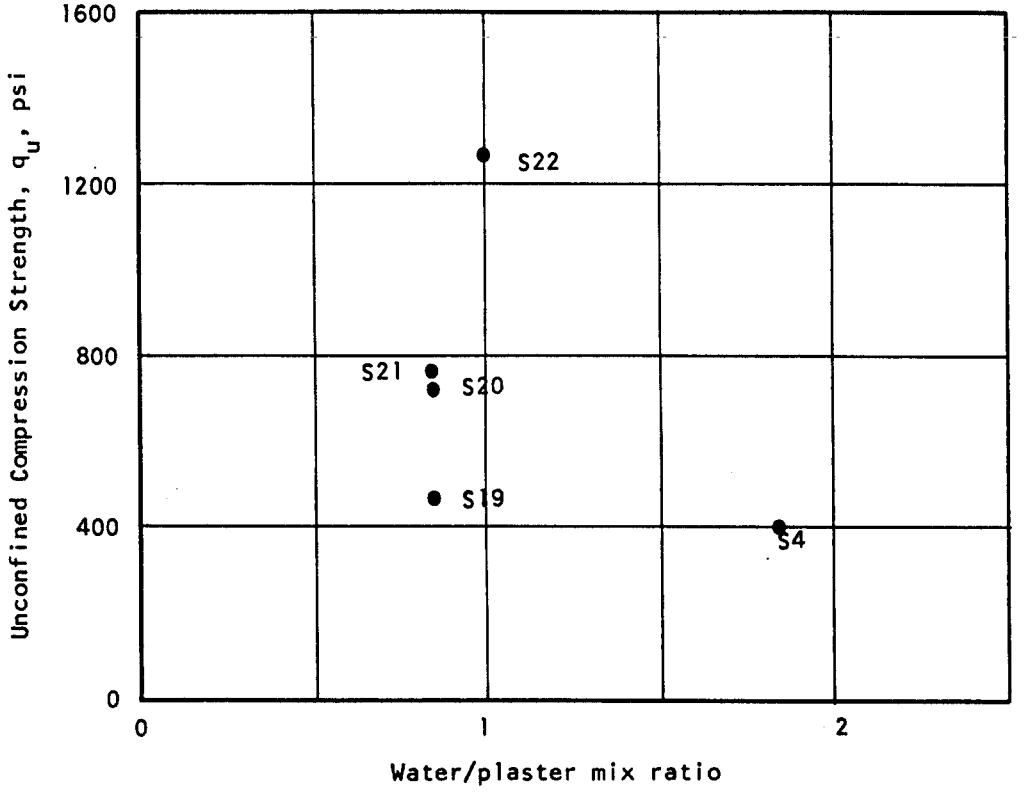

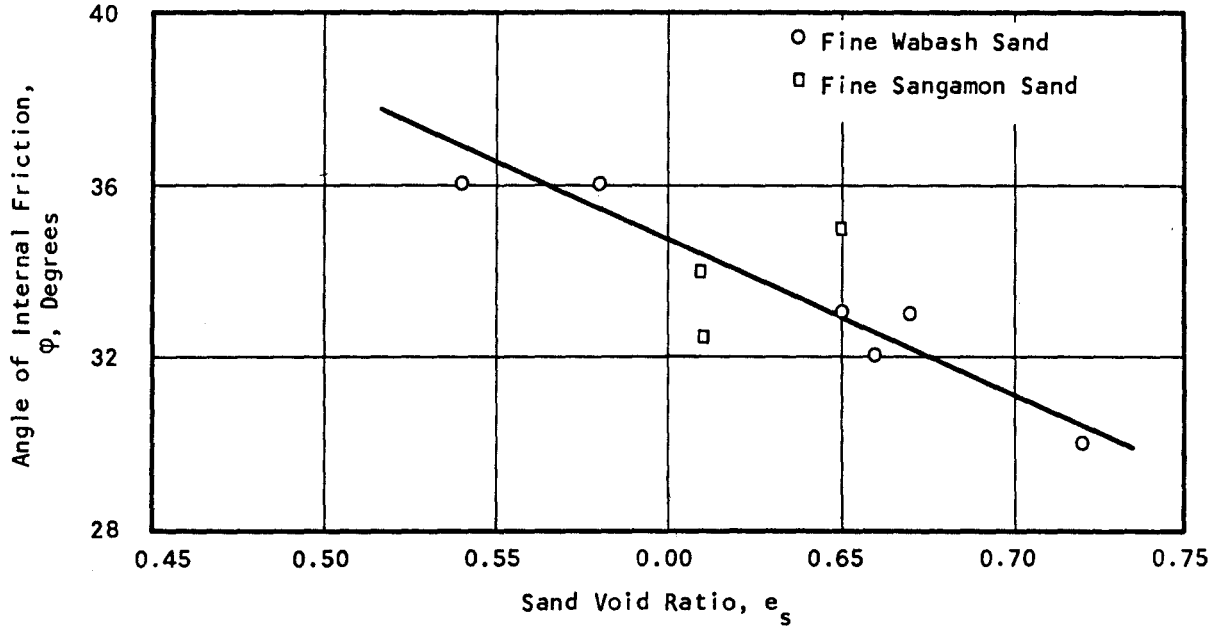

Figure 38 Variation of Internal Friction With Sand Void Ratio

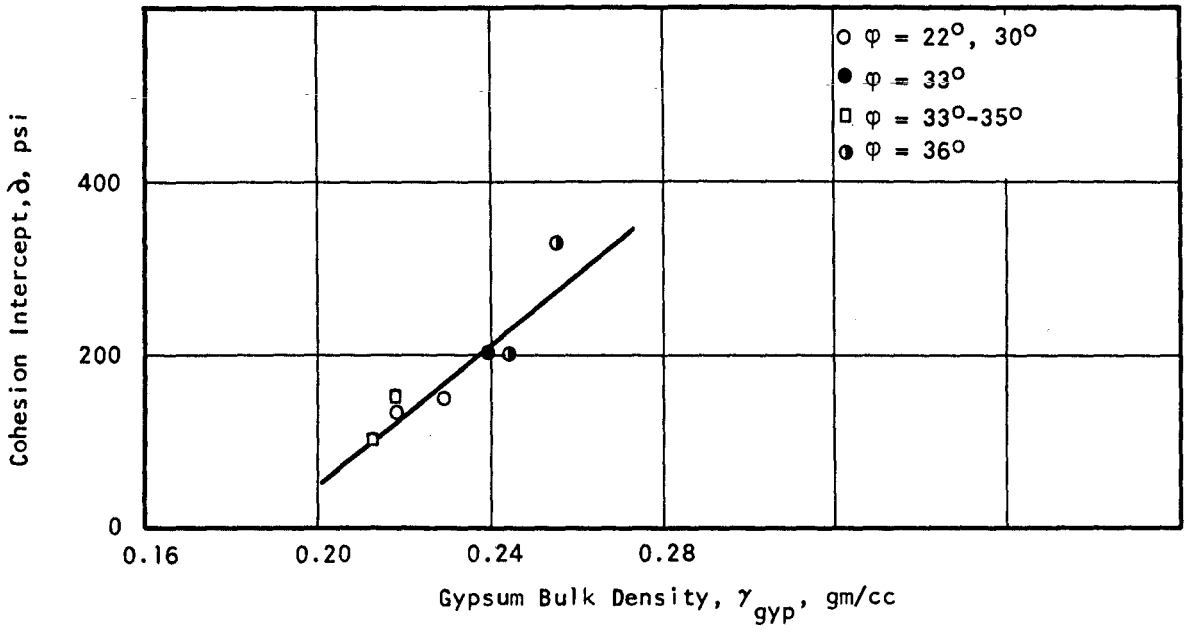

Figure 39 Variation of Cohesion Intercept With Bulk Gypsum Matrix Density Impact Compaction of Water/Plaster/Sand Mixtures

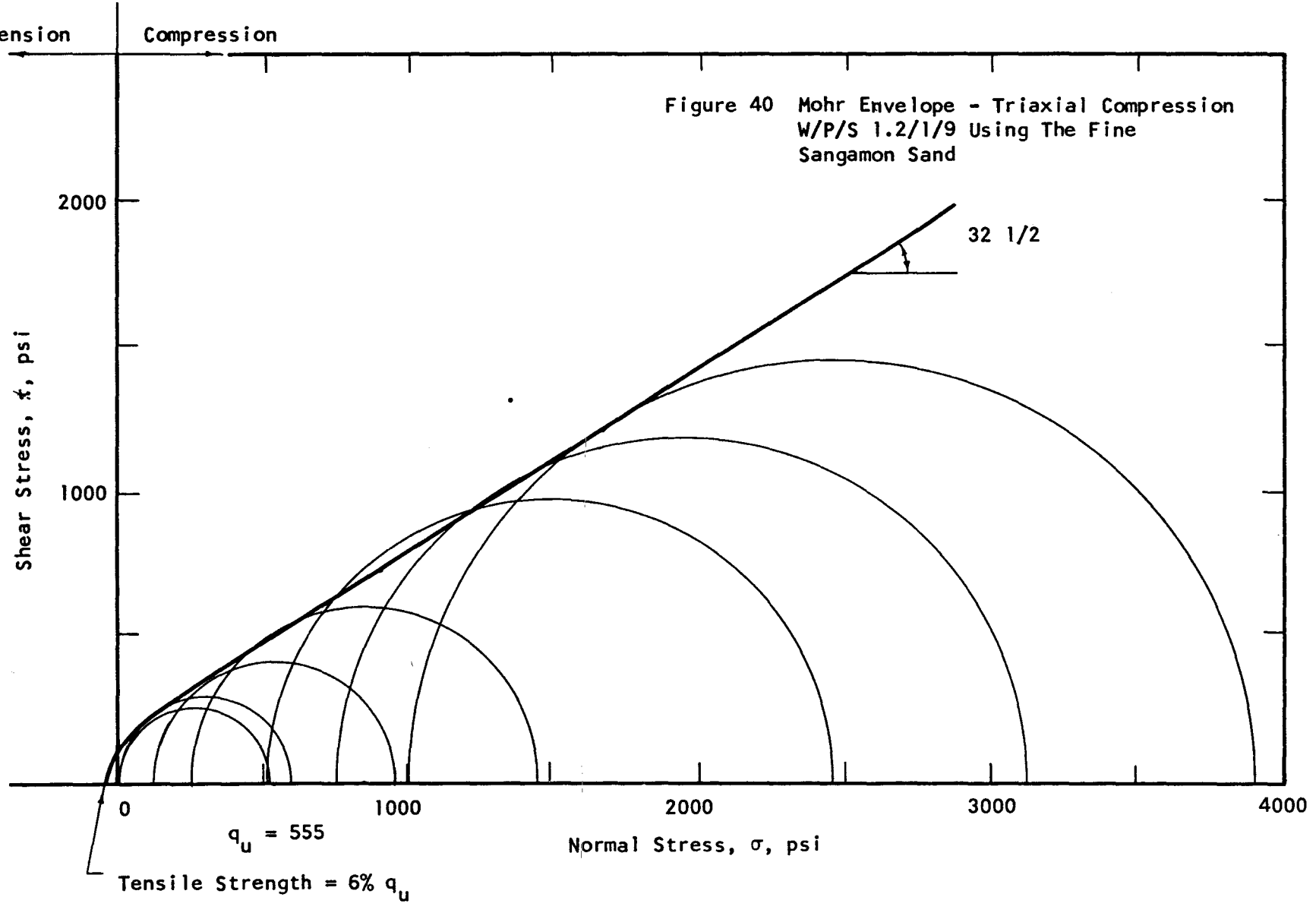

Figure 40 Mohr Envelope - Triaxial Compression W/P/S 1.2/1/9 Using The Fine Sangamon Sand

Figure 41 Stress-Strain Curves-Triaxial Compression Confining Pressures in psi W/P/S = 1.2/1/9 using the Fine Sangamon Sand

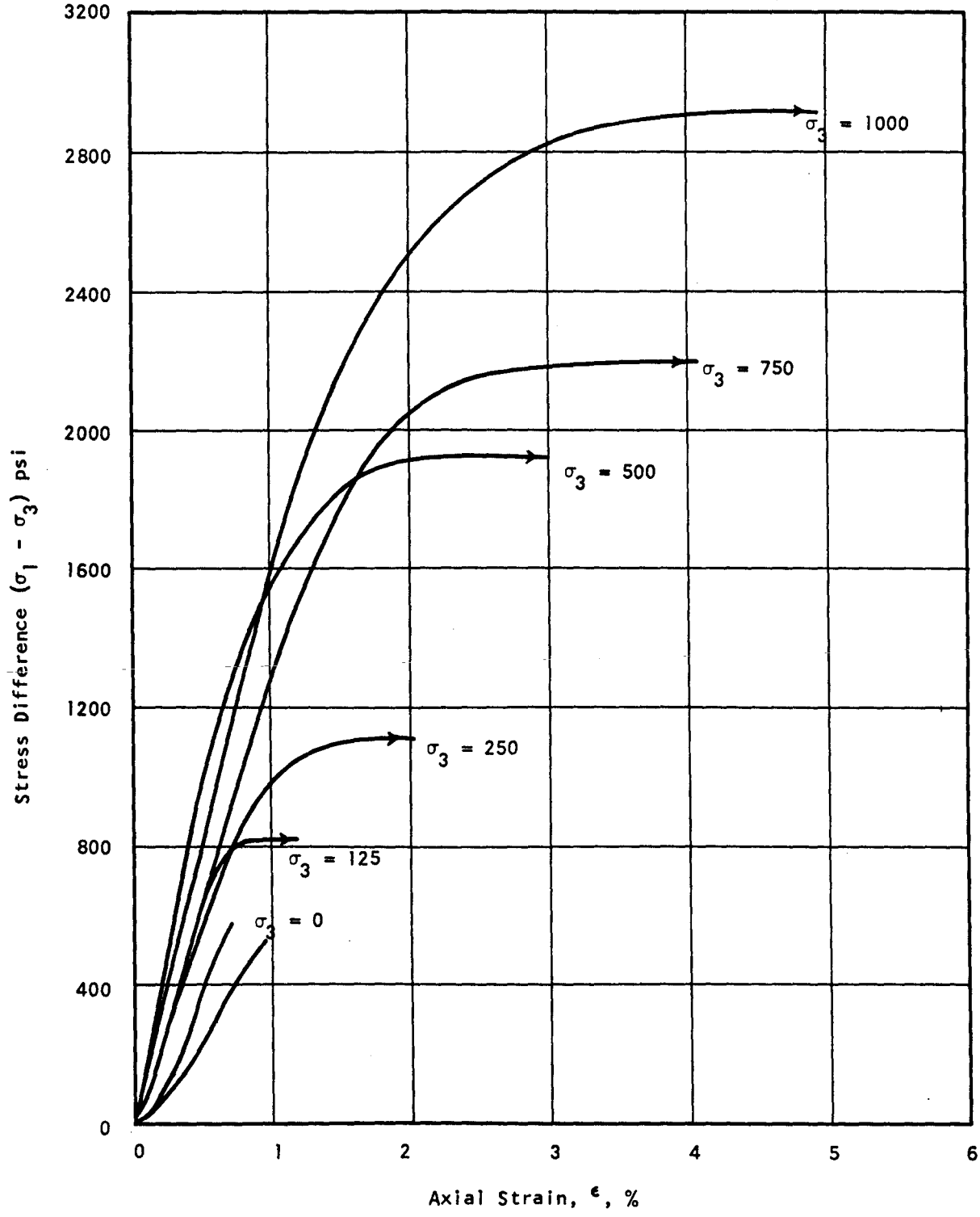

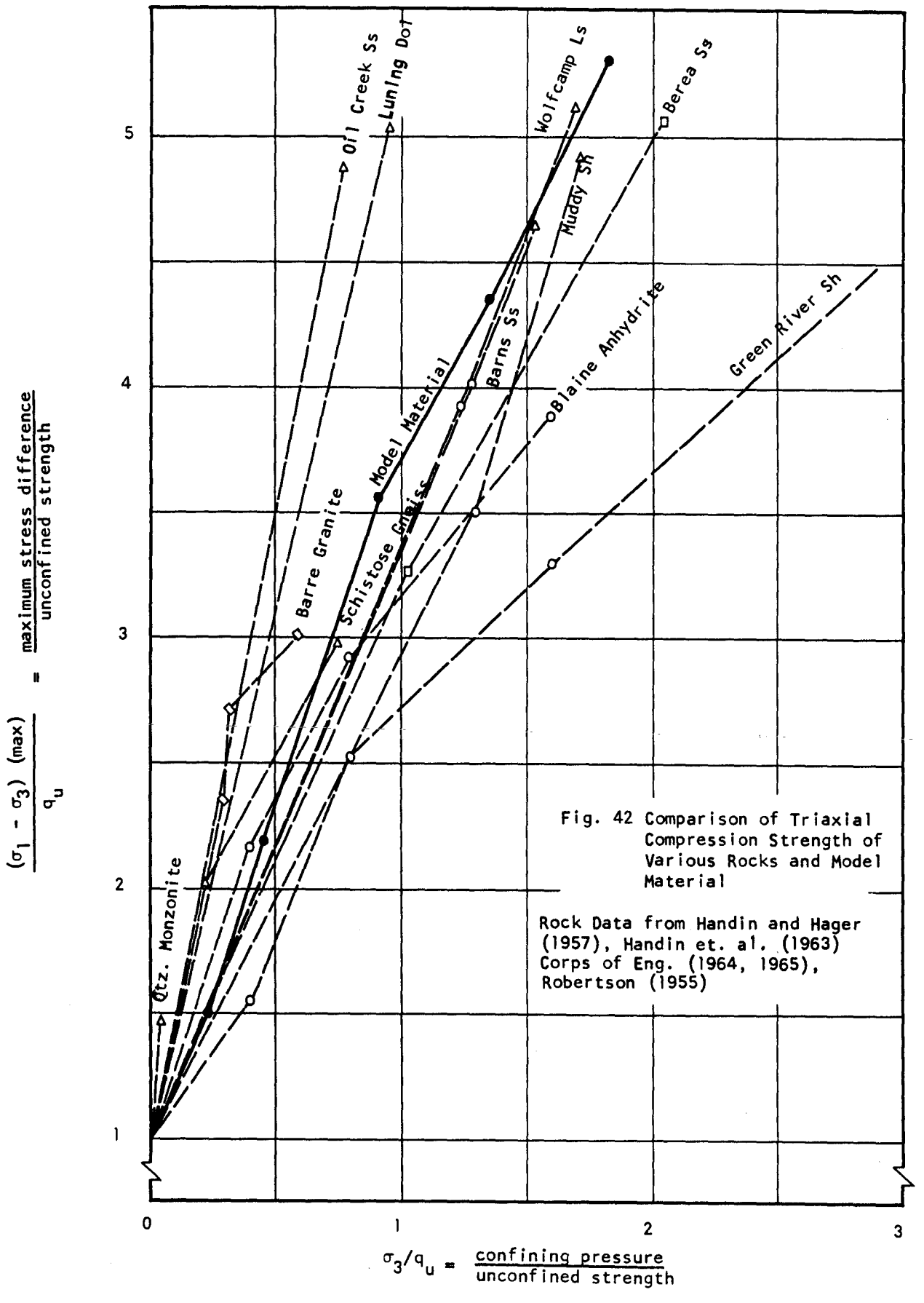

Fig. 42 Comparison of Triaxial Compression Strength of Various Rocks and Model Material

Rock Data from Handin and Hager (1957), Handin et. al. (1963) Corps of Eng. (1964, 1965), Robertson (1955)

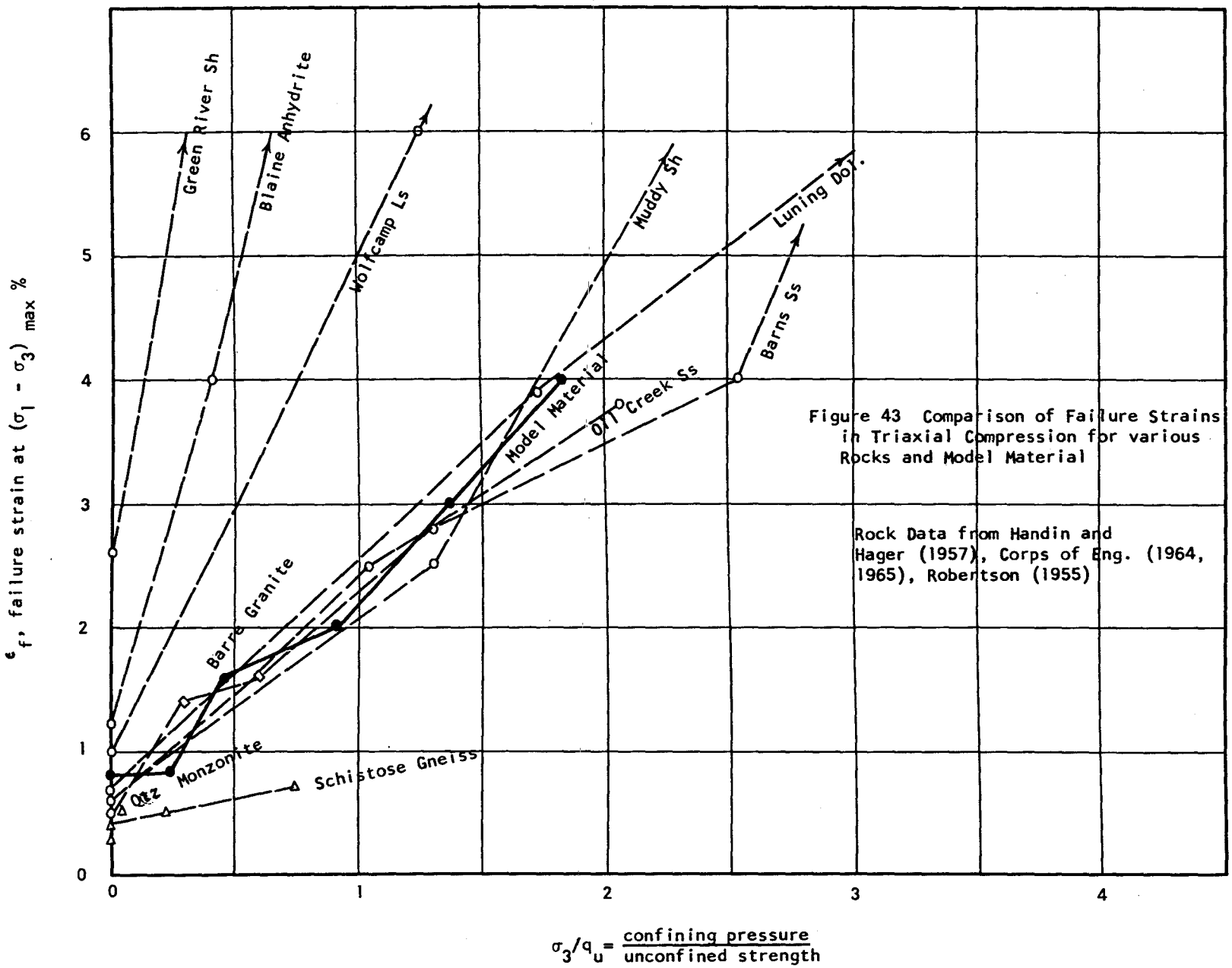

Figure 43 Comparison of Failure Strains in Triaxial Compression for various Rocks and Model Material

Rock Data from Handin and Hager (1957), Corps of Eng. (1964, 1965), Robertson (1955)

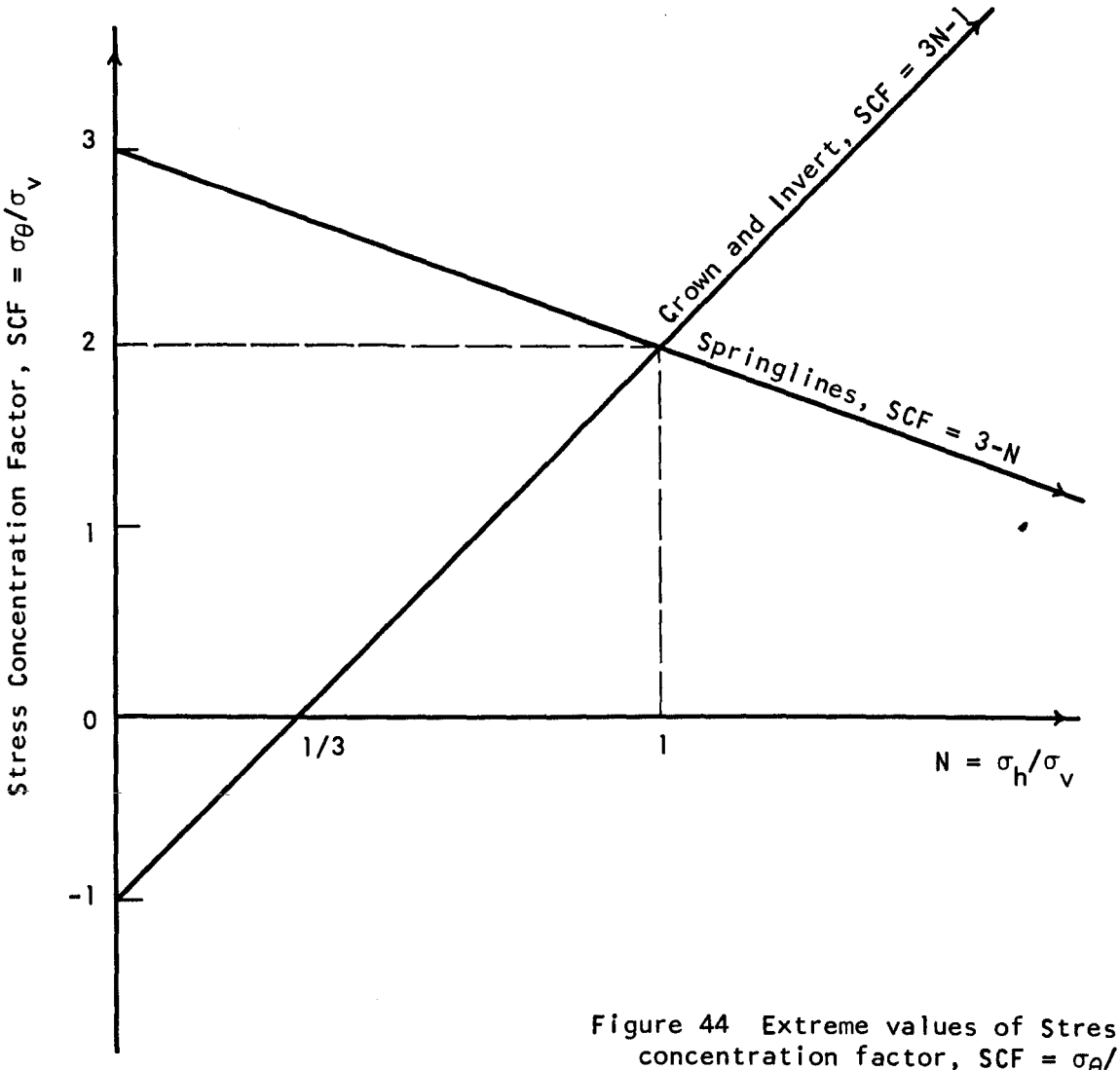

Figure 44 Extreme values of Stress concentration factor, SCF = σ_θ/σ_v, about a circular opening in an elastic medium, based upon the Kirsch equations.

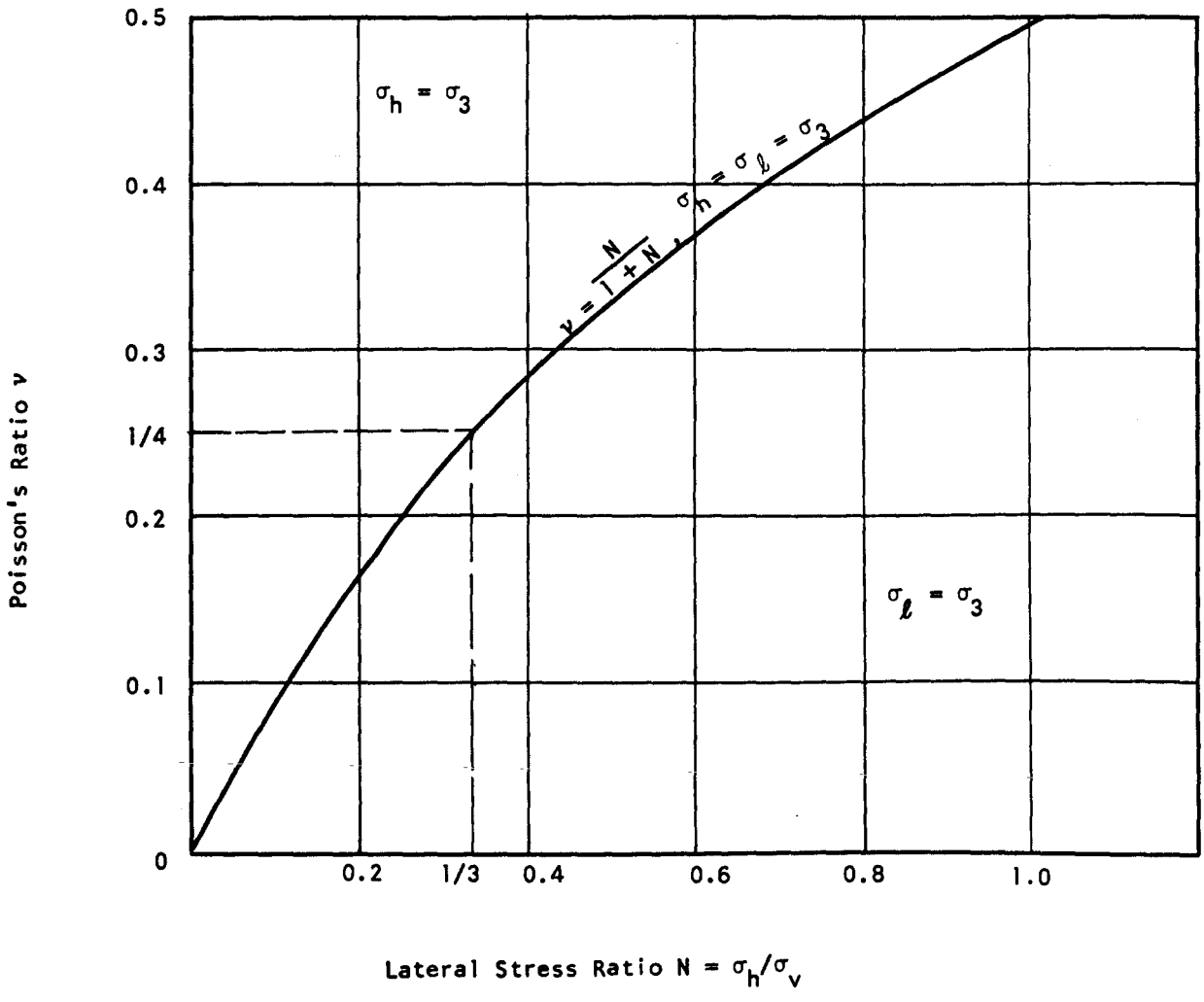

Figure 45 Variation of Minor Principal Stress With Values of N and ν.

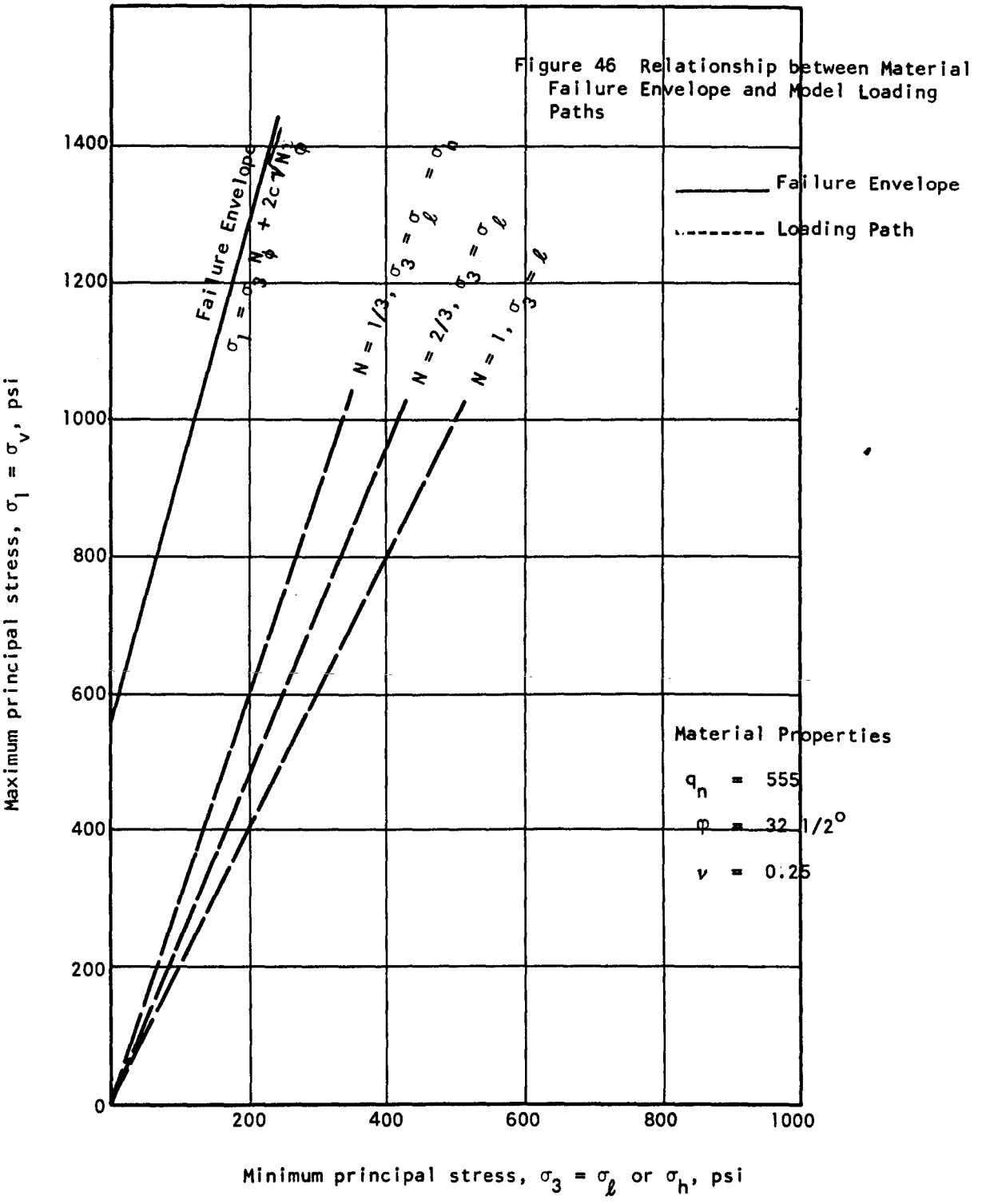

Figure 46 Relationship between Material Failure Envelope and Model Loading Paths

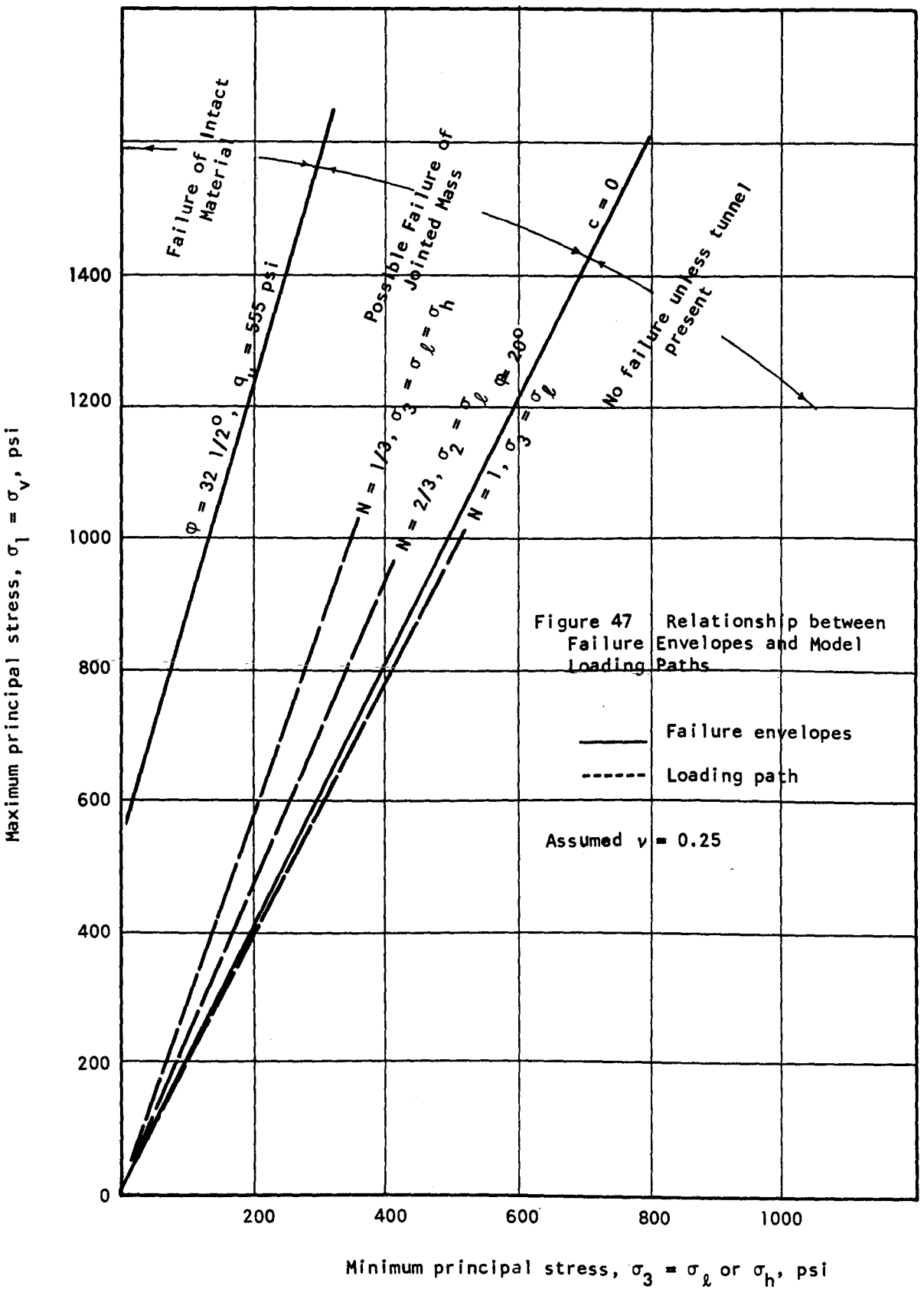

Figure 47 Relationship between Failure Envelopes and Model Loading Paths

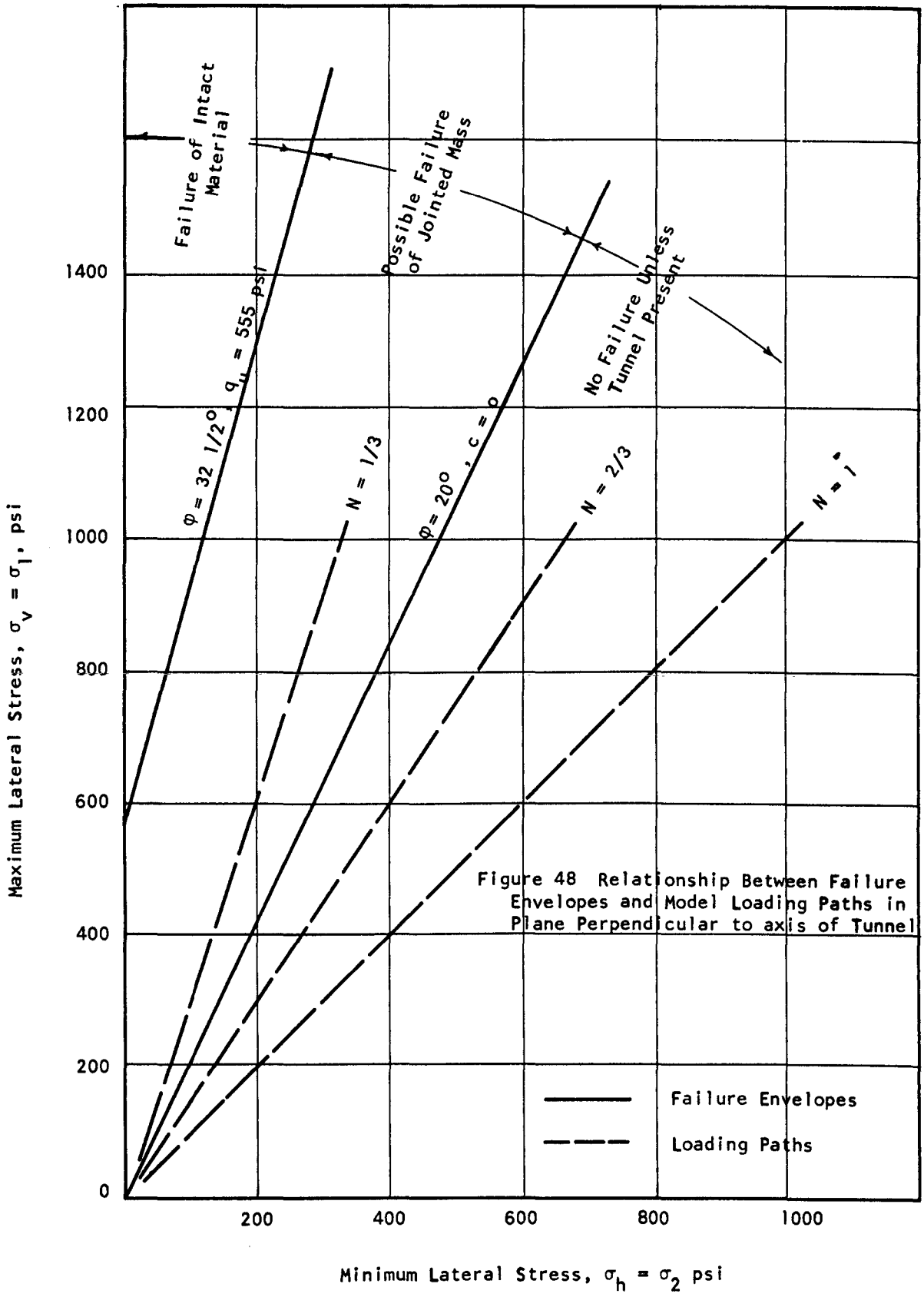

Figure 48 Relationship Between Failure Envelopes and Model Loading Paths in Plane Perpendicular to axis of Tunnel

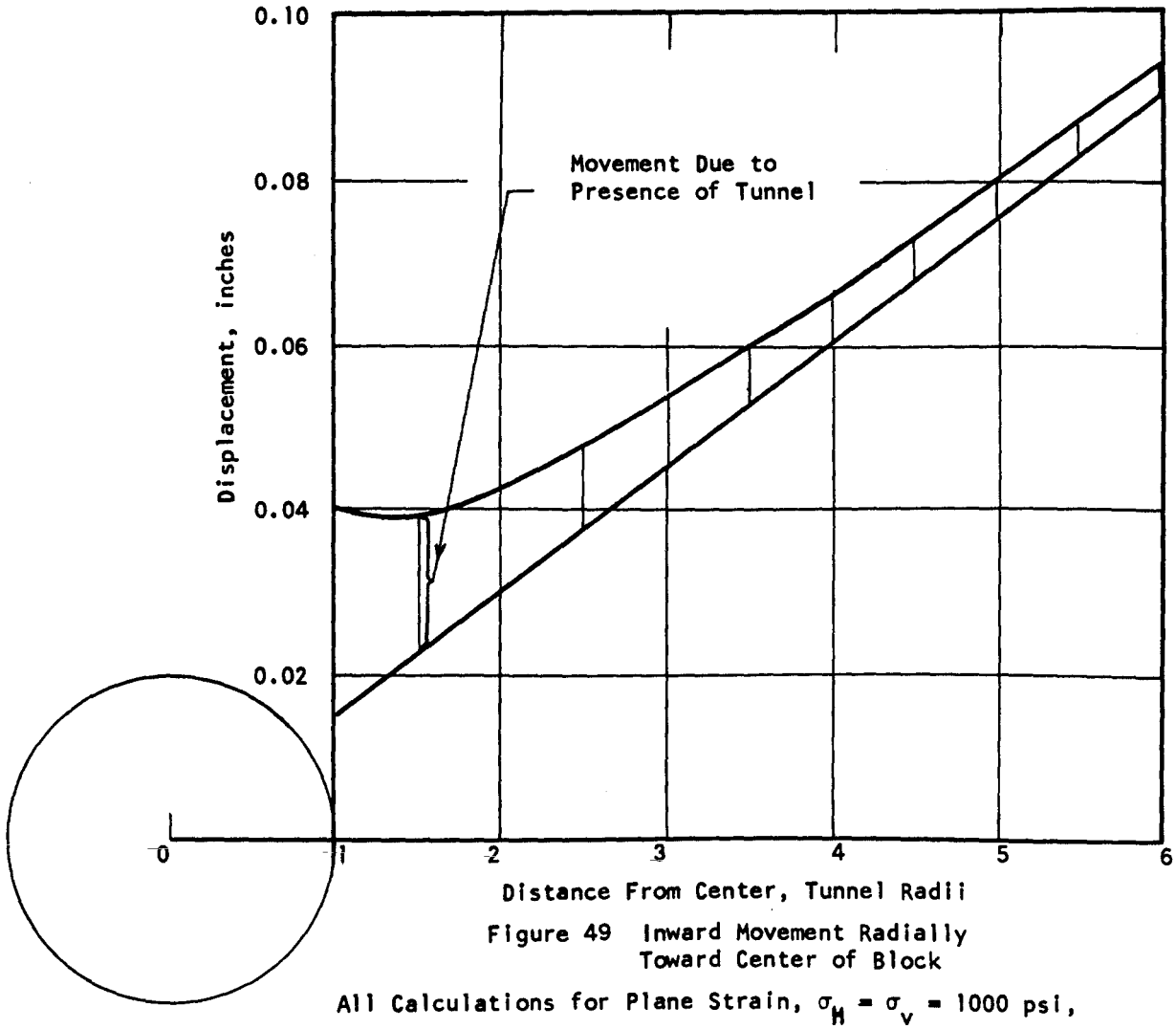

Figure 49 Inward Movement Radially Toward Center of Block

All Calculations for Plane Strain, $\sigma_H = \sigma_v$ = 1000 psi, E = 100,000, ν = 0.25, 4" Diameter Tunnel

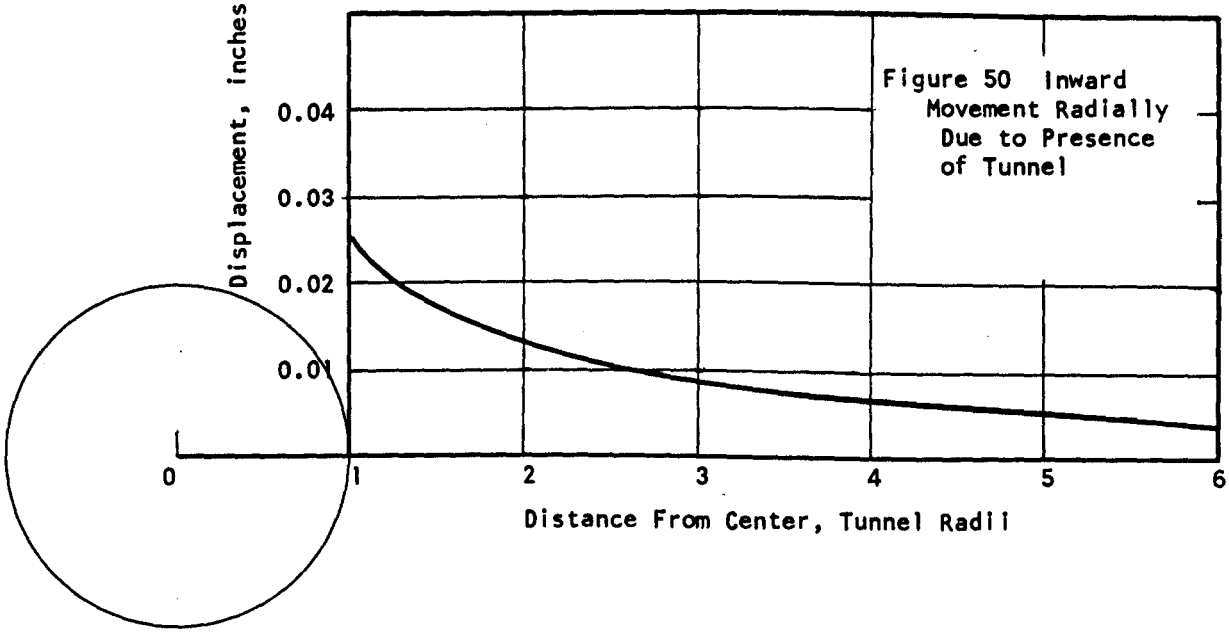

Figure 50 Inward Movement Radially Due to Presence of Tunnel

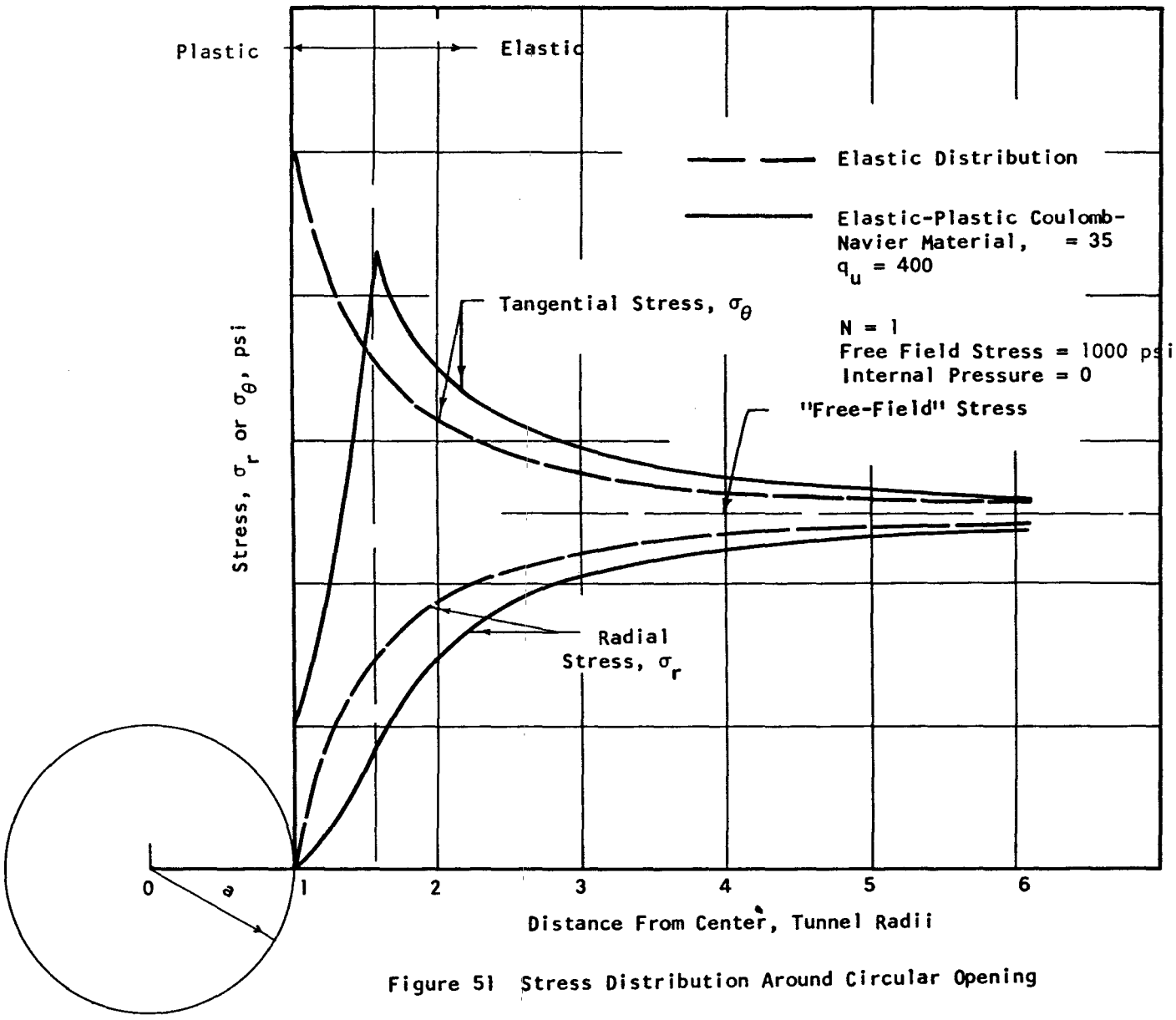

Figure 51 Stress Distribution Around Circular Opening

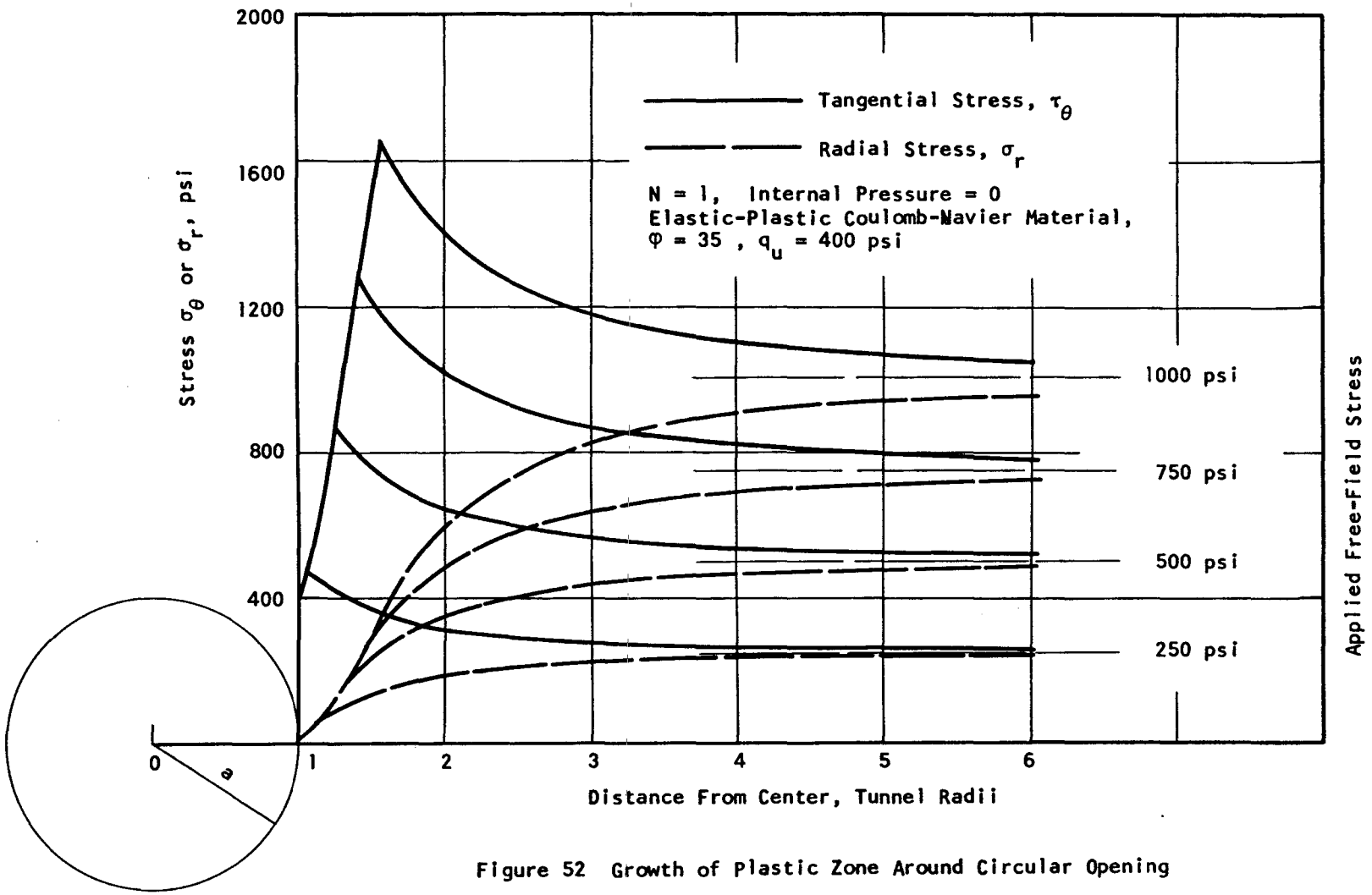

Figure 52 Growth of Plastic Zone Around Circular Opening

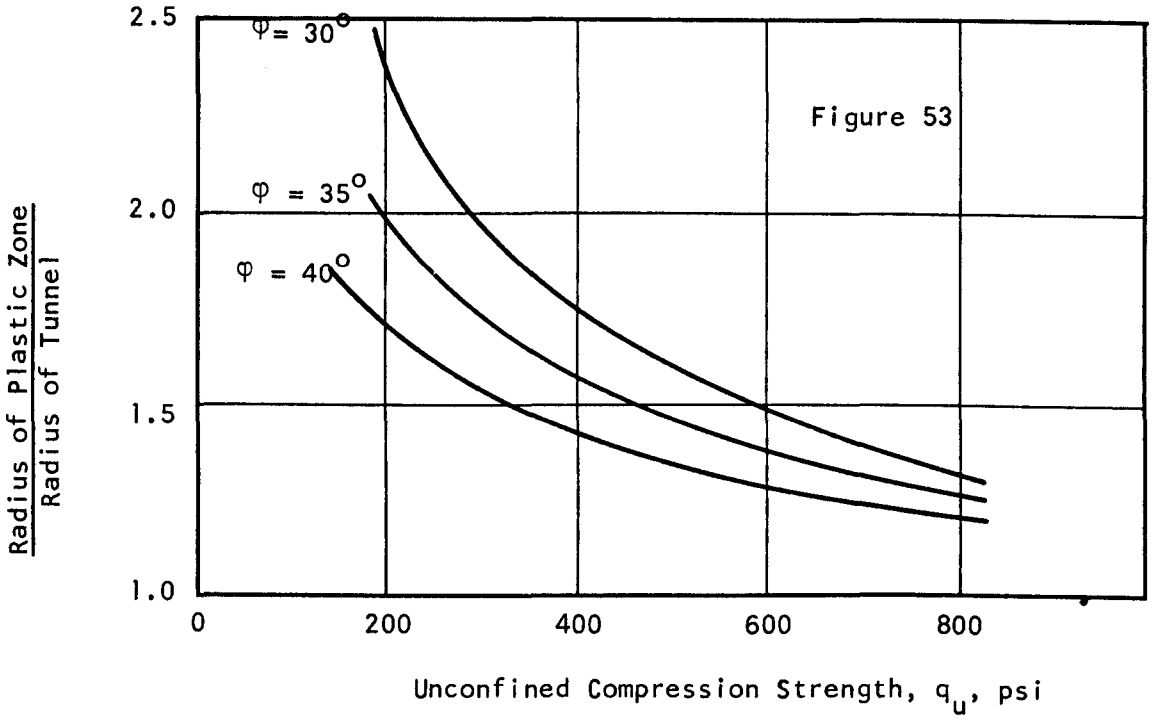

Figures 53 and 54 Depth of Plastic Zone Around Circular Tunnel N = 1, Free Field Stress = 1000 psi Elastic- Plastic Coulomb-Navier material

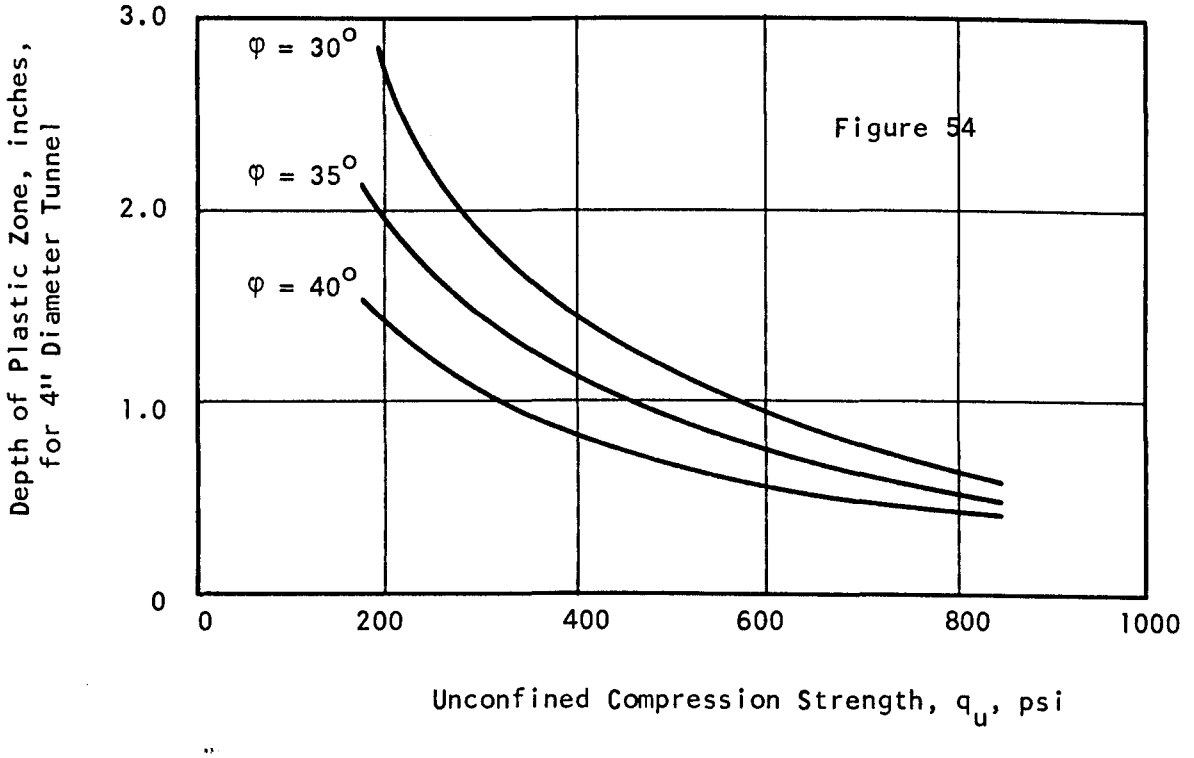

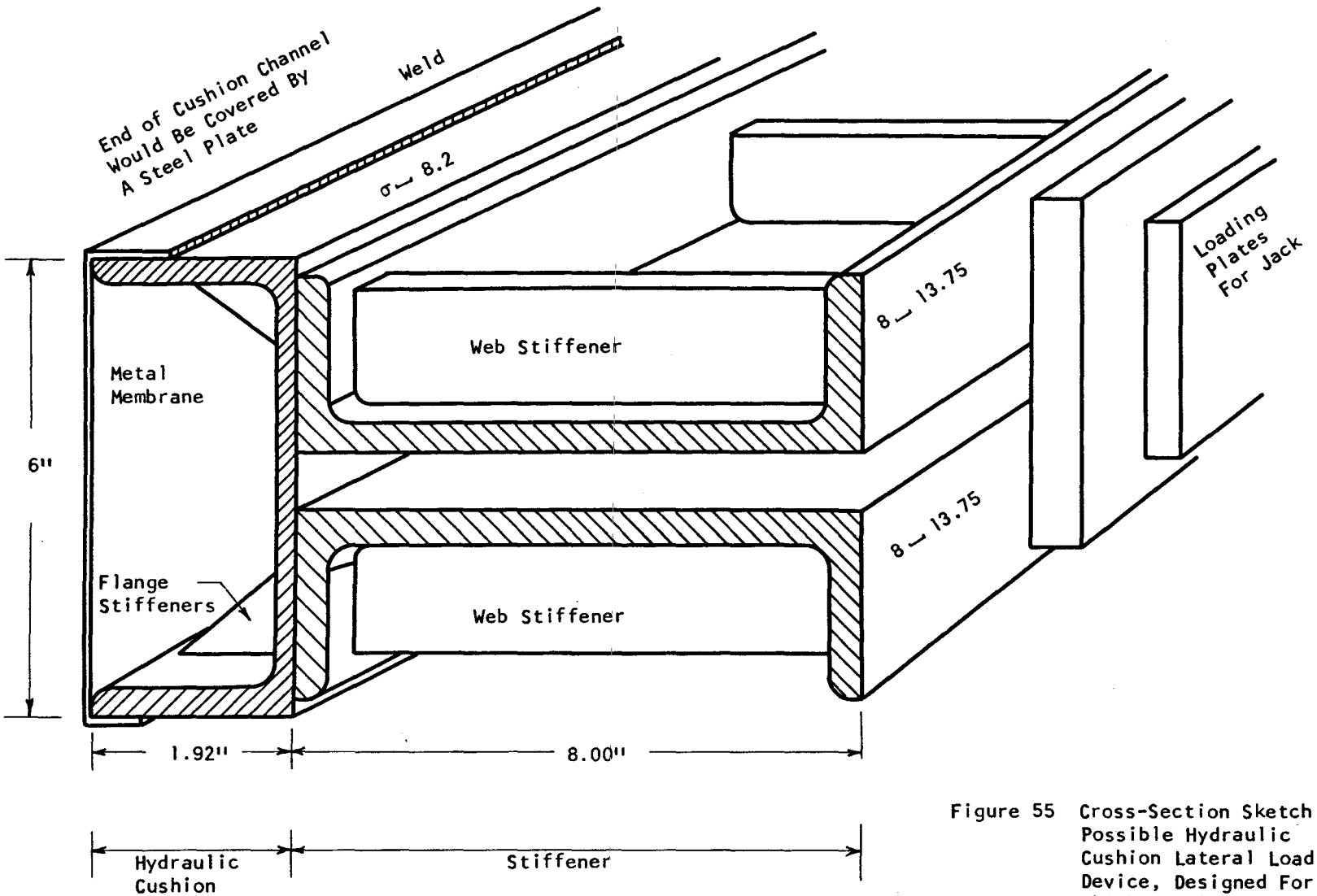

Figure 55 Cross-Section Sketch of Possible Hydraulic Cushion Lateral Loading Device, Designed For 6" Thick Model

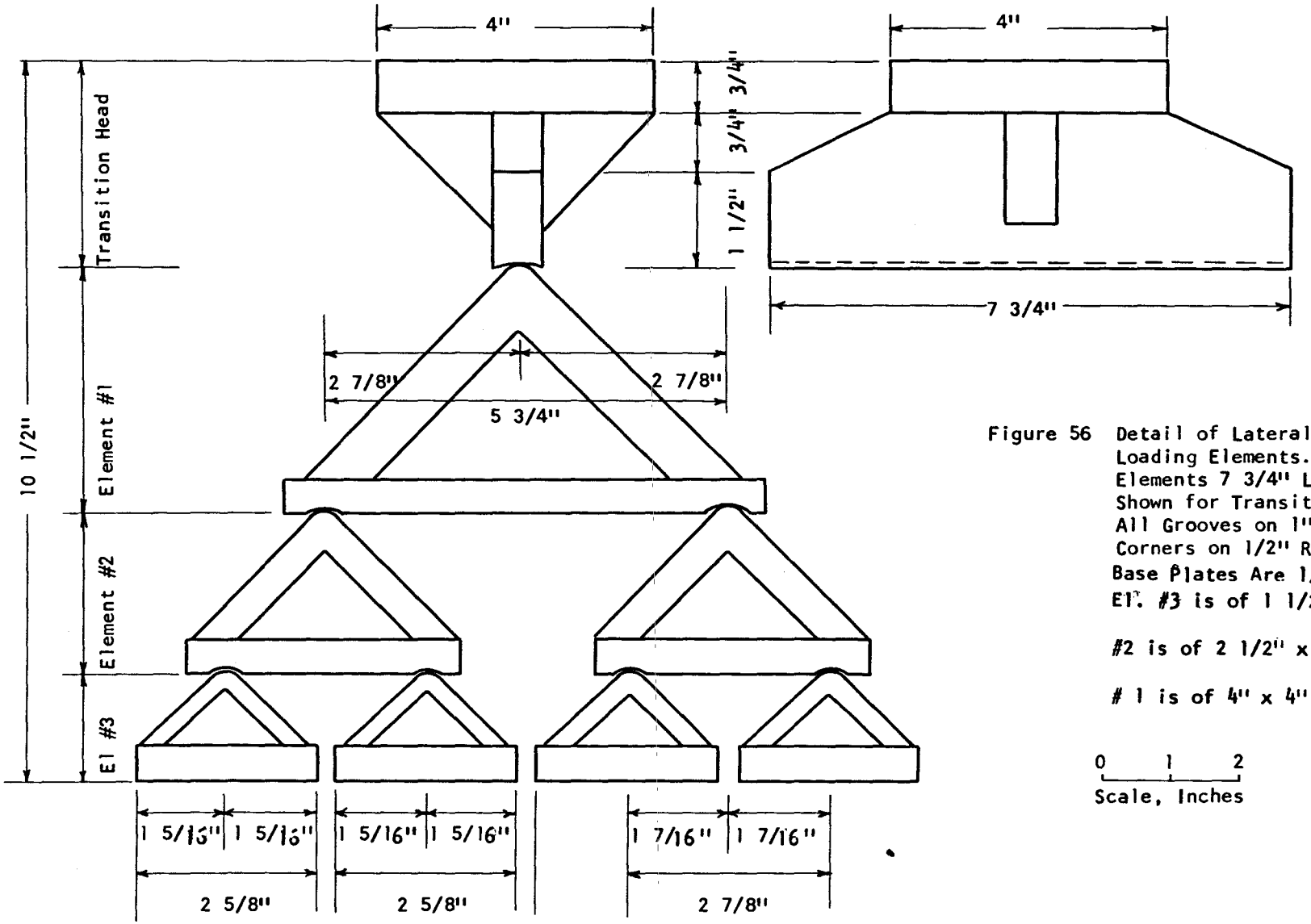

Figure 56 Detail of Lateral Triangular Loading Elements. All Elements 7 3/4" Long as Shown for Transition Head. All Grooves on 1" Radius, Corners on 1/2" Radius
Base Plates Are 1/2" Thick
El. #3 is of 1 1/2 x 1 1/2 x 1/4 Angle.
#2 is of 2 1/2" x 2 1/2" x 1/2" Angle
1 is of 4" x 4" x 3/4" Angle

0 1 2
Scale, Inches

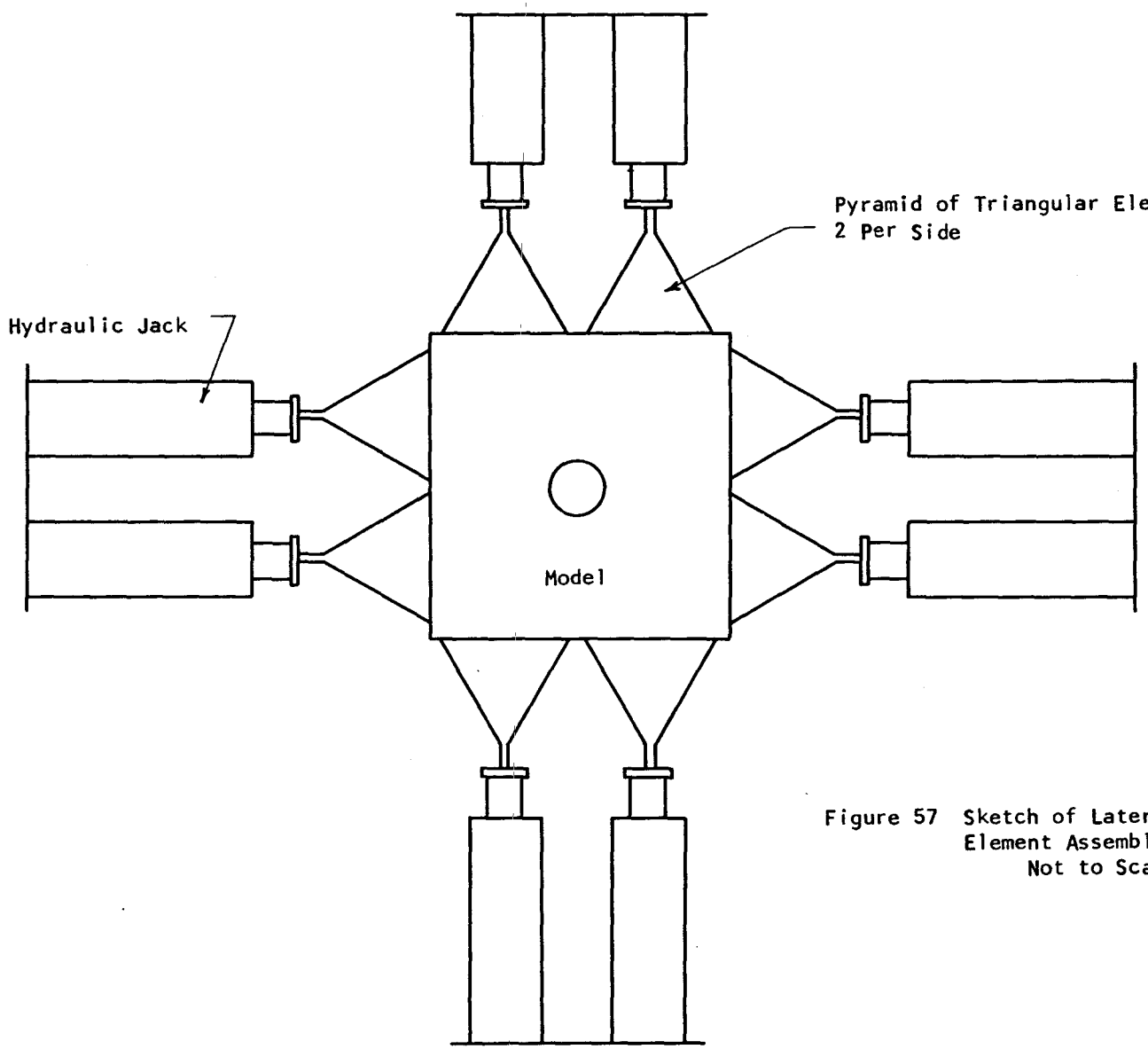

Figure 57 Sketch of Lateral Loading Element Assembly
Not to Scale

Figure 58 One Instrumental Small Triangular Lateral Loading Element

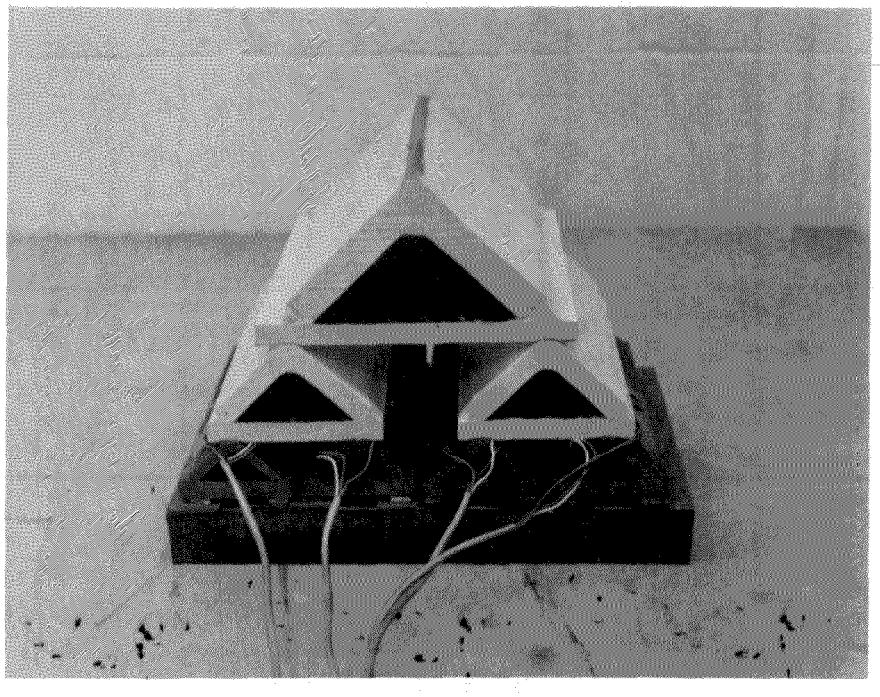

Figure 59 Entire Set of Instrumental Lateral Loading Elements

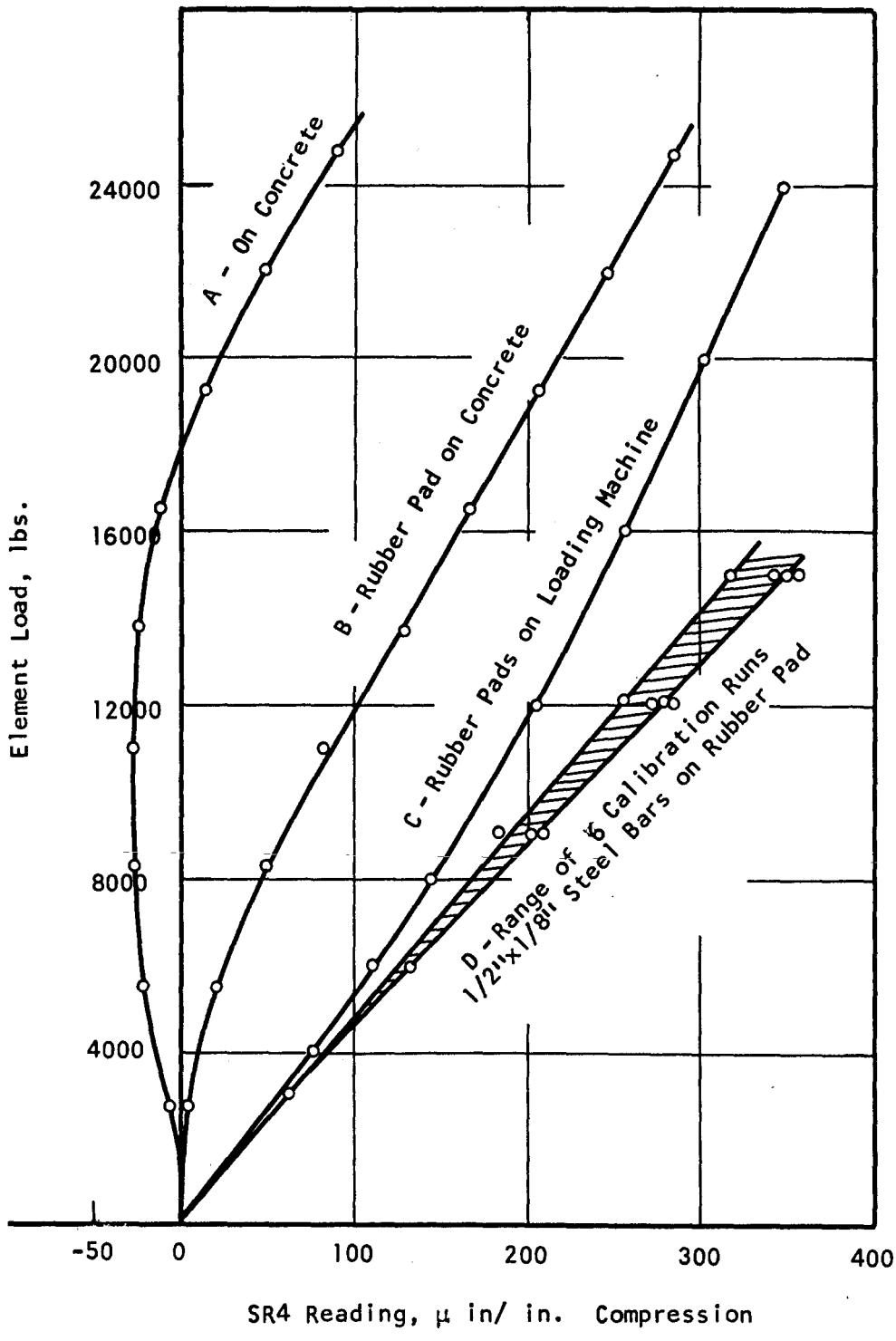

Figure 60 Calibration Curves For Element #3-1 On Different Surfaces

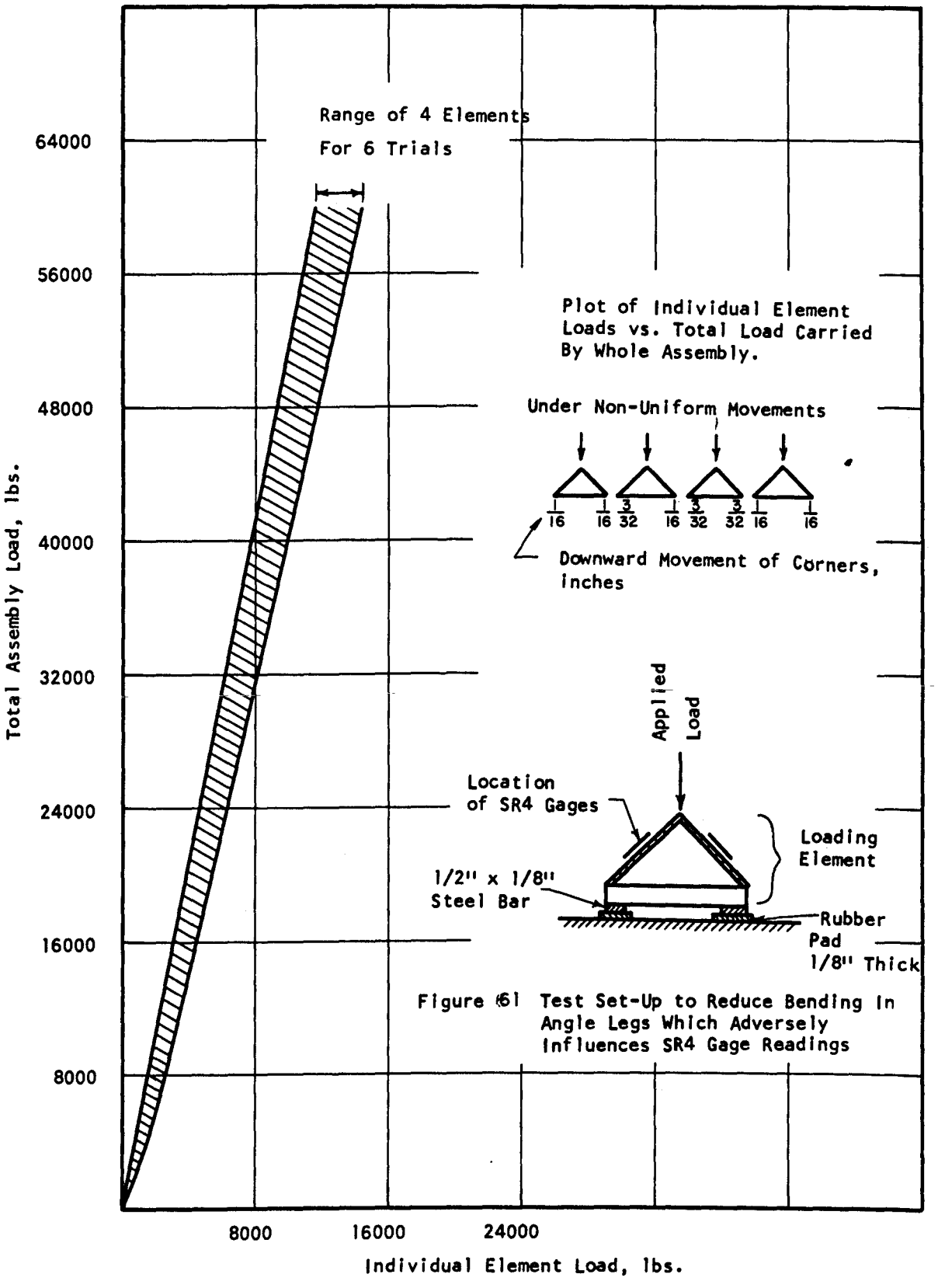

Figure 61 Test Set-Up to Reduce Bending In Angle Legs Which Adversely Influences SR4 Gage Readings

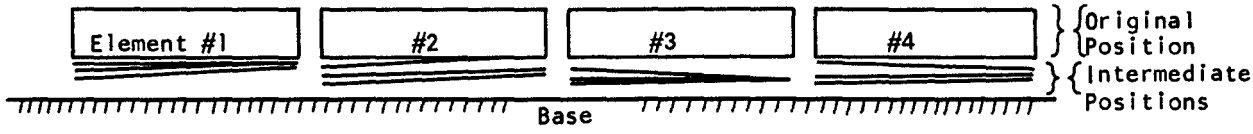

Figure 62 Deformations of Bottom Elements Under Loading of Whole Set - 1/2 Scale Elements Set On Soft Pine

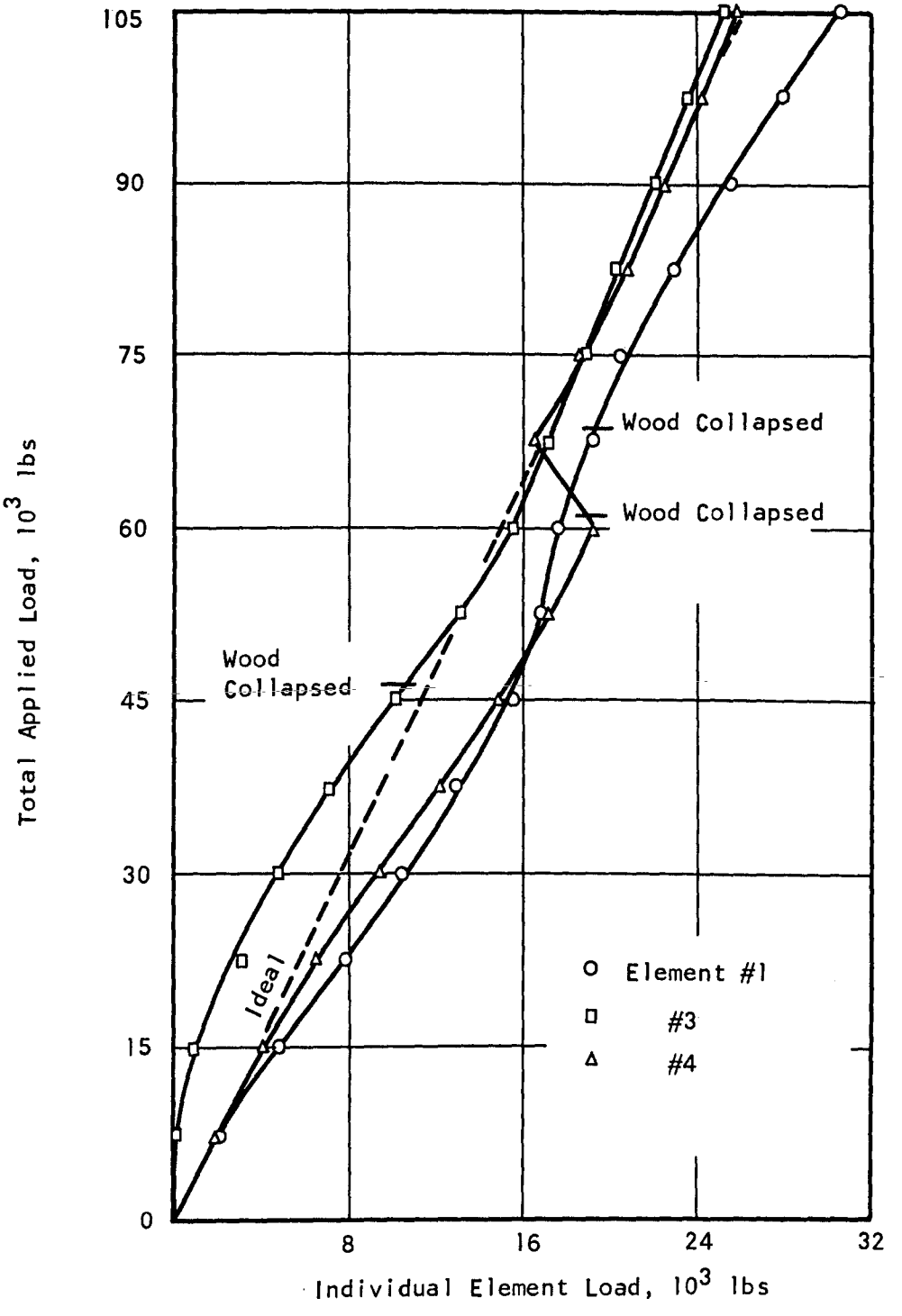

Figure 63 Load Distribution of Set of Triangular Elements

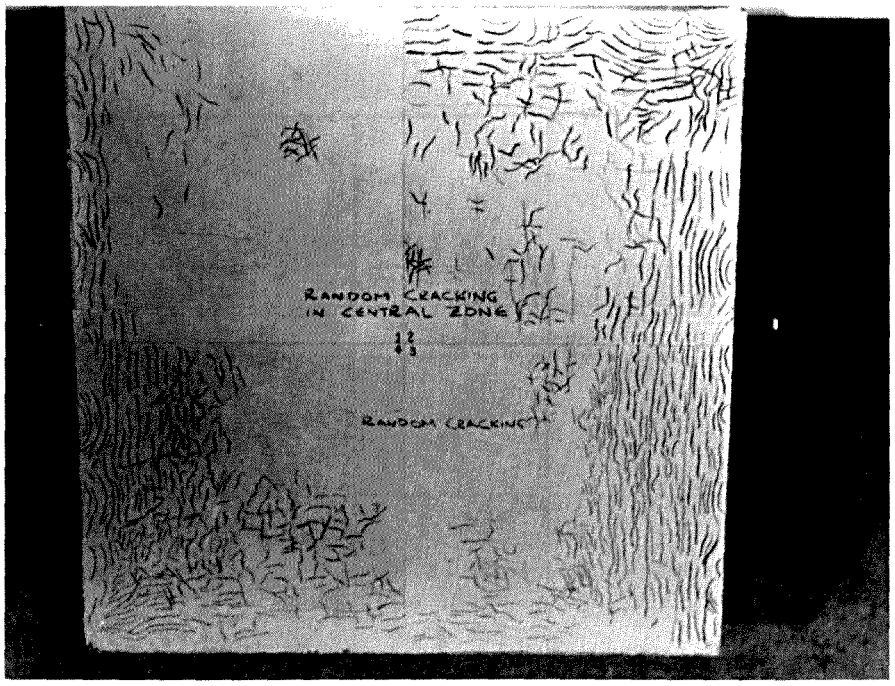

Figure 64 Crash Pattern from Brittle Coating Test No. 1

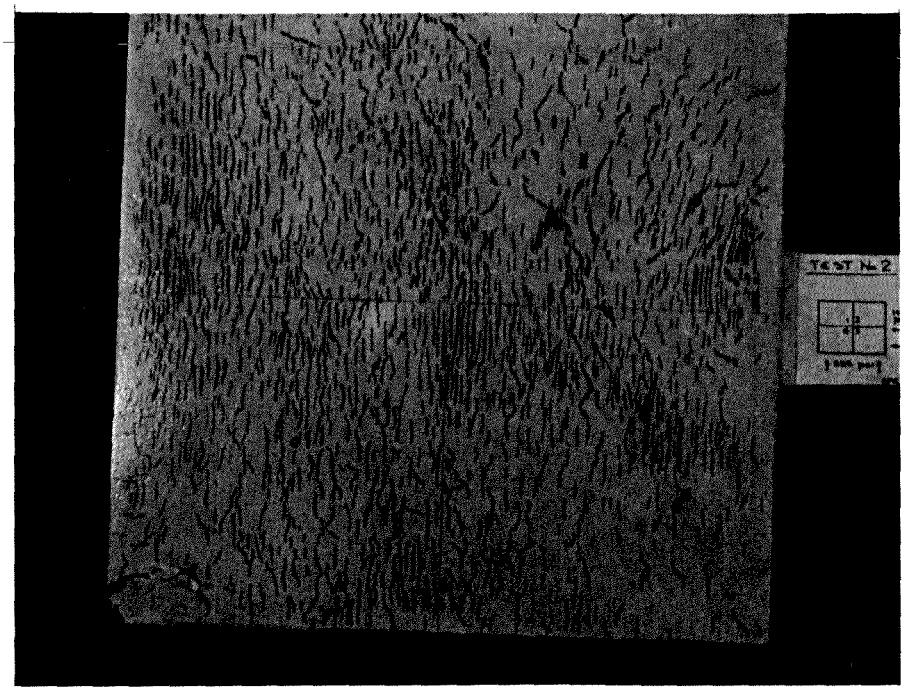

Figure 65 Crash Pattern from Brittle Coating Test No. 2

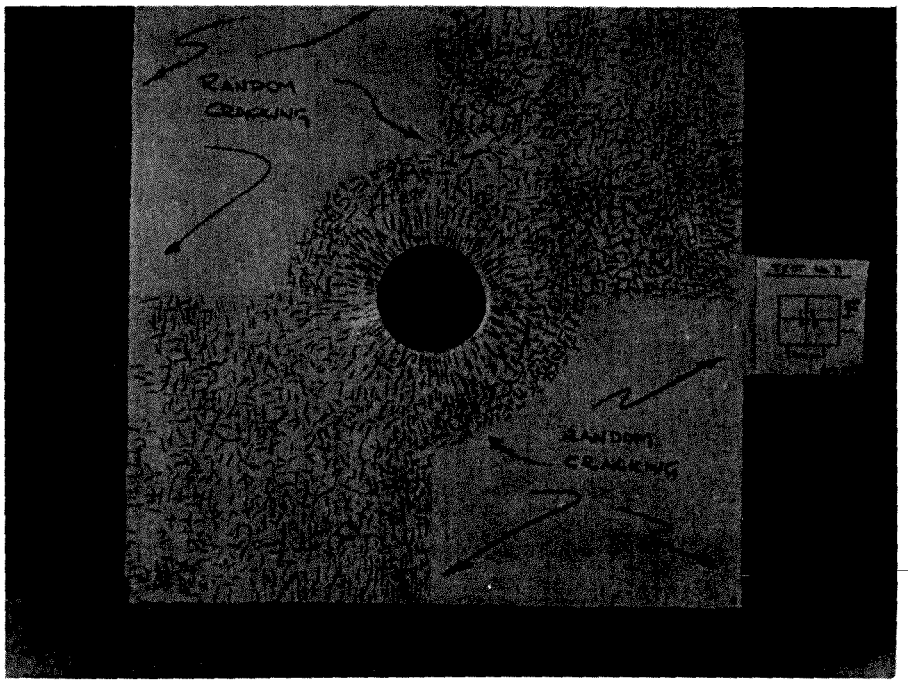

Figure 66 Crash Pattern from Brittle Coating Test No. 3

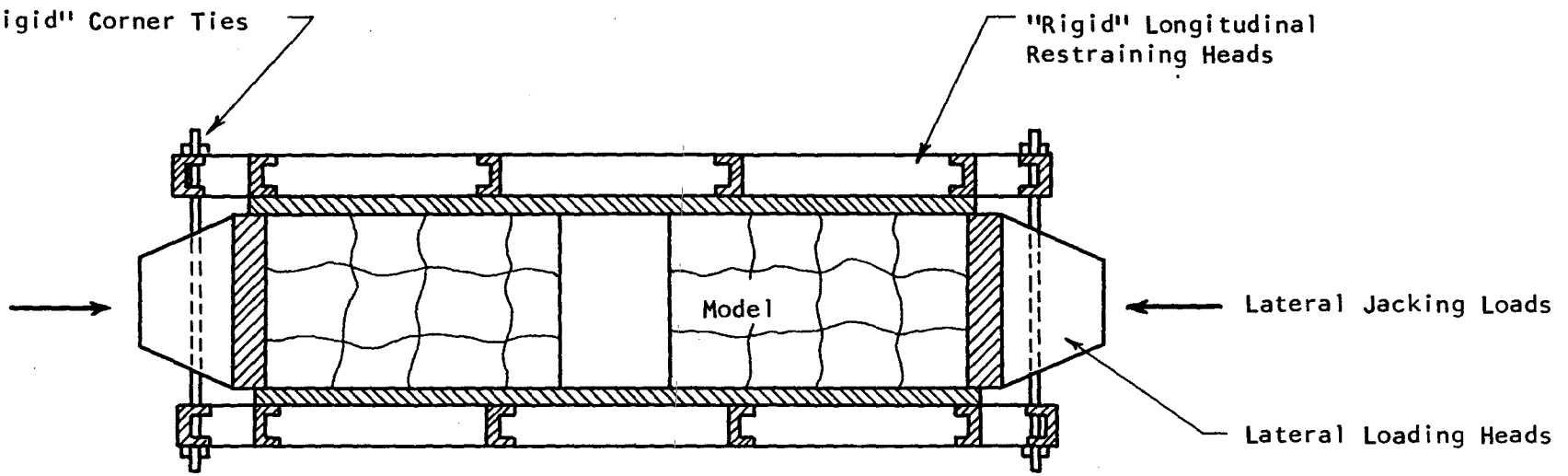

Figure 67 Sketch of Possible Rigid Head System Tied Across Model Not to Scale

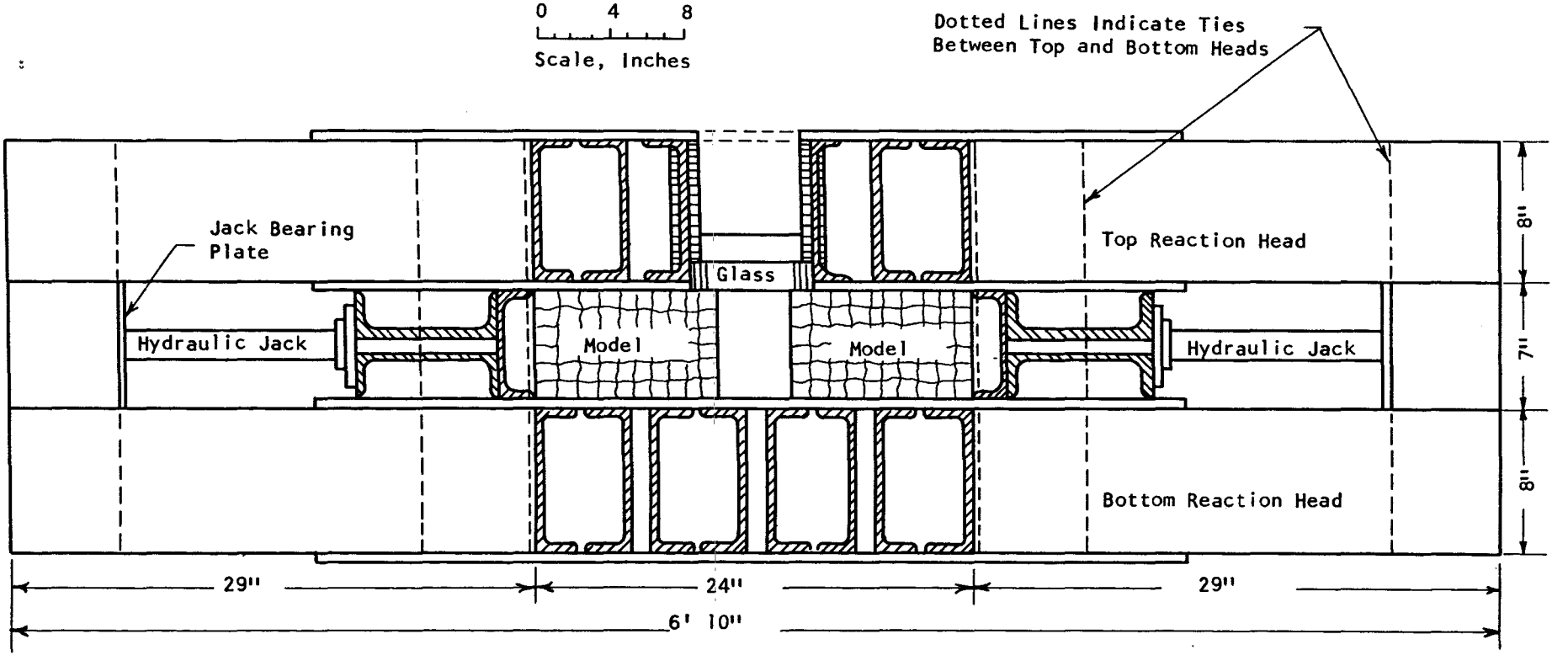

Figure 68 Cross Section of Possible Rigid Loading and Reaction Frame Built Up Out of 8 ⌴ 13.75 and 1/2" Plate, Welded Dimensions Shown Are For Models 24"x24"x6" Shown With Hydraulic Cushion Lateral Loading Elements

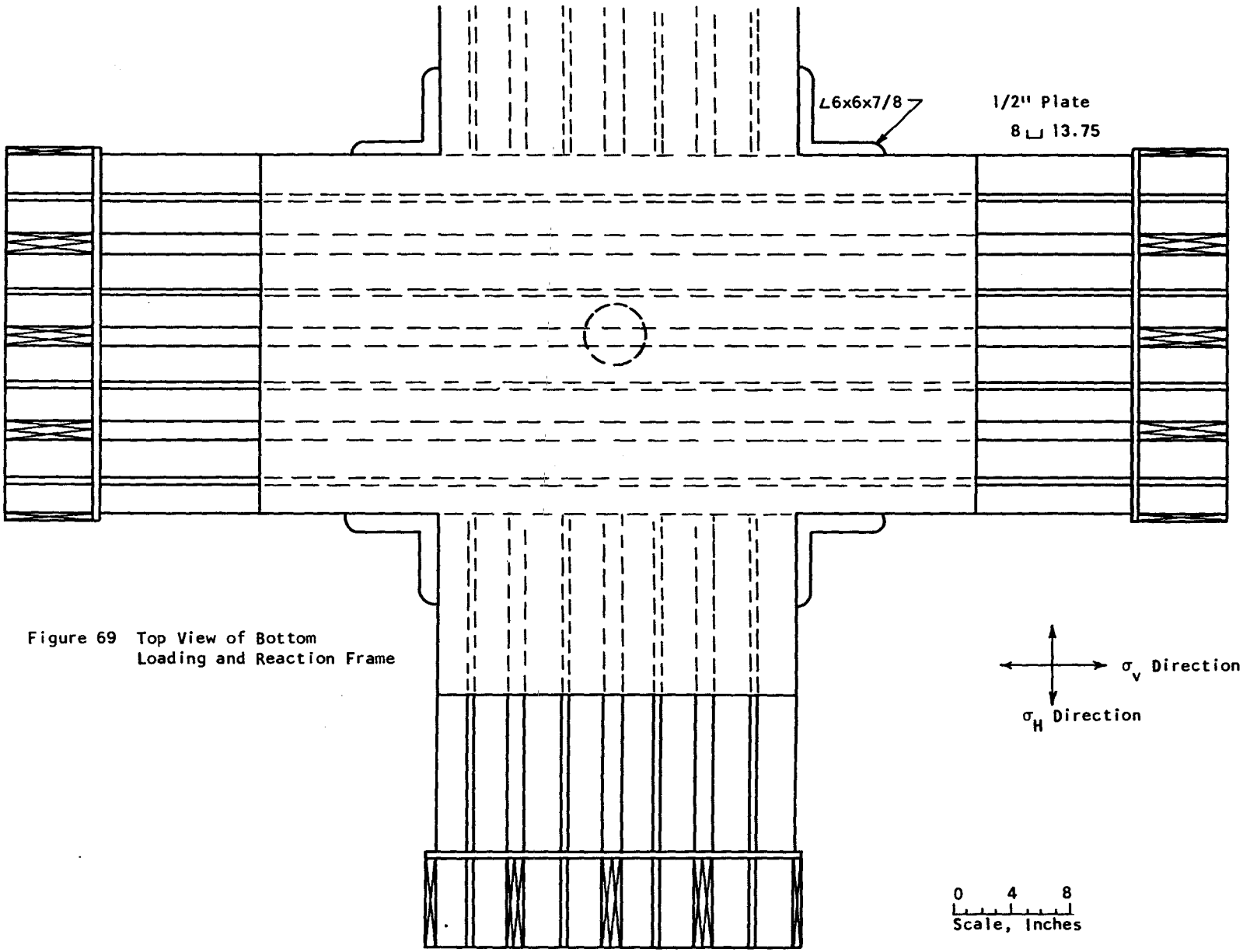

Figure 69 Top View of Bottom Loading and Reaction Frame

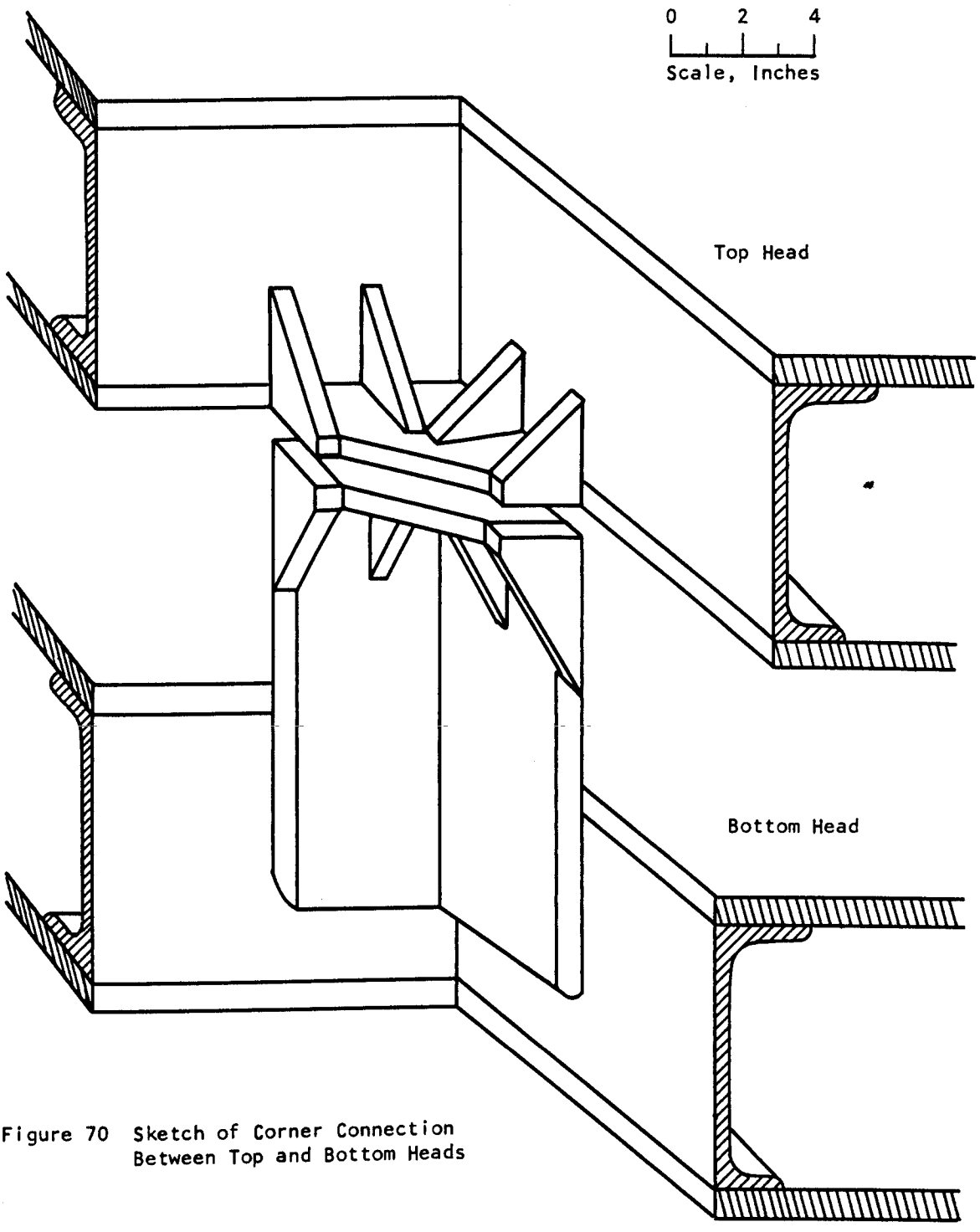

Figure 70 Sketch of Corner Connection Between Top and Bottom Heads

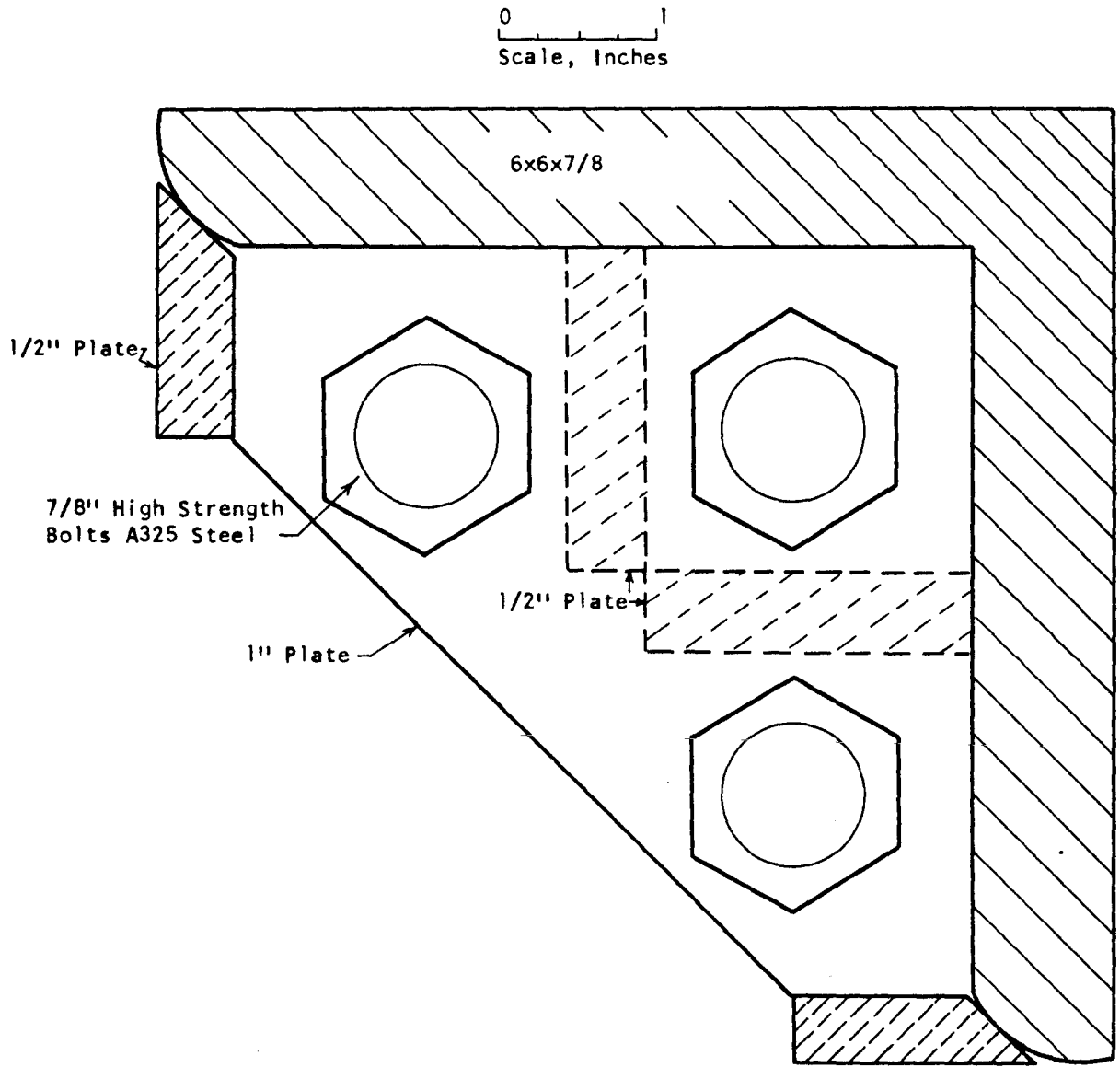

Figure 71 Sketch of Corner Connection
Between Top and Bottom Heads

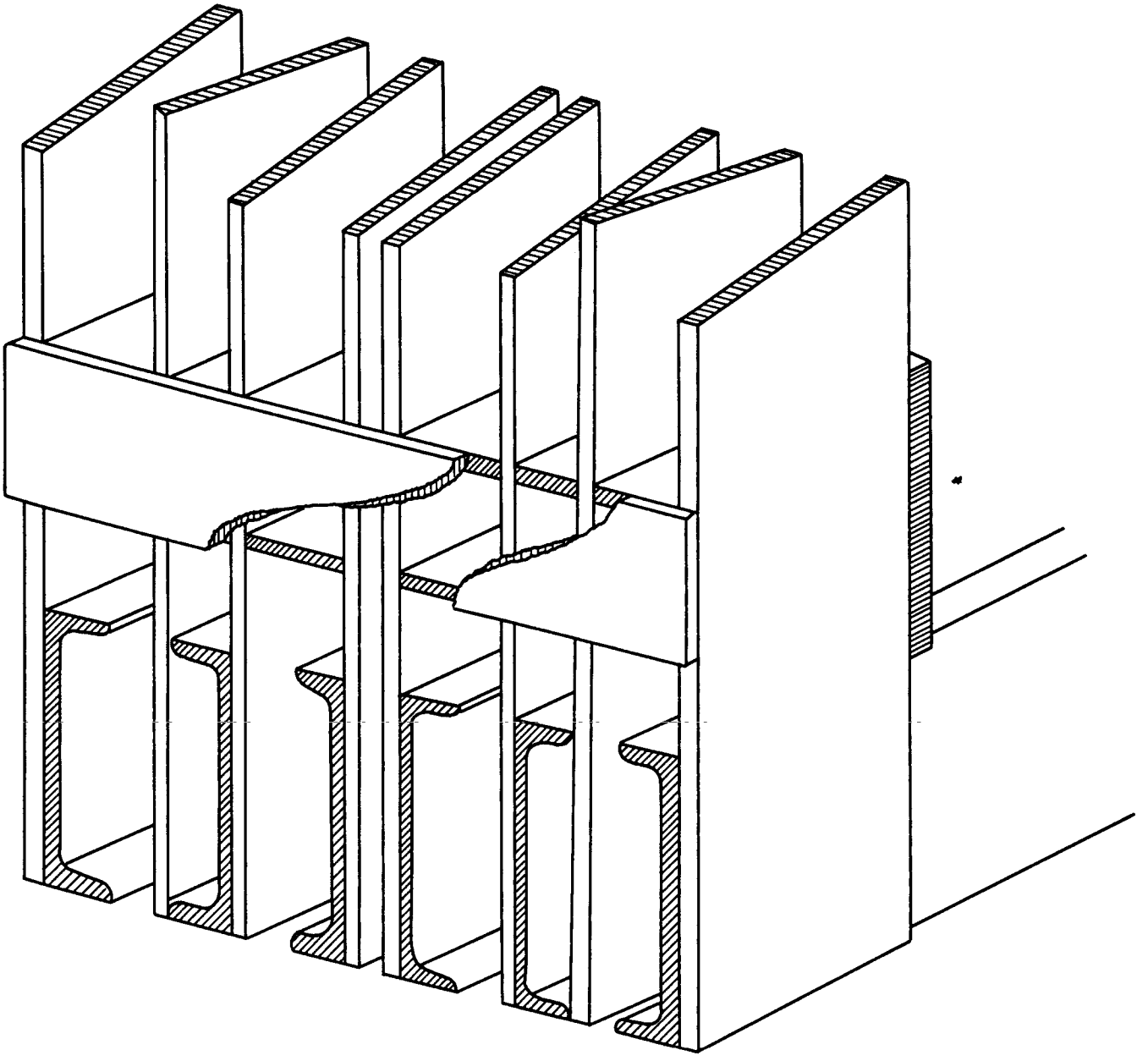

Figure 72 Back Sketch of Jack Reaction

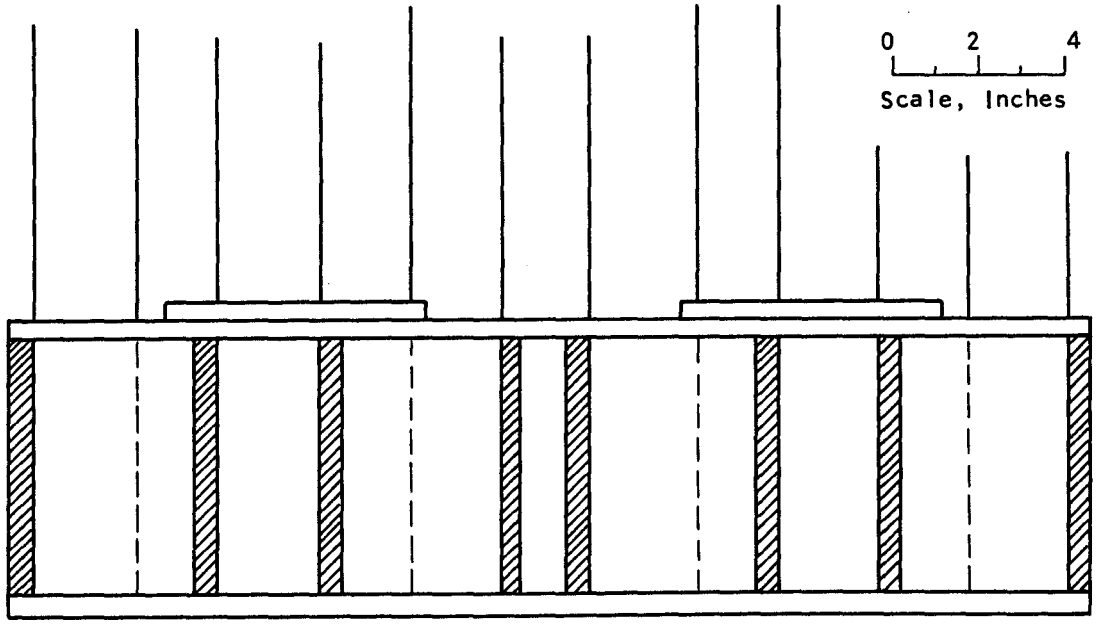

Plan

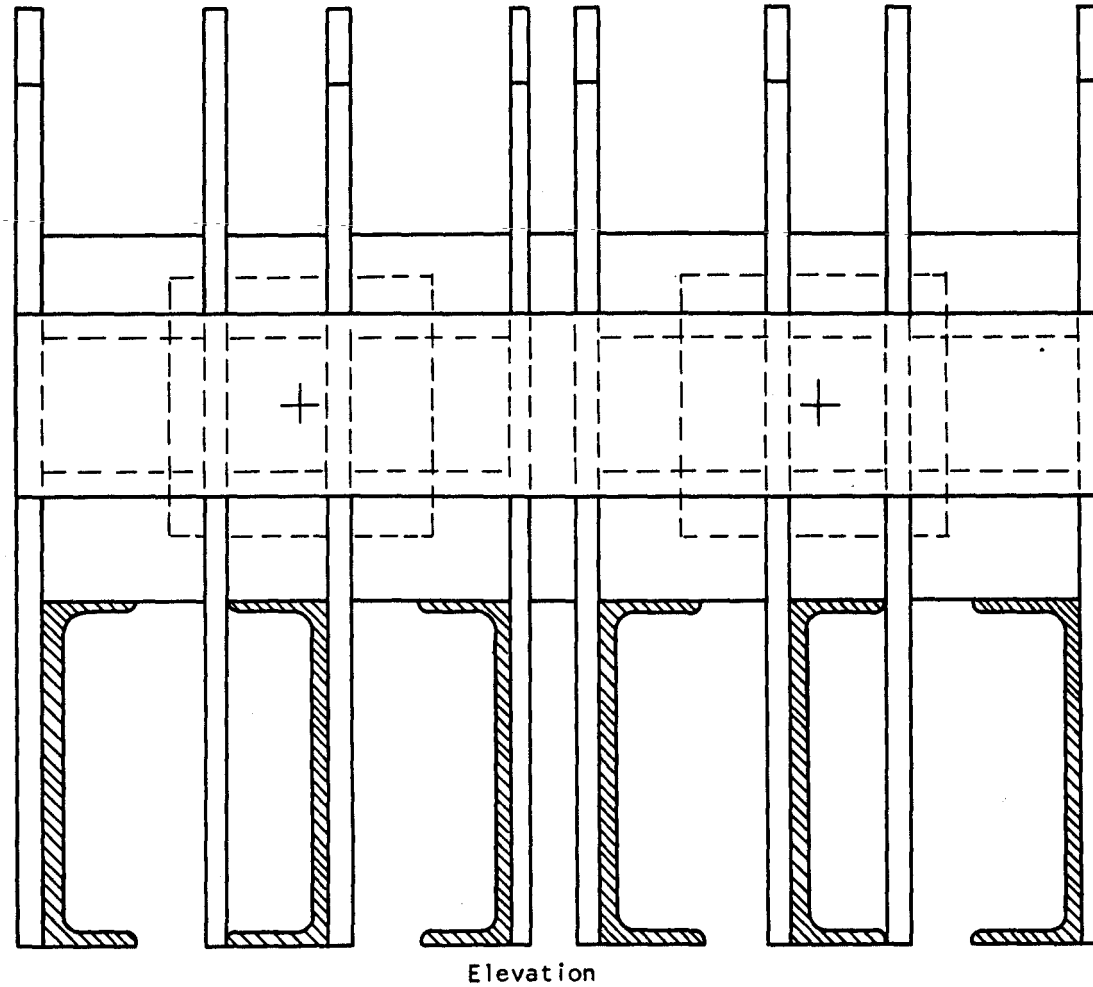

Elevation

Figure 73 Plan and Elevation of Jack Reaction

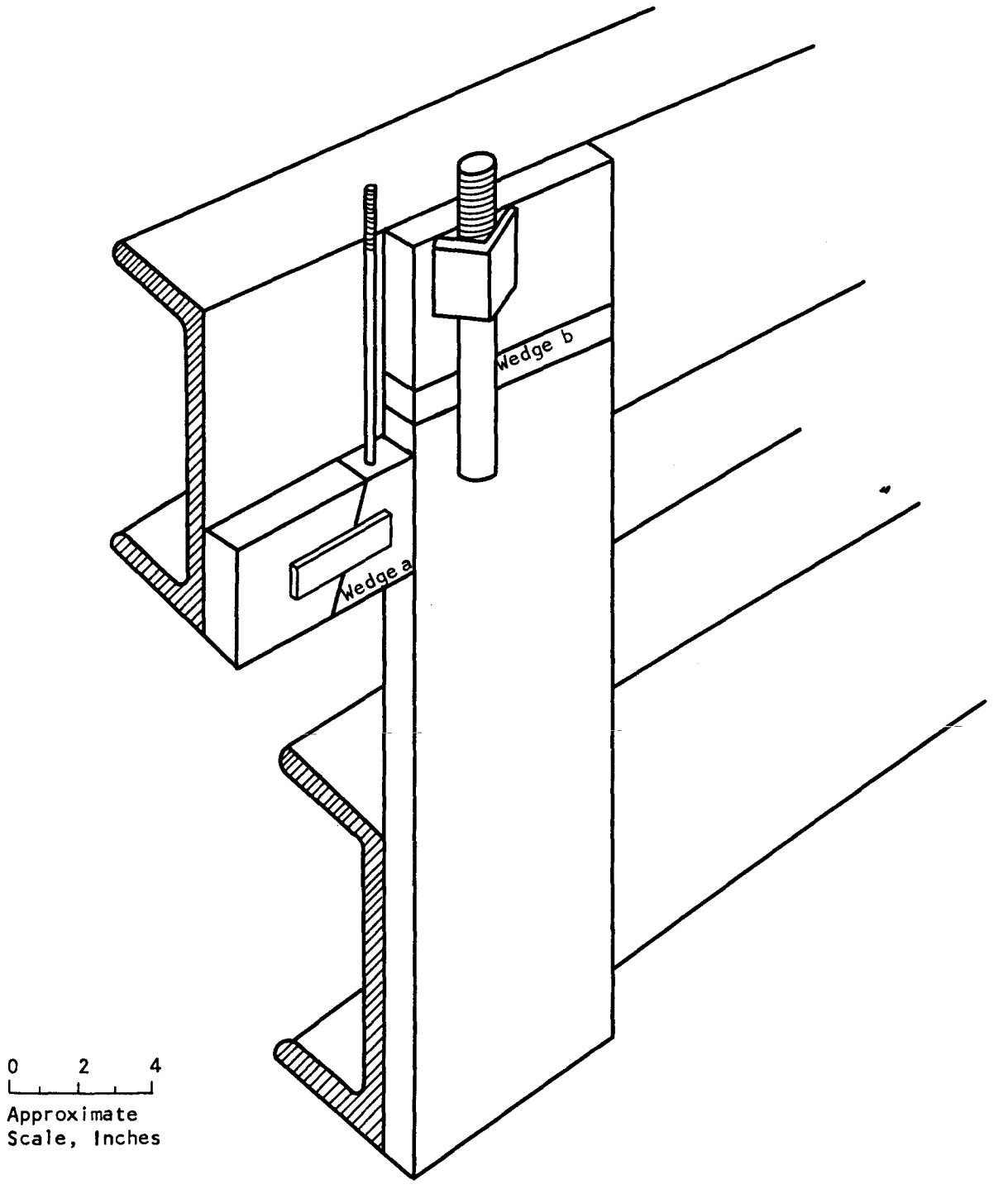

Figure 74 Sketch of End Connection

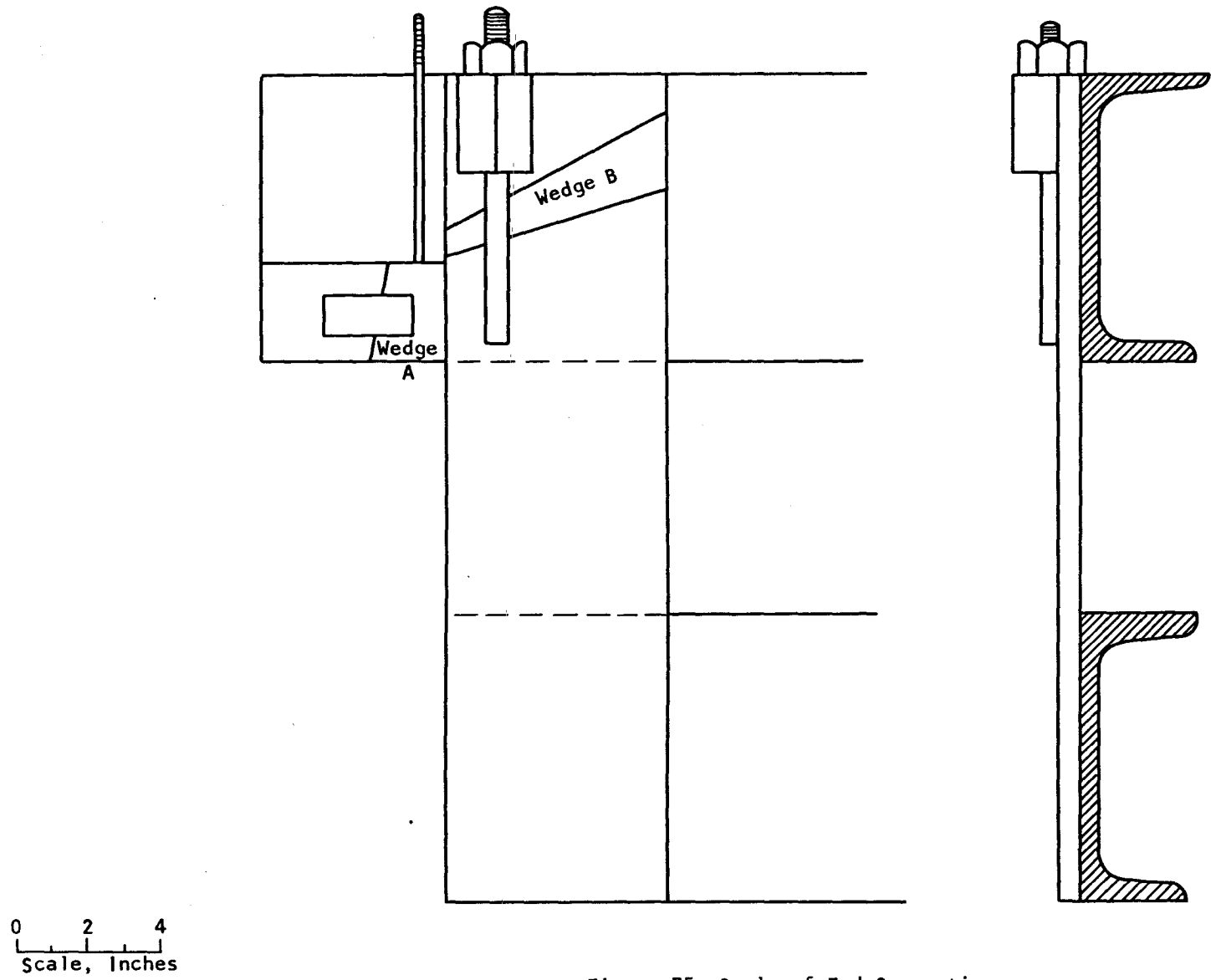

Figure 75 Scale of End Connection

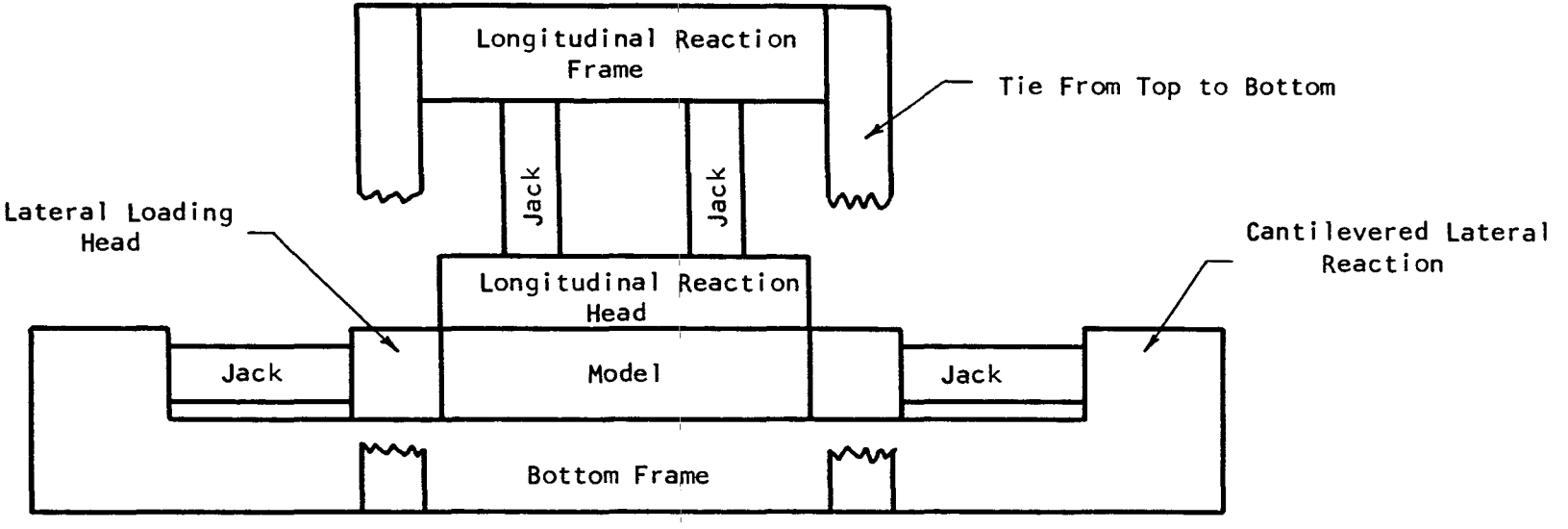

Figure 76 Sketch of Possible Cantilevered Lateral Reaction System Not to Scale

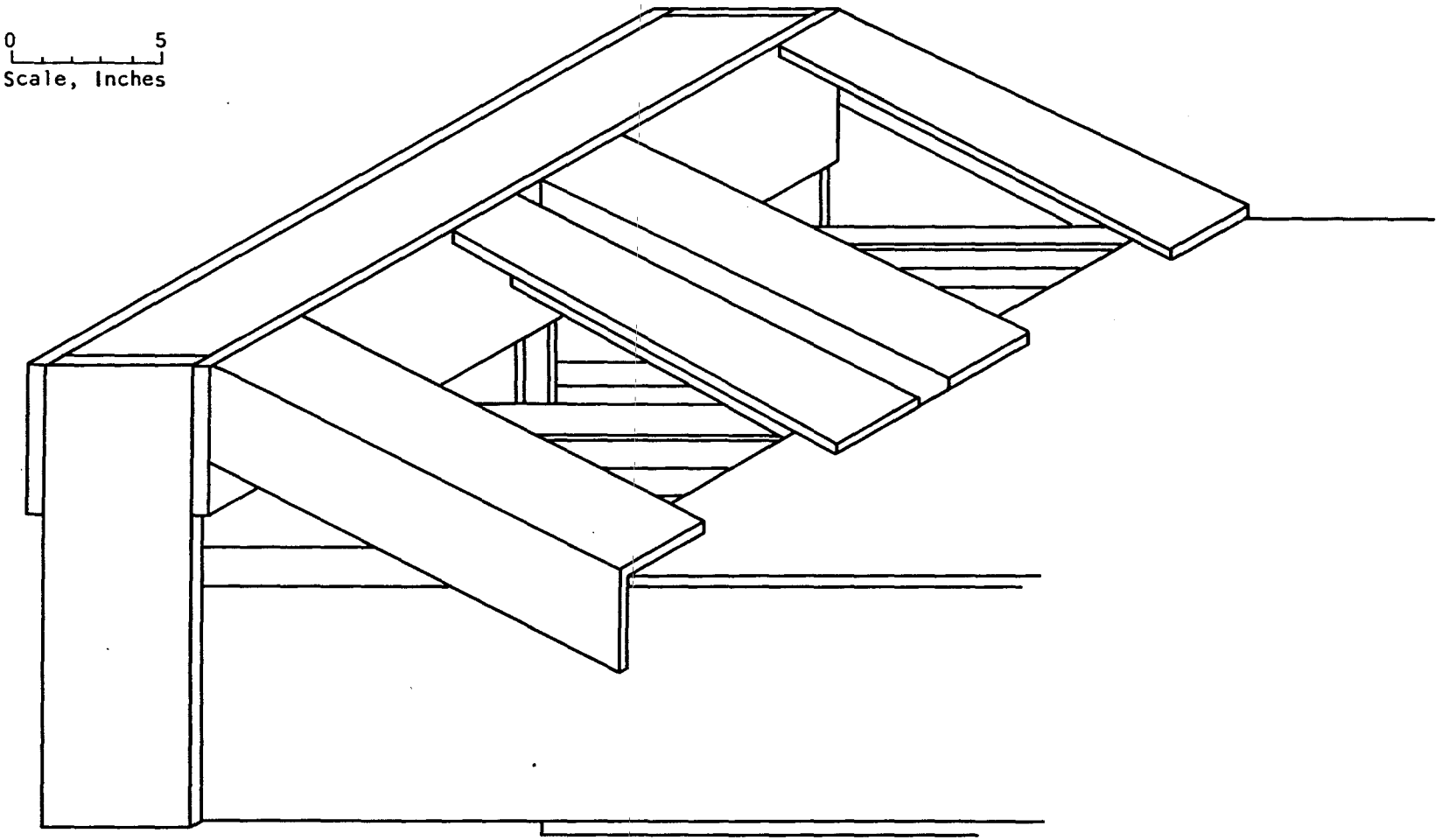

Figure 77 Sketch of Possible Cantilevered End Reaction

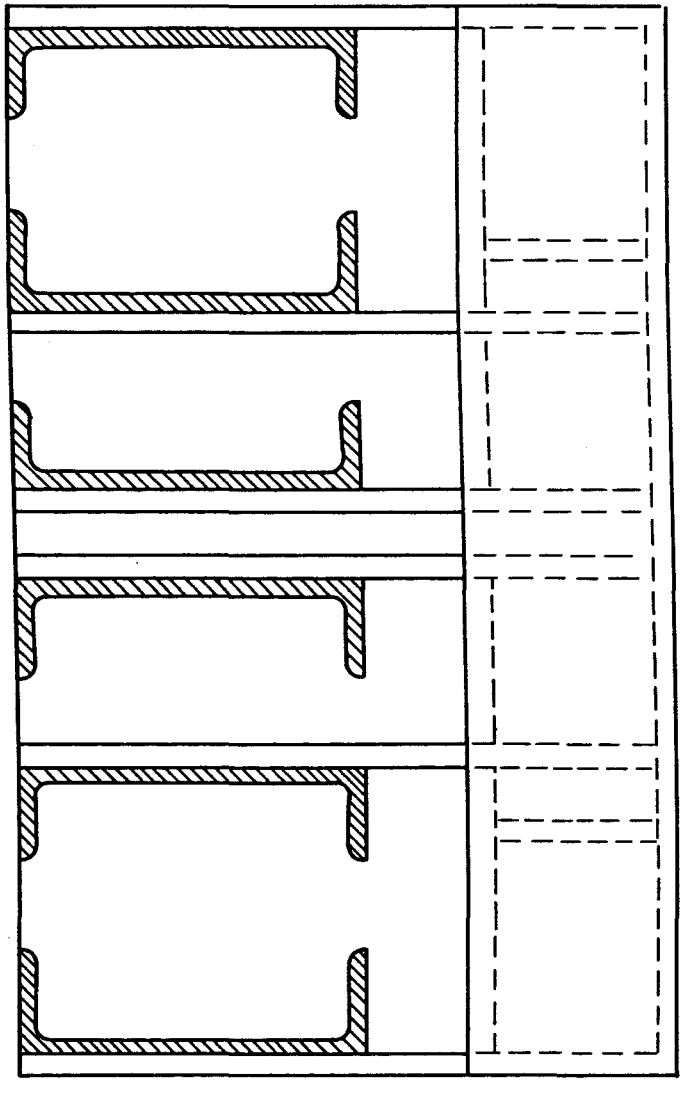

Elevation

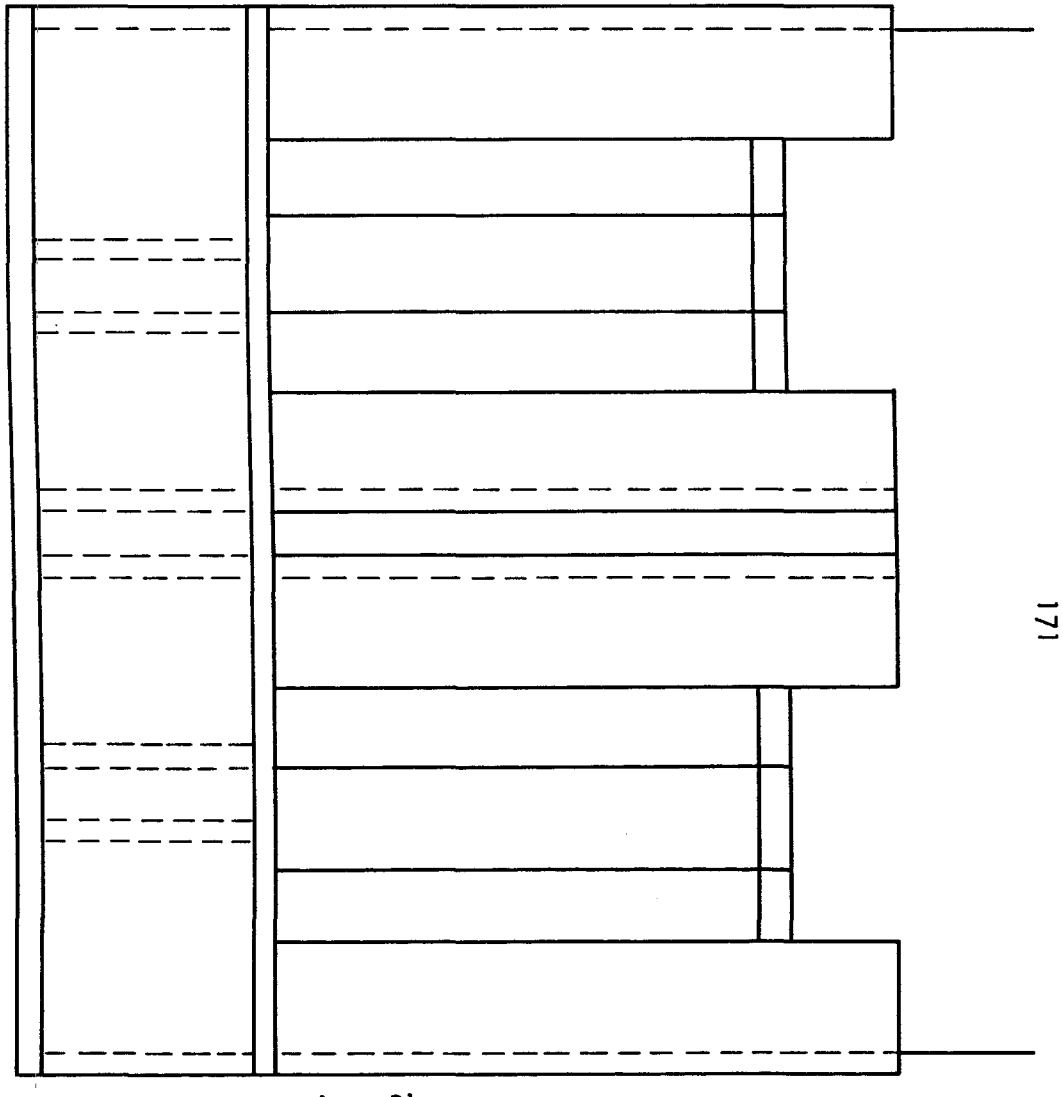

Plan

0 2 4

Scale, Inches

Figure 78 Plan and Elevation Views of Possible Cantilevered End Reaction

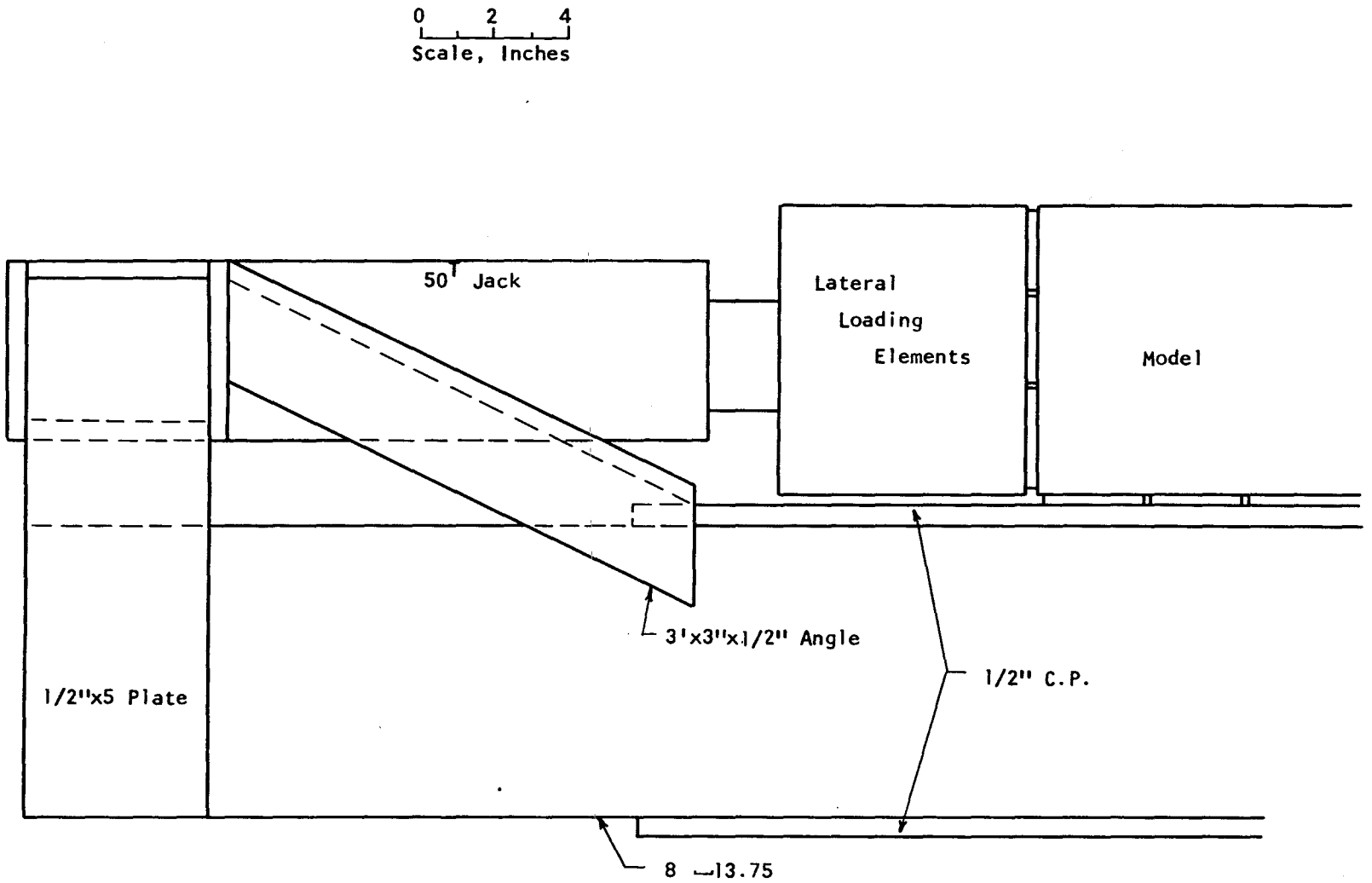

Figure 79 Side View, Possible Cantilevered End Reaction

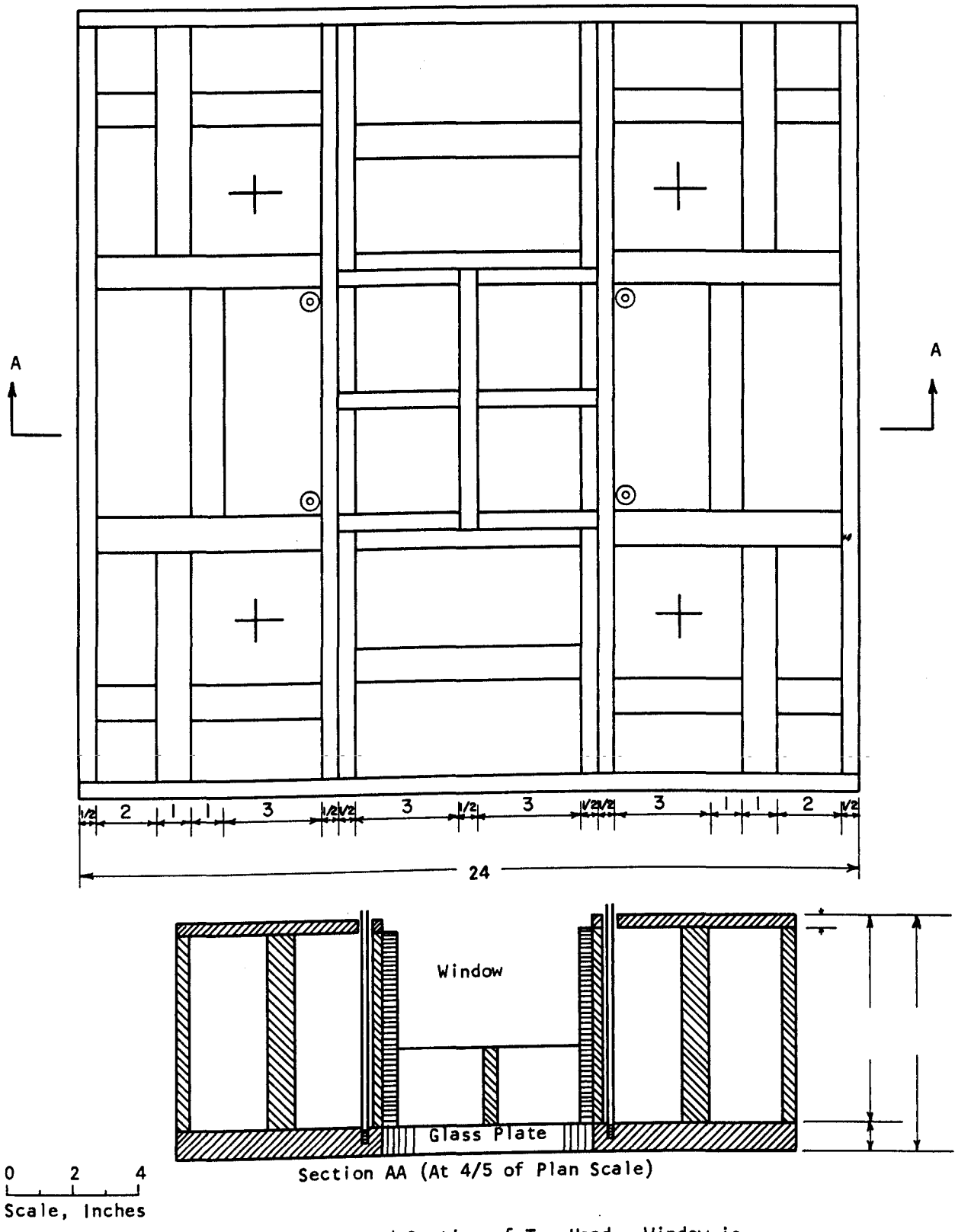

Figure 80 Plan and Section of Top Head. Window is 1"x8"x8" Plate of LOF Tuflex Glass. In Plan View, Crosses Mark Centers of Hydraulic Jacks, Circles Represent 1/2" Holes in Top Plate to Receive 1/4" Rod Threaded Into Bottom Cover Plate.

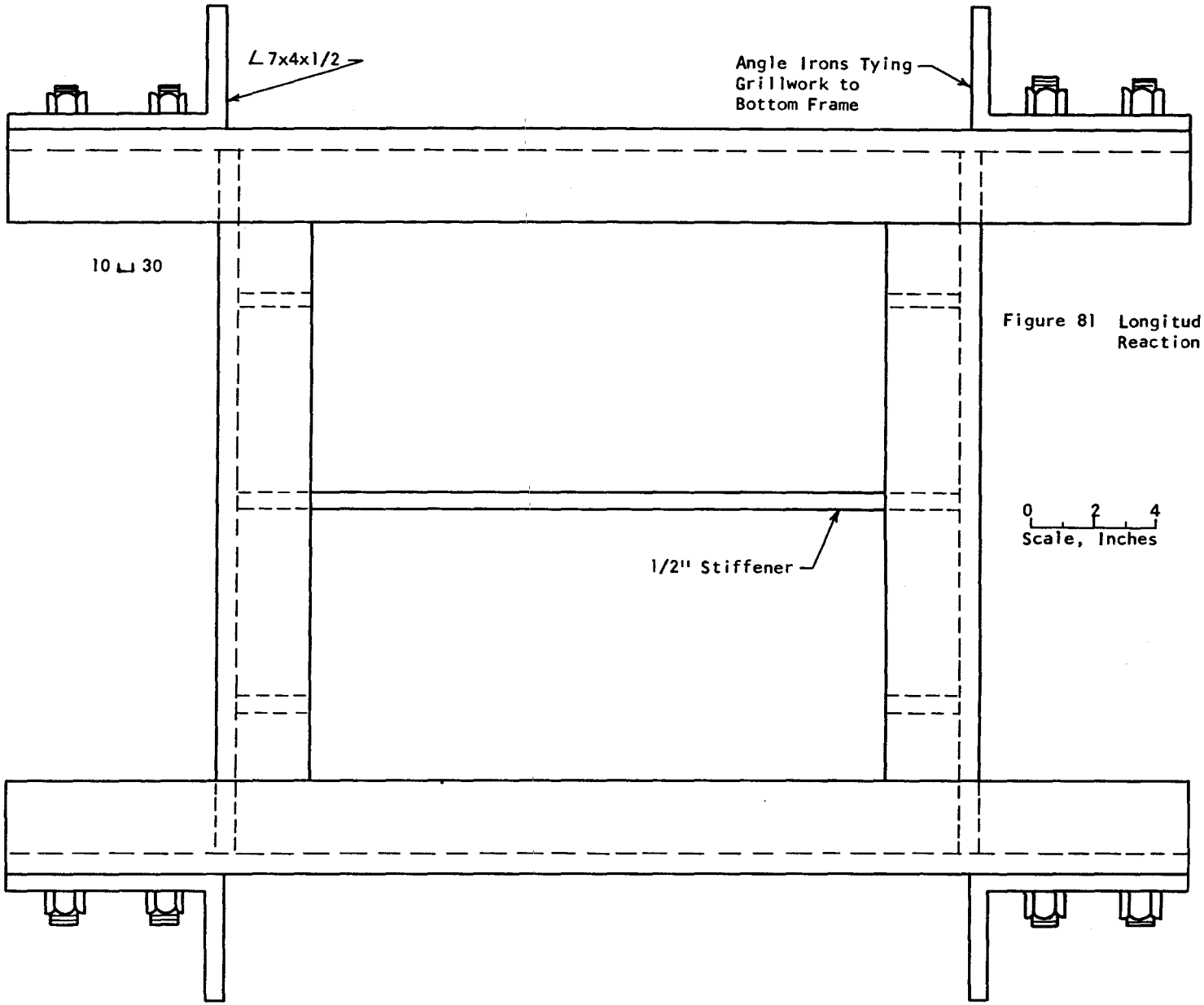

Figure 81 Longitudinal Reaction Head

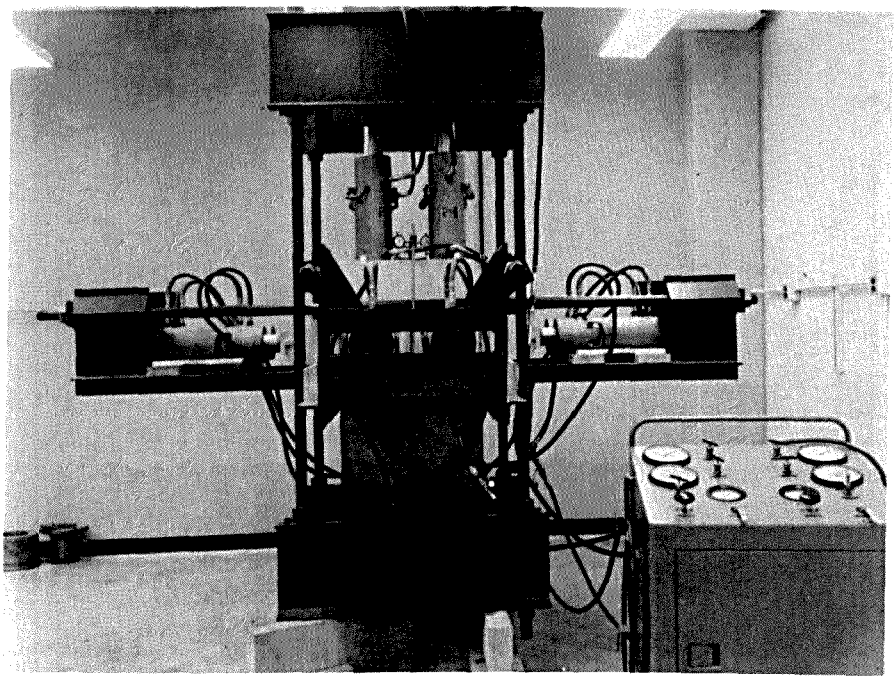

Figure 82a

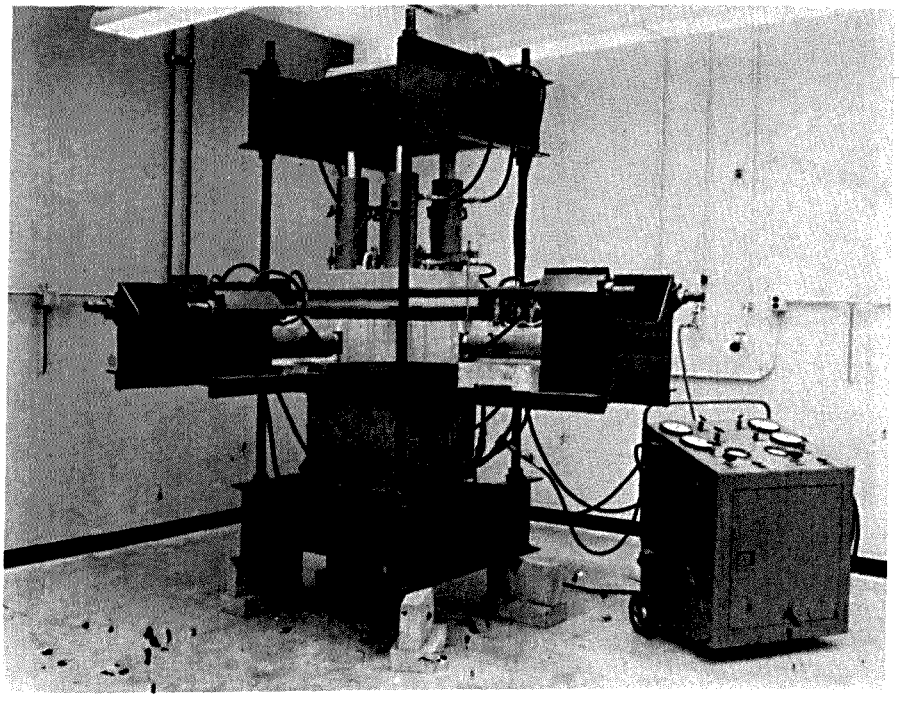

Figure 82b

Figure 82 Eye Level Views of Loading Apparatus

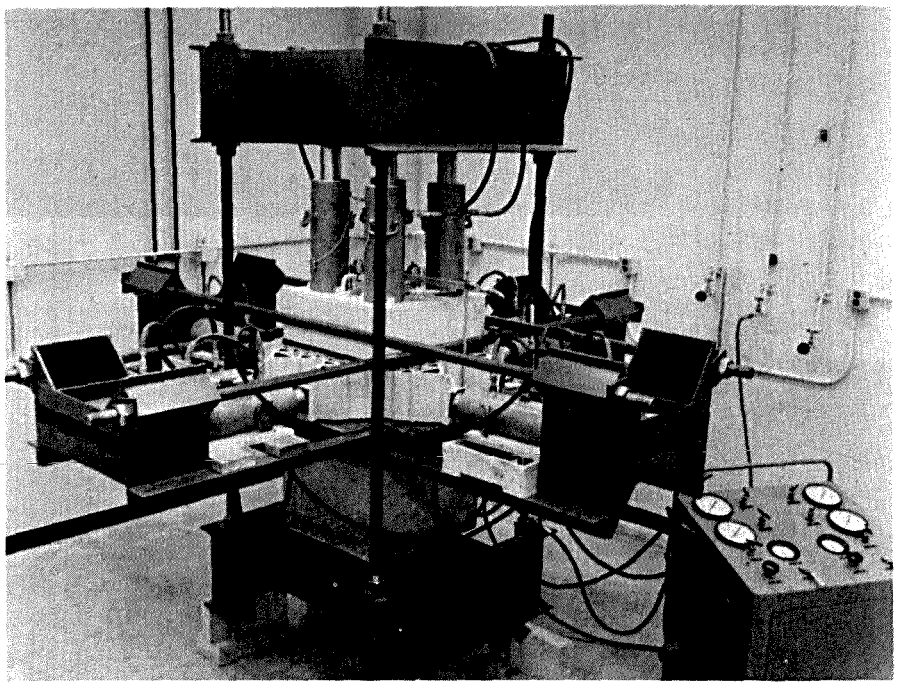

Figure 83 Birds-Eye View of Loading Apparatus

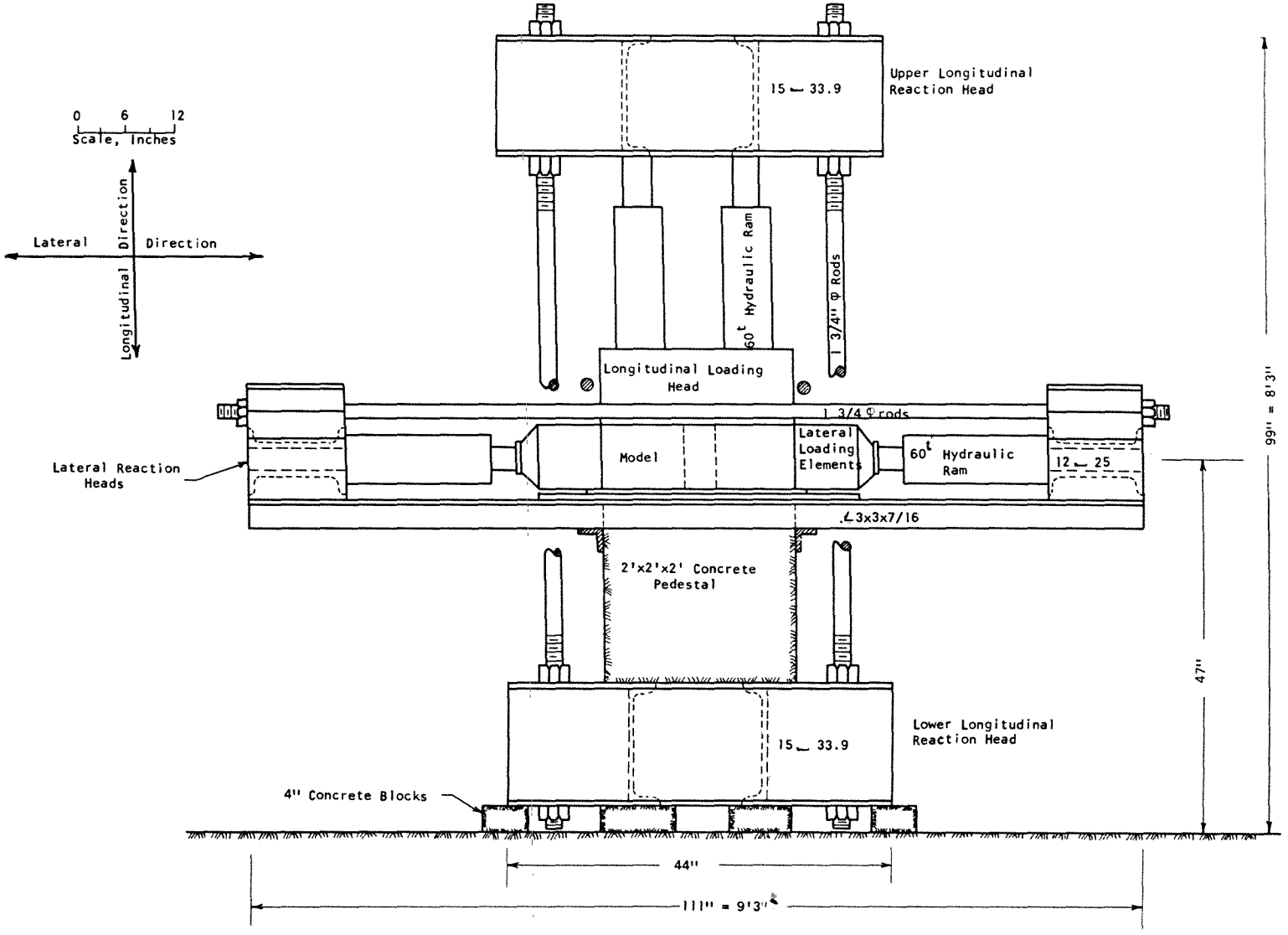

Figure 84 Loading Frame Assembly

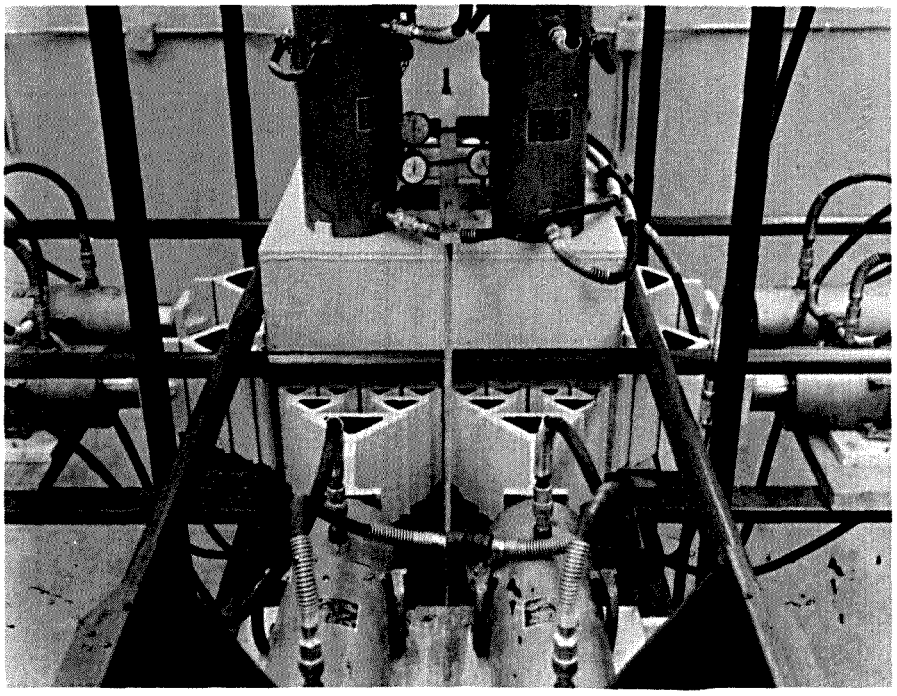

Figure 85a Lateral Loading Elements

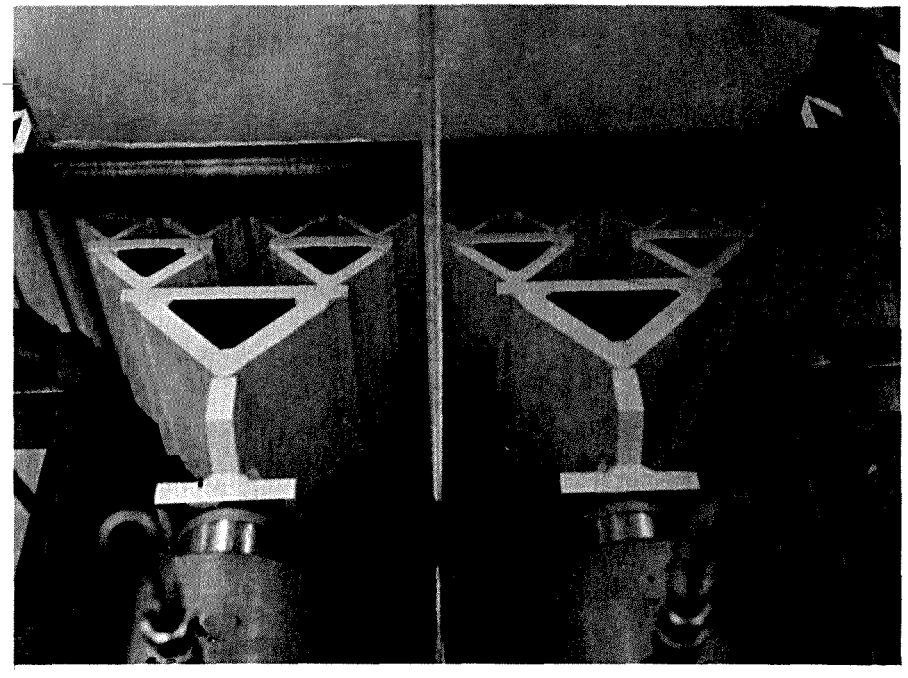

Figure 85b Closeup of Above

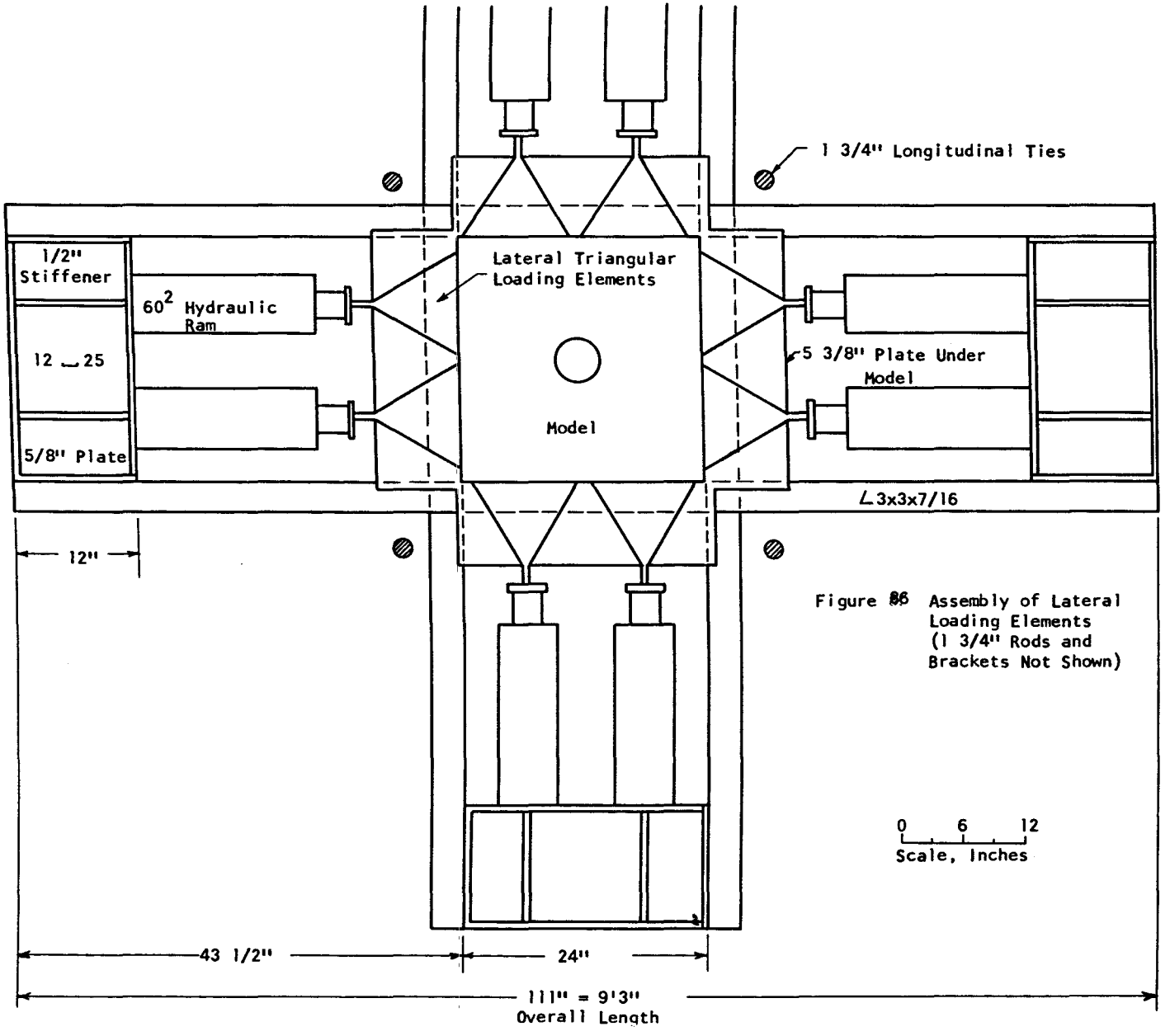

Figure 86 Assembly of Lateral Loading Elements (1 3/4" Rods and Brackets Not Shown)

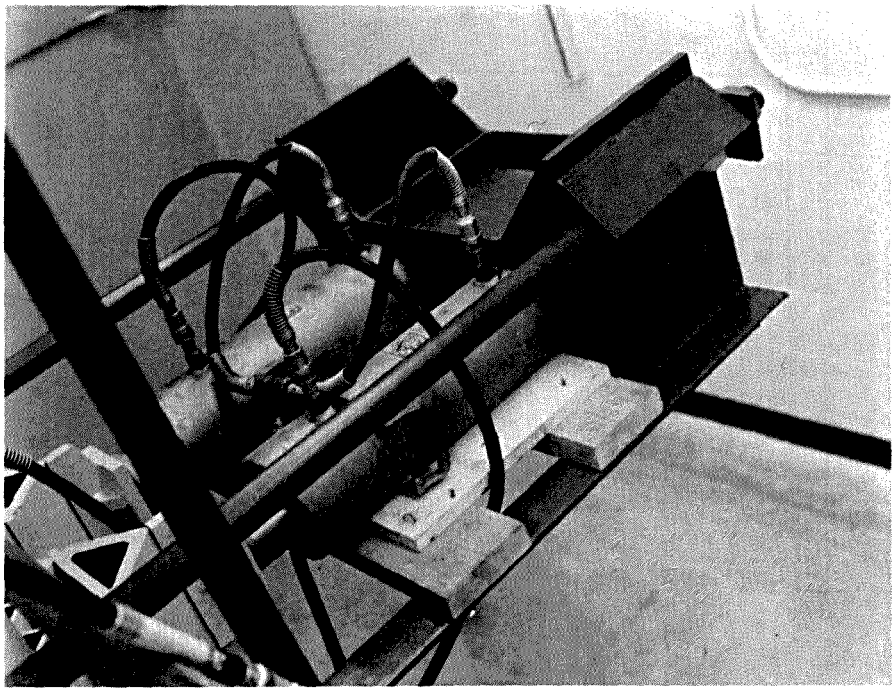

Figure 87a

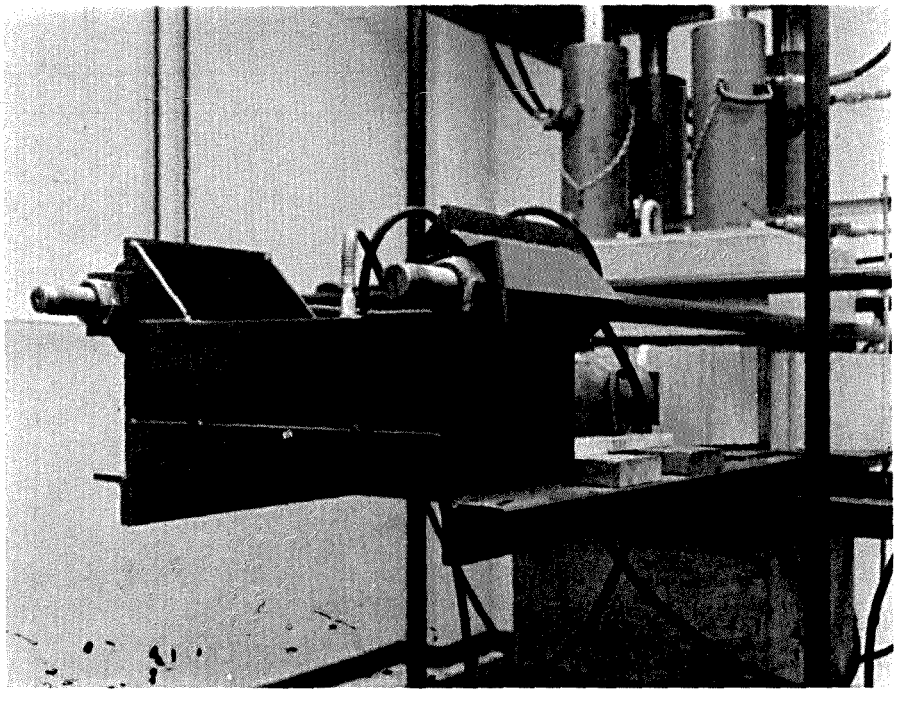

Figure 87b

Figure 87 Lateral End Reactions in σ_v Direction

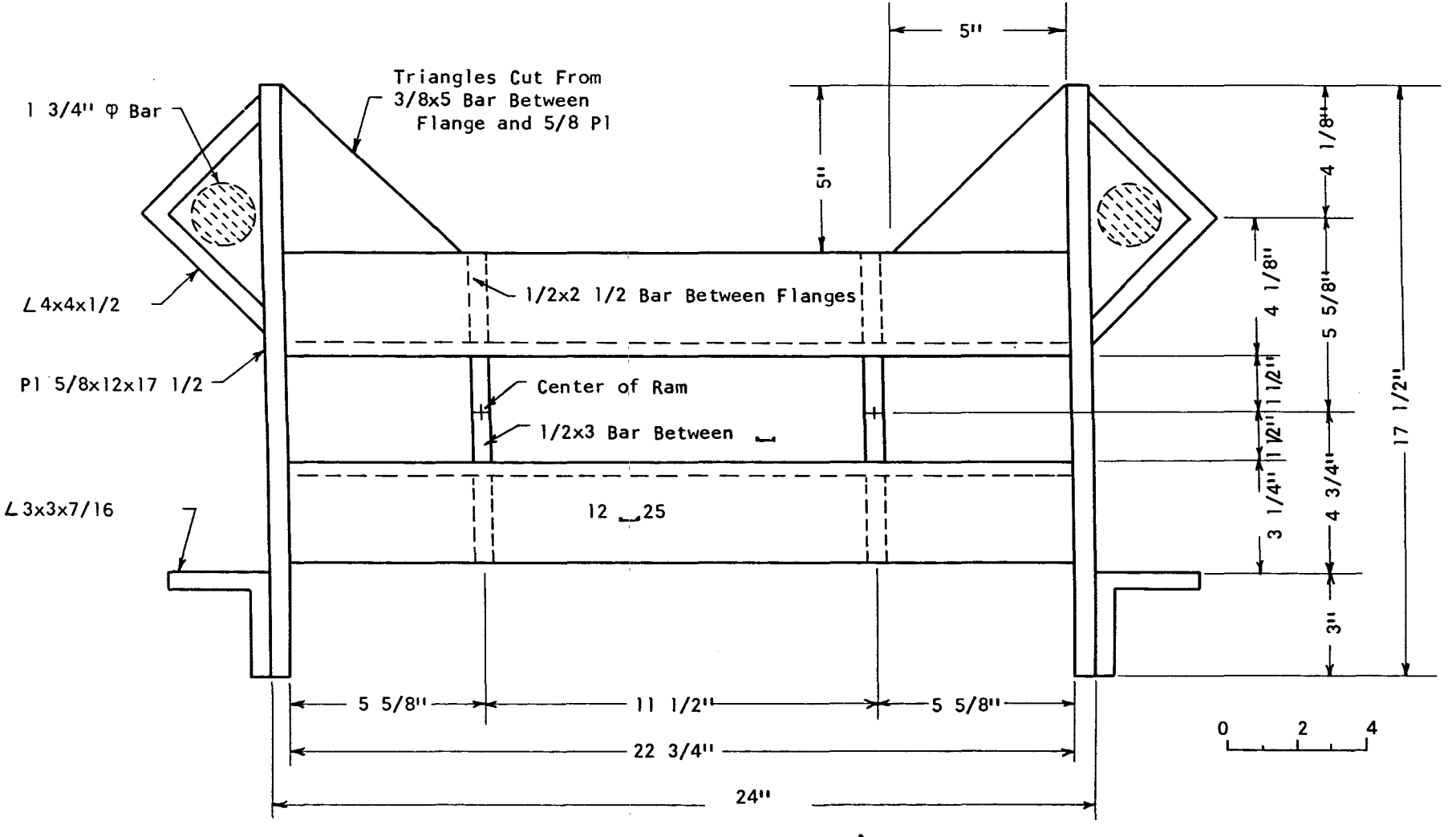

Figure 88 Longitudinal End Reaction in σ_v Direction

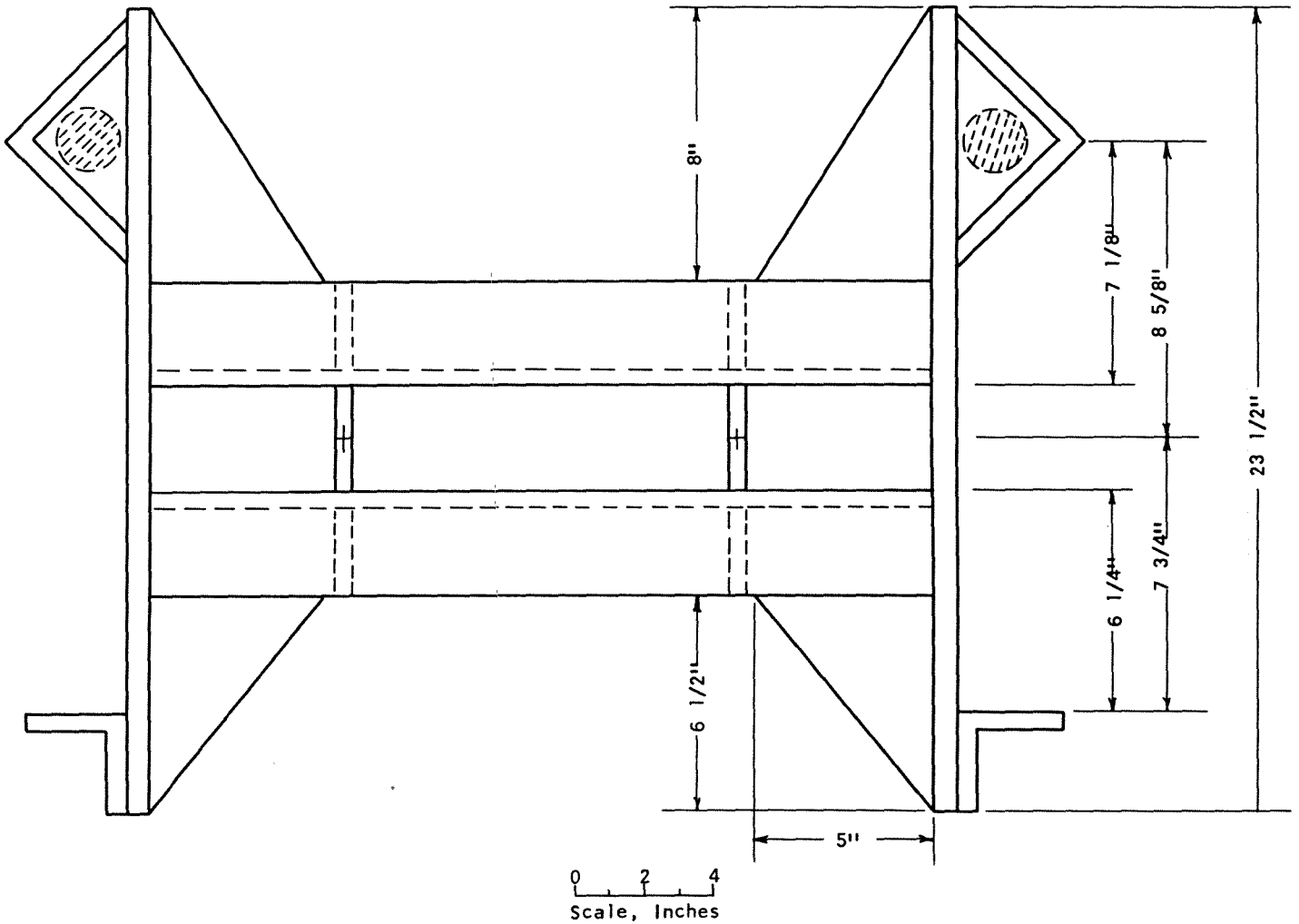

Figure 89 Longitudinal End Reaction in σ_H Direction
Details and Dimensions Not Shown Are
Identical to σ_V Ends

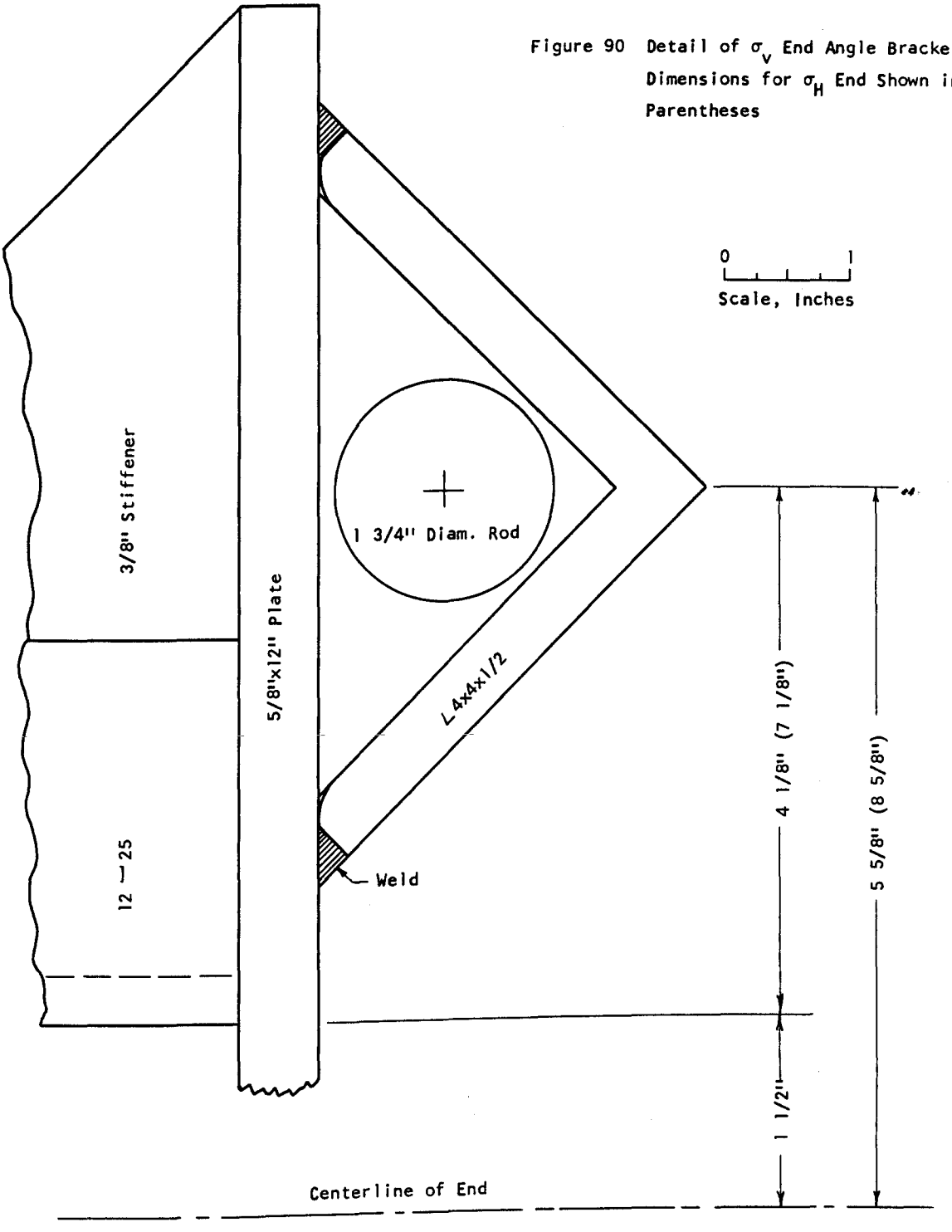

Figure 90 Detail of σ_V End Angle Bracket Dimensions for σ_H End Shown in Parentheses

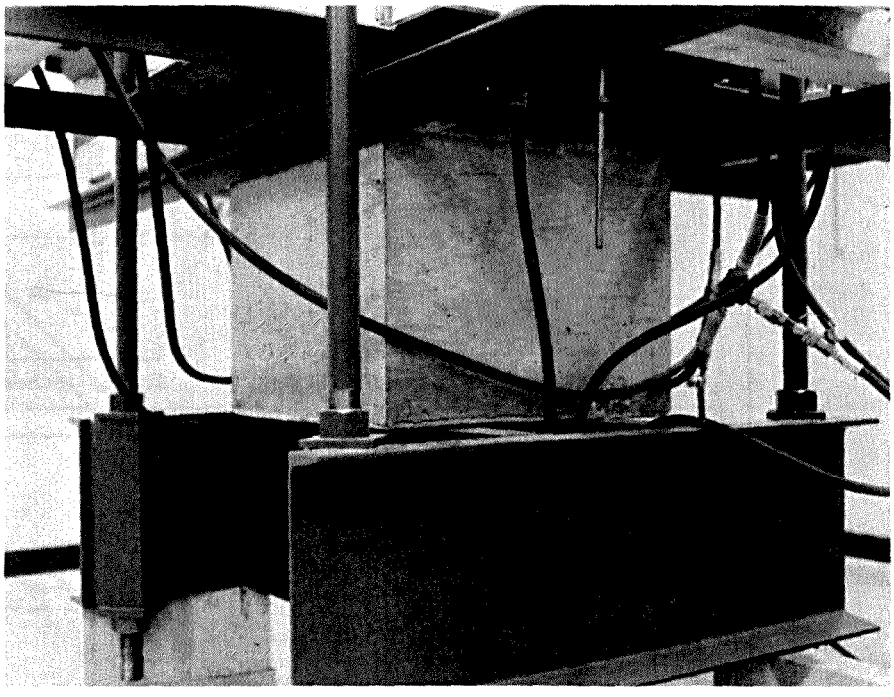

Figure 91 Bottom Longitudinal Reaction Head and Concrete Pedestal

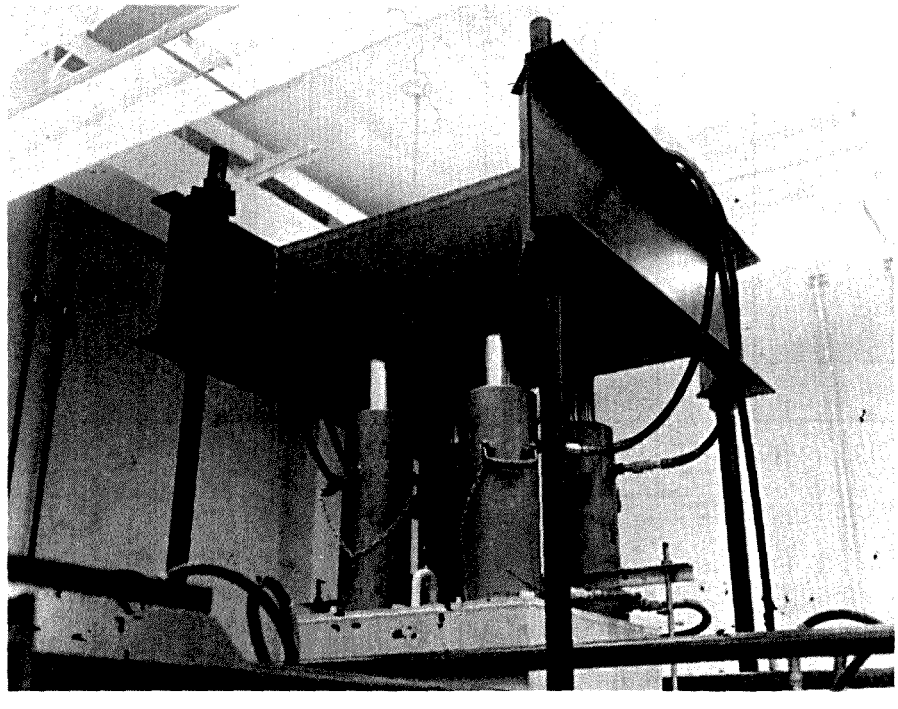

Figure 92 Top Longitudinal Reaction and Jacks

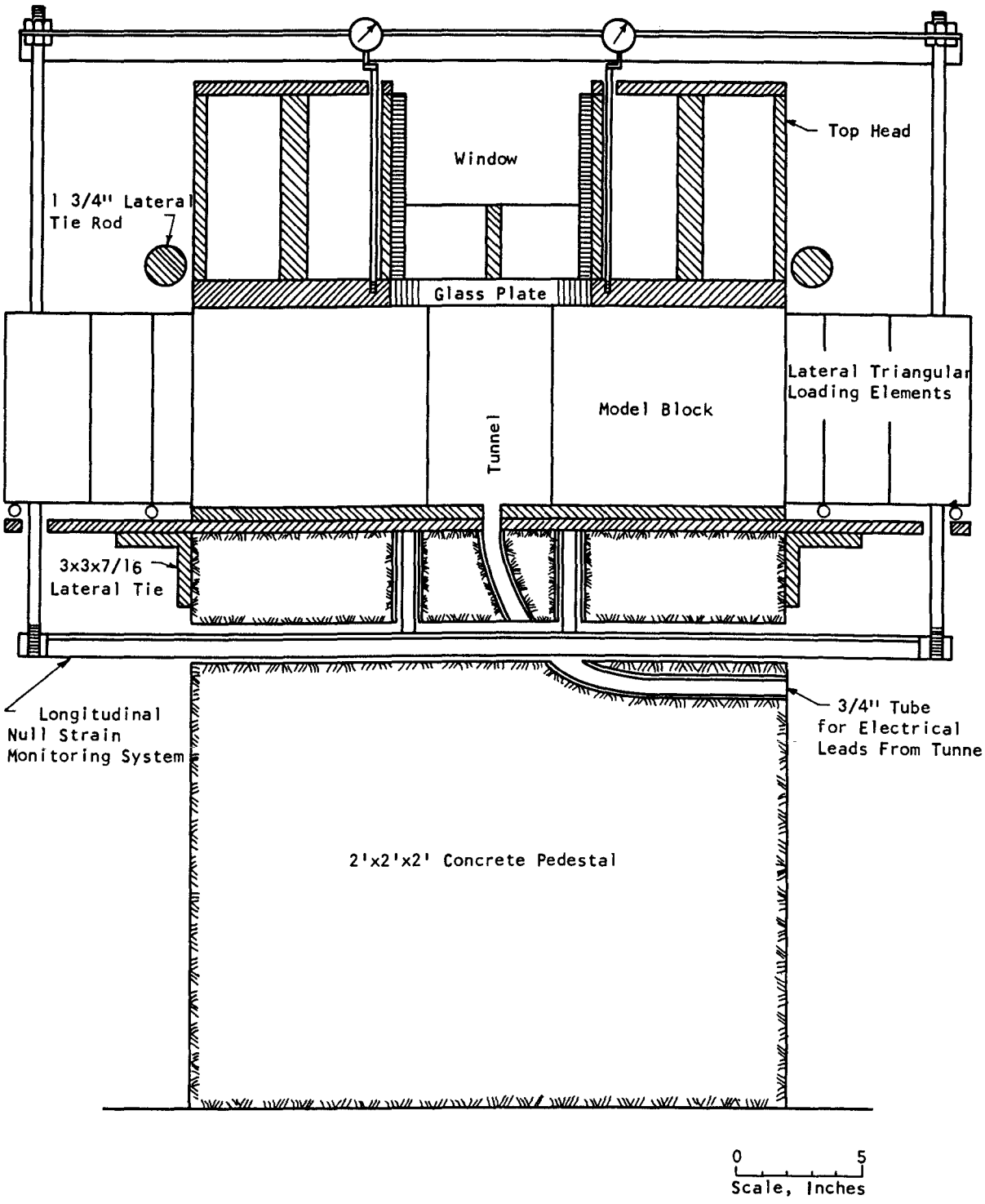

Figure 93 Schematic Diagram of Base and Loading Element Assembly

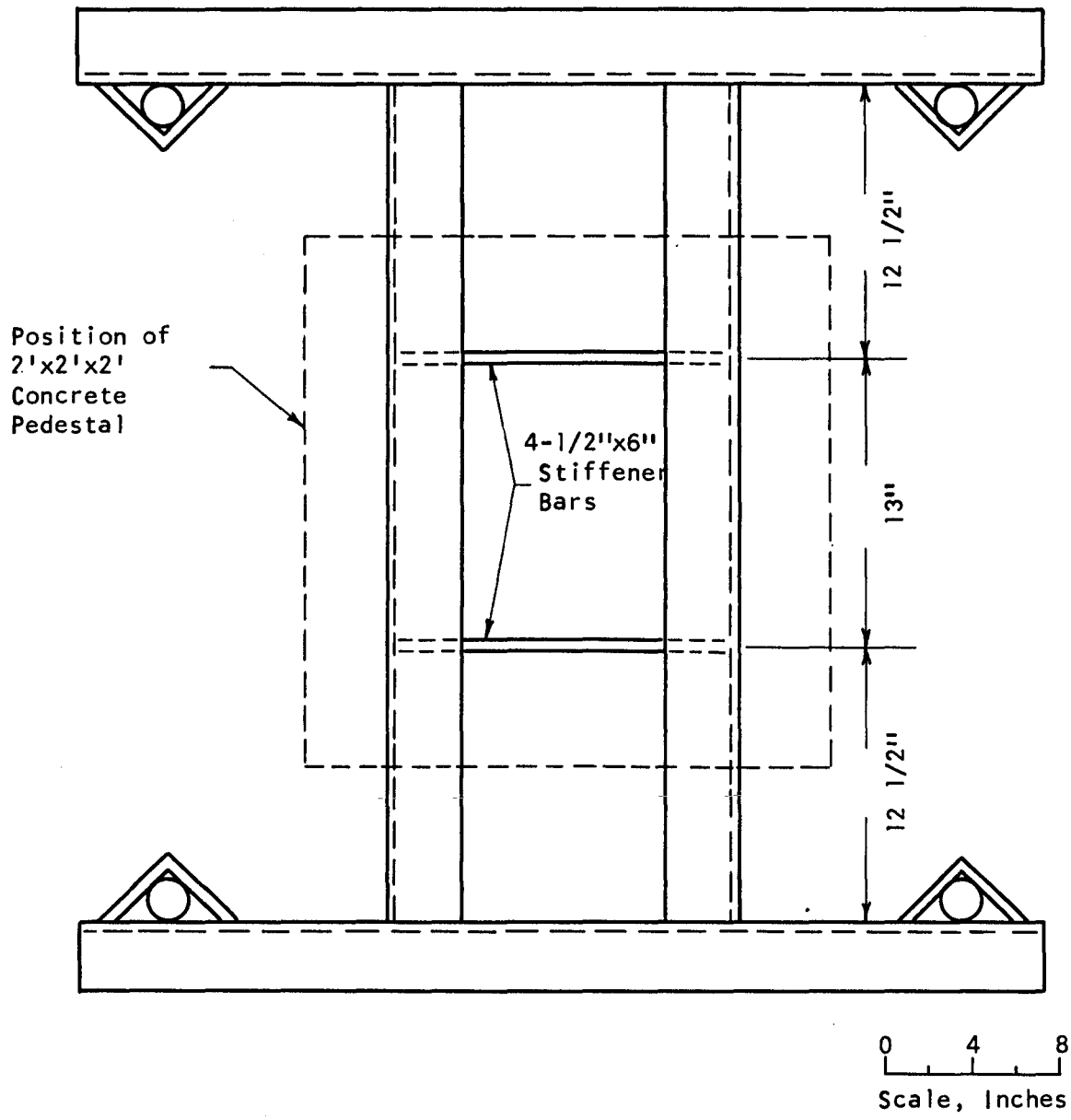

Figure 94 Bottom Longitudinal Reaction Head
Details and Dimensions Not Shown Are
Identical to Top Reaction Head

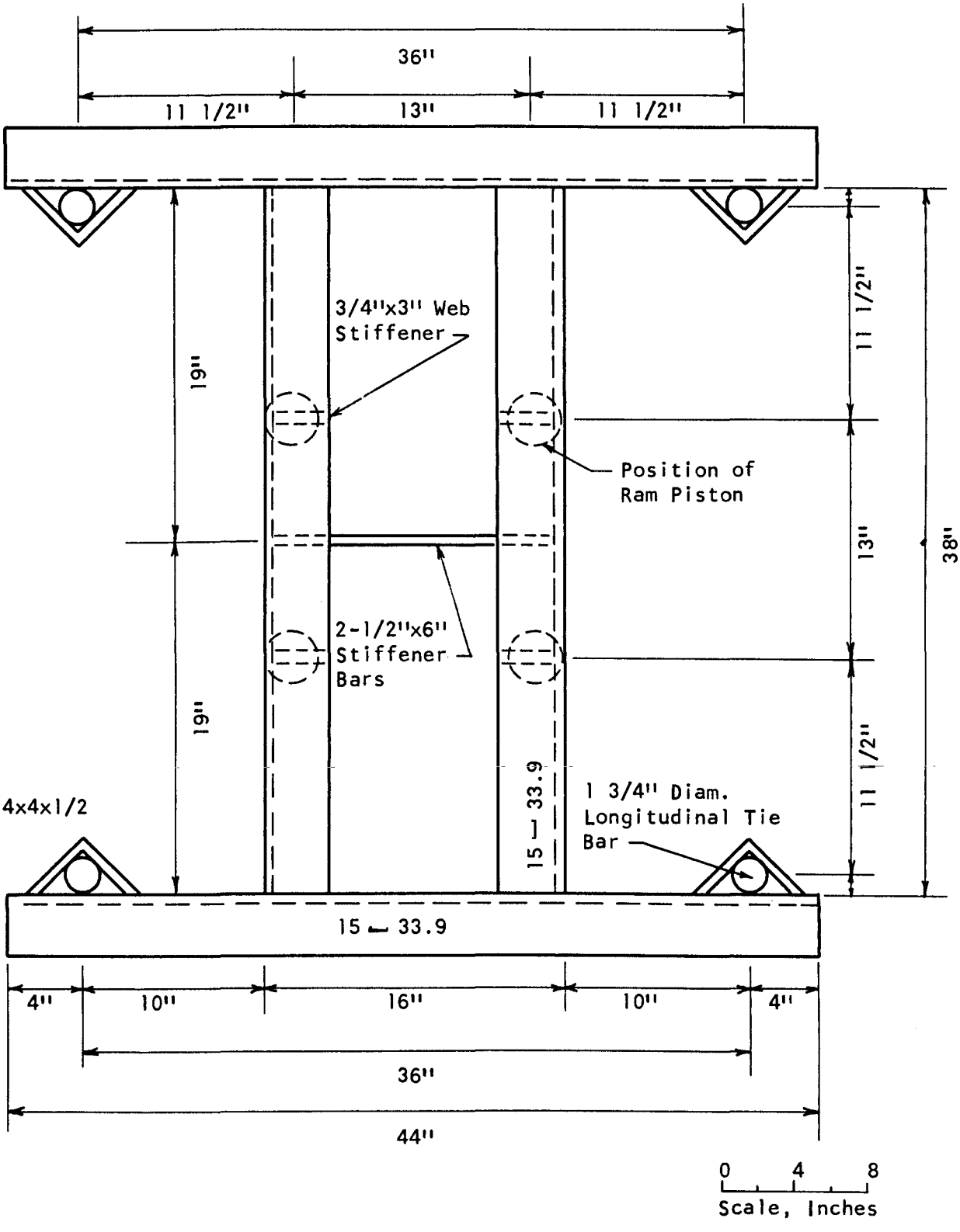

Figure 95 Top Longitudinal Reaction Head

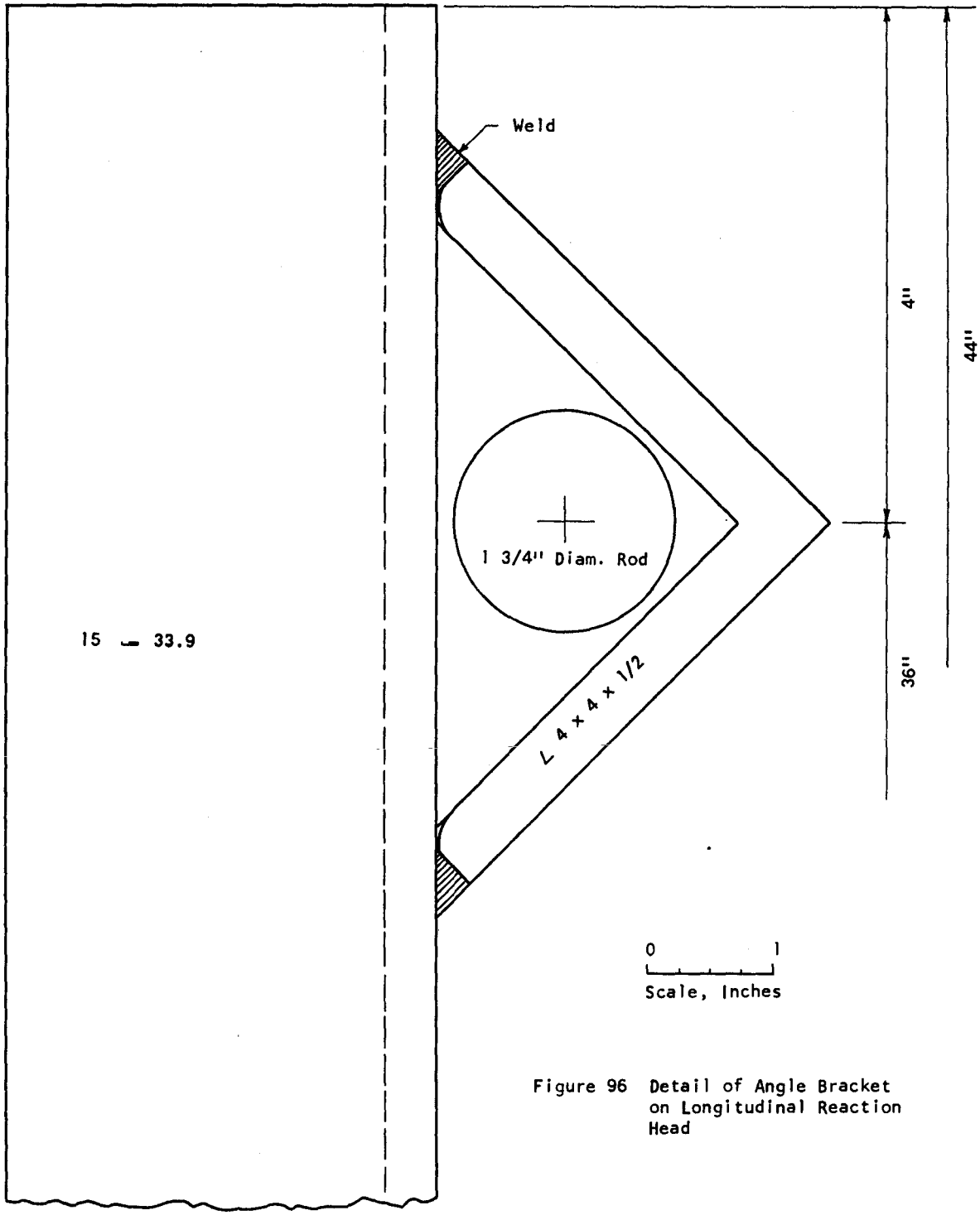

Figure 96 Detail of Angle Bracket on Longitudinal Reaction Head

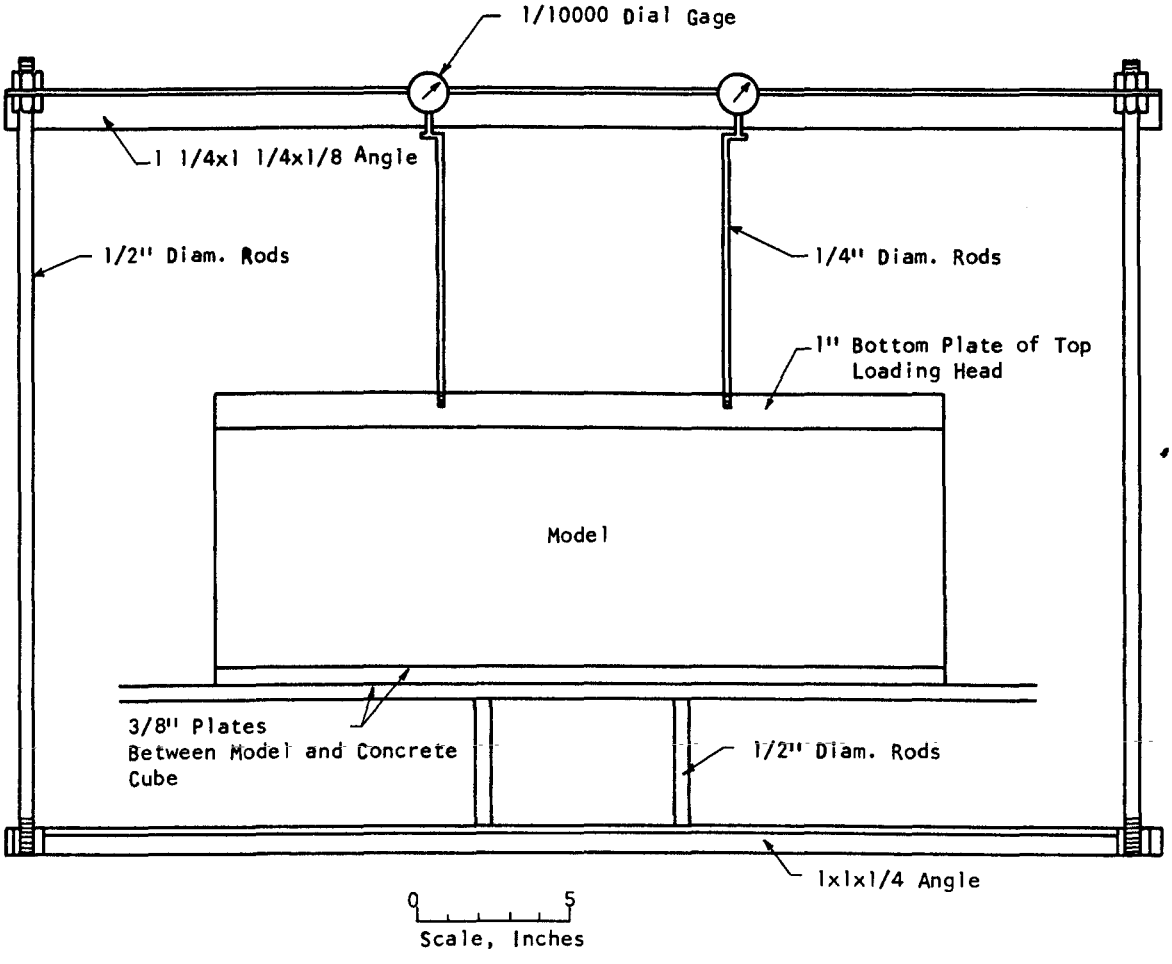

Figure 97 Schematic Diagram of Longitudinal Null Strain Monitoring System

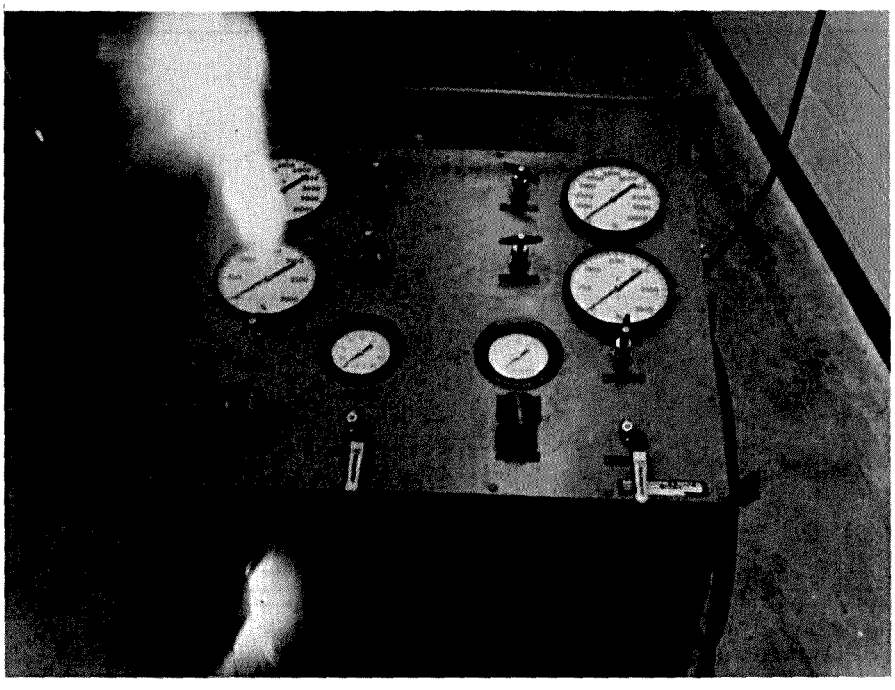

Figure 98 Pressure Console for Driving
Lateral Hydraulic Rams

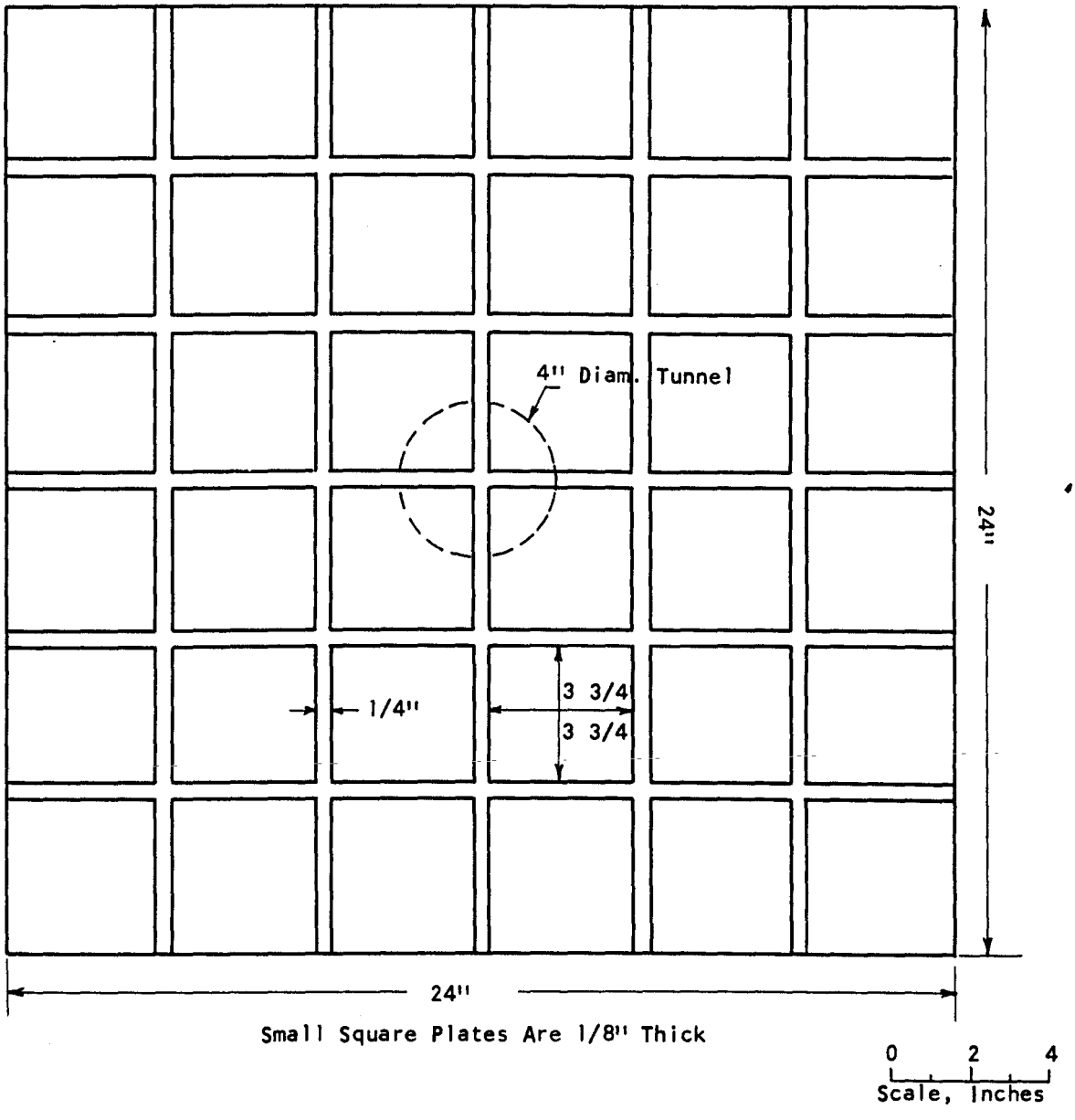

Figure 99 Sketch of Possible Friction Reducing System

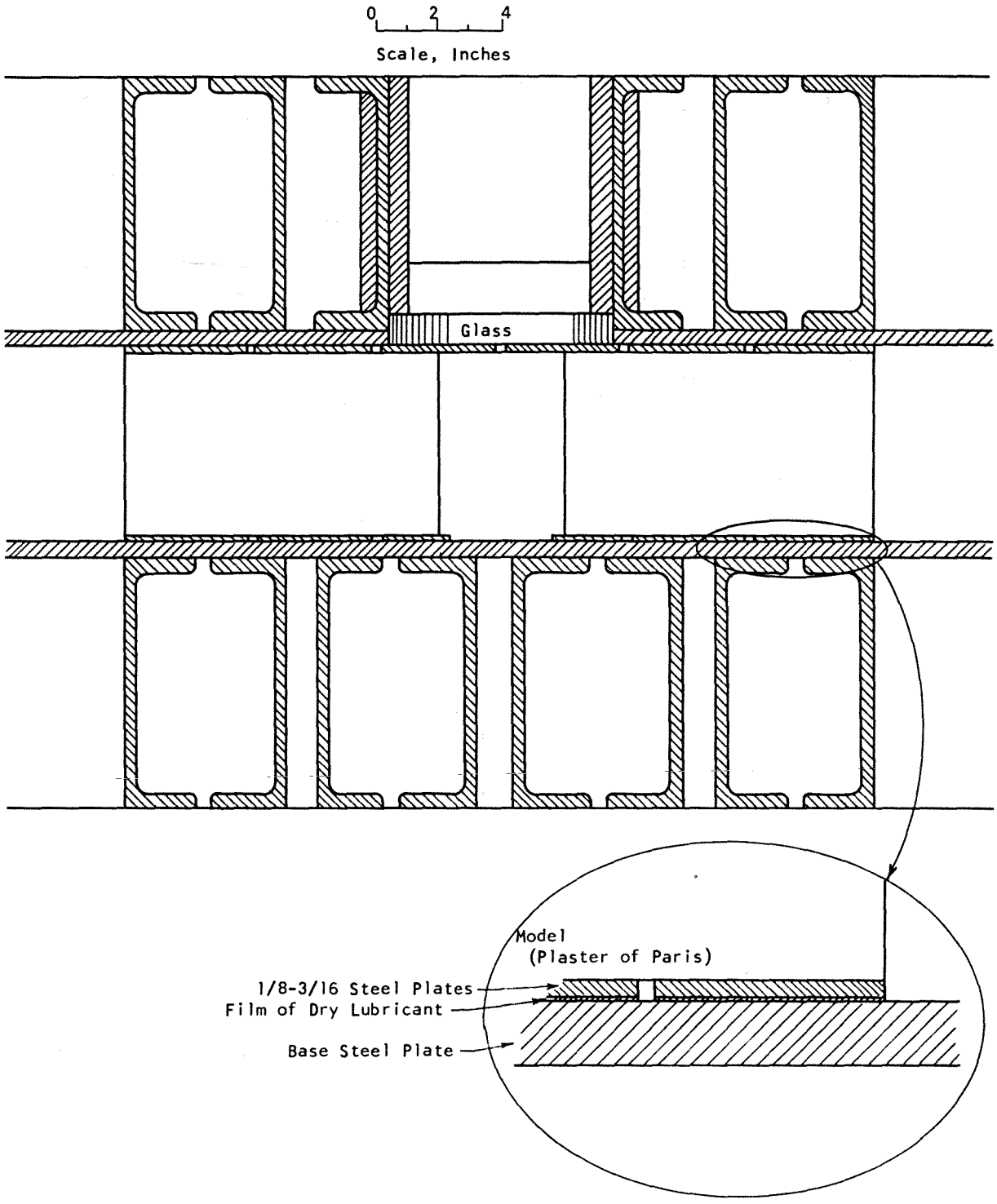

Figure 100 Sketch of Possible Friction Reducing System

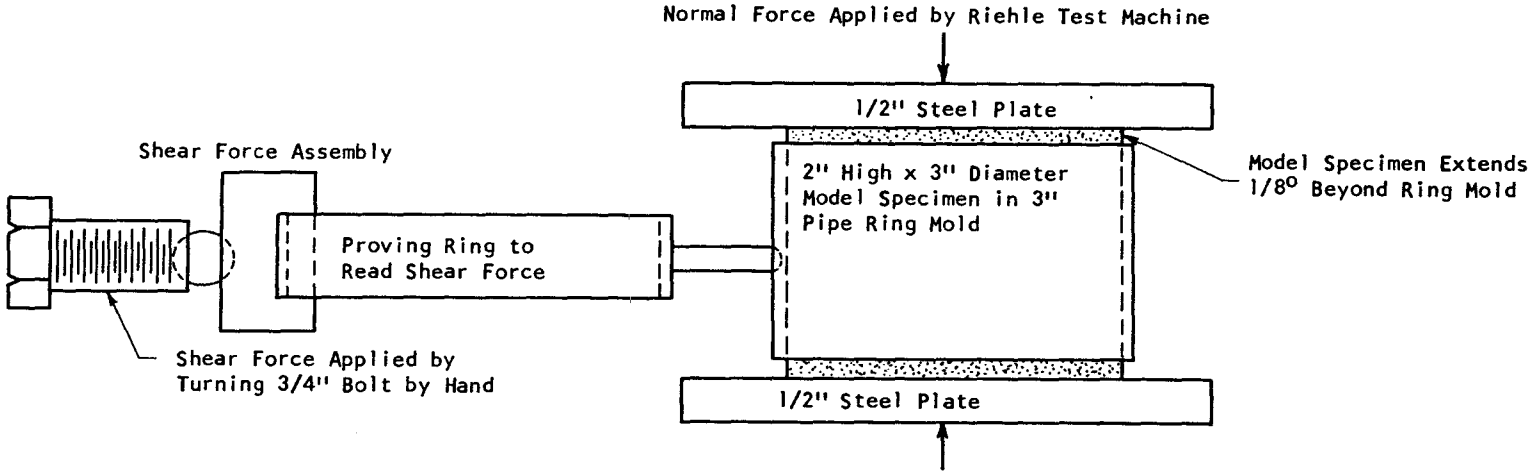

The whole assembly shown above is put inside the rectangular box of 3" channels shown below so the shearing force is self contained and does not apply horizontal thrust against the heads of the test machine applying the normal force.

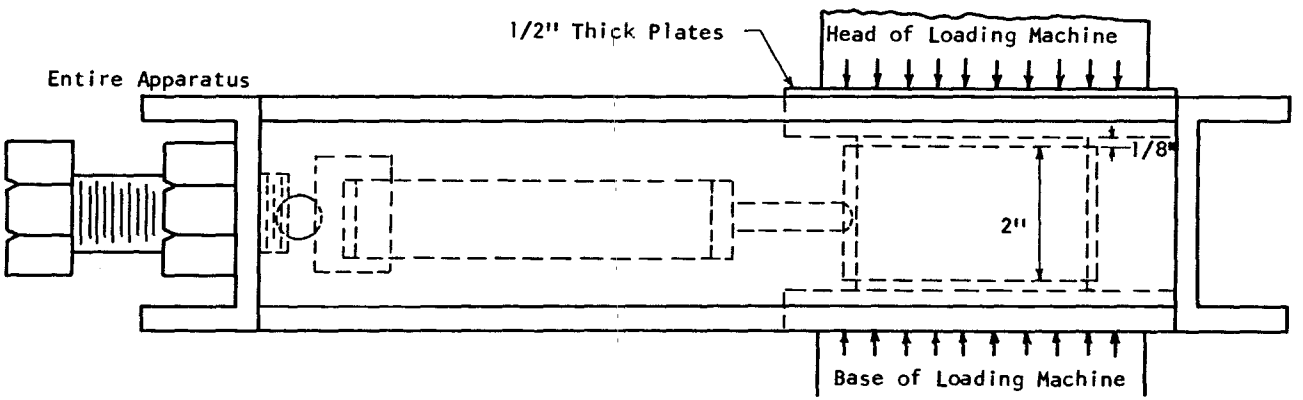

Fig. 101 Double Direct Shear Device For Studying Friction Between Model Material And Steel

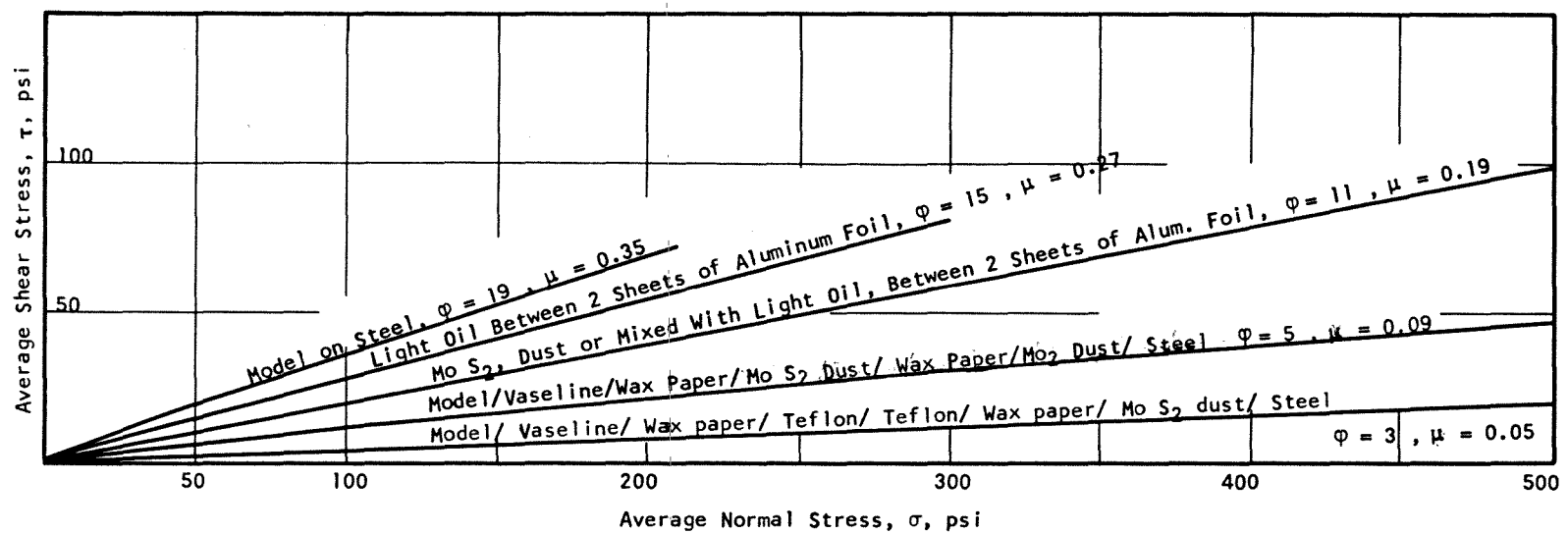

Figure 102 Fricition Between Model Material and Steel Tested in Double Direct Shear, Typical Average Values

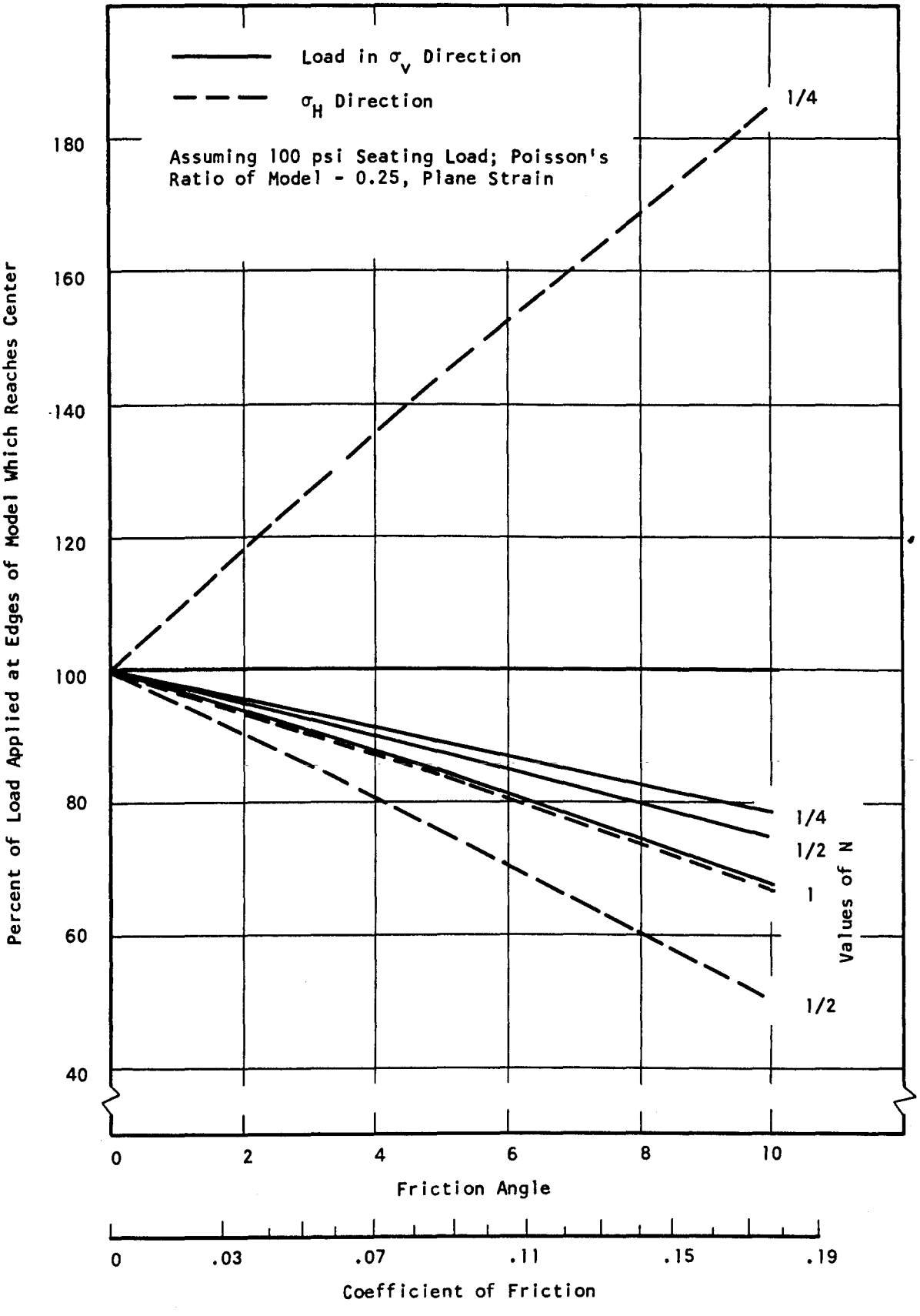

Figure 103 Loss of Applied Lateral Load Due to Friction Between Model and Top Head

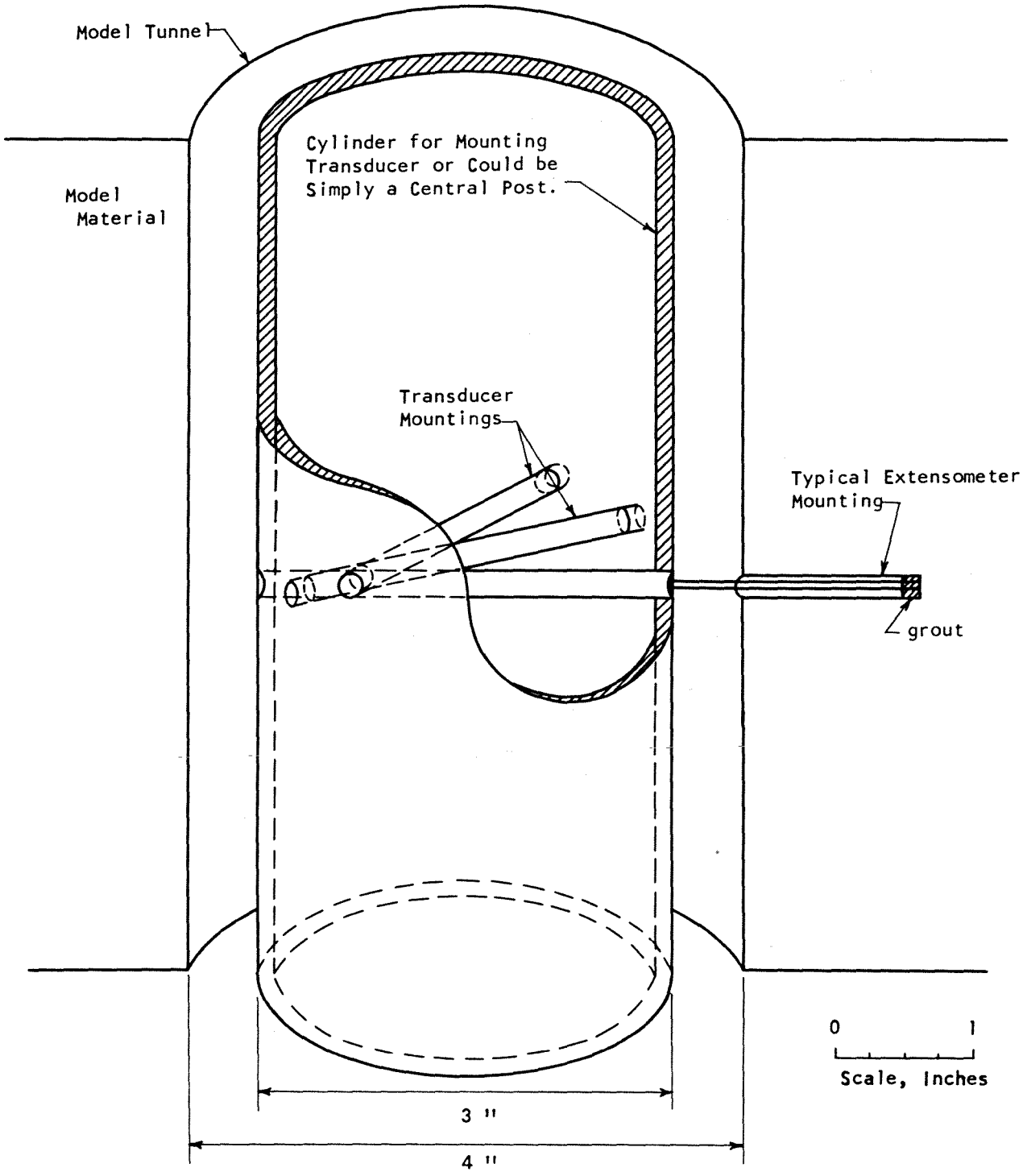

Figure 104 Sketch of Possible Method for Mounting Transducers for Radial Deformation Measurements.

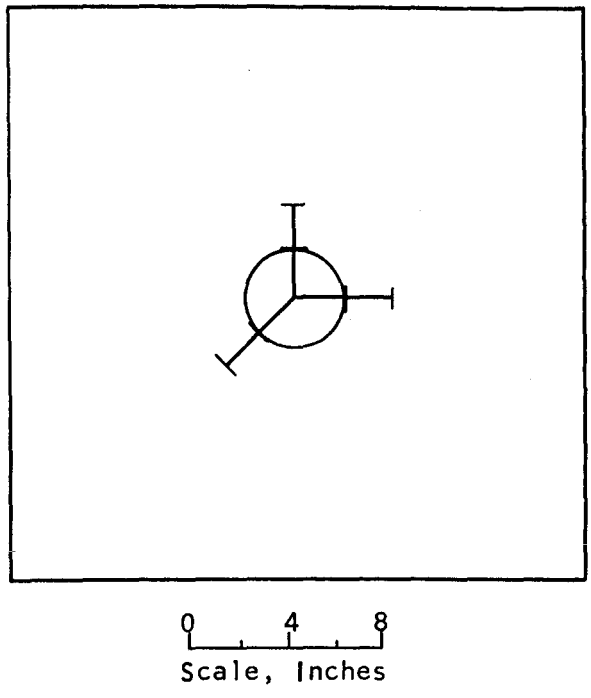

Figure 105 Location of Extensometer

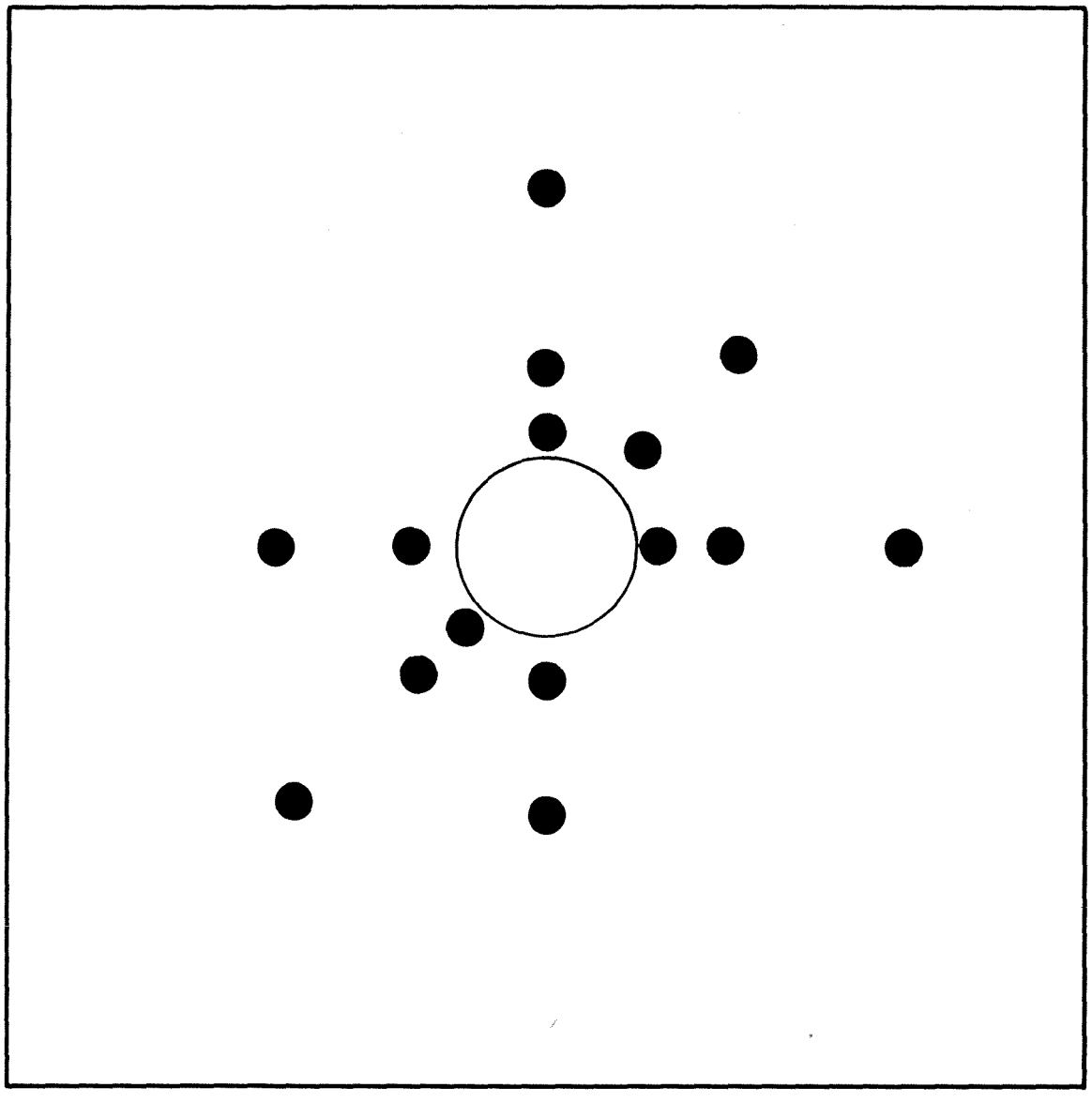

Gage Points 1/4, 1/2, 1, 2, and 3 Radii Behind Wall of Tunnel Shown to Scale, Assuming 3/4 In. Diameter Gages

0 2 4

Scale, Inches

Figure 106 Suggested Internal Gage Locations

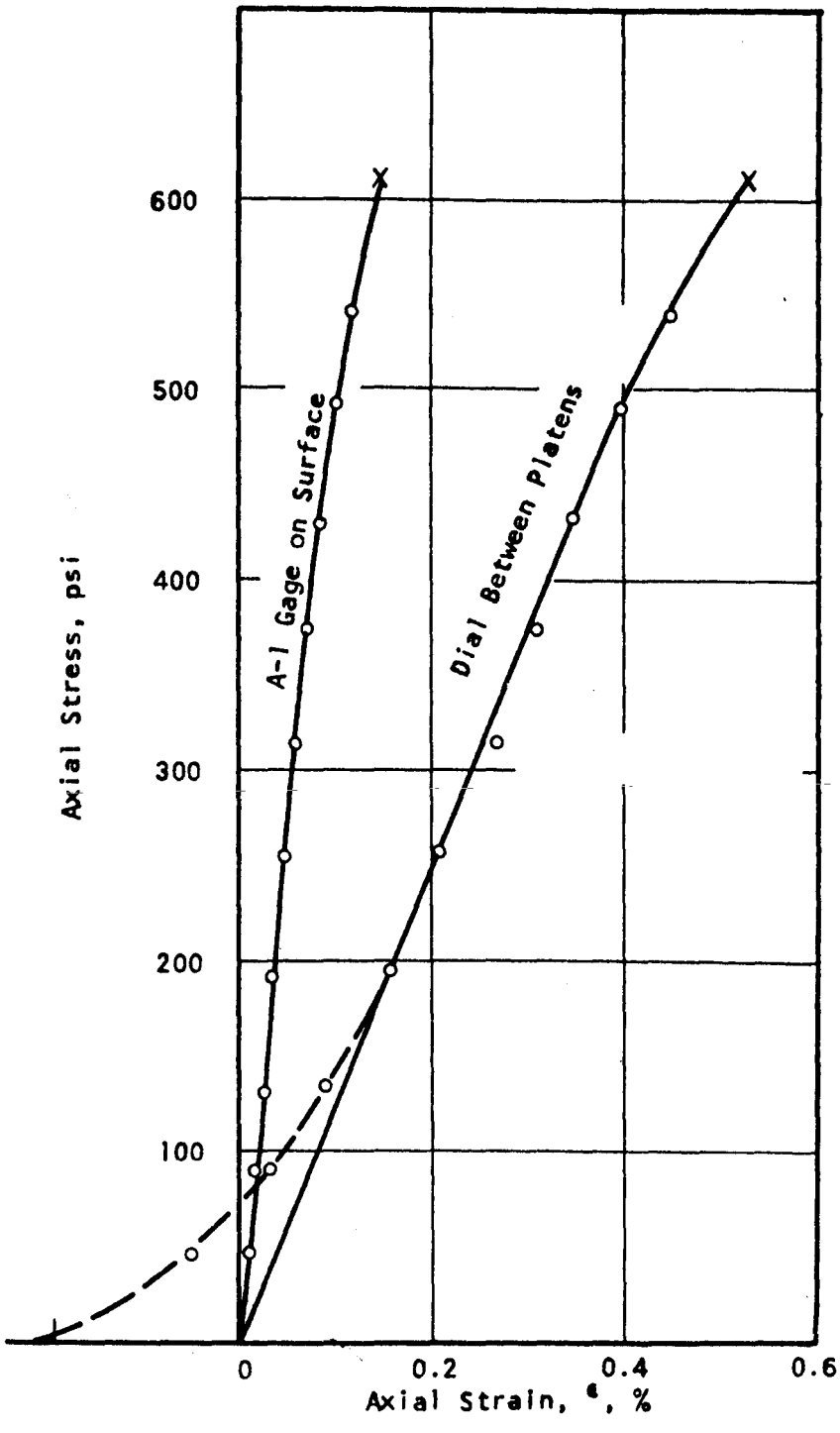

Figure 107 Stress-Strain Curves
$\sigma_3 = 0$
Specimen S29-1

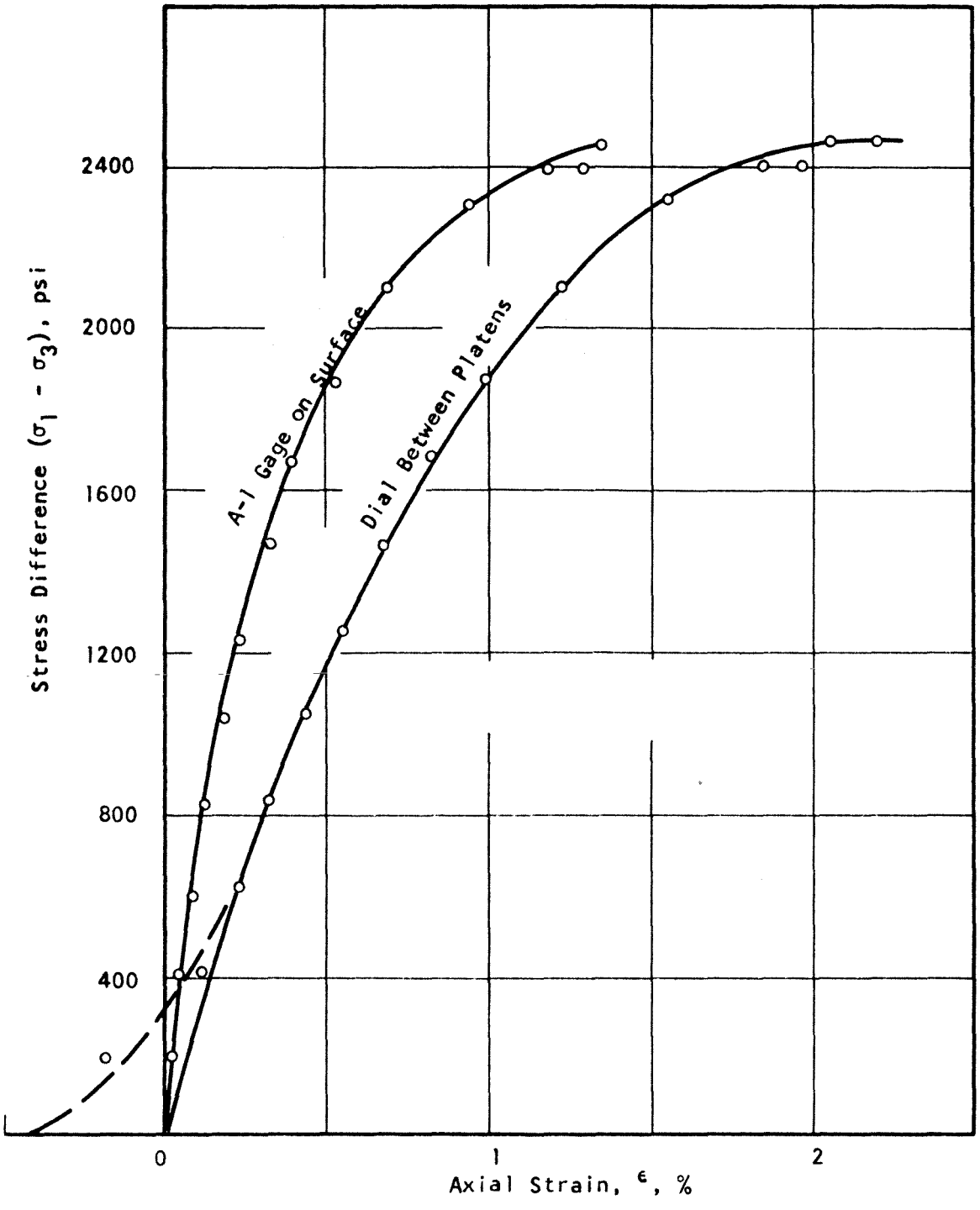

Figure 108 Stress-Strain Curves
σ_3 = 500 psi
Specimen S29-7

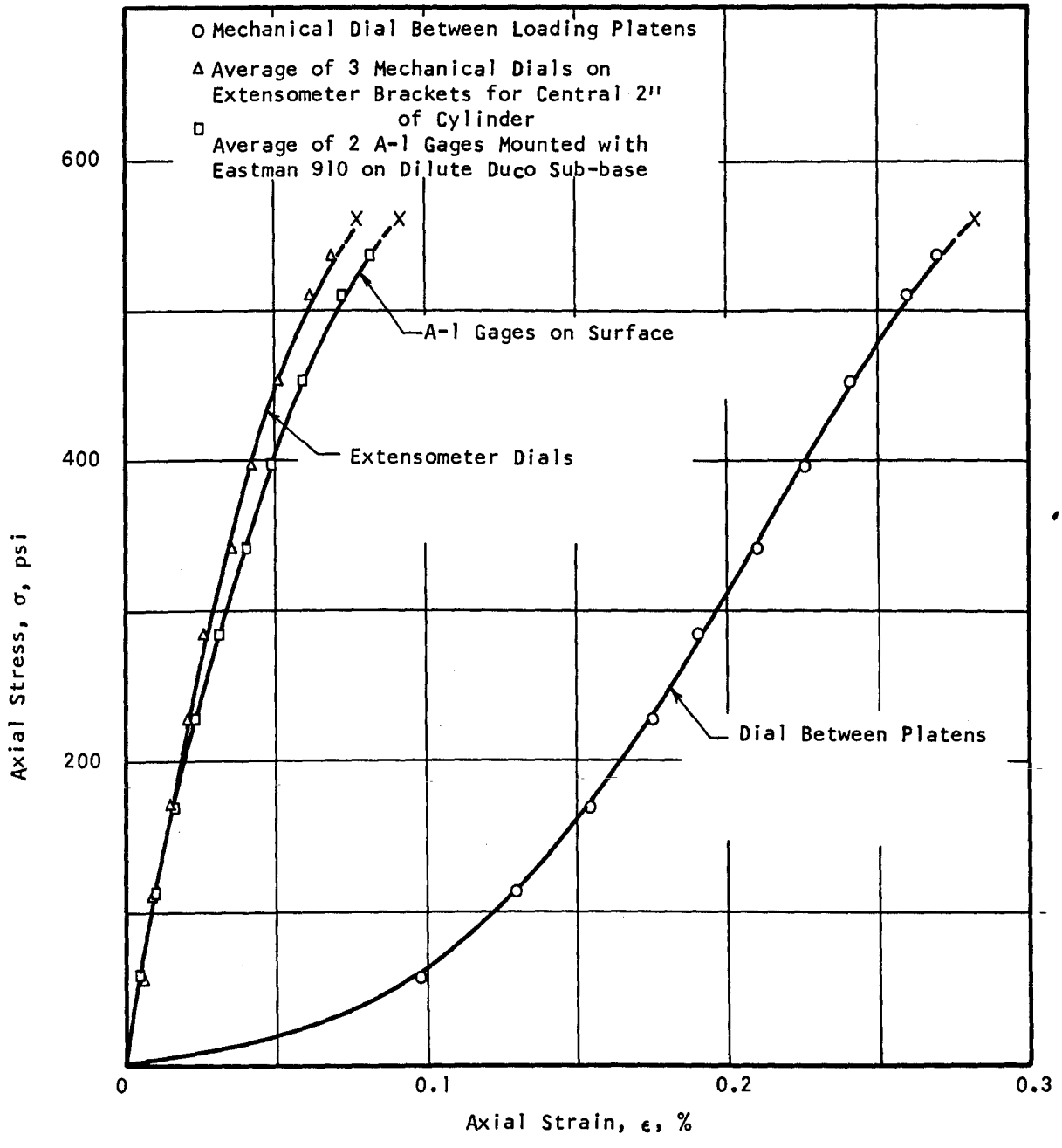

Fig. 109
Stress-Strain Curves
Cylinder LB2-2
Unconfined, Ends Capped
with Hydrocal

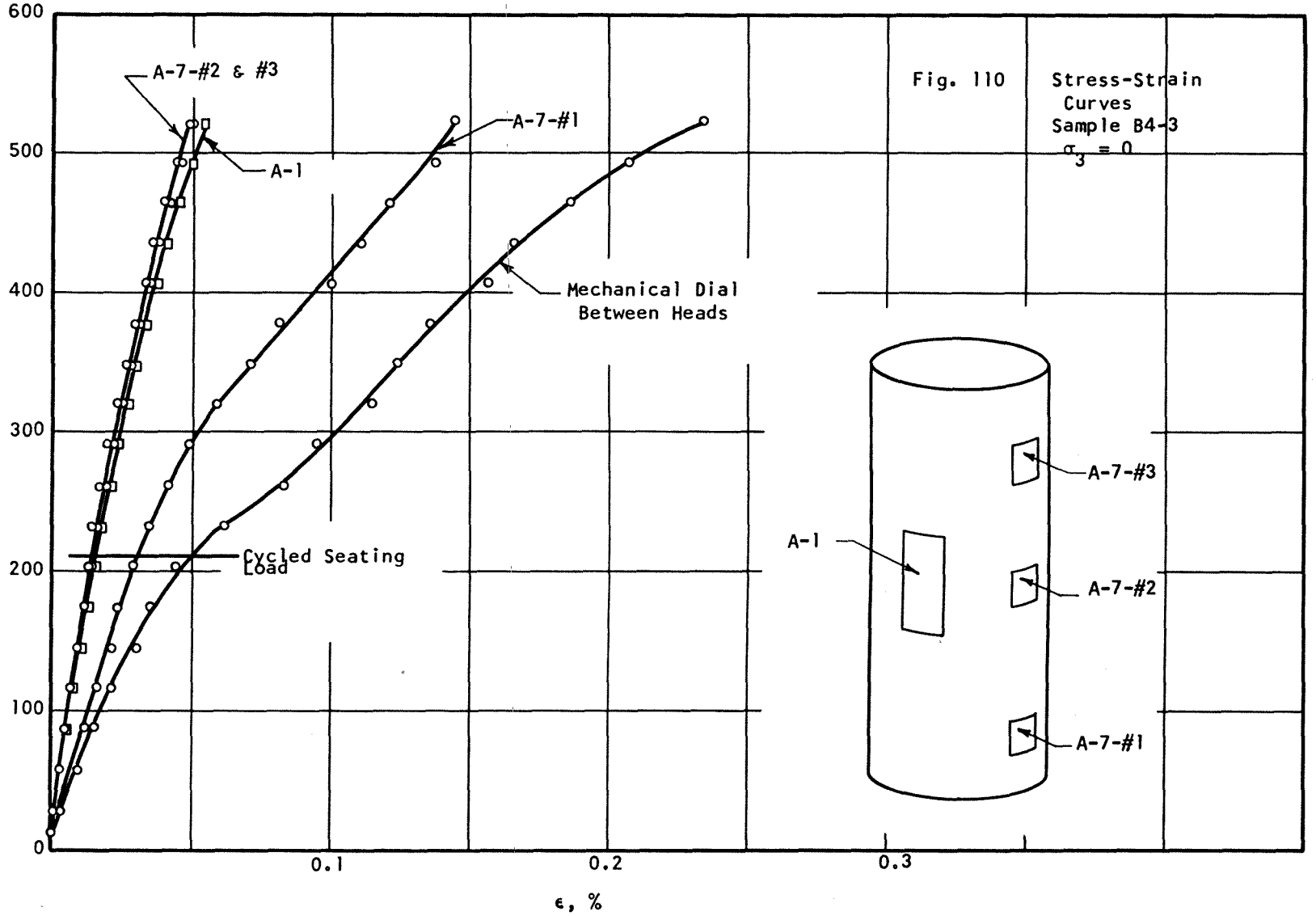

Fig. 110 Stress-Strain Curves Sample B4-3 $\sigma_3 = 0$

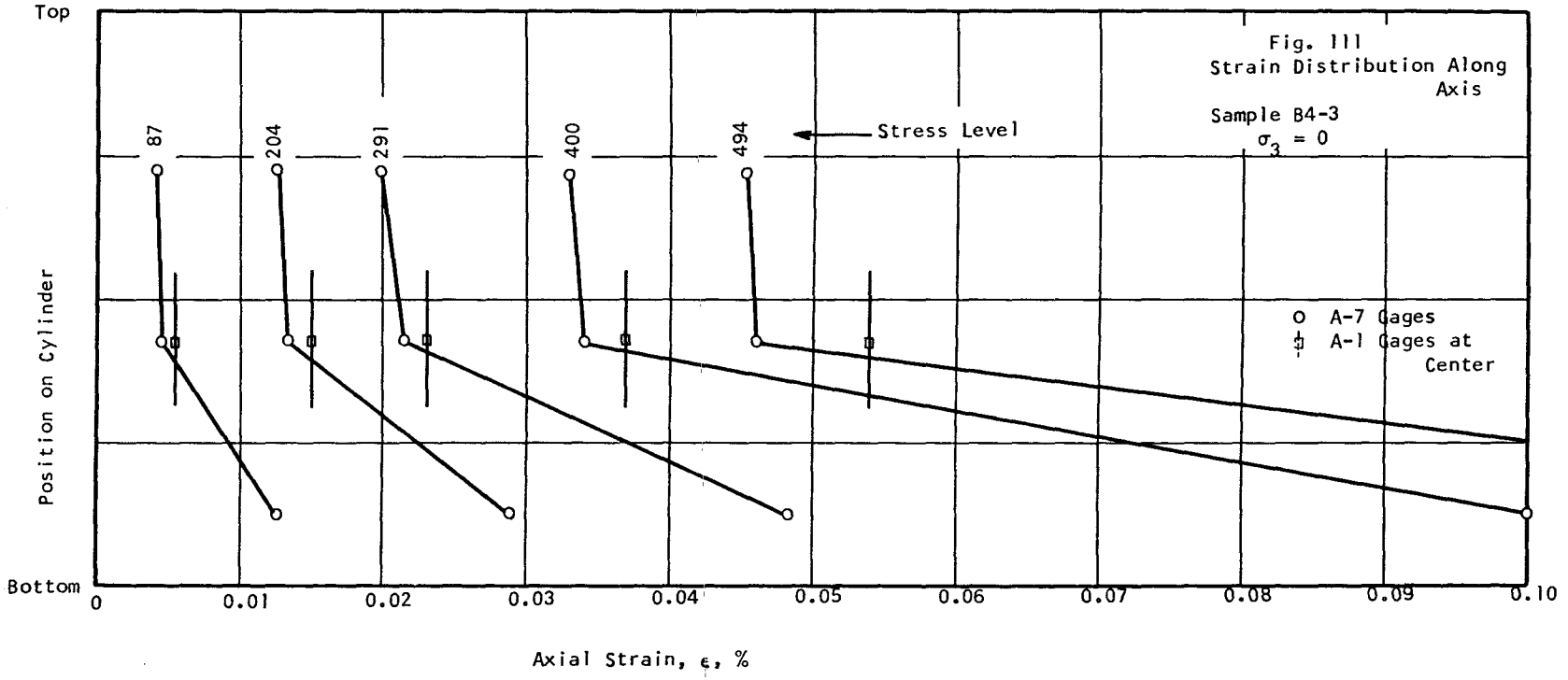
Top
Bottom
Position on Cylinder
87
204
291
400
494
Stress Level
Fig. 111
Strain Distribution Along Axis
Sample B4-3
$\sigma_3 = 0$
o A-7 Gages
⊕ A-1 Gages at Center
0
0.01
0.02
0.03
0.04
0.05
0.06
0.07
0.08
0.09
0.10
Axial Strain, ϵ, %

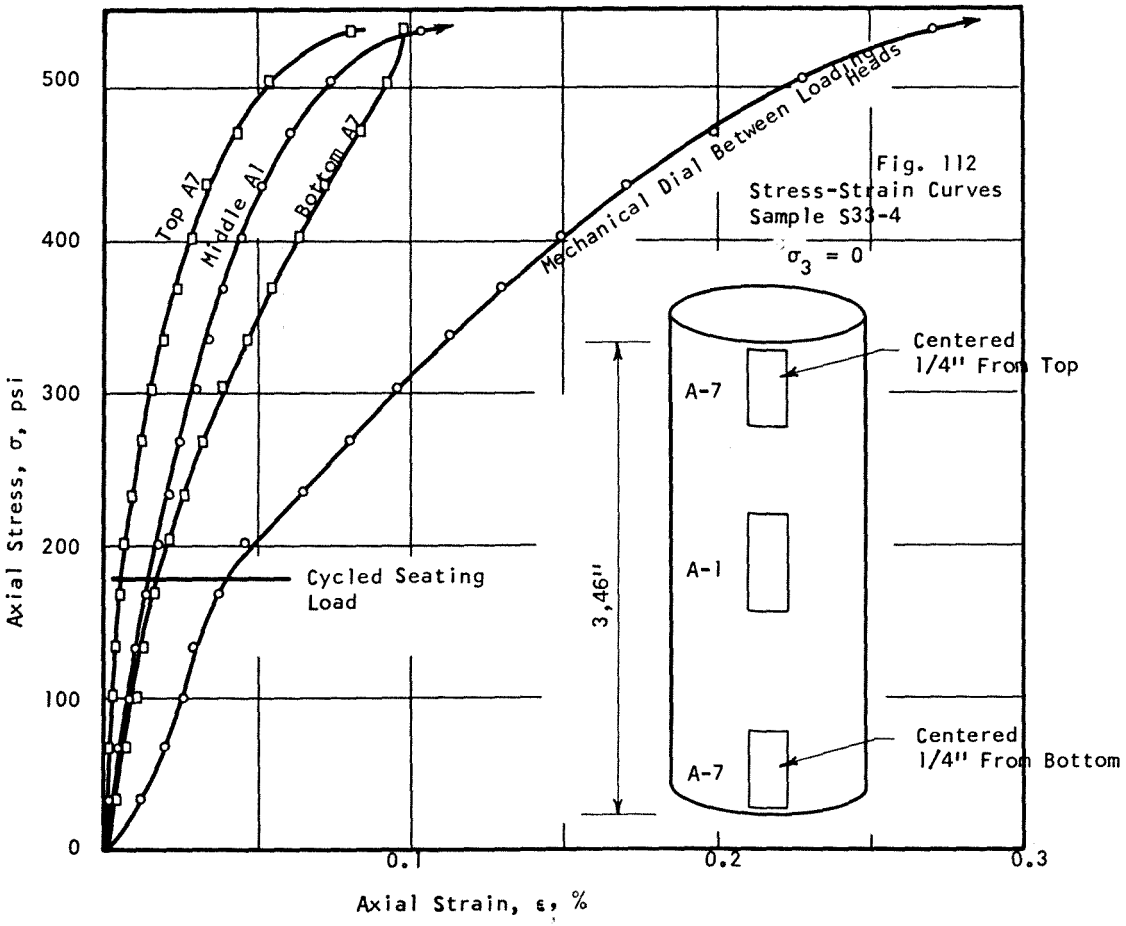

Fig. 112
Stress-Strain Curves
Sample S33-4

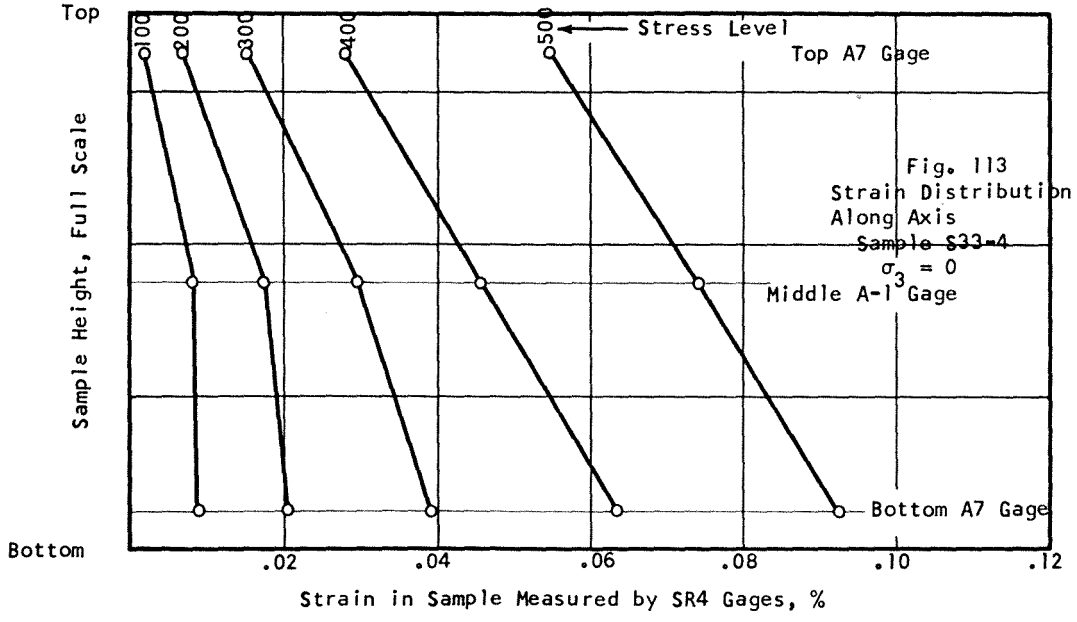

Fig. 113
Strain Distribution
Along Axis
Sample S33-4
$\sigma_3 = 0$

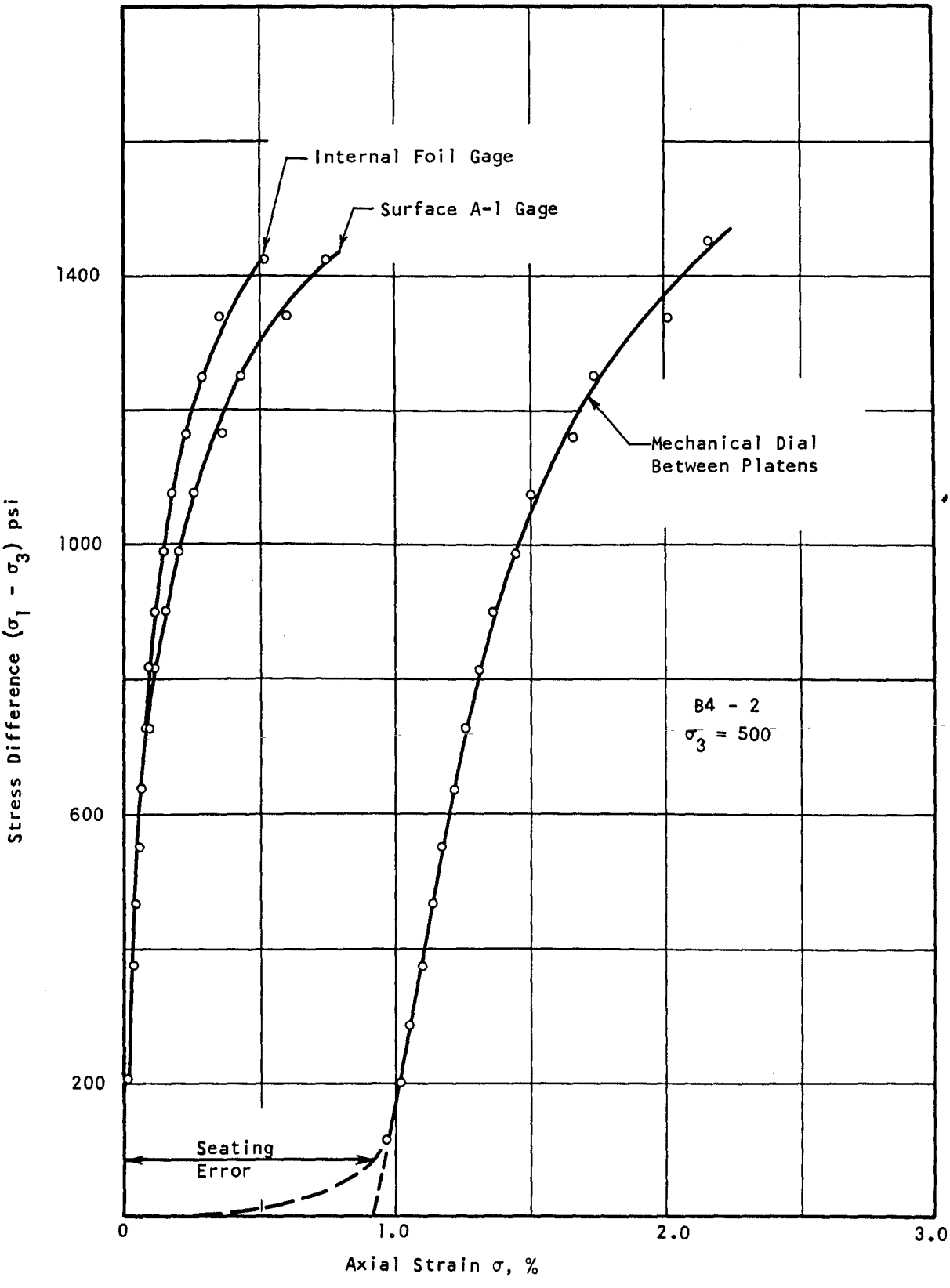

Figure 114 Stress-Strain Curves

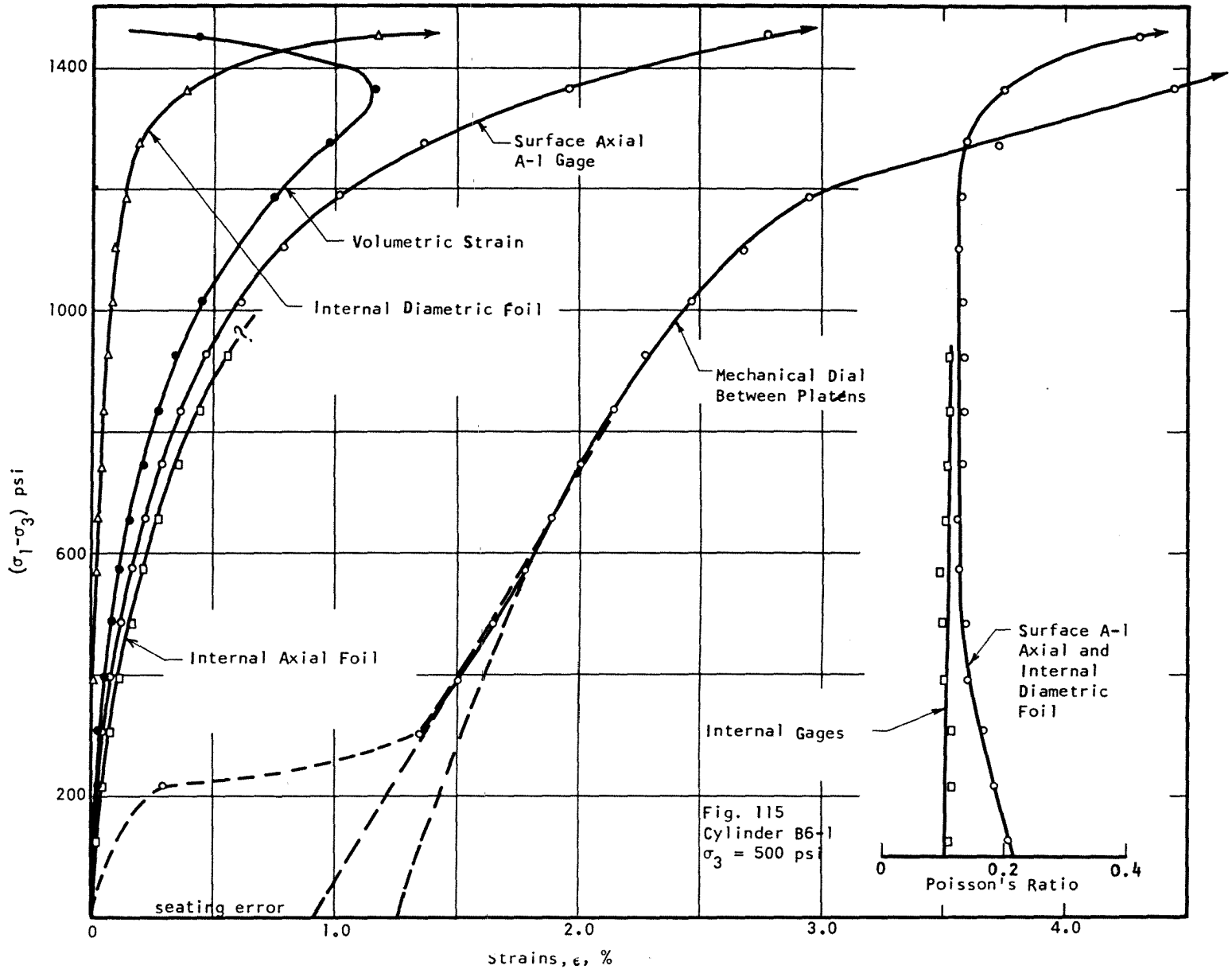

Fig. 115
Cylinder B6-1
σ_3 = 500 psi

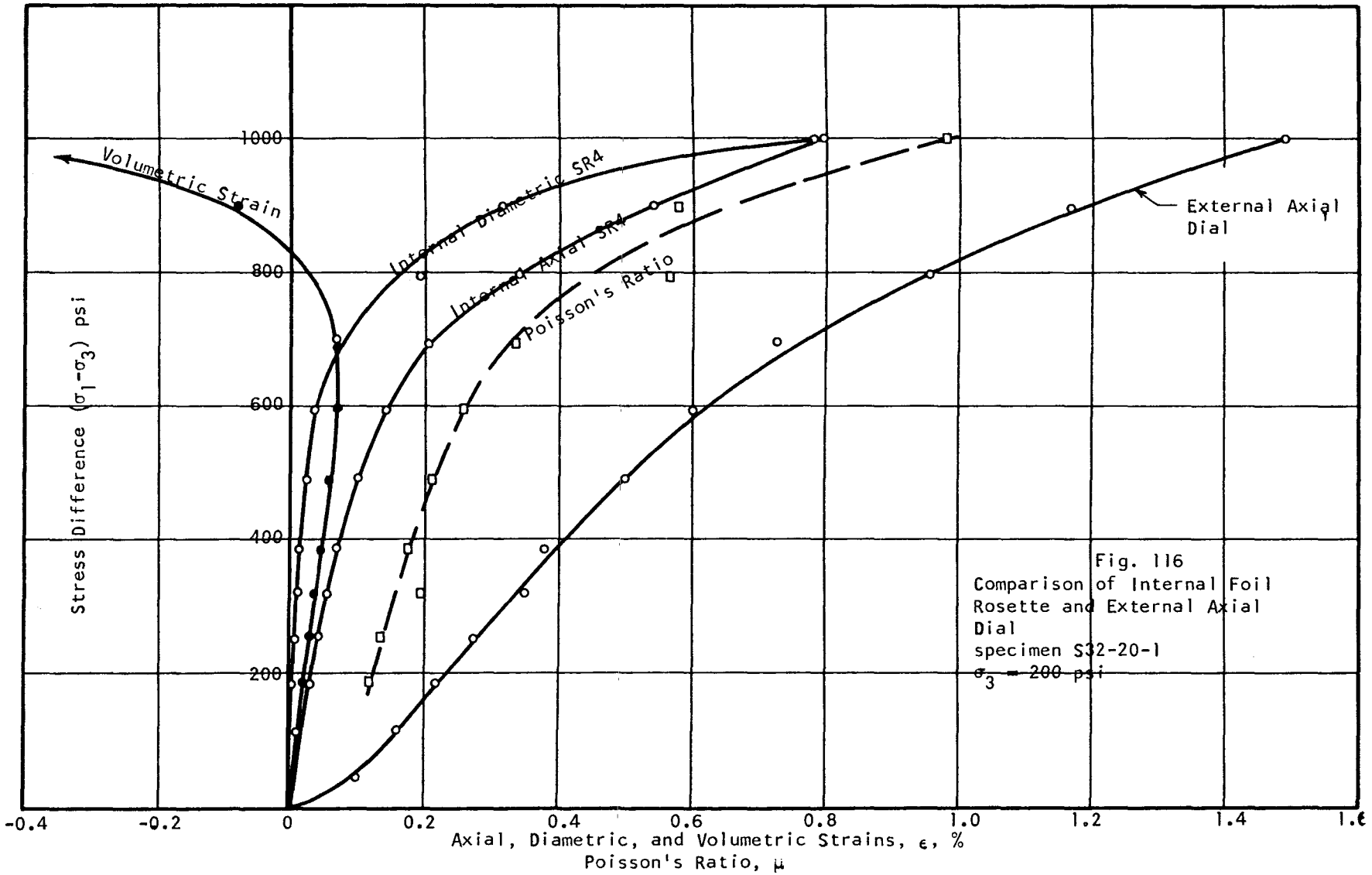

Fig. 116
Comparison of Internal Foil Rosette and External Axial Dial
specimen S32-20-1
σ_3 = 200 psi

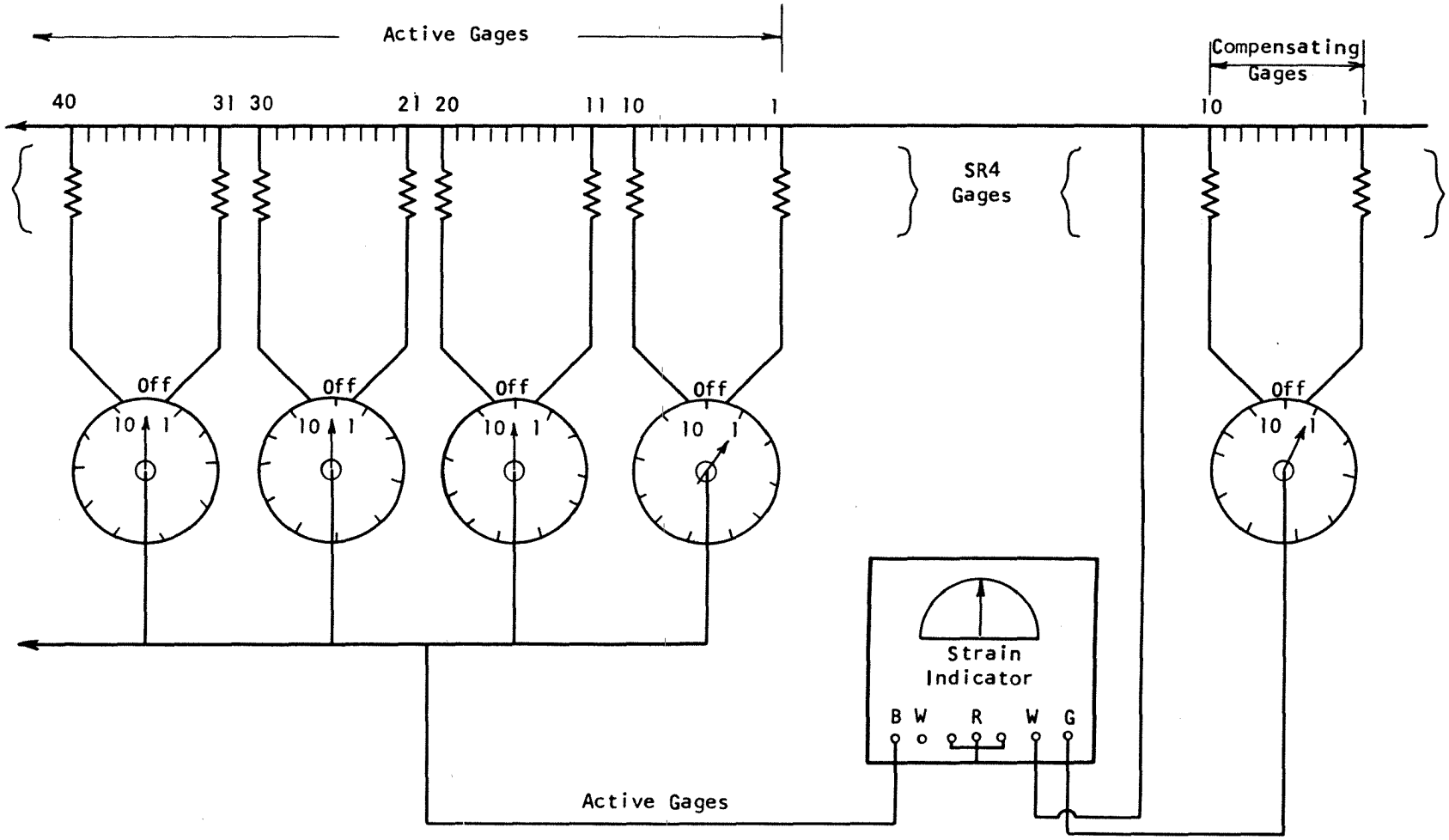

Figure 117 Schematic Diagram of System For Manual Switching of SR4 Gages

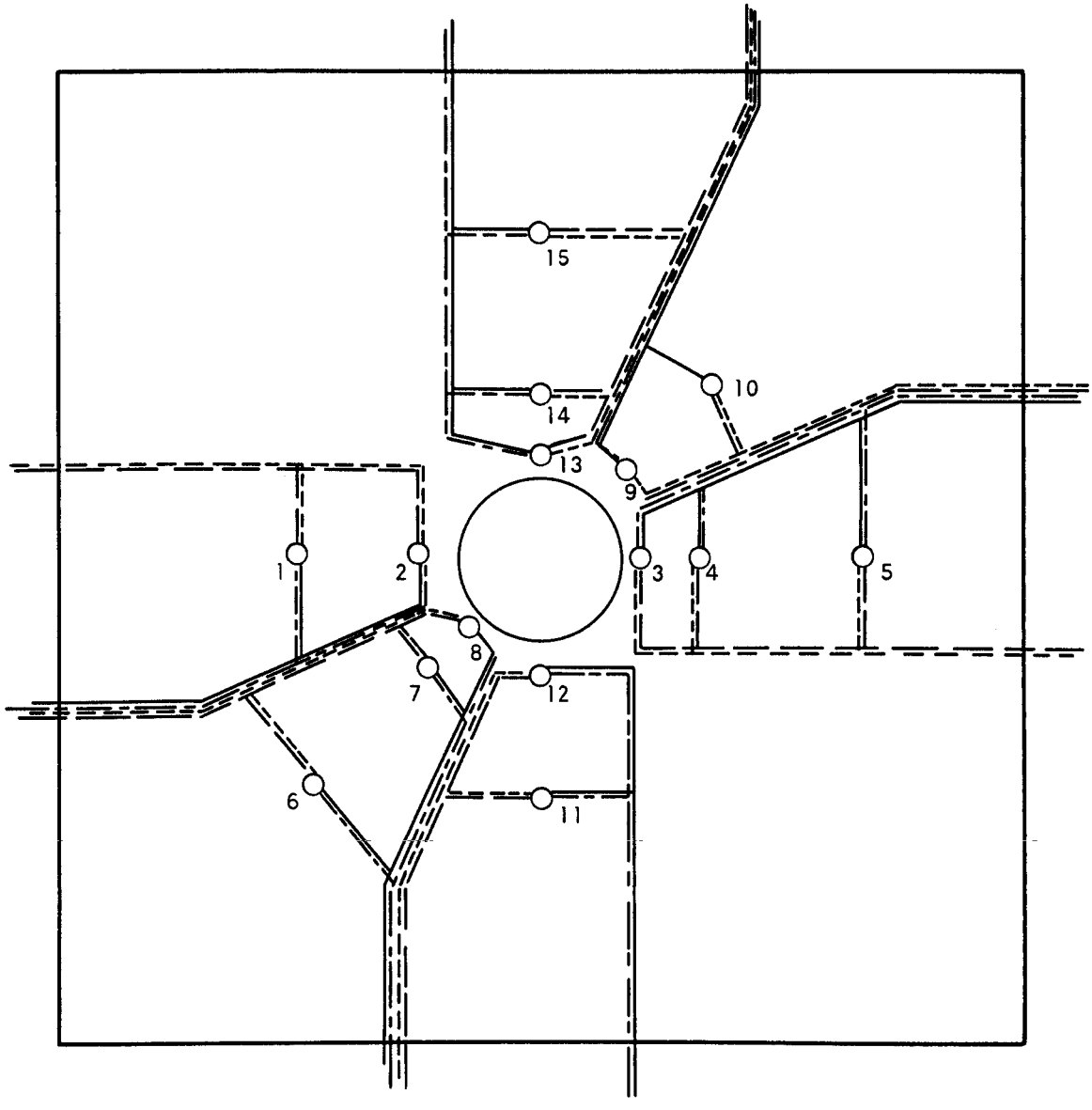

Leads Out of Model

—— – —— Common Lead to All Elements

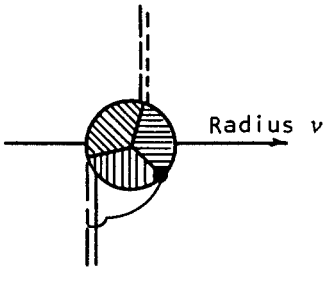

——— Circumferential Lead

– – – – – Radial Lead

—— —— —— 45° Lead

Figure 118 Possible Wiring of Model

NUCLEAR WEAPONS EFFECTS DIVISION REPORTS

DISTRIBUTION LIST

Address	Normal No. of Copies
Army	
Chief of Engineers, Department of the Army, Washington, D. C. 20315	
ATTN: ENGME-S	1
ENGME	1
ENGCW-E	1
ENGCW-Z	1
ENGMC-E	1
ENGMC-EM	1
ENGMC-DE	1
ENGAS-I	2
ENGNA	1
Chief of Research and Development, Headquarters, Department of the Army, Washington, D. C. 20310 ATTN: Director of Army Technical Information	3 copies of Form 1473
Chief of Research and Development, Department of the Army, Washington, D. C. 20310	
ATTN: Atomic Office	1
CRDES	1
Division Engineers, U. S. Army Engineer Divisions, Continental United States	Cy to ea
Commandant, U. S. Army Air Defense School, Fort Bliss, Tex. 79906	1
Commandant, U. S. Army Command & General Staff College, Fort Leavenworth, Kans. 66027 ATTN: Archives	1
Commandant, Army War College, Carlisle Barracks, Pa. 17013 ATTN: Library	1
Commanding General, Aberdeen Proving Ground, Aberdeen, Md. 21005 ATTN: Director, Ballistic Research Laboratories	4
Commanding General, The Engineer Center, Fort Belvoir, Va. 22060 ATTN: Assistant Commandant, Engineer School	1
Commanding General, U. S. A. Electronic R&D Laboratory, Fort Monmouth, N. J. 07703 ATTN: Technical Documents Center, Evans Area	1
Commanding General, USA Missile Command, Huntsville, Ala. 35809	1
Commanding General, USA Munition Command, Dover, N. J. 07801	1
Commanding General, U. S. Continental Army Command, Fort Monroe, Va. 23351	1

Address	Normal No. of Copies
Army (Continued)	
Commanding General, U. S. Army Materiel Command, Washington, D. C. 20310 ATTN: AMCRD-DE-N	2
Commanding Officer, Picatinny Arsenal, Dover, N. J. 07801 ATTN: ORDBB-TK	1
Commanding Officer, U. S. Army Aviation Materiel Laboratories, Fort Eustis, Va. 23604	1
Commanding Officer, U. S. Army Combat Developments Command, Institute of Nuclear Studies, Fort Bliss, Tex. 79916	2
Commanding Officer, U. S. Army Mobility Equipment Research and Development Center Fort Belvoir, Va. 22060 ATTN: Technical Documents Center, Building 315	1
Commanding Officer, U. S. Army Nuclear Defense Laboratory, Edgewood Arsenal Edgewood, Md. 21040 ATTN: Technical Library	1
Department of the Army, CE Ballistic Missile Construction Office, P. O. Box 4187 Norton AFB, Calif. 92409	1
Director of Civil Defense, Office of the Secretary of the Army, Washington, D. C. 20310 ATTN: Mr. George Sisson (RE-ED)	2
Director, Nuclear Cratering Group, U. S. Army Corps of Engineers, Lawrence Radiation Laboratory, P. O. Box 808, Livermore, Calif. 94550	1
Director, Technical Documents Center, Evans Signal Laboratory, Belmar, N. J. 07719	1
Director, U. S. Army Corps of Engineers, Coastal Engineering Research Center Washington, D. C. 20016 ATTN: Mr. T. Saville, Jr.	1
Director, U. S. Army Corps of Engineers, Ohio River Division Laboratories, 5851 Mariemont Avenue, Cincinnati, Ohio 45227	1
Director, U. S. Army Mobility Equipment Research and Development Center Fort Belvoir, Va. 22060 ATTN: Chief, Technical Support Branch	1
Director, U. S. Army CRREL, P. O. Box 282, Hanover, N. H. 03755 ATTN: Mr. K. Boyd	1
Director, U. S. Army Construction Engineering Research Laboratory, P. O. Box 4005, Champaign, Ill. 61820	1

Address	Normal No. of Copies
Army (Continued)	
District Engineer, U. S. Army Engineer District, Omaha, 6012 U. S. Post Office and Court House 215 N. 17th Street, Omaha, Nebr. 68101 ATTN: MROGS-B	1
President, U. S. Army Air Defense Board, Fort Bliss, Tex. 79906	1
Superintendent, U. S. Military Academy, West Point, N. Y. 10996 ATTN: Library	2
U. S. Army Engineer Division, Missouri River, P. O. Box 103, Downtown Station Omaha, Nebr. 68101 ATTN: Mr. Ken Lane	1
Navy	
Commander-in-Chief, Pacific, FPO, San Francisco 94129	1
Commander-in-Chief, U. S. Atlantic Fleet, U. S. Naval Base, Norfolk, Va. 23511	1
Chief of Naval Operations, Navy Department, Washington, D. C. 20350 ATTN: OP-75 OP-03EG	 2 1
Chief of Naval Research, Navy Department, Washington, D. C. 20390 ATTN: Code 811	1
Commandant of the Marine Corps, Navy Department, Washington, D. C. 20380 ATTN: Code A04E	2
Commander, Naval Facilities Engineering Command, Navy Department, Washington, D. C. 20370 ATTN: Code 04 Code 03	 1 1
Commander, Naval Ordnance Systems Command, Washington, D. C. 20360	1
Commander, Naval Ship Engineering Center, Washington, D. C. 20360 ATTN: Code 6115	1
Commanding Officer, Nuclear Weapons Training Center, Atlantic Naval Base, Norfolk, Va. 23511 ATTN: Nuclear Warfare Department	1
Commanding Officer, Nuclear Weapons Training Center, Pacific, Naval Station, North Island San Diego, Calif. 92136	2
Commanding Officer & Director, Naval Electronics Laboratory, San Diego, Calif. 92152	1
Commanding Officer & Director, Naval Ship Research and Development Center Carderock, Md. 20007	1
Commanding General, Marine Corps Development and Education Command, Quantico, Va. 22134 ATTN: Director, Development Center	2

Address	Normal No. of Copies
Navy (Continued)	
Commanding Officer & Director, U. S. Naval Civil Engineering Laboratory Port Hueneme, Calif. 93041 ATTN: Code L31	2
Commanding Officer, U. S. Naval Civil Engineer Corps Officer School, U. S. Naval Construction Battalion Center, Port Hueneme, Calif. 93041	1
Commanding Officer, U. S. Naval Damage Control Training Center, Naval Base Philadelphia, Pa. 19112 ATTN: ABC Defense Course	1
Commanding Officer, U. S. Naval Weapons Evaluation Facility, Kirtland Air Force Base Albuquerque, N. Mex. 87117 ATTN: Code WEVS	1
Commanding Officer, U. S. Naval Weapons Laboratory, Dahlgren, Va. 22448 ATTN: TE	1
Commander, U. S. Naval Oceanographic Office, Suitland, Md. 20023	1
Commander, U. S. Naval Ordnance Laboratory, Silver Spring, Md. 20910 ATTN: EA EU E	 1 1 1
Commander, U. S. Naval Ordnance Test Station, China Lake, Calif. 93555	1
Director, U. S. Naval Research Laboratory, Washington, D. C. 20390	1
President, U. S. Naval War College, Newport, R. I. 02840	1
Special Projects, Navy Department, Washington, D. C. 20360 ATTN: SP-272	1
Superintendent, U. S. Naval Postgraduate School, Monterey, Calif. 93940	1
Underwater Explosions Research Division, Naval Ship Research and Development Center Norfolk Naval Shipyard, Portsmouth, Va. 23511	1
Air Force	
Air Force Flight Dynamics Laboratory, Wright-Patterson AFB, Dayton, Ohio 45433 ATTN: Mr. Frank Janik, Jr.	1
Air Force Institute of Technology, AFIT-L, Building 640, Wright-Patterson AFB, Ohio 45433	1
Commander, Air Force Logistics Command, Wright-Patterson AFB, Ohio 45433	2
Air Force Systems Command, Andrews Air Force Base, Washington, D. C. 20331 ATTN: SCTSW	1

Address	Normal No. of Copies
Air Force (Continued)	
Air Force Technical Applications Center, Department of the Air Force, Washington, D. C. 20333	1
Air Force Weapons Laboratory, Kirtland AFB, N. Mex. 87117	
ATTN: Library	2
WLDC	1
WLDC/R. W. Henny	1
Director, Air University Library, Maxwell AFB, Ala. 36112	2
Commander, Strategic Air Command, Offutt AFB, Nebr. 68113 ATTN: OAWS	1
Commander, Tactical Air Command, Langley AFB, Va. 23365 ATTN: Document Security Branch	1
Space and Missile Systems Organization, Norton AFB, Calif. 92409 ATTN: SAMSO (SMQNM)	1
Headquarters, USAF, Washington, D. C. 20330 ATTN: AFRSTG	1
Director, Air Research and Development Command Headquarters, USAF Washington, D. C. 20330 ATTN: Combat Components Division	1
Director of Civil Engineering, Headquarters, USAF, Washington, D. C. 20330 ATTN: AFOCE	1
Director, U. S. Air Force Project RAND, Via: U. S. Air Force Liaison Office, The RAND Corporation, 1700 Main Street, Santa Monica, Calif. 90406	
ATTN: Library	1
Dr. Harold L. Brode	1
Dr. Olen A. Nance	1
Other DOD Agencies	
Administrator, National Aeronautics & Space Administration, 400 Maryland Avenue, S. W. Washington, D. C. 20546	1
Assistant to the Secretary of Defense (Atomic Energy), Washington, D. C. 20301	1
Commandant, Armed Forces Staff College, Norfolk, Va. 23511 ATTN: Library	1
Commandant, National War College, Washington, D. C. 20310 ATTN: Class Rec. Library	1
Commandant, The Industrial College of the Armed Forces, Fort McNair Washington, D. C. 20310	1

NWED Reports Distribution List

Address	Normal No. of Copies
Other DOD Agencies (Continued)	
Commander, Test Command, DASA, Sandia Base, Albuquerque, N. Mex. 87115 ATTN: TCCOM, TCDT	2
Commander, Field Command, DASA, Sandia Base, Albuquerque, N. Mex. 87115	2
Defense Documentation Center (DDC), Cameron Station, Alexandria, Va. 22314 (NO TOP SECRET TO THIS ADDRESS) ATTN: Mr. Myer Kahn	20
Director, Defense Atomic Support Agency, Washington, D. C. 20301 ATTN: SPSS	5
Director of Defense Research and Engineering, Washington, D. C. 20301 ATTN: Technical Library Mr. Frank J. Thomas	 1 1
Director, Advanced Research Projects Agency, Washington, D. C. 20301 ATTN: NTDO	1
Director, Defense Intelligence Agency, Washington, D. C. 20301 ATTN: DIAAP-IK2	1
Director, Weapons Systems Evaluation Group, Washington, D. C. 20305	1
Langley Research Center, NASA, Langley Field, Hampton, Va. 23365 ATTN: Mr. Philip Donely	1
Manager, Albuquerque Operations Office, USAEC, P. O. Box 5400, Albuquerque, N. Mex. 87115	1
Manager, Nevada Operations Office, USAEC, P. O. Box 1676, Las Vegas, Nev. 89101	1
National Aeronautics & Space Administration, Man-Spacecraft Center, Space Technology Division, Box 1537, Houston, Tex. 77001	1
National Military Command System Support Center, Pentagon BE 685, Washington, D. C. 20301 ATTN: Technical Library	1
U. S. Atomic Energy Commission, Washington, D. C. 20545 ATTN: Chief, Classified Tech Lib, Tech Information Service	1
U. S. Documents Officer, Office of the United States National Military Representative–SHAPE APO New York 09055	1
Other Agencies	
Aerospace Corporation, 1111 E. Mill Street, San Bernardino, Calif. 92408 ATTN: Dr. M. B. Watson	1
Agbabian-Jacobsen Associates, Engineering Consultants, 8939 South Sepulveda Boulevard Los Angeles, Calif. 90045	1

Address	Normal No. of Copies
Other Agencies (Continued)	
Applied Theory, Inc., 1728 Olympic Blvd, Santa Monica, Calif. 90404 ATTN: Dr. John G. Trulio	1
AVCO Corporation, Research and Advanced Development Division, 201 Lowell Street Wilmington, Mass. 01887 ATTN: Mr. R. E. Cooper	1
Battelle Memorial Institute, 505 King Avenue, Columbus, Ohio 43201 ATTN: Dr. P. N. Lamori	1
Bell Telephone Laboratories, Inc., Whippany Road, Whippany, N. J. 07981 ATTN: Mr. R. W. Mayo	1
The Boeing Company, P. O. Box 3707, Seattle, Wash. 98124 ATTN: Technical Library	1
Corrugated Metal Pipe Institute, Crestview Plaza, Port Credit, Ontario, Canada ATTN: Mr. W. A. Porter	1
Defence Research Establishment, Suffield, Ralston, Alberta, Canada	1
Defense Research Corporation, P. O. Box 3587, Santa Barbara, Calif. 93105 ATTN: Mr. Benjamin Alexander	1
Denver Mining Research Center, Building 20, Denver Federal Center, Denver, Colo. 80225 ATTN: Dr. Leonard A. Obert	1
Dynamic Science Corporation, 1900 Walker Avenue, Monrovia, Calif. 91016 ATTN: Dr. J. C. Peck	1
Edgerton, Germeshausen & Grier, Inc., 95 Brookline Avenue, Boston, Mass. 02129 ATTN: D. F. Hansen	1
Engineering Physics Company, 12721 Twinbrook Parkway, Rockville, Md. 20852 ATTN: Dr. Vincent J. Cushing Mr. W. Danek	 1 1
General American Transportation Corporation, General American Research Division 7449 North Natchez Avenue, Niles, Ill. 60648 ATTN: Dr. G. L. Neidhardt	1
General Electric Company, Missile and Space Vehicle Department, Valley Forge Space Technology Center, Goddard Boulevard, King of Prussia, Pa. 19406	1
General Electric Company, TEMPO, 816 State Street, Santa Barbara, Calif. 93101 ATTN: Mr. Warren Chan (DASIAC)	1

Address	Normal No. of Copies
Other Agencies (Continued)	
IIT Research Institute, 10 West 35th Street, Chicago, Ill. 60616 ATTN: Dr. T. Schiffman	1
Kondner Research, Downes Road, Parkton, Md. 21120 ATTN: Dr. R. L. Kondner	1
Lockheed Missile and Space Company, Lockheed Aircraft Corporation, 111 Lockheed Way Sunnyvale, Calif. 94086 ATTN: Dr. R. E. Meyerott	1
Los Alamos Scientific Laboratory, P. O. Box 1663, Los Alamos, N. Mex. 87544 ATTN: Report Librarian	1
Ministry of Defense, MEXE, Christchurch, Hampshire, England ATTN: Dr. Philip S. Bulson Mr. Bruce T. Boswell	 1 1
The Mitre Corporation, Route 62 and Middlesex Turnpike, Bedford, Mass. 01730	1
Physics International Company, 2700 Merced Street, San Leandro, Calif. 94577 ATTN: Dr. Charles Godfrey Mr. Fred M. Sauer	 1 1
Research Analysis Corporation, Document Control Supervisor, McLean, Va. 22101	1
Dr. John S. Rinehart, Senior Research Fellow (R.2), IER/ESSA, Boulder, Colo. 80302	1
Sandia Laboratories, P. O. Box 5800, Albuquerque, N. Mex. 87115 ATTN: Classified Document Division for Dr. M. L. Merritt	1
Southwest Research Institute, 8500 Culebra Road, San Antonio, Tex. 78228 ATTN: Dr. Robert C. DeHart	1
Systems, Science and Software, P. O. Box 1620, La Jolla, Calif. 92037 ATTN: Mr. K. D. Pyatt, Jr.	1
TRW Space Technology Laboratories, One Space Park, Redondo Beach, Calif. 90278 ATTN: Dr. Millard Barton Mr. M. V. Anthony Mr. J. L. Merritt	 1 1 1
URS Corporation, 1811 Trousdale Drive, Burlingame, Calif. 94010 ATTN: Mr. Harold Mason	2
U. S. Department of the Interior, Geological Survey, Geologic Division, Branch of Engineering Geology, 345 Middlefield Road, Menlo Park, Calif. 94025 ATTN: Harold W. Olsen	1
Paul Weidlinger, Consulting Engineer, 110 East 59th Street, New York, N. Y. 10022 ATTN: Dr. M. L. Baron	1

Address	Normal No. of Copies
College and Universities	
University of Arizona, Tucson, Ariz. 85721	
ATTN: Dr. Donald A. DaDeppo, Department of Civil Engineering	1
Professor Bruce G. Johnston, Dept of Civil Engineering	1
Dr. George Howard, College of Engineering	1
University of California, Lawrence Radiation Laboratory, P. O. Box 808 Livermore, Calif. 94550 ATTN: Technical Information Division	2
University of Colorado, School of Architecture, Boulder, Colo. 80304 ATTN: Professor G. K. Vetter	1
University of Detroit, Department of Civil Engineering, 4001 West McNichols Road Detroit, Mich. 48221 ATTN: Professor W. J. Baker	1
University of Florida, Department of Mechanical Engineering, Gainesville, Fla. 32603 ATTN: Professor John A. Samuel	1
Florida State University, Department of Engineering Science, Tallahassee, Fla. 32306 ATTN: Dr. G. L. Rogers	1
University of Illinois, Urbana Campus, Department of Civil Engineering, Urbana, Ill. 61801	
ATTN: Professor N. M. Newmark	1
Professor S. L. Paul	1
Professor M. T. Davisson	1
Professor G. K. Sinnamon	1
Professor W. J. Hall	1
Professor A. J. Hendron, Jr.	1
Professor M. A. Sozen	1
Iowa State University of Science and Technology, Ames, Iowa 50010 ATTN: Professor Glen Murphy	2
Lehigh University, Bethlehem, Pa. 18015	
ATTN: Dr. J. F. Libsch, Materials Research Center	1
Dr. D. A. Van Horn, Department of Civil Engineering	1
University of Massachusetts, Department of Civil Engineering, Amherst, Mass. 01002 ATTN: Dr. M. P. White	1
Massachusetts Institute of Technology, Division of Sponsored Research, 77 Massachusetts Avenue, Cambridge, Mass. 02139	
ATTN: Dr. Robert J. Hansen	1
Dr. Robert V. Whitman	1
University of Michigan, Civil Engineering Department, Ann Arbor, Mich. 48104 ATTN: Professor Frank E. Richart, Jr., Consultant	1

Address	Normal No. of Copies
College and Universities (Continued)	
Dr. George B. Clark, Director, Rock Mechanics Research Group, University of Missouri at Rolla, Rolla, Mo. 65401	1
University of New Mexico, Eric H. Wang Civil Engineer Research Facility, Albuquerque, N. Mex. 87106 ATTN: Dr. Eugene Zwoyer	1
University of New Mexico, Civil Engineering Research Facility, P. O. Box 188 University Station, Albuquerque, N. Mex. 87106	2
Nova Scotia Technical College, School of Graduate Studies, Halifax, Nova Scotia, Canada ATTN: Dr. G. G. Meyerhof	1
Pennsylvania State University, University Park, Pa. 16802	
ATTN: Professor G. Albright, Dept of Architectural Engineering	1
Professor Richard Kummer, 101 Eng. A	1
Purdue University, School of Civil Engineering, Civil Engineering Building, Lafayette, Ind. 47907 ATTN: Professor M. B. Scott	1
Rensselaer Polytechnic Institute, Troy, N. Y. 12180 ATTN: Dr. Clayton Oliver Dohrenwend, Security Officer, Mason House	1
Rice University, Department of Civil Engineering, Houston, Tex. 77001 ATTN: Professor A. S. Veletsos	1
San Jose State College, Department of Civil Engineering, San Jose, Calif. 95114 ATTN: Dr. Franklin J. Agardy	1
University of Texas, Balcones Research Center, Austin, Tex. 78712 ATTN: Dr. J. Neils Thompson	1
Utah State University, Department of Mechanical Engineering, Logan, Utah 84321 ATTN: Professor R. K. Watkins	1
University of Washington, Seattle, Wash. 98105	
ATTN: C. H. Norris, Department of Civil Engineering	1
Dr. A. B. Arons, Department of Physics	1
Professor William Miller, Department of Civil Engineering, 307 More Hall	1
The George Washington University, Nuclear Defense Design Center, School of Engineering and Applied Science, Washington, D. C. 20006	1
Worcester Polytechnic Institute, Department of Civil Engineering, Worcester, Mass. 01609 ATTN: Dr. Carl Koontz	1

Unclassified

Security Classification

DOCUMENT CONTROL DATA - R & D

(Security classification of title, body of abstract and indexing annotation must be entered when the overall report is classified)

1. ORIGINATING ACTIVITY (Corporate author)	2a. REPORT SECURITY CLASSIFICATION
Department of Civil Engineering University of Illinois Urbana, Illinois	Unclassified
	2b. GROUP

3. REPORT TITLE

GEOMECHANICAL MODEL STUDY OF THE BEHAVIOR OF UNDERGROUND OPENINGS IN ROCK SUBJECTED TO STATIC LOADS; Report 1, DEVELOPMENT OF MODELING TECHNIQUES

4. DESCRIPTIVE NOTES (Type of report and inclusive dates)

Report 1 of a series

5. AUTHOR(S) (First name, middle initial, last name)

R. E. Heuer
A. J. Hendron, Jr.

6. REPORT DATE	7a. TOTAL NO. OF PAGES	7b. NO. OF REFS
October 1969	214	57

8a. CONTRACT OR GRANT NO.	9a. ORIGINATOR'S REPORT NUMBER(S)
DACA 39-67-C-0009	
b. PROJECT NO.	
c.	9b. OTHER REPORT NO(S) (Any other numbers that may be assigned this report) U. S. Army Engineer Waterways Experiment Station Contract Report N-69-1, Report 1
d.	

10. DISTRIBUTION STATEMENT

This document has been approved for public release and sale; its distribution is unlimited.

11. SUPPLEMENTARY NOTES	12. SPONSORING MILITARY ACTIVITY
Prepared under contract for U. S. Army Engineer Waterways Experiment Station, Vicksburg, Mississippi	Defense Atomic Support Agency Washington, D. C.

13. ABSTRACT Model laws governing the design of geomechanical model studies of underground openings in rock subjected to static loads are developed using dimensional analysis and the theory of models. The significant variables influencing the prototype which are considered in this study are free-field stresses, intact rock properties, rock mass discontinuity properties, and the opening geometry. Body forces are considered insignificant as a first approximation. The prototype chosen for study is a short section of a long circular tunnel which is underground at a depth of more than 4 tunnel diameters. The development of a modeling material which successfully models the intact properties of rock is described. It was found that modeling materials described in the literature by previous investigators were not satisfactory because they lacked a sufficiently high angle of internal friction. Satisfactory frictional strength in the materials was achieved by developing mixtures of sand and plaster of Paris with a dense packing of sand grains. The size of the model tested is 24" x 24" x 8". The design and development of a loading apparatus which allows independent control of the 3 principal stresses on the block is described. Uniformly distributed loads of 96 tons are applied to the 24" x 8" faces of the model. To maintain a plane strain condition in the model, loads of up to 144 tons are applied to the 24" x 24" faces to null strains parallel to the 8" dimension. Friction along the loading faces is controlled with sheets of teflon. Friction losses are reduced to the order of 10% or less of the applied loads. The development of an instrumentation system for the model is described. Of particular interest is the development of techniques for imbedding electrical resistance strain gages within the model material to measure radial

(continued)

DD FORM 1 NOV 68 1473 REPLACES DD FORM 1473, 1 JAN 64, WHICH IS OBSOLETE FOR ARMY USE.

Unclassified

Security Classification

14. KEY WORDS	LINK A		LINK B		LINK C	
	ROLE	WT	ROLE	WT	ROLE	WT
Dimensional analysis						
Geomechanical models						
Models						
Rock mechanics						
Rock properties						
Static loads						
Tunnels						
Underground openings						

13. ABSTRACT (continued)

and circumferential strains at points within the model around the tunnel. Some tentative observations are made concerning the feasibility of utilizing relatively large scale models to study the behavior of underground openings.